DETERMINE: Novel Radar Techniques for Humanitarian Demining

Federico Lombardi

A dissertation submitted in partial fulfillment

of the requirements for the degree of

Doctor of Philosophy

of

University College London.

Department of Electronic and Electrical Engineering

University College London

July 17, 2019

To my Wife, who always supported me, whatever path I took.
To my Son, who will always support my wife, whatever path I may take.

I, Federico Lombardi, confirm that the work presented in this thesis is my own. Where information has been derived from other sources, I confirm that this has been indicated in the work.

Federico Lombardi

Abstract

Today the plague of landmines represent one of the greatest curses of modern time, killing and maiming innocent people every day. It is not easy to provide a global estimate of the problem dimension, however, reported casualties describe that the majority of the victims are civilians, with almost a half represented by children. Among all the technologies that are currently employed for landmine clearance, Ground Penetrating Radar (GPR) is one of those expected to increase the efficiency of operation, even if its high-resolution imaging capability and the possibility of detecting also non-metallic landmines are unfortunately balanced by the high sensor false alarm rate.

Most landmines may be considered as multiple layered dielectric cylinders that interact with each other to produce multiple reflections, which will be not the case for other common clutter objects. Considering that each scattering component has its own angular radiation pattern, the research has evaluated the improvements that multistatic configurations could bring to the collected information content.

Employing representative landmine models, a number of experimental campaigns have confirmed that GPR is capable of detecting the internal reflections and that the presence of such scattering components could be highlighted changing the antennas offset. In particular, results show that the information that can be extracted relevantly changes with the antenna separation, demonstrating that this approach can provide better confidence in the discrimination and recognition process.

The proposed bistatic approach aims at exploiting possible presence of internal structure beneath the target, which for landmines means the activation or detonation assemblies and possible internal material diversity, maintaining a limited acquisition effort. Such bistatic configurations are then included in a conceptual design of a highly flexible GPR system capable of searching for landmines across a large variety of terrains, at reasonably low cost and targeting operators safety.

Impact Statement

The research programme, funded by the charity Find A Better Way (`http://www.findabetterway.org.uk/`), has been fundamentally directed towards the experimental mapping and characterisation of landmine electromagnetic signatures, as well as developing new configurations for low-cost, accurate and efficient GPR equipment. Special focus has been placed on accurately characterising landmine signatures over a wide range of bistatic angle.

The foremost contribution of the work described in this thesis consists in the perspective of discriminating landmines based on the presence of scattering contributions generated by the internal assemblies of the target, which has demonstrated to be an effective and robust feature for target characterisation. Hence, the presented material, in addition to advancing the knowledge of what can be extracted from the GPR signature of a landmine, opens the possibility to identify targets with internal structure and discriminate the buried anomalies accordingly.

The work has resulted in some key achievements, whose impact is two-fold: firstly, results have highlighted the importance of using neutralised landmines for effectively exploiting the potential of GPR of detecting the internal structure of a target and properly characterising its signature. Secondly, the investigated features are characteristic of the target itself, and are not only source but also scenario independent. This might lead to the development of a common landmine signature database, so that the outcomes can be embedded in a range of GPR systems and made available to a wide range of demining teams.

In addition, yielding the same level of information at a lower computational cost, the suggested bistatic/multistatic approach allows the conceptualisation of a 2D GPR system with the same performance as a 3D one. This consisted of an autonomous ground based platform capable of remotely acquiring dense and regular bistatic data.

Considering that mine clearance operation is a time consuming activity, such conceptual product represents a relevant improvement, outperforming the currently employed hand-held system and possibly relieving the manufacturing cost of such a platform

No clear IP has been identified so far, but might likely emerge in the areas of detection and classification algorithms, signal analysis and processing, bistatic measurement methodologies and antenna development for radar imaging.

Acknowledgements

I would like to thank a number of people who helped me throughout the course of my PhD and contributed to make the work presented in this thesis possible.

First thanks to my supervisor Professor Hugh Griffiths for his constant support and excellent supervision during these years, ensuring successful delivery of this research. This achievement is a result of his constant encouragement and motivation.

My gratitude goes to Dr. Alessio Balleri who has genuinely collaborated for the success of the project and has given me insightful suggestions and counsels throughout the research, as well assistance for the experimental trials. A special mention for Dr. Maurizio Lualdi for his critical insight and constructive collaboration.

The work would not have been possible without the funding support of Find A Better Way, who has sponsored this project, and without the support of the Defence Academy of the UK, who has made available to us the devices employed in the project.

Finally, to my wife Carla who gave me all her unconditional support every day anytime during my PhD.

Last but not least I would like to thank my family and my older and newer friends for their precious support throughout the time of my PhD. Time flies when you're having fun.

Contents

List of Figures

List of Tables

List of Abbreviations

ABC	Absorbing Boundary Condition
ALIS	Advanced Landmine Imaging System
AN/PSS-14	Army-Navy/Portable Special Search
APL	Anti Personnel Landmine
ATL	Anti Tank Landmine
AXO	Abandoned Explosive Ordnance
BLU	Bomb Live Unit
BOR	Body Of Revolution
CCW	Convention on Certain Conventional Weapons
CMP	Common Mid Point
CO	Common Offset
CORD	Collaborative Ordnance data repository
CR	Common Receiver
CS	Common Source
CUDA	Compute Unified Device Architecture
DE	Differential Equation methods
EM	ElectroMagnetic

EOD/IEDD	Explosive ordnance/Improvised Explosive Device Disposal
ERW	Explosive Remnants of War
FAR	False Alarm Rate
FARC	Revolutionary Armed Forces of Colombia
FD	Frequency Domain methods
FDTD	Finite-Difference Time-Domain
FFT	Fast Fourier Transform
GICHD	Geneva International Centre for Humanitarian Demining
GPR	Ground Penetrating Radar
GPU	Graphics Processing Unit
HH	Horizontal Polarisation
HRW	Human Rights Watch
HSTAMIDS	Handheld Standoff Mine Detection System
ICBL	International Campaign to Ban Landmines
ICRC	International Committee of the Red Cross
IDP	Internally Displaced People
IE	Integral Equation methods
IED	Improvised Explosive Devices
IFFT	Inverse Fast Fourier Transform
IS	Islamic State
IWM	Imperial War Museum
JMU	James Madison University

JRC	Joint Research Centre
KCVO	Knight Commander of the Royal Victorian Order
MAG	Mine Advisory Group
MD	Metal Detector
MoM	Method of Moments method
MsMs	Multi-Sensor Mine-Signature
NATO	North Alliance Treaty Organisation
NGO	Non-governmental organization
NQR	Nuclear Quadropole Resonance
OBE	Order of the British Empire
PETN	Pentaerythritol tetranitrate
PHR	Physician for Human Rights
PLS	Proper Lane Sweep
PSG	Pad System for Georadar
RCS	Radar Cross Section
RDX	Research Department Explosive, cyclotrimethylenetrinitramine
SAR	Synthetic Aperture Radar
SF	Single Fold
SNR	Signal to Noise Ratio
SSA	Small Spread Approximation
SVD	Singular Value Decomposition
TD	Time Domain methods

TE	Transverse Electric field
TEM	Transverse ElectroMagnetic
TLM	Transmission Line Matrix method
TM	Transverse Magnetic field
TNA	Thermal Neutron Analysis
TNT	Trinitrotoluene
UAV	Unmanned Aerial Vehicles
UK	United Kingdom
UN	United Nations
US	United States
UXO	Unexploded Ordnance
VNA	Vector Network Analyser
VV	Vertical Polarisation
VVAF	Vietnam Veterans of America Foundation
WWI	First World War
WWII	Second World War

List of Symbols

α	Attenuation parameter
β	Phase parameter
Δf	Frequency step
Δl	Horizontal resolution

Δr	Vertical resolution
ΔT	Time window
Δt	Time step
Δx	Inline sample spacing
$\Delta x, \Delta y, \Delta z$	FDTD model cell size
Δy	Crossline sample spacing
δ	Acquisition error radius
Δ_{off}	Antenna offset sampling
$\varepsilon = \varepsilon' - j\varepsilon''$	Complex permittivity
ε_0	Permittivity of free space
ε_r	Relative permittivity
ε_{tx}, ε_{rx}	Transmitter/Receiver antenna efficiency
λ	Wavelength
μ	Magnetic permeability
μ_0	Magnetic permeability of free space
μ_r	Relative magnetic permeability
ω	Angular frequency
$\sigma = \sigma' - j\sigma''$	Complex conductivity
σ_{RCS}	Radar Cross Section
$\tan\delta = \frac{\sigma' + \omega\varepsilon''}{\omega\varepsilon' - \sigma''}$	Loss tangent
τ_p	Radar pulse width
A_{rx}	Receiver antenna effective area

B	Signal bandwidth
c	Wave velocity in free space
dl	Length of the current element
E	Electric Field
E_i	Incident electric field
E_s	Scattered electric field
f	Wave frequency
f_c	Central frequency
f_t	Transition frequency
G_{tx}, G_{rx}	Transmitter/Receiver antenna gain
H	Magnetic Field
I	Current in the element
I_{TE}, I_{TM}	Incident field strength
k	Phase constant
P_D	Probability of Detection
P_{FA}	Probability of False Alarm
P_{tx}, P_{rx}	Transmitted/Received power
r	Target distance
R_{TE}, R_{TM}	Reflected field strength
T_{TE}, T_{TM}	Transmitted field strength
v	Wave velocity
Y	Admittance

Z	Impedance
Z_0	Impedance of free space
Z_{tx}, Z_{rx}	Transmitter/Receiver coupling losses

If these adults have a problem with these other adults, then go and fight them. [...]. Don't stick a bomb somewhere you'll hurt kids and ordinary women who never did anything to you.

Dolores O'Riordan

Chapter 1

Introduction

A landmine is the perfect soldier: ever courageous, never sleeps, never misses.

P. Jefferson, 1991, [1]

Contamination by landmines and all other types of unexploded ammunitions is a worldwide problem with enormous humanitarian impact [2]. The first antipersonnel mines have been used during World War I, and after that the variety of landmines drastically increased [3]. At the end of the twentieth century, more than 350 types of devices were manufactured in more than 50 countries [4]. A typical landmine consists of a ring mechanism, detonator that sets off the booster charge, and an explosive charge that constitutes the body of the mine and plastic, wood, ceramic or metal casing that contains all of the mentioned elements. A landmine is a type of self-contained explosive device, which is placed into the ground to constitute a mine field, and it is designed to destroy or damage, equipment or personnel. A mine detonates by the action of its target (a vehicle, a person, an animal, etc.), the passage of time, or controlled means.

At least 60 countries are being affected by landmines, but reliable estimates of the area affected worldwide are not readily available. Estimates of the number of mines laid vary, from tens to hundreds of million [5].

While military minefields are laid in a certain order and are reasonably well documented, mines laid by militias are almost never marked or mapped, and when a conflict ends, the landmines are forgotten or deliberately left in the fields, remaining active for decades, becoming a psychological weapon that undermines confidence in the local governments [6]. Although landmines are seen as an effective and inexpensive weapon, they undermine peace and stability and leave behind maimed individuals who require continuing health care and may cease to be fully productive members of society. The war is a cause for displacement, and after hostilities they endanger the lives of returnees and humanitarian aid workers, delay return and impede reintegration and reconstruction, hinder arable land from farming and roads are abandoned due the presence of landmines [7]. Each day these mines are triggered accidentally by civilian activities and animals, ravaging the arable land and killing innocent people [8].

In December 1997, 123 countries signed the Convention on the Prohibition of the Use, Stockpiling, Production and Transfer of Anti-Personnel Mines and on Their Destruction (often called the Ottawa Treaty) in Ottawa, Canada [9]. The Treaty has reduced the number of new mines that are laid every year and the mines that are stockpiled by the signatory countries. However, there are still thousands of hectares of field polluted by landmines. With a current demining rate of approximately 200,000 anti-personnel landmines per year, mine clearance is proving to be a much slower process than was thought in the beginning [10].

Numerous techniques have been used to detect mines, and many of them have demonstrated promising results, but the majority has a low maturity level for field application.

1.1 Motivations of the work

The metal detector, representing the most sophisticated demining tool until recently, suffers from problems such as insufficient detection depth and a high False Alarm Rate (FAR) for landmines with low metal content, due to the high sensitivity required. According to the Geneva International Centre for Humanitarian Demining (GICHD) at present there are few cases of mines laid with no metal content whatsoever, but the so-called minimum metal mines, in which the only metal parts are related to the detonator and contain less than 5 grams of metal, represents a challenging detection task [11].

Without the use of reliable high-tech tools for humanitarian demining, it remains an unsafe (60 casualties were recorded in 2017 among deminers [5]), slow and costly process [12]. According to For military demining, some tools to trigger mines and cause their explosion [13] do exist, but such mechanical demining does not meet the high safety standards for a cleared area established by the United Nations (UN) [14].

In the last decades, a lot of attention has been paid to the application of Ground

Penetrating Radar (GPR) as a landmine sensor, thanks to its capability of successfully detecting minimum metal mines and the possibility of classifying detected objects [15]. A radar signal is sent, and its reflected signal is analysed according to dielectric variations produced from reflections from the soil such as the presence of an object. GPR can detect the soil disturbance due to the mine, which may be either mechanical (deployment of the mine) or hydrological (soil moisture distribution) [16].

GPR has two important features, which makes it an important sensor for landmine detection [17]. First, it is the only advanced sensor that can get horizontal sections of the subsoil at different depths, which constitutes a 3D image of the ground, thus providing volumetric information. Potentially, high-resolution images even allow for classification of landmines. Second, the scatter from a target signal can be used for target classification, as it covers an ultrawide bandwidth. The overall performance of the GPR sensor for landmine detection heavily depends on the way in which it is used and what processing algorithms are implemented in it [18, 19].

Although Ground Penetrating Radar for landmine technology is established, it is capable of further developments to enable continued classification of evolving targets and continued reduction of the size, weight and power of equipment, at the same time to reduce the human presence and supervision [20].

At present, GPR systems do not fully exploit the information available in the reflected signal, which could be used to identify particular types of landmine. This would allow a greater breadth of capability and performance [21].

As inferable from its operational principles, GPR implemented as a subsurface anomaly detector may potentially detect any subsurface object. Typical minefield environments include natural structures, such as rocks, roots or animal burrows, and man-made debris, such as shell casings and urban debris, and these may constitute the vast majority of subsurface scatterers. As a result, the false alarm rate may rise, particularly when considering the extremely high probability of detection required by mine detection sensors.

Landmines are not the only explosive threats to civilian populations once a war ends. Often, bombs, artillery shells, mortars, rockets and grenades, or cluster munitions that did not explode when they were employed, still pose a risk of detonation, sometimes many decades after they were used or discarded. Also, many post-modernist conflicts have seen the wide-spread use of improvised explosive devices.

The principal question is, are there scattering features that can uniquely define the nature of the target and unambiguously characterise a landmine? And, would it be feasible to increase the achievable level of information without increasing the complexity of demining operations?

Theoretically, the reflector can be fully identified based on its shape, size, and spatial distribution of dielectric permittivity [22]. All these features can be provided by solving the inverse problem [23]. However, the huge total amount of necessary measurements of the reflected fields and the very high computational costs involved prevent practical realisation of this approach.

The ability to separate landmines from clutter targets is essential if a sensor is to exhibit both a high probability of detection and an acceptable false alarm rate. When a buried target is illuminated by an electromagnetic wave, energy scatters via several mechanisms, each of them containing characteristic information that is essential for target recognition. Therefore, the key to better target recognition lies in understanding and analysing the electromagnetic signatures of landmines.

Mines (as a man-made objects) exhibit a level of vertical or circular symmetry that is not prevalent in other clutter targets. A scatterer that exhibits these planes of vertical symmetry will have unique scattering responses in terms of bistatic scattering angle and polarisation. As a result, a radar that can make independent bistatic scattering, as well as diverse polarisation observations, can provide important information for separating targets with some symmetry from subsurface objects that do not have this characteristic. In this manner, the scattering response can be used to identify landmines and reject non-symmetric clutter targets. Still, given the resolution capability, a large number of false alarms can fall in this category, if one just relies on shape considerations. In addition, a large number of landmines have been moulded in irregular shape to impede a visual detection and the symmetry and regularity feature could vanish when the target is inclined, hence the shape could not be a discriminant feature. In a radar image, a symmetric target will nearly always appear symmetric, whereas an asymmetric target will often appears asymmetric.

To overcome this problem, advanced descriptors that could exploit features beyond the physical properties of the object need to be collected and extracted from the radar data in order to identify a discriminant property.

A discriminant plane can be found in the nature of the target. A landmine is a complex object, composed by a number of different assemblies and structures to allow a proper detonation and activation of the mine, thus its signature would likely differ from the one collected from a natural clutter object. The potential of GPR imaging to show the internal structure of a landmine, given the prohibitive false alarm rate, can be a significant improvement for the detection and especially the identification of buried landmines. The presence of internal scattering components in the target radar signature represents a discriminant feature, and it can be unambiguously associated with a composite objects, hardly found in the majority of clutter targets.

1.2 Research scope and methods

The approach developed in this Thesis aims at exploiting possible presence of internal structure beneath the target, which for landmines means the activation or detonation assemblies and possible internal material diversity, maintaining a limited acquisition effort. Under this perspective, the point in question is whether this family of targets could benefit from angular diversity, as few contributions have been found addressing this issue. Indisputably, identification and recognition are only possible if these reflections are detected, therefore the first consideration is that a sufficient resolution is needed in the collected data.

Three major milestones and research challenges have been identified:

- **Evidence of internal reflections from landmines**: as these contributions are hardly to be present in other targets than landmines (or generally buried man-made threats), the challenge is to be able to effectively sense these internal reflections and evaluate the level of accuracy of the GPR images. Ideally, being able to delineate the internal design of a target could fill the gap between detection and recognition, breaching also the path to target identification.
- **Bistatic signature analysis and characterisation**: as per previous considerations, each of the internal components of a landmine will have its angular scattering pattern, consequently, a change in the separation between the transmitter and the receiver could better highlight these events and bring an improved target characterisation.

- **Design of a bistatic system**: the optimum configuration is intended to be deployed in a highly mobile ground penetrating radar system capable of searching for landmines across several terrain conditions. This equipment must be reasonably low cost and affordable to meet the dynamics of the humanitarian demining market and to make it effectively deployable.

Ideally, the ultimate outcome needs to be as simplest as possible, i.e. an image with only landmines positions highlighted, regardless of any physical, geometrical and environmental matters. The system architecture should not only provide a logistical progress over the current operations methodologies, but also improve the safety and reduce the hassle of the operator. Area surveying and object detection are repetitive, meticulous and painstaking steps in demining operations, reasons for which a machine-based approach, rather than a manual sensing, can provide important advances in operations quality. From a practical point of view, an autonomous solution will eliminate the need for extensive training of operators, which is a time consuming and subjected to a performance decay, and ideally allows continuous operations, handing down to the human the manual removal of the identified objects only. Even if the last step can be regarded as the only really dangerous part of manual mine clearance, it strongly relies on the performance of the area sweeping step. Finally, as GPR imaging performance depend of the data collection accuracy, the constancy of operations of an automatic solution can hardly be matched by manual surveying. A reliable unmanned platform is required as the ultimate solution. The target robot should have the capability to operate in different control modes, should have reliable navigation capabilities over an area to be cleared with efficient and flexible locomotion capability. It should be easy to use, as even someone with only basic training should be able to operate the system. Lastly, the cost of the equipment should not be significantly more expensive on a sensor to sensor basis than current metal detectors.

The mentioned research question and the related milestones have been addressed by analysing the GPR responses of a number of landmines characterised by different design and structure, with different environment conditions and geometry, and evaluating the information that can be extracted from the different operational mode in which GPR can be operated. For each step, a comparison to a solid replica of the target has been computed to verify the results.

An introductory evaluation has been obtained through the employment of FDTD numerical simulations, to gain a fundamental understanding of the scattering mechanisms that contribute to the overall target signature and to validate the research scope. An additional preliminary analysis has been made carrying out a series of free space measurements, with a consistent wavelength to target size ratio (compared to the subsequent field experiments) to give the off the ground signatures a meaningful value. Experimental trials have been performed in controlled conditions and using a dedicated GPR platform assembled for the purpose of the study and based on already available technology.

It is essential that properly constructed landmine models are used for test and development, otherwise their signatures could differ from real ones. Considering that landmines are objects which are difficult to replicate, it was the first priority to obtain reliable inert (or neutralised) landmines to ensure the collection of landmine signatures as close as possible to those of a real live device. Three representative landmines, provided by the Defence Academy of the UK, have been used. These were complete with all their external and internal components and were filled with a high explosive simulant commonly used to train UK Ammunition Technical Officers.

Given the reliability of the proposed approach, in particular the employment of inert device and the controlled conditions of the trials, the collected signatures and images can constitute a preparatory basis for the development of a catalogue of landmines signature, which could benefit future works and researches. This possibility is of notable importance also for target recognition/identification algorithms, for which a large number of observations, as much accurate as possible, are needed. If one considers the large number of research institutes that are currently involved in the topic, it is obvious that the learning curve can rise faster if a reliable and consistent database is available.

1.3 Scientific innovation and perspective

The foremost novelty aspect of the work described in this Thesis consists in the perspective of discriminating landmines based on the presence of scattering contributions generated by the internal assemblies of the target. Following this direction, the main original contributions are listed below.

- Demonstration of the capability of GPR methodology of discriminating the internal structure of the target, both through a numerical prediction and employing a realistic GPR platform in controlled conditions. A thorough evaluation of this GPR potential is previously not found in the literature.

- Accurate delineation of the internal design of landmines from a series of dense 3D GPR images. The close agreement with the actual structure could pave the way for target recognition scheme, as the internal assemblies could be uniquely associated with a particular family of landmines.
- Employment of different bistatic geometries to additionally characterise the internal design of the target, including the location and spatial extension of the scattering contributions, showing that the same level of information can be obtained through a more efficient survey scheme (compared to a dense and accurate 3D volume).
- Validation of the previous results varying the inclination angle of the buried target towards the surface to prove that the strategy could provide the same performance even when the symmetry of the target is not maintained.

1.4 Personal publications

The following publications have resulted from the work presented in this thesis.

Journal Papers

- **Lombardi**, F., Griffiths, H., Wright, L., Balleri, A., ”Dependence of landmine radar signature on aspect angle”, *IET Radar, Sonar & Navigation*, 11(6): 892-902, 06/2017.
- **Lombardi**, F., Griffiths, H., Lualdi, M., ”Sparse ground penetrating radar acquisition: implication for buried landmine localization and reconstruction”, *IEEE Geoscience and Remote Sensing Letters*, 16(3): 362-366, 03/2019.

Conference Papers

- Wright, L., Balleri, A., Griffiths, H., **Lombardi**, F., ”Multi-perspective high range resolution profiles of landmines”, *IEEE Radar Conference, 2015*, Johannesburg, South Africa, 51-55, 10/2015.
- **Lombardi**, F., Griffiths, H., Lualdi, M., ”The influence of the spatial sampling in GPR surveys for the detection of landmines and IEDs”, *13th European Radar*

Conference (EURAD). London, United Kingdom, 322-325, 10/2016.

- **Lombardi**, F., Griffiths, H., Balleri, A., ”Influence of internal structure on landmine radar signatures”, *13th European Radar Conference (EURAD)*. London, United Kingdom, 161-164, 10/2016.
- **Lombardi**, F., Griffiths, H., Balleri, A., Lualdi, M., ”Preliminary results on multi offset imaging of landmines”, *2017 9th International Workshop on Advanced Ground Penetrating Radar (IWAGPR)*, Edinburgh, United Kingdom, 1-6, 06/2017.
- Lameri, S., **Lombardi**, F., Bestagini, P., Lualdi, M., Tubaro, S., ”Landmine detection from GPR data using convolutional neural networks”, *2017 25th European Conference on Signal Processing (EUSIPCO)*, Kos, Greece, 508-512, 09/2017.
- **Lombardi**, F., Griffiths, H., Balleri, A., ”Bistatic radar signature of buried landmines”, *2017 IET International Conference on Radar Systems*, Belfast, United Kingdom, 1-6,10/2017.
- **Lombardi**, F., Griffiths, H., Balleri, A., ”Landmine internal structure detection from ground penetrating radar images”, *2018 IEEE Radar Conference*, Oklahoma City, United States, 1201-1206, 04/2018.
- Picetti, F., Testa, G., **Lombardi**, F., Bestagini, P., Lualdi, M., Tubaro, S., ”Convolutional autoencoder for landmine detection on GPR scans”, *41st International Conference on Telecommunications and Signal Processing (TSP)*, Athens, Greece, 1-4, 07/2018.

1.5 Thesis outline

The thesis is split into 7 Chapters. The Chapter following this introduction provides a detailed and comprehensive description of the landmine problem, analysed in all his facets, from its socio-economic impact to the technological challenges. Chapter 3 develops a critical review of the main publications relevant to the research context, covering the existing literature with respect to the highlighted milestones. A particular focus is put on publications covering the radar application for sensing and identifying the scattering contributions from the internal structure of landmines, including bistatic and/or multistatic and polarimetric strategies. Weaknesses and limitations of the listed contributions are also given to motivate the originality of this work.

Chapter 4 provides the analytical basis for addressed problem and the subsequent experimental section. This chapter is roughly divided in two, where the first part covers the fundamental principles governing the GPR methodology and summarises the key concepts influencing electromagnetic wave propagation from a theoretical perspective. Special attention is put on the constraints that the demining framework possesses. Discussed theory is then investigated in the second part of the Chapter, in which a series of numerical simulations involving the key variables affecting the imaging performance is developed and assessed in the light of the research objectives here described.

Chapter 5 is dedicated to the assessment of the design and the outcomes of the experimental campaigns. The contents of this chapter includes: a set of initial measurements of the landmine signature changing the antenna orientation and target aspect angle. This dataset, acquired both in free space and in a sand pit, provides a preliminary evidence of the effects generated by the target internal structure. After highlighting some limitations related to unfavourable geometries and complex target design, and after showing that neither a 2D profile can guarantee the detection of the internal contributions, the Chapter presents the results obtained from a 3D GPR experimental campaign which demonstrate the capability of accurately delineating the internal design from a set of images, confirming the suitability of the methodology and the validity of the approach. Some limiting considerations on the acquisition constraints for producing such high resolution images are illustrated as well, underlining the required acquisition effort. Finally, two different bistatic geometries, a common receiver (CR) and a common mid point (CMP) scheme, are evaluated in the light of assessing the benefits that a variation in the antenna separation could bring for target characterisation and acquisition efficiency. A summary of the findings is appended to each section.

After a detailed overview of the logistical and economical context for a successful deployment of a landmine detection system, the results of the experimental campaigns are analysed in Chapter 6 in the light of a conceptualisation of an unmanned bistatic GPR platform. The aim of this Chapter is to provide a series of operational parameters that should be considered when designing such a platform.

The conclusion of this work and suggestions for future research are given together in Chapter 7.

Chapter 2

The landmine problem and the response of technology

Technological progress has merely provided us with more efficient means for going backwards.

A. Huxley, 1937, [24]

In the last decades landmine [1] detection has become a major topic in sensor development and research. The main reasons that have pushed and are still pushing countries for the clearance of mine-affected territories are not only injuries caused to innocent people by these remnants, but also the usage denial of substantial areas of land for agricultural and other economic purposes, which may be critical in countries where the threshold of poverty is already low [25].

Cheap and easy to use, they are favourite weapons in civil wars and wars of insurgency, used by governments and guerrillas alike in flagrant violation of international humanitarian law. These ”eternal sentinels” stand guard long after the conflicts have ended and kill and maim without mercy or discrimination. Unlike a bomb or artillery shell which explodes when it approaches or hits its target, a landmine lies dormant until a person, vehicle, or animal triggers its firing mechanism. Landmines are blind weapons that recognise no ceasefire and cannot distinguish between the footfall of a soldier and that of an old woman gathering firewood [26].

[1] defined from United Nations (UN) protocols as a *munition placed under, on or near the ground or other surface area and designed to be exploded by the presence, proximity or contact of a person or vehicle*.

In the five decades since the end of the Second World War, mine warfare has gained increasing importance on the battlefield. Given the range of tactical situations, terrain and types of force that used them, mines have undoubtedly been one of the most flexible weapon systems of the late twentieth century. Mines became a significant problem after a war because little or no effort was made to clear them and few if any records of them existed. Most mines were laid in close proximity to areas frequented by civilians and the victims of mines were often the very people whom they were supposed to protect. Returning refugees generally had no knowledge of mined areas and were especially prone to treading on them [27, 28].

That mines were not cleared by government forces at the end of conflict was the result of several factors. In general, many of the conflicts did not end in a simple manner, the security situation remained tense even after the official ceasefire. Government forces rarely saw any advantages in marking mines as these were the very weapons on which they relied.

The presence of vast numbers of live mines renders large areas of land inaccessible, prevents refugees and displaced people from returning home, precludes farmers and shepherds from working their fields, and hinders development and rebuilding following the end of war. During and after hostilities, mines can hinder, or even prevent humanitarian activities. The presence of mines also increases the cost of delivering relief supplies [29]. Relief workers obviously are less likely to enter areas heavily infested by mines. Mines can also be used to harm and terrorise peacekeeping forces, as happened in August 1993 when Somali militia used a landmine to attack a U.S. military vehicle in Mogadishu, killing four soldiers. In Bosnia, there have been incidents in which refugee convoys have been blocked by mines on roads intended as evacuation routes. In Afghanistan, some provinces are inaccessible to mine action operators. In 2017, three humanitarian deminers were killed and one injured in conflict-related attacks [30]. In 2017 and 2018, humanitarian demining operators had vehicles seized and damaged by Colombian FARC dissidents, in some cases resulting in the suspension of operations[31]. In South Sudan, four mine action personnel were seriously injured in an ambush, and there were several instances of criminality in which teams were robbed by armed groups.

There are no precise figures on the total number of landmines in the ground, but the number is less important than the impact — it only takes a couple of mines or the mere suspicion of their presence to render a land area unusable. As of December 2018, sixty states and areas have an identified threat of anti-personnel mine contamination, with a further 10 countries having either suspected or residual anti-personnel mine contamination. However, several of the states for which no estimate is provided are heavily or massively contaminated. Total global clearance of landmines in 2017 was about 128 km^2, declined for the third year in a row although in some areas the amount of land release through survey was doubled, with at least 168,000 anti-personnel mines destroyed, figures that are possibly underestimated due to the lack in reporting from some actors (armies or even informal clearance).

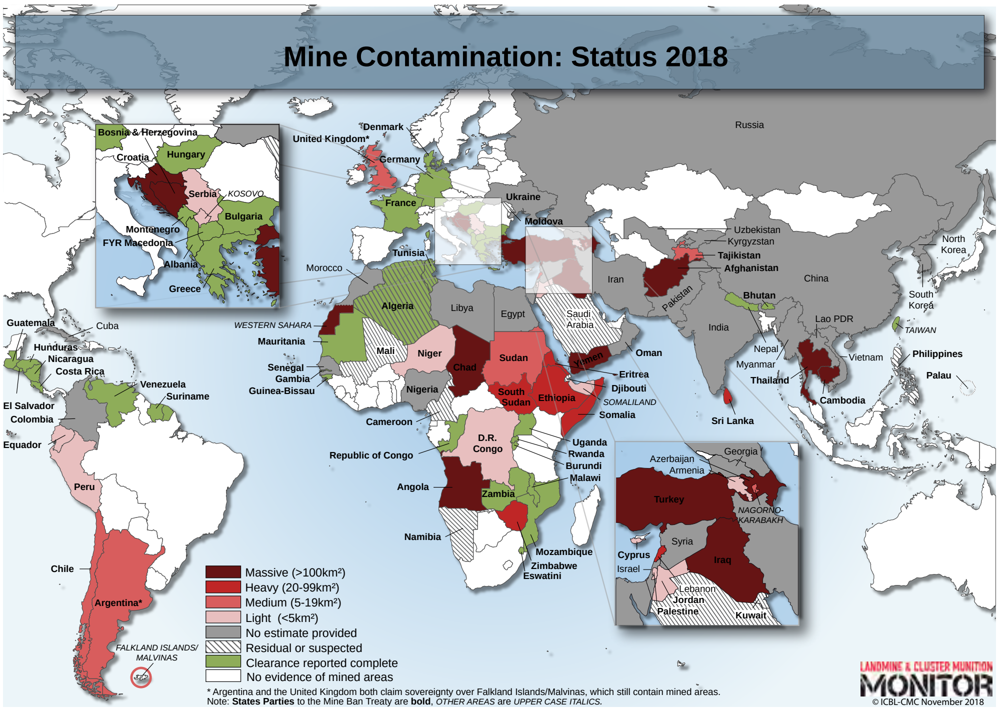

Figure 2.1: Contamination status as of December 2017. *Courtesy of icbl.org campaign.*

High numbers of casualties continued to be recorded in 2017, following a sharp rise in 2015, with a total of more than 7,000 people killed or injured by antipersonnel and antivehicle landmines, including improvised landmines, as well as unexploded cluster submunitions and other explosive remnants of war (Fig. 2.2).

While remaining very high, the total for 2017 marks a decrease on the casualties recorded for 2016. However, it is certain that numerous casualties went unrecorded, as some of the most affected countries do not have national casualty surveillance systems nor adequate reporting in place [5, 32].

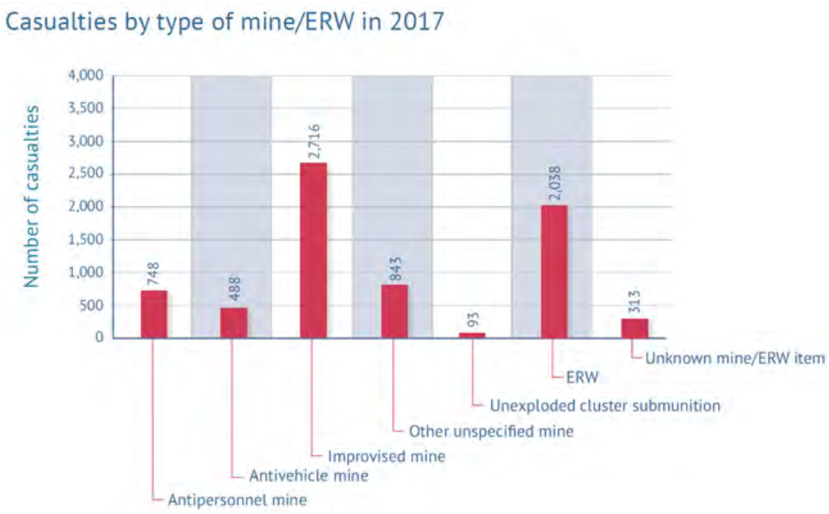

Figure 2.2: Casualties from remnants of war as of December 2017. *Courtesy of icbl.org campaign.*

The primary victims are unarmed civilians, and children are particularly affected, compared to military and security forces, continuing the well-established trend of civilian harm that influenced the adoption of the Mine Ban Treaty: 87% of casualties were civilians in 2017 where the status was known [33]. Of the total recorded casualties in 2017, 60% occurred in 35 States Parties to the Mine Ban Treaty (Fig. 2.3).

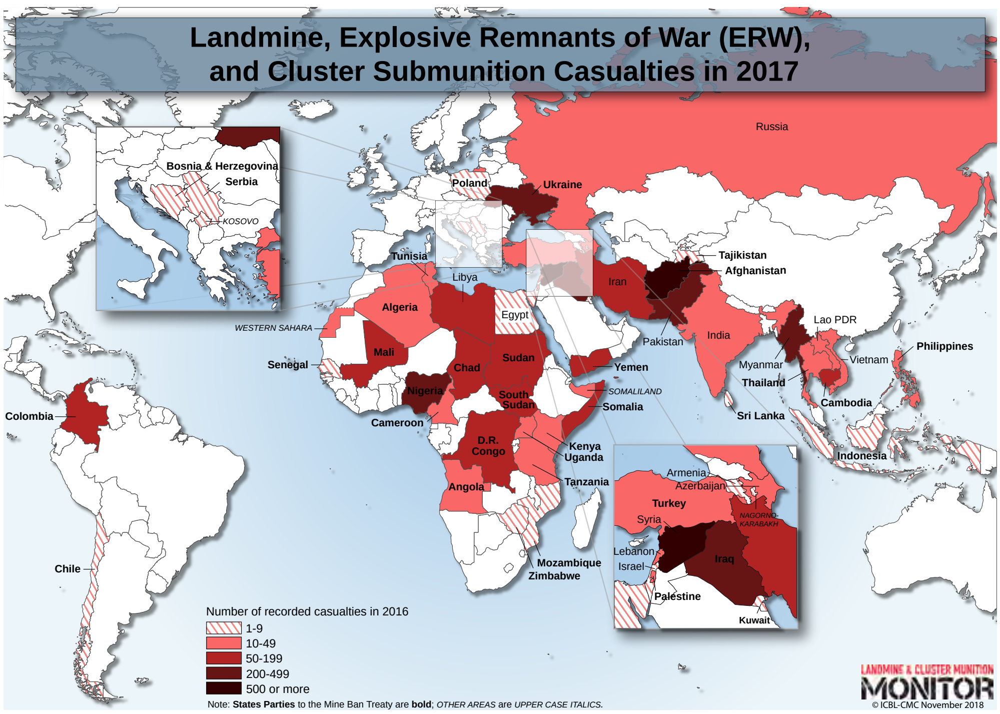

Figure 2.3: Recorded casualties as of December 2017. *Courtesy of icbl.org campaign.*

Government forces of Myanmar used anti-personnel landmines in 2017 [34], while in at least eight countries, including Yemen and Colombia, armed factions and terrorist groups have produced and used improvised landmines [31, 35]. Again, lack of available information meant that it is not possible to determine if mine incidents are the result of new use of antipersonnel mines or due to legacy contamination of mines laid in previous years.

The existence of landmines is considered a vital socio-economic and environmental problem facing many countries exposed to their use. More than half of the affected countries are among the least developed countries, those least able to bear the burden posed by the threat posed by these remains as they fall behind in growth and sustainable development.

In countries emerging from conflict, mines and other ERW slow the repatriation of refugees and internally displaced people (IDPs, whose numbers have reached over 60 million), hamper the provision of aid and relief and deprive communities of the productive and safe use of land for cultivation, the gathering of firewood and other necessities, reconstruction and water. Their presence on roads and infrastructure not only restricts freedom of movement but also makes travelling and rehabilitation efforts hazardous. Their removal requires surveys, clearance and the development of mine action programmes. The world has responded to the risks posed by landmines and UXO by spending over $ 5 billion on mine clearance in the last 10 years (Fig. 2.4), with the highest level of international support recorded in 2017 (more than $673 million). The overall trend is for spending to rise, with over $ 395 million (93% of total contribution) spent on mine clearance and risk education in 2017.

Tragically, removing landmines is far more expensive than putting them into the ground in the first place. The cost of removing a landmine is considered ten times more than the price for its production and installation.

Cost–benefit evaluations of landmine clearance are contradictory, probably influenced by inadequate data. Benefits from clearance include human benefits, the value of casualties and medical costs saved, and development benefits, revenue from new production or tourism and travel costs saved. To estimate human benefits it is commonly assumed that clearance reduces relevant casualties in proportion to the area of land cleared, based on the productive value of victims.

The methods of estimating development benefits depend on land use. For agri-

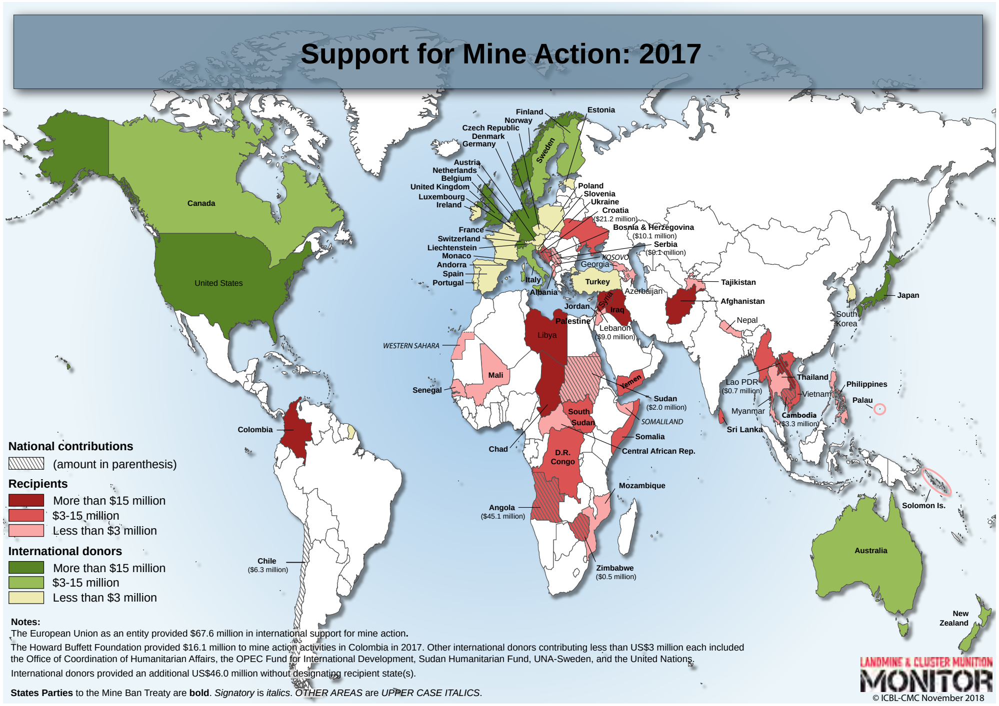

Figure 2.4: Support for mine action as of December 2017.

cultural land and irrigation systems they are based on the additional value of farm revenues. For roads and bridges, wells and water supplies, schools, and health stations estimates are based on reductions in travel costs, while for historical and cultural sites additional tourist revenue is calculated.

Landmine programs typically involve targeted clearance operations rather than an average clearance task so that mine fields with the greatest benefits are likely to be cleared first. For example, the clearance of landmines that prevent the use of existing infrastructure or allow new development projects such as access roads, water systems, and irrigation works are likely to yield significant economic returns. As a result, the true economic benefits of real landmine programs are seriously underestimated.

2.1 Evolution of mine warfare

Landmines today range from very simple devices improvised in the field by soldiers to high-technology, sensor-activated weapons. Landmines are small, usually round devices designed to injure or kill people by an explosive blast or flying fragments. Most modern mines are fabricated from sophisticated non-metallic materials and incorporate advanced electronics, making them increasingly smart.

Modern landmines trace their lineage from non-explosive predecessors (Fig. 2.5) such as the spikes and stakes that were employed by ancient armies [1]. The word ”mine” is derived from the Latin word *mina* which means ‘vein of ore’ and was originally applied to the excavation of minerals from the earth. The term was then borrowed by military engineers whose job it was to dig mines in the ground during sieges of forts and castles, often under walls to cause them to collapse.

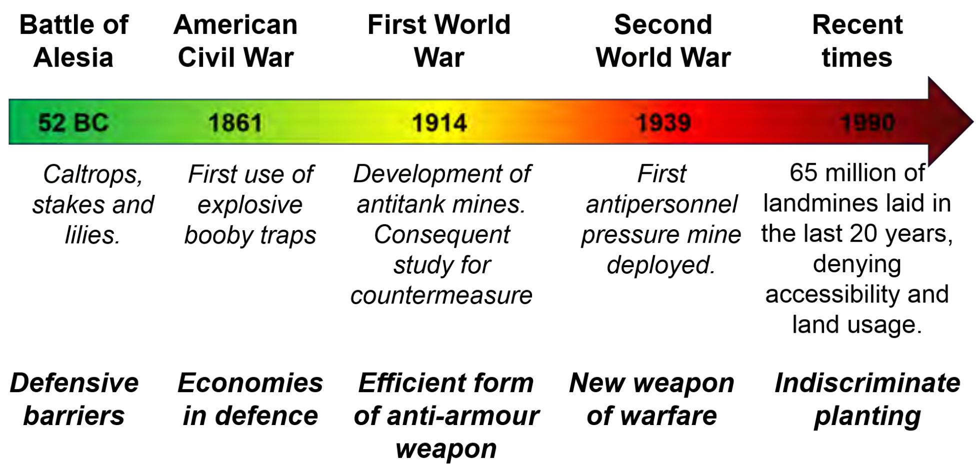

Figure 2.5: From defensive barriers to contamination: the evolution of concealed traps.

The first use of concealed traps in a tactical defensive context to gain advantage on the battlefield dates back to the Siege of Alesia, in 52 B.C., when Emperor Caesar used pits, arrays of stakes and devices called *caltrops* to impede the progress of the Gauls (Fig. 2.6(a)). Similar devices were used in the battle of Bannockburn (1314) and the Wars of the Roses (1455 - 1485). After the discovery of gunpowder in the 13th century, explosive charges were used in siege warfare. This led to the development of the *fougasse* – essentially an underground cannon, placed forward of a defensive position to shower rocks and debris over a wide area (Fig. 2.6(b)). In the mid 1950s the concept of the fougasse was reborn in the guise of the extremely lethal American M18A1 anti-personnel directional fragmentation mine, better known as the ”claymore”.

Precursors of conventional landmines appeared in the 15th century at the Battle of Agincourt in France and in the 18th century during the American Civil War, when the first devices designed to explode on target contact were first employed by the US Confederate Navy as floating mines. Even at that early date, the use of mines raised strong feelings, with many judging them as ”unworthy and improper to the conduct of war”. However, the ability of a cheap mine to destroy an expensive warship was an

(a) (b)

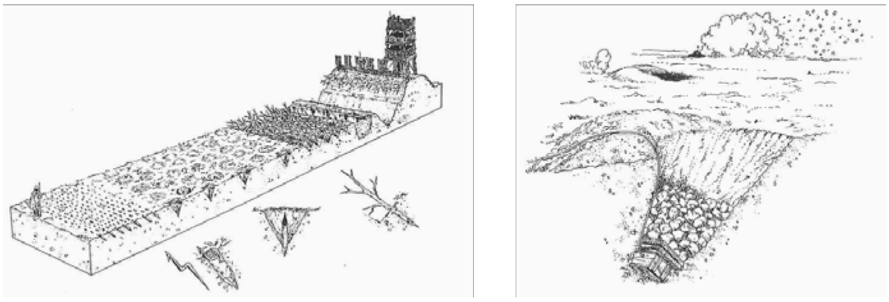

Figure 2.6: Landmine warfare precursors. (a) Romans fortification. (b) American fougasse. *Taken from [1]*

irresistible economic argument for its deployment [36].

On 4 May 1862, while scouting along a road leading to Yorktown, a horse rider activated one of the earliest landmines, which had been fabricated by assembling artillery shells so that they could be exploded by pulling trip wires, becoming the first person to be killed by a pressure-operated landmine. After his troops encountered these devices, the commander of the Union Army, General William T. Sherman, said that the use of landmines "was not war, but murder". The Civil War experience also demonstrated the longevity of mines in the ground. In 1960 five landmines belonging to this period were recovered in Alabama, still potentially functioning.

The British Army was keen to use landmines during their African campaigns in the 1880s. During these wars they used *fougasses* and tripwire/pressure-operated mines that were generally manufactured in the field. By the 20th century the concept of landmine warfare had permeated through most regular armies.

The development and use of the landmines became a major military strategy between 1918 and 1939. Mines only began to appear on a large scale in 1918, as an answer to another new piece of weaponry, the assault tank. To combat the growing number and effectiveness of Allied tanks, the Germans needed to design new weapons. Initially they used artillery shells dug into the ground and covered with wooden boards, to give a wide pressure plate (Fig. 2.7(a)). A number of anti-personnel mines and booby-traps were laid in abandoned positions in anticipation of an enemy advance. These weapons were adapted from artillery shells, with specially designed fuzes screwed into the bottom of the shell. The Germans entered the Second World War with just two types of anti-tank mines and one anti-personnel mine. By the end of the war they had manufactured sixteen different types of anti-tank mines, ten different types of anti-personnel mines (Fig. 2.7(b)) and employed many different types of booby traps (improvised devices). From 1942 they fought almost constantly on the defensive, placing increasing importance on mines as a weapon of attrition.

In 1940 French troops encountered a new device that leapt out of the ground before detonating. The *Schrapnellmine* was the size of a beer can and was activated by a three-pronged push device or a pull igniter attached to a tripwire. When fired, a cannister was launched about one metre into the air by a primary charge before it was detonated by a secondary charge scattering 350 steel balls out to a range of 150 m [37].

(a) **(b)**

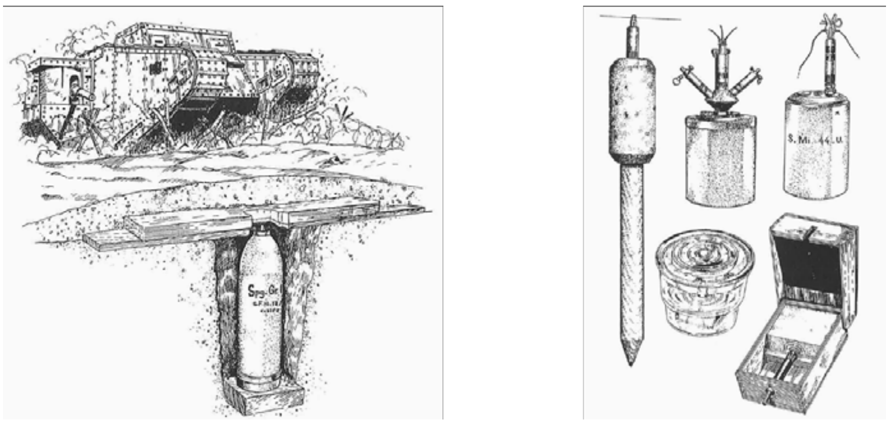

Figure 2.7: Early German landmines. (a) Anti-tank mines from WWI. (b) Anti-personnel mines from WWII. *Taken from [1]*

The first major innovation of the war was in 1942, with the introduction of the wooden-cased mine. The smaller amount of explosive that the case could contain was sufficient to leave its victim limbless but not strong enough to kill him, opening the way to the practical intention of maiming rather than killing. Towards the end of 1944 American soldiers first came across non-metal mines in Lorraine, France. In a single minefield they found 12,000 mines made out of bakelite plastic or wood, which made them more difficult to locate with metal detectors. Still, at this time, mines were used in a controlled manner and specifically targeted at soldiers. It was not until the 1960s that the random distribution of landmines began [38].

Advances in mine technology, as in all areas of weaponry, accelerated in the decades following World War II, primarily in response to changing battlefield requirements, in the nature of warfare and the development of new military technologies. With the end of fighting and the dawning of the Cold War, barrier minefields became a common feature of national border defences, sometimes, as in the case of East Germany, designed to keep the population in rather than the more traditional role of keeping the enemy out [39].

In the early 1960s, the United States first introduced the use of a new and sophisticated class of contact antipersonnel mines, known as remotely delivered mines or scatterables (Fig. 2.8), to stop the flow of men and materiel from North to South Vietnam through Laos and Cambodia [1].

(a) **(b)**

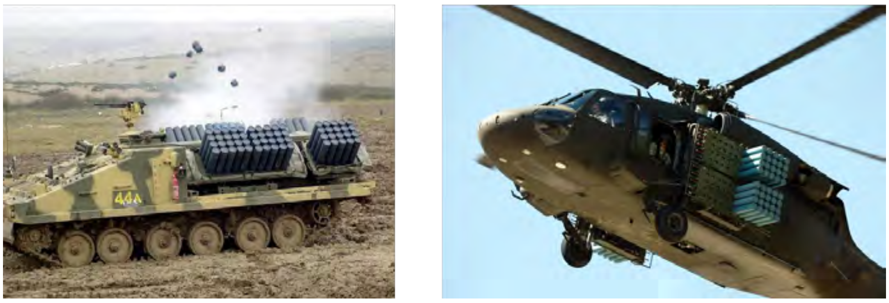

Figure 2.8: Remotely delivering mine system. (a) British Shielder Vehicle-Launched Scatterable Mine System. (b) US M139 Volcano Mine System. *Taken from wikipedia.org*

The most commonly deployed devices were the BLU-43 and BLU-44, weighting only 20 grams but capable of tearing off a foot. These were the forerunners of the Soviet PFM-1, or ”butterfly” mine, used extensively in Afghanistan during the late 1970s. Because of the hit-and-run nature of the Vietnam War, American ground forces often found themselves retreating through areas that their own pilots had previously saturated with mines.

During the Cambodian conflict, government troops used mines offensively by placing them around the perimeters of enemy villages. They then bombarded the villages with artillery fire so that the enemy, mainly non-combatant civilians, was forced to flee into minefields. Other examples of mines being used intentionally against civilian populations include Afghanistan, where Soviet and Kabul forces mined grazing areas, agricultural land, and irrigation systems in an effort to undermine civilian support of the Mujahidin, and Northern Somalia, where Siad Barre’s forces mined wells and grazing lands [40]. In both cases, there was no pretence that the widescale use of mines was directed purely at the military opposition. Landmines were used extensively throughout the conflict following the breakup of Yugoslavia (Fig. 2.9), as one of the aims of the fighting was to drive people out of their homes and keep them away, generating the so called Europe's biggest minefields [41]. As well, when Saddam Hussein's Iraqi forces occupied Kuwait, they set about encircling that country with a double ring of minefields to seal off the Kuwait City area.

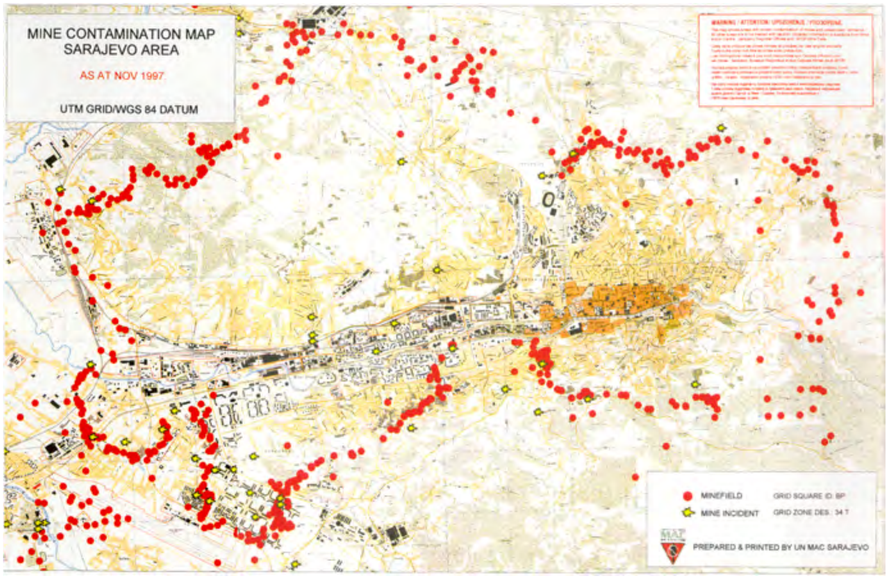

Figure 2.9: Mine contamination of the Sarajevo area in 1997. *Taken from balkansnet.org*

In Angola, Cambodia, Ethiopia, Mozambique, Nicaragua, Iraq, Somalia, Sudan, and more recently Ukraine, Syria and along the territories occupied by the IS forces, anti-personnel mines have been widely used as part of military strategy or simply to terrorise civilians or control their movements.

As can be inferred, mine have had a part to play at every level of conflict, in any terrain, against a variety of targets. They can be laid in advance, thus allowing the most economical use to be made of scarce engineer resources. For a fraction of the cost of a main battle tank, a mine can wreak devastating and disruptive damage upon that, as well as decimating an infantry squad as easily as a machine gun, but at lower expense. Of all the hazards of war, the mine was the most insidious and the most feared, providing a disturbing psychological dimension, as highlighted by the British officer Colonel J.M. Lambert in 1952:

> Mine warfare is an unpleasant business. It is foreign to our character to set traps cold bloodedly, or to kill a man fortnight in arrears, when you yourself are out of harm's way; and most British soldiers who have experienced it will own a rooted dislike of mine warfare in principle and practice.

and, more recently, from a letter recovered from a colombian eradication man to his commanding officer [42]:

> It's a silent killer which stalks us and threatens us, and yes, we admit it, frightens us.

2.2 The path to the global ban

Concerning international law, on August 1949 the Geneva Conventions, Fig. 2.10, were updated to reflect the changes in the nature of warfare in the previous decade. Apart from forbidding prisoners of war from employment on mine clearance duties, no specific restriction was placed on the use of mines. Even the 1980 *Convention on Prohibition or Restrictions on the Use of Certain Conventional Weapons Which May be Deemed to be Excessively Injurious and to have Indiscriminate Effects* (or CCW), did not adequately address the problem of the unique threat that mines posed to civilians, as it had two important shortcomings: it did not formally apply to internal conflicts and there was no means of implementing it.

Figure 2.10: The 1949 Geneva Convention. *Courtesy of icrc.org*

After the Vietnam War, the inability of landmines to stave off an attack, while stressing the horrific injuries they had caused to people, was worldwide clear and manifest. However, it was not until the early 1990s that the issue of landmines really became a matter of international attention. By that time, it was clear that thousands of civilians were victims of mines that had been laid without reference to the CCW and it was contended that mines had been used specifically to target civilians. In 1991 *Human Rights Watch* and *Physicians for Human Rights* published the first detailed study of how landmines were actually being used [43]. The book made a strong case for humanitarian demining, which aims to make the land completely safe for human use - a far cry from stock military mine clearing techniques.

October 1992 marked the real beginning of the *International Campaign to Ban Landmines* (ICBL) when a coalition of six non-governmental organisations combined their separate initiatives and harnessed popular support, sponsoring the creation of the campaign: *Handicap International*, *Human Rights Watch*, *Medico International*, *Mines Advisory Group*, *Physicians for Human Rights* and *Vietnam Veterans of America Foundation*. None of the six groups on the steering committee of the International Campaign came from the disarmament community [44]. By 1995 the Campaign had embraced a multitude of groups from all corners of the world, and been given a huge boost when the *International Committee of the Red Cross* overcame its usual reluctance to deal with political issues and launched its parallel, well-documented campaign. Bypassing the failure of consensus politics, a Canadian initiative in October 1996 convened an historic conference in Ottawa (Fig. 2.11 (a)) [45]. The 50 governments who fully participated signed a declaration recognising the urgent need to ban anti-personnel landmines.

Against the backdrop of the intensive campaigning was the growing involvement of Diana Spencer, Princess of Wales, in the global landmine issue. Before her untimely death, the Princess had been actively speaking out against the production and use of landmines and she made several visits to affected countries. In 1997 at the invitation from the International Red Cross, Princess Diana visited Angola in an effort to create an international awareness of landmines, including the plight of Angolan children [46]. During her visit she was invited by the HALO Trust, a British demining agency, to view and walk through an active minefield. The visit by Princess Diana to Angola received extensive media coverage, and gave the ICBL campaign a welcome boost. Her crusade against landmines led also to her three-day visit to Bosnia in August, 1997, during which she met victims who had sustained injuries from devices planted during the savage civil war in the 1990s [47].

Unbeknown to her, several high profile UK politicians took offence at what she was saying publicly at the time and publicly distanced themselves from her. This caused further publicity and news items which ultimately benefited the campaign. Lou McGrath OBE, the founder of the British organisation Mine Advisory Group, speaking on the 20$^{\text{th}}$ anniversary of her death, said [48]:

> Without her we couldn't have brought forward what was the fastest arms control

treaty in the world.

This concerted effort culminated in 1997 with the adoption of the Ottawa Treaty, becoming a milestone in international law, at a conference in Oslo, Norway [49]. The ICBL received a further boost in October of the same year when the Nobel Peace Prize was awarded jointly to the International Campaign to Ban Landmines and its co-ordinator Jody Williams "*for their work for the banning and clearing of anti-personnel mines*" (Fig. 2.11 (b)) [50].

Figure 2.11: The Ban campaign. (a) Princess Diana walking through a minefield. *Courtesy of halotrust.org*. (b) The Treaty signing ceremony. The ICBL Coordinator Jody Williams is the first on the left. *Courtesy of canadianlandmine.org*. (b) Nobel Peace Prize award, Oslo, December 1997. *Courtesy of handicap-international.ca*

The *Convention on the Prohibition of the Use, Stockpiling, Production and Transfer of Anti-Personnel Mines and on their Destruction*, shortly known as the Ottawa Treaty, made a significant effort to stop the diffusion of anti-personnel landmines worldwide, stating right at the beginning of the treaty [9] that:

1. *Each State Party undertakes never under any circumstances:*
   (a) *To use anti-personnel mines;*
   (b) *To develop, produce, otherwise acquire, stockpile, retain or transfer to anyone, directly or indirectly, anti-personnel mines;*
   (c) *To assist, encourage or induce, in any way, anyone to engage in any activity prohibited to a State Party under this Convention.*
2. *Each State Party undertakes to destroy or ensure the destruction of all anti-personnel mines in accordance with the provisions of this Convention.*

In summary, the Ottawa Convention bans States Parties from using "victim-activated" explosive devices, but the convention does not ban mines that are designed to be exploded by the presence, proximity or contact of a vehicle (i.e. anti-vehicle and anti-tank mines) and explosive devices that are remotely controlled [51]. This is the most argued issue of the Treaty, as its opponents point out that the inhumane nature of landmines stems not from whether they are anti-personnel as opposed to anti-vehicle, but from their persistence in the ground.

Although a triumph for popular will (to date there are 164 States Parties to the treaty plus one that has yet to ratify), 35 member states, including the United States, China and Russia (the three largest military powers) did not sign the treaty and are still are non-signatories (Fig. 2.12). The majority of non-signatories claim that when used correctly, anti-personnel mines are defensive weapons that harm only attackers, and that the psychological effect of mines increases the threshold to attack and thus reduces the risk of war. Furthermore, some states felt that a ban on such weapons would compromise their national security to an unacceptable degree [2]. Presumably they believe that the humanitarian dimension lies in protecting their people from aggressors rather than from the residual effect that mines may have.

Figure 2.12: Mine Ban accomplishments as of December 2017. *Courtesy of icbl.org campaign.*

Since the Convention came into force in 1999, the use of anti-personnel mines has decreased, as well the active production of these devices. However, non-signatory

[2]"Even as we take this further step, the unique circumstances on the Korean Peninsula and our commitment to the defence of the Republic of Korea preclude us from changing our anti-personnel landmine policy there at this time." *US Department of State*; "A mine-free world remains our common goal. Nonetheless, our movement towards this goal has to be realistic and gradual, sustaining the necessary level of security and stability." *Statement of Russia*; "We are still obliged to maintain anti-personnel landmines as necessary for self-defence and security needs. Israel regrettably cannot commit to a total ban as they are a legitimate means for defending its borders." *Israeli Ministry of Foreign Affairs*; "As a country with long land borders, China must reserve the right to use anti-personnel mines on its territory. The Treaty addresses only the humanitarian concerns, thus China is not able to sign". *Statement of China*.

States to the treaty continue to use and stockpile these landmines, and more than 82 countries have some form of widespread landmine contamination from past and ongoing conflicts. The use of anti-personnel mines by states remains a relatively rare phenomenon, even if there are confirmation of their employment by non-state armed groups in dozens of countries, due to the recent proliferation of low intensity conflicts [52, 53]. Of course, although governments may sign on to the International Campaign to Ban Landmines, terrorist groups do not conform to such [54].

In this respect the United Nations reported estimates and statistics illustrating the scale of the disaster: 120 million landmines still in the ground and a comparable number in military stockpiles, which could be eliminated after 1100 years (provided that no additional mines are planted) at a cost of more than 30 billion dollars. This means 1 landmine for every 16 children in the world. On the basis of the figures currently being promoted, the clearance of mine affected areas would be next to impossible and politically unfeasible.

(a) **(b)** **(c)**

Figure 2.13: Pyramid of Shoes against landmines. (a) Place de la Republique, Paris.(b) Trafalgar Square, London. (c) Capitol Hill, Washington. *Taken from the web.*

Certainly, the campaign has brought a great deal of publicity to the issue (Fig. 2.13), but it has distorted the size and the shape of the problem and distracted attention from the crux of the issue (the clearance of redundant minefields), making a moral issue out of a practical problem. Indisputably, the massive circulation and promotion estimates, statistics and figures on landmines and landmine victims has played a central role in efforts aimed at reaching a total legal ban on landmines but the dissemination of grossly exaggerated estimates do not serve the interests of potential victims.

Even if it will make no difference to a farming community whether a given square kilometre of land may be infested with one, a hundred or ten thousand mines, since the risk of death or injury precludes its use unless cleared, and the concentration of mines may not be the prime factors determining the speed of mine clearance, since the time required for its humanitarian clearance roughly remains the same, a precise appreciation of the landmine contamination in a given territory is indispensable to evaluate and plan mine clearance programmes. [3]

2.3 Landmine classification

There are currently more than 600 different types of landmines (black market production excluded) available, not only to official armies but essentially to all fighting groups and armed factions worldwide, as well as many improvised mines made by military forces engaged in fighting (*ordata.info*).

They are grouped into two broad categories: anti-personnel mines (*APL*) and anti-vehicle mines, also commonly referred to as anti-tank mines (*ATL*).

AP mines can be found on the ground, buried or fixed above ground and are generally small devices that come in many different shapes. Often, they are camouflaged to help them blend into the surroundings and can be fabricated from wood, plastic or metal. Once triggered, AP mines cause death or serious injury by an explosive blast and/or flying fragments. They are grouped according to their design, or to the manner in which they inflict injuries:

- **Blast** (Fig. 2.14): designed to be triggered by the pressure caused by physical contact with the mine, mostly by stepping on them. Most mines of this type are designed to cause serious injury, rather than death. They create a blast shock wave consisting of hot gases travelling upward at extremely high velocity. In addition to buried blast mines, a common type of mine is the scatterable mine, so-called as it is scattered over the ground by aircraft or artillery fire.

[3] A useful essay on the landmine estimation controversy can be found in [55].

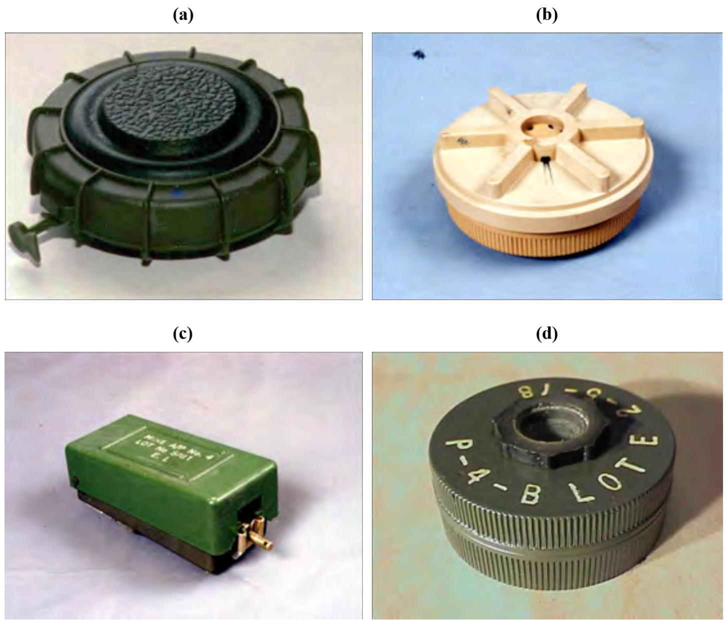

Figure 2.14: Examples of blast mines. (a) Italian VS-Mk2. (b) Belgian PRB M409. (c) Israel No. 4. (d) Spanish P-4-B. *Taken from ordata.info*

- **Fragmentation**, typically designed to cause death, often to a large number of people, from fragments propelled by the mine's explosive charge. Most of these mines have metal casings, or contain ball bearings or metal fragments that are turned into lethal projectiles by the detonation of the mine. There are three basic types of fragmentation AP mines:
  i) **stake mines** (Fig. 2.15), fitted with one or more tripwires that set the mine off when pulled or cut. Tripwires are very hard to see, and may be strung across paths or doorways, and attached to a solid object such as a tree, or to another mine. Once set off, metal fragments are projected over a 360-degree radius, causing lethal injury to anyone within an unobstructed four metre range and causing death or serious injury to people at much greater distances. Beyond this, the uneven size and distribution of the fragments makes the effect unpredictable; over time, stake mines may fall over or the stake on which they rest may disintegrate, making them even more dangerous.

Figure 2.15: Examples of stake-mounted fragmentation mines. (a) Chinese type 59. (b) Soviet POMZ. *Taken from jmu.edu*

ii) **directional mines** (Fig. 2.16), or ”Claymore” type, are designed to project a dense pattern of fragments in a specified direction. Directional fragmentation AP mines are usually command-detonated, but they can also be initiated by tripwire. Once detonated, most mines of this type project their fragments within a 60-degree horizontal arc and to a height of about two metres. Most are designed to have an effective range (causing serious injury or death) of around 50 metres. They are capable of killing people, as well as disabling or destroying passenger and pick-up vehicles.

Figure 2.16: Examples of directional fragmentation mines. (a) US M18 Claymore (note the well-known inscriptions *FRONT TOWARDS THE ENEMY*. (b) Yugoslavian VMRUD *Taken from iwm.org.uk*

iii) **bounding mines** (Fig. 2.17), normally buried and triggered by tripwires or direct pressure. Once triggered, an initial explosion lifts the mine out of the ground to about waist height before the main charge detonates. Upon detonation, the explosion shoots out metal fragments over a 360-degrees horizontal radius. Design variations mean that the number, size and distribution of fragments vary widely, but a typical bounding mine is likely to be lethal within 25 metres and capable of inflicting serious injury at ranges up to 100 metres.

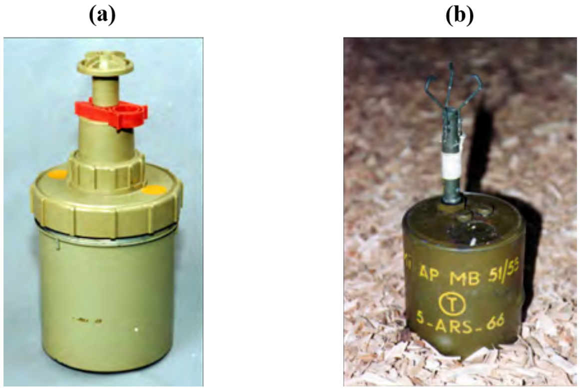

Figure 2.17: Examples of bounding fragmentation mines. (a) Italian P-40. (b) French 51/55. *Taken from ordata.info*

Anti-vehicle landmines, instead, are designed to disable or destroy vehicles. Like anti-personnel mines, AT mines can be detonated by pressure (though normally much greater weight is needed), by remote control, by magnetic influence or through the disturbance of a tilt rod (a sort of vertical tripwire). Because AT mines are made to destroy vehicles, they are generally found on roads, roadsides, paths and tracks. Clearly, this family of mines are much larger than their anti-personnel equivalent, and have a far heavier explosive charge (Fig. 2.18). It normally takes considerable pressure to detonate a standard anti-vehicle mine, around 120 kg to 150 kg.

Figure 2.18: Examples of anti-vehicle landmines. (a) Italian Bakelite type II. (b) Russian PG-MDM. (c) German T-42. (d) British Mk-V. *Taken from iwm.org.uk*

This does not necessarily mean that people weighing less can safely step on them.

Fuze systems may deteriorate or be deliberately adjusted, resulting in a reduction in pressure required to detonate. In some cases AP mines have been laid on top of AT mines which, when initiated, will generally cause the anti-vehicle one to detonate as well. Anti-personnel mines are often used to prevent the recovering of the anti-vehicle ones, and the technique of laying these two families of landmines together in clusters is common [56].

There are two further categories of explosive devices which eventually could have the same effects of landmines, even if their main purpose is different:

- **Explosive Remnants of War** (Fig. 2.19): explosive ordnance which has been primed, fuzed or otherwise prepared for action, and which has been fired, dropped, launched, projected or placed in such a manner as to constitute a hazard to operations, installations, personnel or material and remains unexploded either by malfunction or design or for any other cause. Under the international legal definition, they consist of unexploded ordnance (UXO) and abandoned explosive ordnance (AXO), but they do not consist of mines, because of the different primary aim of these weapons.

(a) (b)

Figure 2.19: Examples of explosive remnants. (a) Unexploded mortar bomb in Cambodia. (b) Israeli cluster bomb with penetrating submunitions. *Taken from icrc.org and wikipedia.org*.

- **Improvised Explosive Devices** (Fig. 2.20): dating back to the bombs made by the Irish Republican Army using explosive based on fertiliser [57], they are a type of unconventional explosive device placed or fabricated in an improvised manner and designed to destroy, incapacitate, harass or distract. They may incorporate military explosive items, but are often devised from non-military component and can come in many forms. Improvised devices can be carried or delivered in a vehicle; carried, placed, or thrown by a person; delivered in a package; or concealed on the roadside.

Figure 2.20: Examples of improvised explosive devices. (a) Victim activated fuel container in Afghanistan. (b) Mortars and shells in Nigeria. (c) Mortars and landmines in Iraq. (d) Ordinary items used for IEDs. *Pictures taken from wikipedia.org, nato.int and courtesy of the Defence Academy of the UK.*

Acting *de facto* as anti-personnel landmines, IEDs account for 25% of the total casualties every year and countless more injuries [5].

2.4 Standards and Definitions

There are two principal types of mine clearance operations: military and humanitarian [14]. Military demining is conducted for a strategic advantage, i.e. the clearance of a path through a minefield, and it is about reducing risk, therefore casualties may be accepted. Normally the clearance is performed with armoured vehicles equipped with hardened roller, steel flail or similar tools capable of neutralising objects on or near the surface (Fig. 2.21).

Otherwise known as minefield breaching, military mine clearance does not normally expect to achieve more than 60-75% clearance of a given mined area (up to 90% when employing explosive breaching machines).

Humanitarian mine clearance, on the other hand, aims to return land to the civilian population, with civilians being the beneficiaries of the activity. Clearance means that

Figure 2.21: Route clearance and minefield breaching machines. (a) Toothed rake machine. (b) Mine flail. (c) Mine roller. (d) Typical route clearance trails. *Taken from nolandmines.com and wikipedia.org*

there is nothing dangerous left in the ground till an agreed depth. The UN statement of requirement [14] defines the clearance criteria as follows:

> The area should be cleared of mines and UXOs to a standard and depth, which is agreed to be appropriate to the residual/planned use of the land and which is achievable in terms of the resources and time available. The contractor must achieve at least 99.6% of the agreed standard of clearance. The target for all *UN* sponsored clearance programmes is the removal of all mines and UXOs to a depth of 130 mm.

Demining time is not considered to be a major factor in humanitarian operations, in particular less important than the safety of the clearance personnel and the reliability and accuracy of the process. Safety is of utmost importance, and casualties are unacceptable. Another consideration by humanitarian demining is the use of land for development, as there is a need to reduce the environmental and ecological impacts that may results from the demining operation [58].

The process has the primary aim of safely returning the area to its normal use, so no explosive hazards can be left behind. It must be noted that the solutions developed for the military are generally *for* the military and cannot be used for the purposes of humanitarian demining. Military procedures cannot be employed in humanitarian operations because they cannot achieve what is defined as ”clearance”, i.e. *the identification and removal or destruction of all mine and ERW hazards from a specified area to a specific depth*. The techniques for breaching the minefields are not effective enough. Flails, tillers and rollers can be useful when trying to make a fast breach. Ploughs can push the mines aside, leaving them buried at unpredictable angles and burying them under piles of earth, causing further difficulties for mine clearers. Some machines are useful for breaching a single lane through a minefield in battle, but achieving close to the clearance rates demanded of humanitarian mine clearance has proved elusive [59]. The flail chain and hammers can damage munitions but very rarely detonate them. The explosive methods can be ruled out because they would be potentially polluting. Ultimately, they are also usually expensive.

The need for a systematic, 100% clearance of a contaminated land generally results in the decision to conduct manual clearance, as had been done since the Second World War, using probes, sniffer dogs and metal detectors (Fig. 2.22) [60]. It is widely acknowledged that current mine clearance techniques are extremely slow, the technology having barely advanced since the 1940s [4].

Most mine clearance is done manually in lanes, with one or more individuals using a mine detector and/or a metal prodder to locate each mine (Fig. 2.23) . Vegetation must be cleared with extreme caution, as tripwires will otherwise detonate surface-laid mines. This clearance is often done manually using hand tools such as shears and sickles, but in some case petrol strimmers can be adopted. Large machines are used to both remove the undergrowth and prepare the ground surface. Such methods are difficult, expensive, labour intensive, and not without risk. In addition, the efficacy of manual clearance is reduced from the fact that mines are increasingly being made of plastic materials, minimising the more easily detectable metal components. Then, mined areas are often spread with metal debris creating a high false alarm rate (FAR). Even if anti-personnel landmines are commonly shallow-buried to guarantee detonation, once

[4]The first mine detector was developed in 1941 by a Polish officer, Lt. Kozacki, who escaped to Britain at the beginning of the war. He was requested the manufacture of such a device as a result of the need to move or relay minefields laid to protect Britain’s beaches. The British Army was still using a version of the same device up to 1995 [1].

Figure 2.22: Manual demining operations. (a) Mine detection dog in Lebanon. (b) Vegetation clearance in Colombia, (c) snowy operations in the Balkan region, and (d) clearing in urban scenario. *Taken from halotrust.org*

the mines are in place vegetation grows uncontrolled in the minefield areas. On the occasions when storms causes flooding, the vegetation traps mud and silt carried by the water, increasing the ground level [61]. In this way, mines could gradually be buried up to a metre below the surface. In addition, mines can be deliberately buried deeply to defeat conventional mine detection techniques [62].

Figure 2.23: Mine clearance operations. (a) Afghanistan, (b) Kurdistan. *Taken from maginternational.org*

In the age of stealth aircraft it seems ironic, if not tragic, that such primitive methods are still necessary. Daily progress varies greatly depending on the method and technology used as well as the operating terrain, type of soil and current weather. Daily clearance output for one deminer has been observed between five and 150 sqm. Manual clearance is most effective and efficient when integrated with other detection and clearance methods. The employment of animals, such as dogs and rats, can be faster and more cost-effective than manual demining detector methods. Daily progress has been recorded from 300 m^2 to 2000 m^2, depending on environmental conditions, the type of task and the operational concept in use. Animals are at their best when indicating individual mines or minefield boundaries, rather than trying to work within dense concentrations of mines, and have the strong limitations of inconsistency in performance.

A detailed survey of landmine status and problem understanding can be found in [63].

The development of standard cost models for manual mine clearance programmes is far from straightforward. While many organisations have come to believe that the simple division of total programme costs by the number of square metres of land cleared will provide a satisfactory solution, the reality is somewhat more clouded than that. The full cost is at least the sum that allows an organisation to continue operating at the same level for an indefinite period. A complete accounting of full costs would include direct cost, directly related to the demining operations such as cost of personnel, facilities, materials and equipment, and indirect cost, necessary to the organisation but hard to couple their impacts on the demining activities. Ideally, it is this figure that should be used when comparing costs across demining operations.

2.5 Background on Sensor Technology

Following a vicious circle, landmine design has followed, often anticipating, the evolution of countermine equipment.

If all mines were metal cased or had substantial metallic content, all that would be required for detection are metal detectors. The widespread use of minimum metal landmines necessitates development and deployment of more sophisticated detection technologies, which attempt to exploit ancillary disturbances in the background, such as thermal, chemical, or dielectric. Further, due to changing environment conditions that influence measurements and existence of other natural or man-made objects that give sensor readings similar to the landmine, the interpretation of sensor data for landmine detection is a complicated task [64, 65].

Here lies the cornerstone: once a subsurface feature has been detected, the employed technology should be capable of recognising its signature and differentiating it from the surrounding environment. A landmine detection system should be able to detect mines regardless of the type of explosive used, since mines are made of a variety of explosive materials. Mines come in a variety of shapes and in various types of casings, and therefore a detection system should be either insensitive to the geometrical shape of the mine and the type of casing material, or preferably provide imaging information. This latter feature will enable the system to better distinguish mines from background clutter. Since mines can be buried at different depths under the ground surface, the detection system should not be overly sensitive to the depth of burial. The operator of a detection system should be able to avoid close proximity to the position of the mine to minimise the possibility of inadvertent triggering of the mine. The detection process should also be speeded up and detection reliability and accuracy maximised. In addition, the system should not represent a logistical burden by requiring complex machines and operations. The diversity of the mine threat points out the need for different types of sensors and equipment to detect and neutralise landmines [66].

Detection techniques that are in development can be grouped depending either on their operational characteristics (Fig. 2.24):

- Electromagnetic;
- Optical;
- Acoustic;
- Nuclear;
- Biological.

or on their final results:

- sensors that see an image of the landmine through scattering;
- sensors that detect anomalies at the surface or in the soil;
- sensors that detect landmines explosive or associated chemicals.

Their operational characteristics are listed in Table 2.1. Detailed descriptions and further analysis can be found in [63, 67, 68].

The key issue with any sensor for mine detection is the probability of detection

Table 2.1: Outline of sensors

Technology	Sensor	Operative principle	Strength	Limitations
Electro-Magnetic	Metal Detector [69]	Induction of electric currents in metal components.	Ready-to-use and lightweight. Still on the forefront of demining operations. [70]	Minimum content metal mines, metal-cluttered urban environments and mineralised soil.
	GPR [71]	Reflection of EM waves at the boundaries of dielectric contrast.	Detects all anomalies, even if non-metallic. [72]	Natural and hand-made clutter, soil conditions. Technologically complex and limited resolution.
	Electrical Tomography [73]	Determines electrical conductivity distribution.	Detects all types of mines. Suitable for wet environment. [74]	Deep buried mines. Contact required. Dry and non-conductive environments.
Electro-Optical	Hyperspectral [75]	Detects differences in material reflectivity	Discriminates different surface-laid materials from stand-off distance. [76]	Extremely variable due to changing environment, weathering can eliminate anomalies.
	Thermography [77]	Study of the temporal evolution of temperature profiles.	Detects every type of mine [78].	Significant variability. Early stage of thermal signature understanding.
Acoustic & Seismic	Seismic [79] Sensors	Response of the ground to an applied shock.	Detects all types of buried mines. Low soil moisture impact. [80]	Man made clutter and deep buried mines.
	Ultrasonic [81] Sensors	Backscattered ultrasonic wave.	Low false alarm rate and unaffected by moisture and weather. [82]	Soil condition for ultrasonic wave propagation. Heavy vegetations.
Explosive Vapour Detection	Biological [83]	Odour discriminating skills of living organism (dogs, rats and bees).	Explosives presence confirmation and material characterization. [84]	Extensive training and difficulty in maintaining continuous operations.
	Chemical [85]	Chemical identification of microscopic residues of explosive compound.	Lightweight and simple to operate. Low detection threshold. [86]	Suffers from residual vapours and chemical clutter, complexity of collecting enough explosive molecules.
Bulk Explosive Detection	NQR [87]	Resonation of the chemical bonds when subjected to RF pulse.	Very low false alarm rate (not driven by clutter). Specific for landmines [88].	Susceptibility to RF interference. Low SNR and stationary detection required.
	TNA [89]	Radiation emissions from atomic nuclei in explosives.	Low strength source radiation. Identifies the elemental content. [90]	Ground surface fluctuations. High false alarm in wet environment (sensitive to hydrogen content).
	X-ray [91]	Difference in mass densities and atomic number.	High resolution imaging capabilities. Potential lightweight and portable. [92]	Shallow penetration and sensitivity to soil topography. Long time for image generation.

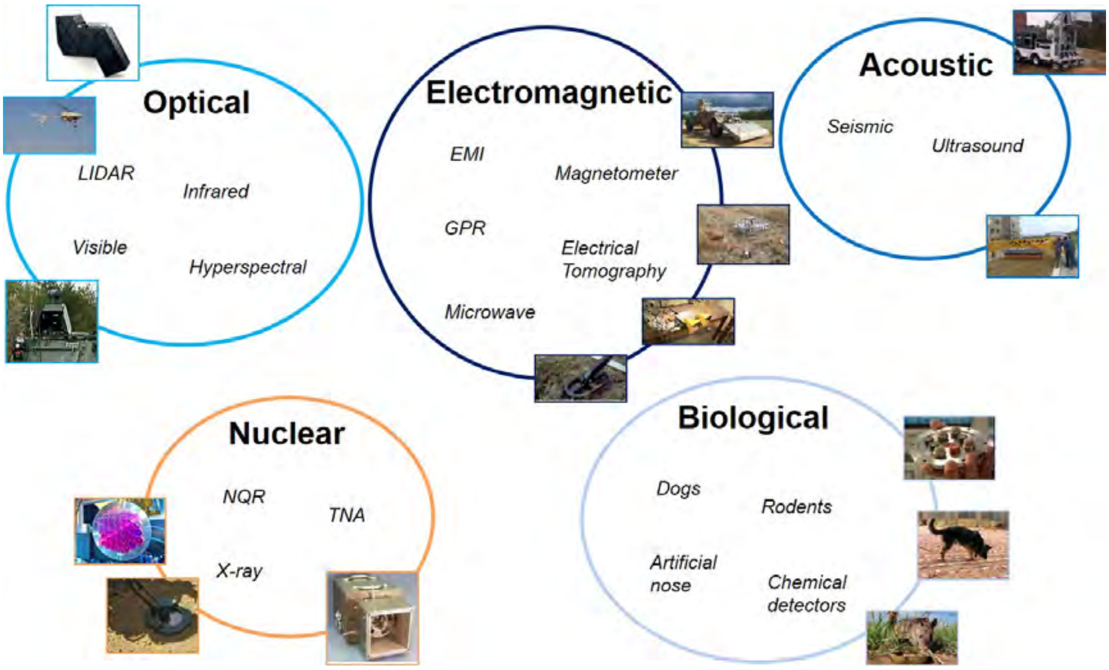

Figure 2.24: Outline of remote sensing technologies for landmine detection.

(P_D, the amplitude of the signal being higher than the threshold whenever the target is present) and false alarm rate (P_{FA}, an erroneous decision caused by noise or other interfering signals exceeding the detection threshold) [93]. Table 2.2 shows the efficiency of different demining methods (derived from [94]).

Table 2.2: Probability of detection by various demining methods.

Type of asset	Assessment of quality	Probability of detection
Manual mine clearance	All mines and ERW are found to the required depth	100%
Mine detection dogs	Verification of dogs indications is conducted manually	100%
Flail and tillers	Performance is variable, very poor for some ERW	40 - 80%
Rollers	Performance depends on the ground and type of mines	0 - 40%

The two quantities are strictly bounded, as a decreasing of the detection threshold could ensure a comprehensive detection, but also may lead to the detection of smaller misleading detections, generating a high false alarms rate and slowing down the operations. The two different approaches to landmine clearance, military and humanitarian operations, can be plainly explained considering these two factors (Fig. 2.25): the first procedure follows the idea of not identifying a target as a mine unless there is an absolutely certainty that it is a mine, while for the latter a landmine is marked even if there is a low suspect on its presence.

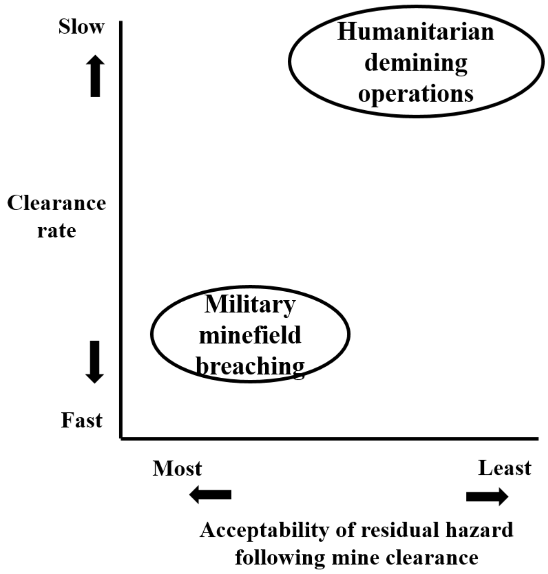

Figure 2.25: Operational mode for landmine clearance procedures.

While the detection probability is mostly dependent on the target properties and the specifications of the system, the false alarm rate instead is affected by all the surrounding objects and minefield scenario. Clutter can be either man-made, such as metal fragments, pipes or building remnants just to mention a few, and natural, such as rocks, tree roots or water ponds. Depending on the physical principle of the employed technique, the source of false alarms could be very different (Table 2.3).

Table 2.3: Common sources of false alarms for mine detection.

Detection technology	Source of false alarms
Induction	Metal scrap, natural soil conductivity and magnetisation
Radar	Natural clutter (roots, rocks) and metal debris
Acoustic	Hollow, man-made objects
Nuclear	Radio frequency interference
Optical	Man-made objects.
Biological	Explosive leakage, battlefield debris

Any new technology product being offered must provide good detection performance, significant improvements in false alarm rate over current technology, must be simple and easy to use, in all countries, and not significantly more expensive on a sensor to sensor basis than current metal detectors (approximately $ 5k) [95]. Technologies to be developed should take into account the facts that many of the demining operators will have had minimal formal education and that the countries where the equipment is to be used have poor technological infrastructure for equipment maintenance, operation, and deployment.

New sensors should detect minimum metal/non-metallic mines and ideally the explosive contained therein. It is clear that no single technology has the capability to detect and recognise a variety of mines under all circumstances. Some of them are more suitable for confirmation than for primary detection. The most efficient way to increase the detection probability while minimising the false alarm rate consists of using several complementary sensors in parallel and then combining the information collected by these sensors. The main benefit for using a multi-sensor systems lies in the potential for a reduction in the number of false alarms and/or improved probability of detection against a wider variety of mine types and terrains. Several analysis have shown that by reducing the false alarm rate (expressed in false alarms per square metre) by a factor of the order of 10 could result in an improvement in the overall mine clearance rate of a factor of 2.

Technically this is possible, but reliable explosive detection technology may not meet cost, weight or low power requirements. Many technologies are promising, but few of them are of the sensitivity, size, weight, manufacturability and price range required for humanitarian demining (Fig. 2.26) [96]. Even if it is rather difficult to get detailed price estimates (as most systems are prototypes), this price level makes it difficult for dual or generally multi-sensor technology to compete and even the most developed systems are significantly more expensive, although once produced in volume it would be reasonable to expect that price will reduce.

A promising solution to reduce false alarm rates and to overcome current landmine detection limitations will be by applying fusion of sensory information from various sensor outputs through the use of advanced signal processing techniques, by integrating different sensor technologies reacting to different physical characteristics of buried objects.

Mutual processing of the data coming from different sensors is called data fusion and a distinction is commonly made between three different levels of sensor fusion: (1) data-level fusion, (2) feature-level fusion, and (3) decision-level fusion. In the majority

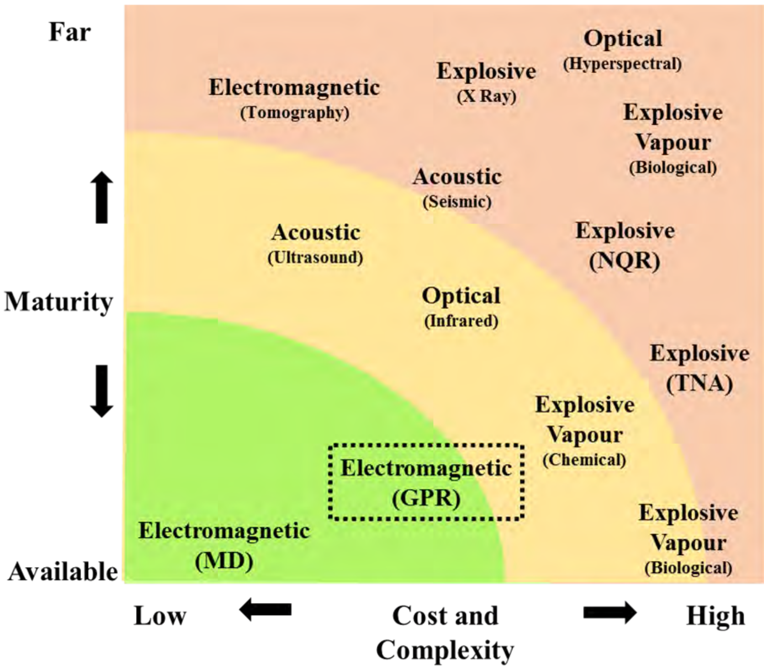

Figure 2.26: Inferences about the maturity of mine detection technologies.

of multisensor systems developed so far, data acquired by different sensors are fused at a decision level. Fusion at lower levels requires more computational power and a deep knowledge of the performance of each sensor, as well as access to the raw data of these sensors. Despite evident difficulties with its realisation, feature-level fusion can provide much better results in terms of detection and FAR.

The feature-level sensor fusion process starts with the selection of the regions of interest with their features as measured by the individual sensor and consists of three steps: feature extraction, feature reconciliation or object association, and decision making. In principle, feature-level fusion can handle all features from all sensors. However, the number of selected features should be kept to a minimum as an exhaustive search over all feature combinations would require an enormous amount of evaluations and is not feasible.

This work will focus on Ground Penetrating Radar (*GPR*) technology, one of the technologies that have been extensively researched as a means of improving mine detection efficiency and considered one of the few that can provide meaningful operational capabilities.

GPR is beginning to be fielded as a sensor for mine detection, where its ability against the minimum metal mine often surpasses the ubiquitous metal detector. Reports on the successful field deployment of GPR can be found in [97, 98, 99, 100, 101]. Considering the operating principle, it is more than likely that a GPR system will be combined with a metal detector, although some work has been carried out on the integration of metal detector, GPR and Nuclear Quadrupole Resonance techniques for detecting explosive as well as microwave and millimetre wave radiometers [102] [103]. However the complexity and cost of these systems has made them uncompetitive with the conventional induction technique.

In terms of technology readiness level, the most advanced systems are the US Army AN/PSS-14 (formerly HSTAMIDS) hand-held detector [104] developed by CyTerra (now L-3 Communications, US), the Anglo-German Vallon - Cobham VMR3 Minehound (formerly MINETECT) humanitarian detector [105, 106], and the ALIS, developed by Tohoku University Sedai, Japan [107]. The three platforms are depicted in Fig. 2.27.

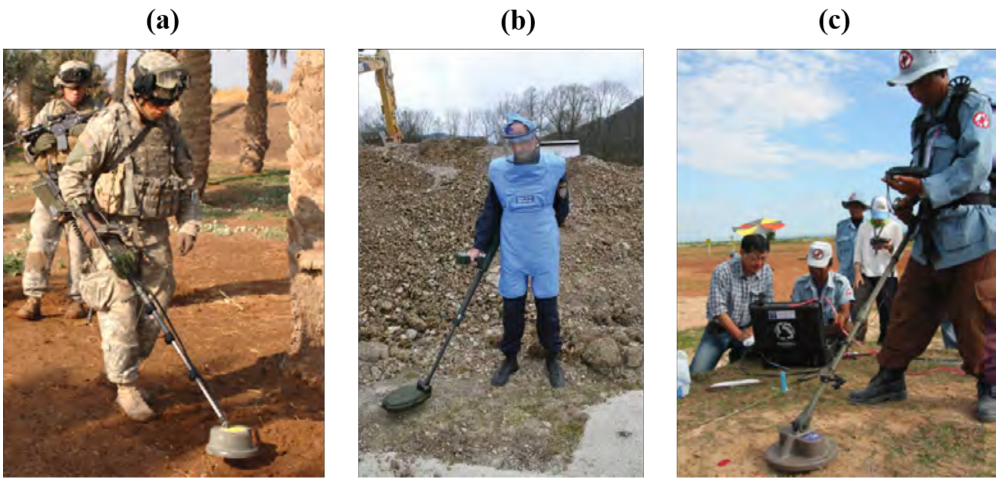

Figure 2.27: Deployed GPR equipment. (a) AN/PSS-14. (b) VMR3. (c) ALIS

The HSTAMIDS system combines a metal detector system manufactured by MineLab of Australia with a three antennas stepped frequency GPR system developed under US Army funding by CyTerra. The MINEHOUND system combines a metal detector system manufactured by Vallon of Germany with a two antenna impulse radar GPR system developed by ERA Technology. ALIS is a combination of a metal detector (produced by CEIA, Italy) and can select one from two different GPR systems,a stepped frequency radar and an impulse radar system.

Operationally, the signal from the metal detector, representing the prime search capability, is used to trigger the GPR, methodology which constitutes the simplest form of data fusion. Each sensor returns a unique audio signal and can be heard by operators individually or in combination with the other. Following the MD alert, the GPR unit checks the area around the metal reading to verify whether the response of can be associated to a landmine like material. Joint occurrence of these two events confirms the presence of landmine. In ALIS, accurate positioning information is available, allowing for computing 3D subsurface image and image-based object detection. In all handheld systems, classification of detected objects is left to the operator.

In the field trials of produced handheld mine detectors, it has been demonstrated that the GPR sensor improves the overall performance of the whole detection system. Statistics of the operational use of AN/PSS shows improvement from 7 to 17 times in comparison with a single metal detector, while operational testing of VMR3 has demonstrated reduction of the false alarms by a factor of better than 5:1 and 7:1 depending on the soil conditions. Similar performance of ALIS has been reported.

Reports on field evaluation trials for the described equipments can be found on the *gichd.org* repository.

2.6 Ground Penetrating Radar

From the early beginnings the development of GPR took place in parallel to the development of radar and in 1910, only six years after Hülsmeyer applied for a patent and performed experiments with anti-collision devices for ships, Leimbach and Löwy applied for a patent to locate buried objects with radar technology (Fig. 2.28) [108]. Their technique consisted of burying dipole antennas in an array of vertical boreholes and comparing the magnitude of signals received when successive pairs were used to transmit and receive.

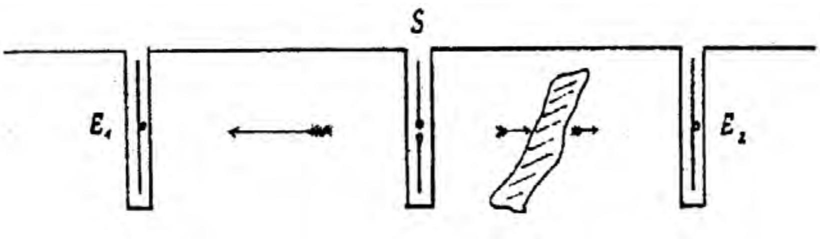

Figure 2.28: Sketch of the first GPR system comprising an array of borehole antennas. Original sketch taken from [108]

However, the technology was largely forgotten until in the 1950s a U.S. Air Force plane crashed in Greenland, because its radars were seeing through the ice layer and misread the altitude [109]. This was the initial spark for investigating into the ability of radar to see into the subsurface not only for ice sounding but also for mapping subsurface properties. Different scientific teams began to work on radar systems for viewing into the ground in the early 1970s, including the lunar science mission planning for the Apollo program [110]. In the beginning, these radars were developed for military applications such as locating tunnels constructed by the Viet Cong during the Vietnam War and in the demilitarised zone between North and South Korea [111, 112]. Soon thereafter public utility and construction companies were interested in such radars as a practical tool to map pipes and utility lines under city streets [113]. GPR has been very successfully used in forensic investigations [114], with the most notorious case occurring in the United Kingdom in 1994 when the grave sites, under concrete and in the house of Fred West, of the victims of the serial murderer were pinpointed [115] [116]. Nowadays, Ground Penetrating Radar is widely accepted for subsurface sensing in the fields of geology, archaeology and utility detection (just to mention, see [16] and [117]). GPR technology is being applied to abandoned landmines as a means of reducing the false alarm rate and providing improved detection of low metal content mines [118, 119].

Compared with other subsurface sensing technologies, the potential benefits of GPR can be summarised as follows:

- False alarm reduction by target identification based on measured target responses.
- Ability to detect both metal and non metal cased landmines, and generally every dielectric discontinuities occurring in the subsurface.
- Ability to detect both surface laid and buried landmines, theoretically without the need of being in contact with the surface.
- High resolution 3D imaging capability.
- Unmanned operations and sensor combination suitability.

GPR is a non-destructive technique that can provide a 3-D pseudo image of the subsurface [120], including the fourth dimension of colour (scaled to signal amplitude), and can also provide accurate depth estimates for many common subsurface objects [121] as well as precise information on its nature, under favourable conditions.

GPR is an electromagnetic method similar in principle to the seismic reflection technique, except that it is based on the propagation and reflection of electromagnetic waves rather than acoustic ones. The electromagnetic wave is radiated from a transmitting antenna and travels through the material at a velocity which is determined primarily by the permittivity of the material. The wave spreads out and travels downward until it hits an object that has different electrical properties from the surrounding medium, is scattered from the object, and is detected and recorded by a receiving antenna.

When a wave impinges on interface, it scatters the energy according to the shape and roughness of the interface and the contrast of electrical properties between the host material and the object. Part of the energy is scattered back into the host material, while the other portion of the energy may travel into the object.

Since the dielectric properties of the soil control the attenuation of the signal, and the contrast between the landmine and the background medium controls the scattering and reflection strength, the electromagnetic properties of both mine and soil are crucial variables [122]. A reflection occurs when the electromagnetic wave encounters any electrically heterogeneous material, and its magnitude depends on the boundary dielectric contrast.

2.6.1 Operational principles and survey techniques

GPR Equipment can be broadly categorised as frequency or time-domain systems, depending on the operating principles:

- **Time Domain Radar**: the transmitter emits a short pulse of electromagnetic energy and the receiver collects the echo for a certain time period. The exact type of the transmitter and receiver, shape of the electromagnetic pulse, and system set-up depend on the specific application;
- **Frequency Domain Radar** [123]: a stepped-frequency signal probes the environment with a discrete set of frequencies The main advantage is the greater measurement accuracy inherent in a frequency domain system and the flexibility to adjust the operating frequency range to suit the specific ground conditions.

The application of GPR is mostly related to the use of impulse radar systems, due to a major easiness of usage and data interpretation. For both types of GPR the total subsurface response, formed from a combination of the responses from all reflectors within the medium, can be inverted using various imaging algorithms [124].

Concerning the configurations of the antennas, a GPR system is configured as:

- **Monostatic**: a unique antenna operates as both transmitter and receiver.
- **Bistatic** or **Multistatic**: transmitter and receiver are separated and independently managed.

Most GPR systems employ separate antennas for transmitting and receiving, although the antenna elements are housed in a single module with no means of varying the antenna geometry, commonly referred to quasi-monostatic configuration.

Further on, an additional distinction is commonly made between **ground coupled** and **air launched** systems, defining whether the equipment is working in contact with the surface or above it (Fig. 2.29).

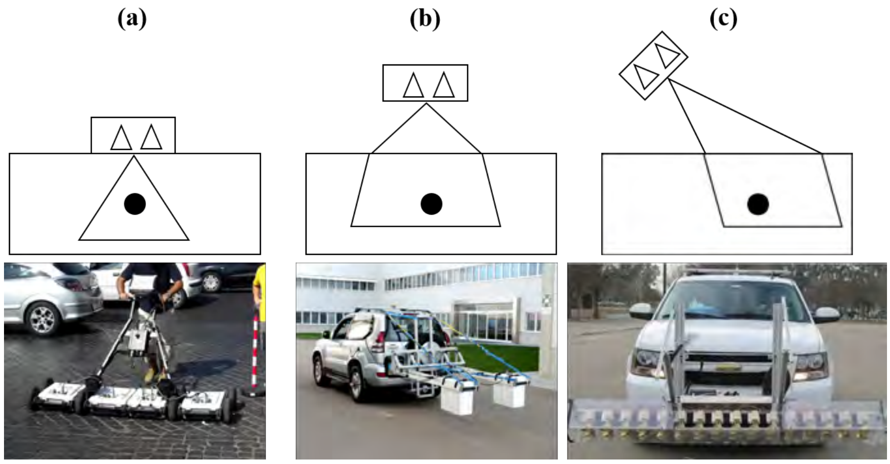

Figure 2.29: Examples of GPR survey strategy. (a) Ground coupled, (b) air launched, and (c) forward looking. *Courtesy of idscorporation.com*

The selection of deployment approach represents a trade-off between both operational simplicity and data quality or interpretability. It should be noted that the height at which antennas need to be placed for the configuration to be considered air-launched is poorly defined, as well as how close is close enough to be considered ground coupled.

Figure 2.30 presents a simulated example of the effects originated by elevating the antennas from the ground.

Generally, the probability of detection by close-in sensors such as GPR degrades rapidly as the sensor is lifted from the ground due to reductions in both the ground coupling and reduced sensitivity caused by the spreading loss resulting from the increased distance to the mines [125, 126].

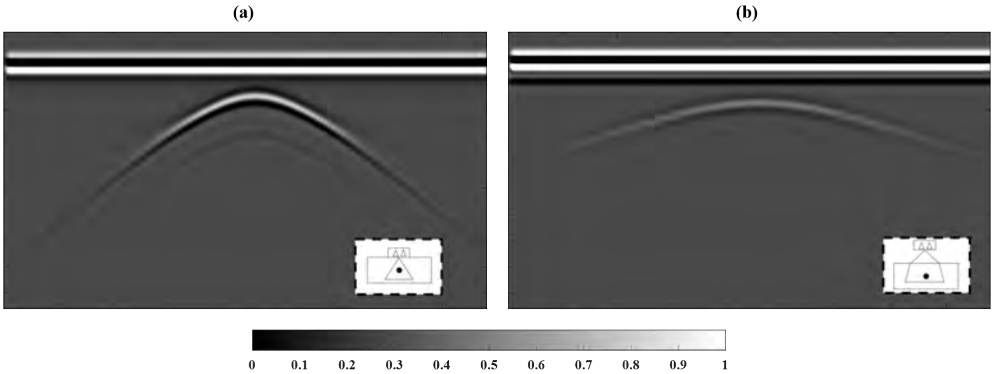

Figure 2.30: Comparison of GPR imaging performance of a dielectric target buried at 13cm in low loss soil. (a) Ground coupled data. (b) Elevated antennas (5 cm).

Ground coupled GPR measurements are generally more effective, since raising the antennas off the ground surface degrades lateral spatial resolution. In addition, despite being intuitively an optimal choice, the efficacy of airborne GPR systems is limited by the rough air/ground interface, below which landmines are typically buried. Stand-off radar systems suffer from a low energy coupling process efficiency since, in the presence of lossy materials, complex angles of refraction may occur. At larger incident angles than the Brewster angle the losses at the air/ground interface increase rapidly. A rough surface would scatter GPR waves randomly, making the received data difficult to analyse, as well as complicating the prediction of the the effective propagating waveform [127, 128]. In addition to the problem of coupling energy into the ground, one should take into account that the scattering amplitude of all landmines decreases when they are buried. Obviously, working at a stand-off distance has its straightforward advantages, especially considering that it can be operated at high speed and is more flexible to vehicle mountings [129].

Conversely, employing a ground coupled platform could improve signal penetration and data resolution [130]. When the antennas are in contact with the ground, the subsurface waveform is nearly unaffected by the roughness of the soil and therefore is predictable and easy to analyse [131]. Ground coupled systems survey an area at slower speeds and cannot be operated on every surface topography, but are less prone to external noise, surface clutter (as it is incorporated into the first echo), and take advantage of a theoretically perfect coupling between the antennas and the soil interface [132].

Typical GPR surveys are collected in common offset (CO) or single-fold (SF) mode. CO acquisition deploys one transmitting and one receiving antenna that move together along the surface keeping a constant offset. When a single antenna acts alternately as transmitting or receiving one (monostatic configuration), the configuration is called zero-offset conditions. During a survey, a fixed geometry is usually applied, using not only a constant separation but also a fixed orientation between the antennas (Fig. 2.31). From a practical point of view, this method allow easy access to most survey area and a relatively fast and simple acquisition.

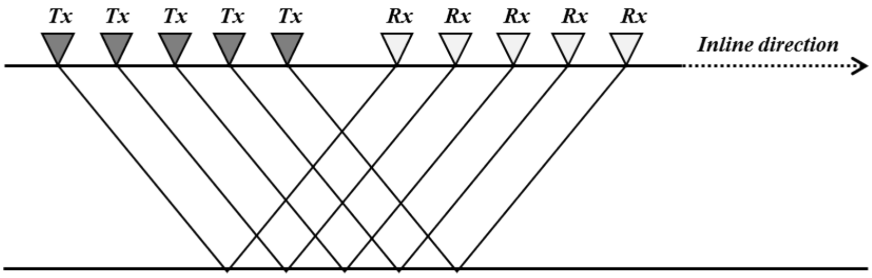

Figure 2.31: Common offset GPR survey. Tx and Rx represents respectively the transmitter and the receiver.

To maximise target coupling, antennas should be spaced such that the refraction focusing peak in the transmitter and receiver antenna patterns points to the common depth to be investigated. In practice, a small antenna offset is often used because operational logistics usually demand simplicity of operation.

In general, survey lines run perpendicular to the trend of subsurface features object of investigation, as for discrete objects it will result in hyperbolic radargram signatures which can be easily interpreted. In addition, more information can be gathered using fewer survey lines.

Until about 20 years ago, surface GPR studies were based on sparse 2D profiles. Unfortunately, interpretation is often not sufficient for complex scenarios or extended targets and thus recognition and identification remains a challenge. This challenge could be mitigated if a properly sampled 3D dataset is available, allowing the extraction of physical and geometrical information of the buried target, as well as eliminating ambiguities due to soil effects and other spatially-extended noise artefacts.

3D GPR is able to provide a deeper insight of the subsurface features, as well as to visualise their spatial extent. Although the significant advantages of three dimensional surveying strategies are well documented [133, 134, 135], they generally require much greater acquisition expenditure and effort than traditional sparse bidimensional acquisitions. Three dimensional imaging with GPR has been tested in most domains of shallow subsurface disciplines [136, 137, 138]. The price to pay is a very high accuracy in trace positioning and acquisition regularity [139, 140, 141].

As the objective of GPR surveys is to obtain information about the subsurface structures, the wavefield as a function of space and time must be properly sampled and recorded. Therefore, survey design must adhere to fundamental sampling principles [142, 143]. Certain important limitations of sampling interval should be noted. From the sampling theorem [144], in order to reconstruct the buried features as accurately as possible, trace spacing should be dense enough for the unaliased recording of all diffraction hyperbolae:

$$\Delta x \geq \frac{v}{4 \cdot f \cdot sin\theta} \tag{2.1}$$

where v is the wave velocity, f is the working frequency and θ is the dip angle along a diffraction hyperbola. For large angles, the *sin* function could be approximated as unity, thus leading to the common adopted sampling parameter of $\lambda/4$.

Applying the Nyquist criterion requires the GPR measurements to be spaced by quarter of the wavelength of the highest frequency in all directions, because diffraction hyperbola cones have rotational symmetry. In principle, the technology for performing 3D GPR acquisitions is readily available, but in practice the density specifications that are implicit in all 3D surveys can be a demanding requirement [139, 140, 145, 146], as summarised in Table 2.4.

Table 2.4: GPR spatial sampling criterion for different frequencies and soil velocities.

Frequency	**Velocity** 8 [cm/ns]	**Velocity** 12 [cm/ns]	**Velocity** 18 [cm/ns]
200 MHz	10 cm	15 cm	22.5 cm
600 MHz	3.3 cm	5 cm	7.5 cm
1 GHz	2 cm	3 cm	4.5 cm
3 GHz	0.66 cm	1 cm	1.5 cm

In some instances, it may be possible to increase the sampling interval slightly beyond what is quoted, but only when data volume and speed of acquisition are at a premium over integrity of the data. When the station spacing is too large, the data will become unable to adequately define structures such as steeply dipping layers. Although adequate spatial sampling is important, there are no significant benefits from over-sampling. Survey line spacing depends on the extent of variation in subsurface features along the trend direction (for example, pipe orientation or strike direction). If there is little to no variation, only one profile line may be needed to accurately characterise the target features. If there are significant variations, the profile line spacing should be set according to the Nyquist sampling interval.

Despite the majority of experimental trials have been performed with a fixed antenna separation, a bistatic geometry in which the transmitter and the receiver are independently managed may offer several key benefits, especially for low-observable targets or low Signal to Noise Ratio (*SNR*) scenarios [117, 147]. Common offset data is always limited in imaging capabilities because it provides only a single look at the subsurface, as only a single near offset trace is acquired for each position along the profile. In comparison, multi-offset data involves multiple reflection angles of investigation, equivalent to multiple looks at each subsurface position [148]. A separate receiving antenna allows to record the character of the transmitted signal as it appears entering the ground. Objects with irregular or rough shape could reflect the incident wave in a particular direction far from the monostatic receiver, thus multiple looks at a target from a variety of antenna spacing could make it easier to distinguish target of interest from clutter features [149].

Multi-offset GPR data offers numerous imaging benefits over common offset survey, such as increased signal to noise ratio and depth penetration, and improved reflector continuity and dip imaging [150, 151]. Another relevant benefit of multi-offset data is the improved lateral imaging capabilities it provides [152]. Further on, it will be useful for remotely surveying the area by setting a transmitter at a fixed position and only the receiver scanning the ground surface. Obviously an accurate relative antenna position knowledge is required. These systems provide more information as pairs of antennas provide different views of the target.

Finally, GPR propagation is along raypaths defined by Snell's law, hence wave propagation and target scattering characteristics are equally affected by directional dependencies, and they have a significant impact on the final image. Polarisation is one of the fundamental feature of radar, as the way in which a target scatters signal of different polarisations provides important additional information [153]. In addition, even the subsurface, under certain conditions, is capable of depolarising the EM wave ([154, 155]) as a result of combination of multiple reflection phenomena [156, 157, 158]. The same considerations apply for a change in the angle of incident of the wave, i.e., a variation of the antenna separation [159]. For example, targets designed to minimise backscatter might be easily detected by a bistatic configuration. Separating the transmitter and the receiver will allow the ground wave to detach from the surface reflection, providing a finer estimate of the dielectric characteristics of the propagating soil, and surface clutter effect can be reduced through a bistatic acquisition.

All the above described procedures suffer from some constraints and limitations that depend on the physics of the EM wave propagation and on the instrumentation. Since the antenna dimensions have an inverse correlation with their central frequency due to physical constraints, the minimum offset for a bistatic antenna pair cannot be too small. Moreover, several commercial systems use shielded antennas, which are bigger than the corresponding unshielded ones. In addition to these logistical constraints there are some physical limitations that cannot be overcome. The immediate vicinity (less than about one wavelength) of an antenna is usually referred as near field, and is characterised by a strong electromagnetic field that theoretically prevents true wave propagation, as this energy is not yet coupled with the ground.

Therefore, in the GPR experiments the offset should be set large enough to assure far field conditions, at the same time the offset cannot be too large especially where high conductive subsurface materials are present. The maximum separation distance generally does not exceed 1-2 times the depth of the target interface.

In addition, the minimum transmitter-receiver separation should not exceed the Nyquist sampling interval defined above. Therefore, for each successive reading, the transmitter-receiver separation should increase by Δx, meaning that the transmitter and receiver should be moved a distance $\Delta x/2$.

2.6.2 Performance factors

Easy understandable, the major design control in a GPR system is the frequency of the emitted wave, and thus its wavelength and bandwidth. Image quality improves as the wavelength decreases and the frequency increases. However, at high frequencies, penetration of the incident wave into the soil can be poor. When choosing equipment for a particular application it is necessary to find a compromise between these parameters.

The performance of a radar system can be evaluated through two major factors, namely maximum detectable range and radar resolution. The maximum detectable range is defined by the maximum distance at which the radar can detect the object, while the radar resolution is defined by the Rayleigh criterion as the limit of certainty in distinguishing between two close signals obtained during the GPR mapping, before their separate identity is lost and they appear to be one event (Fig. 2.32) [15].

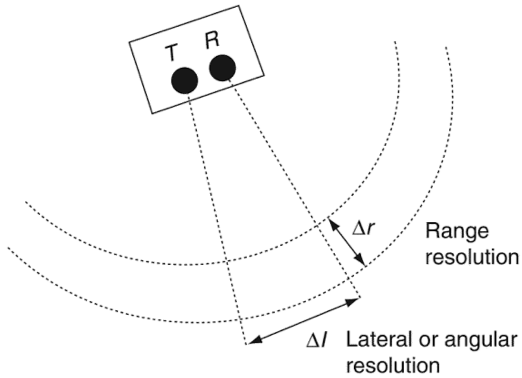

Figure 2.32: Resolution concept for GPR.

The vertical (also range or depth) resolution provides information about the system ability to differentiate, in time, two adjacent reflections as different events. The vertical resolution for unmodulated transmissions mainly depends on the effective duration of the radar pulse, obtained from the width of the signal envelope. Note that GPR systems are designed to achieve bandwidths that are about equal to the centre frequency and thus the pulse period is inversely proportional to the centre frequency. This is why GPR frequency and bandwidth are often interchangeable.

This suggests that the shorter the pulse duration (i.e. the wider the bandwidth), the better its resolution, and that the slower the propagation in the medium the higher the discrimination performance, as the effective pulse duration depends on the wave propagation velocity in the medium.

Theoretically, taking into account Fig. 2.33, Δt can be defined as:

$$\Delta t = t_2 - t_1 = \frac{2\Delta r}{v} \tag{2.2}$$

where t_1 and t_2 are the travel times for reflections r_1 and r_2 and v is the wave velocity.

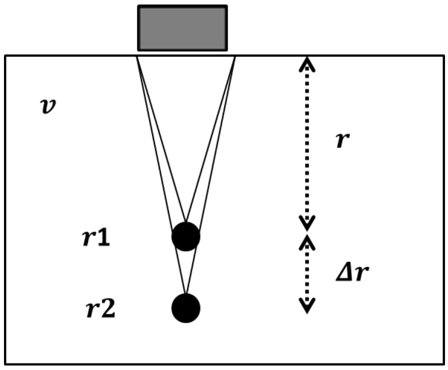

Figure 2.33: GPR vertical resolution concept.

In general, it is accepted that two close events can be distinguished if the targets are separated in time by a difference of half the effective pulse duration (i.e. twice the bandwidth). Therefore, the expected spatial vertical resolution can be calculated from the effective duration of the radar pulse (τ_p) and the wave propagation velocity in the medium:

$$\Delta r \geq \frac{\tau_p v}{4} = \frac{v}{4B} = \frac{\lambda}{4} \tag{2.3}$$

in which is clear that the pulse width and the velocity in the material dictate the range resolution.

Practically, two pulses, one reflected from the top and the other from the bottom of the target are distinguishable from each other when offset by a quarter of the wavelength of the GPR signal (for a 100% fractional bandwidth system).

Table 2.5 lists achievable values for vertical resolution for different materials and typical bandwidth.

This is theoretically independent of distance from the source in an ideal world, but in practice in most natural materials, the attenuation of the electromagnetic waves increases with frequency, widely known as the dispersion effect. This low-pass filter effect within the propagating materials causes an increase in the duration of the pulse and, therefore, worsens the resolution. As the wave propagates, it loses its high frequency components; although in some cases the resolution is approximately independent of this loss. Earth materials with significant water content tend to have higher attenuation properties but this characteristic is balanced out with the reduction of the pulse length due to a slower wave velocity in wetter materials.

Obviously, a signal having very large bandwidth is needed to be able to distinguish

Table 2.5: Vertical resolution of GPR systems.

Soil type	**Soil velocity** [cm/ns]	**Bandwidth** [GHz]	**Resolution** [cm]
Dry Sand	15	0.6 3	6.3 1.3
Limestone	12	0.6 3	5 1
Clay	6	0.6 3	2.5 0.5
Silt	8	0.6 3	3.3 0.7
Ice	16	0.6 3	6.6 1.4
Air	30	0.6 3	12.5 2.5

between closely spaced targets and to show the detailed structure of a buried target.

Horizontal (also lateral or angular) resolution indicates the minimum distance that should exist between two reflectors located next to the other at the same depth (parallel to the analyzed medium surface) so that the radar detects them as separate events. It mainly depends on the radiation characteristics of the antenna and the depth of investigation. The farther the targets are from the source, the larger the wavefield footprint, the worse the resolution. It is closely related to the Fresnel zone concept.

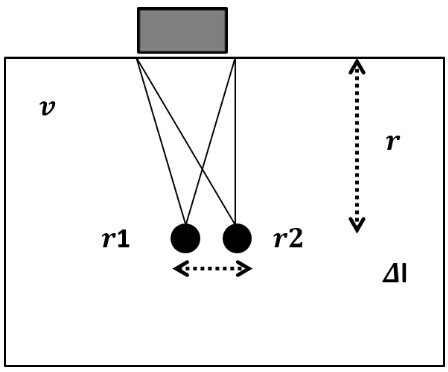

Figure 2.34: GPR horizontal resolution concept.

The zone of influence is defined as the area which can contain a second target that cannot be uniquely resolved. Hence, horizontal resolution can be identified with the footprint size, commonly identified with the diameter of the first Fresnel Zone. As before, the time difference between the two events is expressed as:

$$\Delta t = t_2 - t_1 = \frac{2(\sqrt{r^2 + \Delta l^2} - r)}{v} \tag{2.4}$$

Employing the approximation of considering the target sufficiently distant from the antennas, the time difference becomes:

$$\Delta t = t_2 - t_1 = \frac{\Delta l^2}{vr} \tag{2.5}$$

and therefore the horizontal resolution must be:

$$\Delta l = \sqrt{\frac{\lambda}{2} r} \tag{2.6}$$

which is identical to the Fresnel zone radius for monochromatic signals of that particular frequency. Note also that the horizontal resolution defines an area of resolution since all targets encompassed by a radius of $\Delta l/2$, perpendicular to r cannot be resolved. Finally, at best it is equal to the distance between transmitting and receiving antenna.

Table 2.6 lists achievable values for horizontal resolution for different materials and typical bandwidth, considering a target buried at 10 cm.

Table 2.6: Horizontal resolution of GPR systems for a 10 cm buried target.

Soil type	**Soil velocity** [cm/ns]	**Bandwidth** [GHz]	**Resolution** [cm]
Dry Sand	15	0.6 3	11 5
Limestone	12	0.6 3	10 4.4
Clay	6	0.6 3	7 3
Silt	8	0.6 3	8 3.7
Ice	16	0.6 3	11.5 5.3
Air	30	0.6 3	15.8 7

In general, to achieve an acceptable lateral resolution, a sharp beam is needed. However, small antennas with significant gain require a high carrier frequency, which may not penetrate the material to a satisfying depth. The footprint dimensions are related to the propagating material, hence plan resolution improves as attenuation increases, provided that there is sufficient signal to discriminate under the prevailing clutter conditions [126]. In addition, it is dependent on the survey design, which will determine the lateral variations able to be imaged.

Figure 2.35 shows the effect of resolution for targets discrimination using a system with a central frequency of 1.5 GHz.

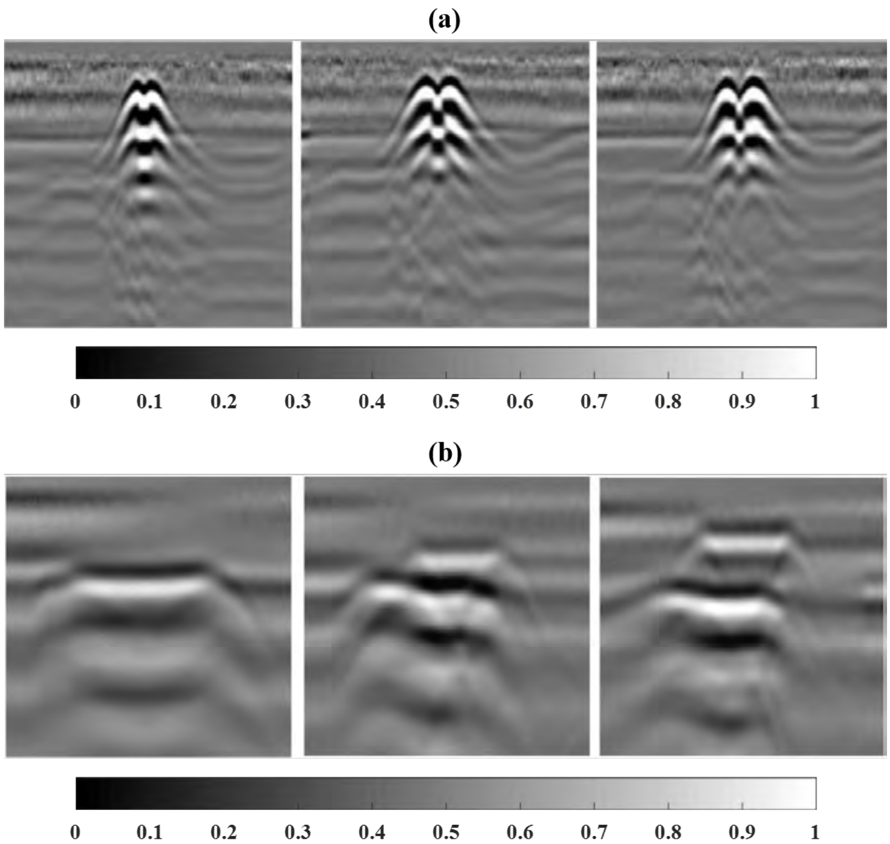

Figure 2.35: Examples of GPR resolution concept. (a) Horizontal resolution. Objects separation is respectively 100 mm, 200 mm and 250 mm. (b) Vertical resolution. Objects separation is respectively 0 mm, 50 mm and 100 mm. *Courtesy of geoscanners.com*

The maximum detectable range, which is the maximum detectable depth in GPR, is determined by the ratio of the transmitted power and the minimum detectable signal level, which is normally the noise level of the receiver. The detectable range in a free space is determined by the radar equation, but for GPR, the detectable depth is strongly dependent on the subsurface material. Therefore, GPR penetration performance cannot be defined in an absolute way.

The image of a buried target generated by a GPR radar will not correspond to its geometrical representation. The fundamental reasons for this are related to the ratio of the wavelength of the radiation and the physical dimensions of the target, which generally is close to unity. This compares very differently with an optical image, which is obtained with wavelengths such that the ratio is considerably greater than unity. This results in a GPR image with a much lower definition and that is highly dependent on the propagation characteristics of the surrounding ground.

2.6.3 Radar cross section and clutter

Both propagation parameters and the target Radar Cross Section (*RCS*) define the fundamental system detection performance. The RCS represents a convenient way to describe the strength of scattered fields observed in the far-field, theoretically defined in Eq.2.7 as the area intercepting the amount of power that when scattered isotropically, produces at the receiver a density that is equal to the density scattered by the actual target [156].

$$\sigma_{RCS} = \lim_{r \to \infty} 4\pi r^2 \left| \frac{E_s}{E_i} \right|^2 \tag{2.7}$$

where E_s and E_i are the far field scattered and incident electric field intensities, respectively, and r is the target distance. It depends mainly on target dimensions (compared with the wavelength), shape, materials, polarisation and aspect angle [160]. In particular, it has been demonstrated that targets showing some directional features have a significant polarisation dependent scattering [161]. This is particularly true for elongated objects, as pipes and cables [162], but even complex targets could show a polarimetric behaviour [163].

In practice, it describes the spatial distribution of the reflected energy throughout the surrounding medium. This property can be interpreted as a consequence of constructive and destructive interference of the field reflected from a collection of coherently illuminated point scatterers.

Examples of RCS diagram for different targets are provided in Fig. 2.36.

When the scattering object is small its RCS is proportional to its physical size, thus the complexity of detecting landmines. Given this, it is very important to under-

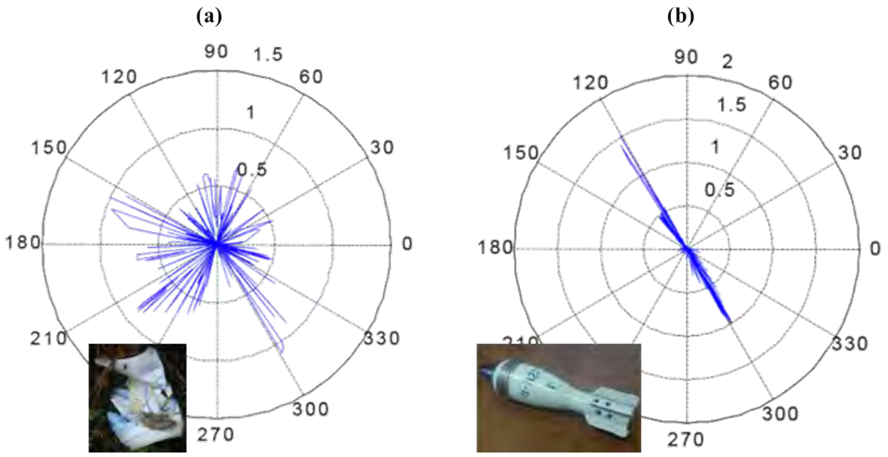

Figure 2.36: Examples of typical RCS diagram for: (a) Random - shaped target. (b) Elongated object.

stand the physical construction of landmines as this has a major influence on their RCS [164, 165].

The majority of landmines are moulded from plastic materials, the metallic components being minimal or absent. A landmine may be characterised by a number of scattering centres, each with its own angular radiation pattern, in particular when the plastic content of the internal structure is high. Most landmines may be considered as multiple layered dielectric cylinders that interact with each other to produce multiple reflections, and it is expected to have a certain impact on the overall target signature and RCS. For example, some minimum metal landmines are substantially solid explosive, but others have significant air gaps or composite assemblies to allow movement behind the pressure plate. Other aspects of the radar cross section of landmines are concerned with the relative contributions of specular reflection, diffraction of discontinuities, travelling waves including direct illumination running wave, creeping wave on metal, trapped guided wave on dielectric as well as the contribution due to resonant scatterers, which are a combination of discontinuities that allow the echo to build up. The ensemble of these events enhances the RCS, beneficial for target detection.

Both target and clutter RCS are a function of the look angle and hence multiple looks at a target from the variety of antenna spacings could make it easier to distinguish targets of interest from clutter, as landmines could have some geometrical features and symmetry that are not present in clutter signature [166].

Clutter in radar technology is defined as reflections coming from events which are unrelated to the target scattering characteristics but occur in the same time window and have similar spectral characteristics to the target wavelet. This disturbance is a deterministic signal, stable in time, thus it cannot be removed via traditional radar clutter filtering and might reduce the detection threshold of the system. In the world of subsurface imaging, clutter represents a large variety of sources [167, 168] .

Soil heterogeneity, in terms of high fluctuations of the dielectric permittivity and conductive texture of soil, causes the electromagnetic wave to be reflected and results in very high level of ground clutter which could mask weak target signatures. Small stones and gravel, as well as tree roots, animal burrows, metal fragments and other debris included in the soil are causes of undesired reflections [169, 170]. These conditions are often found in minefields, as for example shown in Fig. 2.37. The type of clutter is just as important in that other subsurface heterogeneity, such as rocks, roots, surface roughness, and soil spatial variations also yield a signature. [171].

Figure 2.37: Examples of minefield scenarios.Taken from *cmas.gov.kh*.

Seeming unusual, these disadvantages brings equally significant benefits: imaging all discontinuities in the subsurface brings a large amount of data yielding a significant amount of information. Features can then be extracted and behaviour outlined, making the methodology suitable for classification and identification processing.

In conclusion, GPR performance as a landmine detector is governed in terms of detection by the RCS of the mine, its depth of cover from the top of the mine to the surface of the soil, and the propagation properties of the surrounding medium.

2.6.4 GPR Data presentation

GPR data can be displayed in a number of different formats. These are generally represented as a one-, two-, or three-dimensional dataset, denominated by the acoustic terminology A-, B- and C- scans. Each presentation mode provides a different way of looking at and evaluating the investigated target:

- **A-scan**, Fig. 2.38(a), displays the amount of received energy as a function of time. The energy is plotted along the vertical axis and the elapsed time is displayed along the horizontal axis. In the A-scan presentation, changes in the impedance of the different materials can be estimated by comparing the signal amplitude obtained from an unknown reflector to that from a known reflector. Reflector depth can be determined by the position of the signal on the horizontal sweep.
- **B-scan**, Fig. 2.38(b), is a two dimensional plot representing an ensemble of A-scan acquired moving the equipment on a straight line. The horizontal axis stands for the number of inline traces or scan length, whereas the vertical axis represents the time scale.
- **C-scan**, Fig. 2.38(c), is a three dimensional display of GPR data resulting from a side by side arrangement of several B-scans. It can be seen also as a collection of horizontal slices, where each slice corresponds to a particular depth.

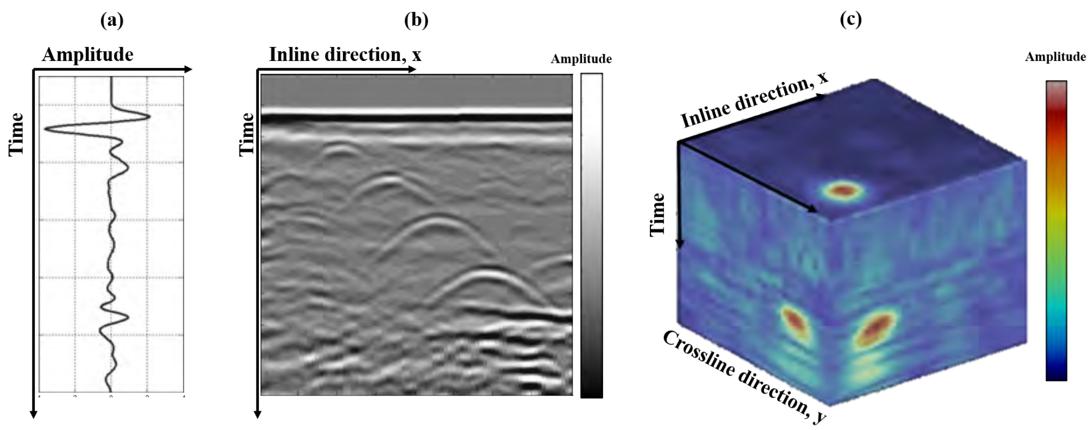

Figure 2.38: GPR results visualisation techniques. (a) A-scan. (b) B-scan. (c) C-scan

A-scans and their energies are generally used for target detection tests at the corresponding scan positions. The hyperbolic response can be easily obtained by the geometry of the scanning system. It is important to note that this hyperbolic response due to a single target will shift in the scanning direction if the inline position of the target also shifts. The shape of the hyperbola is the same for targets at the same depth but shape changes with depth. In particular, the hyperbola becomes more flat for deeper targets.

It is obvious that the three display modes are in ascending order according to the acquisition effort, but also by increasing level of information that can be gathered.

2.7 Summary

Landmines are a persistent and complex problem. Although numbers have declined significantly in the last two decades, landmines still affect almost 30 per cent of countries, and have caused an average of more than 5,000 casualties per year in the last 5 years, with sharp rise in the last two. Landmines still pose a serious and global problem despite the work of engineers, NGOs, and policymakers, who have made real headway in the last 20 years, reducing both the number of landmines deployed, and their use. Moreover, landmines pose a problem that is complex, seen in different terms by different players, and therefore defies a clear solution.

Conventional antipersonnel mine detection has not evolved as much as one would like. The most widely used method for detecting and removing antipersonnel mines follows the same techniques developed during the Second World War, and directly involves human beings. Metal detectors for identification are used and a detailed and slow analysis of the affected zone is made. Every suspicious element found is meticulously checked.

Difficulty in detecting tiny amounts of metal in a minimum metal landmine with a metal detector has led to the surfacing of Ground Penetrating Radar as a promising technology. GPR has been extensively applied to investigate subsurface structures or buried objects in geology, civil engineering, environmental and soil science. This non-destructive method of subsurface analysis is becoming increasingly important for many environmental and shallow geophysical applications. GPR can quickly and accurately determine the subsurface structure, can easily move on the ground surface but does not have to touch it, and it can detect both metallic and non-metallic objects in the soil.

Due to these features, detection of buried landmines has proved to be a successful application of GPR technique. GPR has a number of advantages over other landmine detection sensors. First, it is complementary to conventional metal detectors. Rather than detecting exclusively the presence of metal, it senses variations in the electromagnetic variations of the ground, and therefore it can find mines with a wide variety of casing, including minimum metal landmines. Second, it can generate an image of the mine or another buried object, on which basis the detected object can be confidently identified and classified. Third, GPR scans at a rate comparable to that of an EMI system.

However, GPR is not a specific sensor for explosives, and it detects only secondary signs of explosive devices. Because the technique responds to all electromagnetic inhomogeneities of the ground, all natural subsurface inhomogeneities will be a source of false alarms, which should be discriminated in later processing. Whether or not a GPR will detect a landmine highly depends on soil moisture, surface roughness, and mine location; such complex interplays make its performance highly variable and difficult to predict. Due to the above-mentioned reasons, a GPR sensor will hardly perform the role of standalone sensor for landmine detection, but it can play a crucial role within a multisensor platform, as for the deployed systems described above.

While considerable research into target recognition techniques has been carried out, the variability of the soil and target parameters has challenged the development and implementation of robust and reliable signal processing methods, meaning that there are still considerable opportunities for improvements in detection performance as well as reduction of false alarms.

Chapter 3

Research Context

The saddest aspect of life right now is that science gathers knowledge faster than society gathers wisdom.

Isaac Asimov [172]

Ground Penetrating Radar surveying is aimed at retrieving unknown physical properties of the internal status of the structure under investigation by making use of limited measurements of scattered electric fields. Traditional radar approaches allow the extraction of qualitative information from the radar echoes, whereas in many cases, such as for instance demining applications or archaeological surveys, there is the need of obtaining quantitative information on the buried targets. This requires to cope with an electromagnetic inverse scattering problem that is non-linear and ill-posed [23]. Inverse scattering theory demonstrated that ideal noise-free data for orthogonal polarisation and all aspect angle can uniquely determine a target. In reality, due to measurements uncertainties and errors, the inversion is strongly ill posed, thus only approximate solution can be retrieved [173].

The application of Ground Penetrating Radar for landmine clearance is by no means an undiscovered topic in scientific literature. However, the development is not straightforward, due to a number of physical or operational limitations. Many anti-personnel landmines are mostly dielectric objects with little metal content and a size less than 15 cm. This requires a very high spatial resolution. Lossy soils act as a frequency low-pass filter, whereas in low-loss soils, the dielectric contrast between the mine and the surroundings can be very low. In both cases, a very weak signal needs to be detected in the presence of strong disturbances and clutter. Although technologically advanced, GPR systems still suffer from severe limitations concerning clutter reduction and image resolution. The effects of surrounding soil, landmine characteristics (both geometrical and physical), equipment design and acquisition strategies are only a few of the major aspects affecting the quality of the outcomes [174].

The next challenge is therefore to move from qualitative interpretation, which depends heavily on the human visual interaction with the data, towards the extraction of quantitative target parameters and identify target attributes quickly and (possibly) automatically.

To cover the research in these areas, contributions from several research communities have been evaluated and the main contributions have been reviewed.

3.1 Scattering from composite targets - landmines perspective

An important aspect that needs to be considered when studying scattering from plastic cased landmines is their internal structure. Each type of landmine has its own operation principle and hence internal structure varies. Nevertheless, certain common characteristics may be identified.

For a pressure actuated blast mine, which is the most common type of anti-personnel mine, the internal structure may roughly be subdivided into the following four components: (1) the external mine casing, (2) the main explosive charge, (3) the fuze, and (4) the trigger mechanism. Since plastic materials have permittivity similar to those of explosives (Table 4.4), from an electromagnetic point of view the casing and the explosives may be considered as one.

The explosives include the main charge, which is set off by a smaller amount of explosive called the detonator. Sometimes the firing train also contains a booster charge to amplify the ignition by the detonator. Different types of fuze mechanisms exist, such as the mechanical pressure fuze or the chemical pressure one. Usually the fuze is the only component of a plastic cased landmine that contains parts of metal, however its metal content may be limited to no more than a small firing pin or a striker spring [175]. In particular the presence of air gaps is expected to amplify the target response when the mine is buried and hence should facilitate its detection with GPR. Furthermore, due

Table 3.1: Relative dielectric constant of landmine constituents.

Material	**Relative dielectric constant ε_r**
Neoprene rubber	6-9
Bakelite	3-5
Polycarbonate	2.9-3.5
Polyethylene	2-2.5
Epoxy resin	3-4
TNT	2.7
PETN	2.72
Comp B (RDX TNT)	2.9
Tetryl	2.9
Semtex (RDX PETN)	3
Comp C-4 (RDX)	3.14
Nytroglycerine	19

to their particularity, the potential of imaging these components (location and spatial extension) could be beneficial for target classification and identification.

Figure 3.1 shows some examples of disassembled landmines.

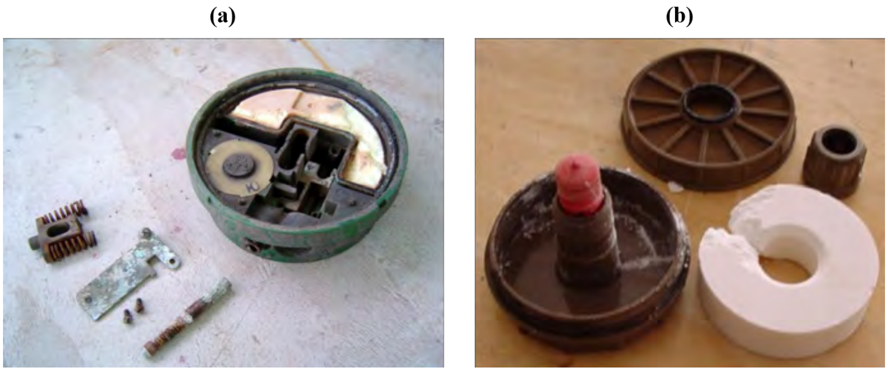

Figure 3.1: Examples of anti-personnel landmines internal design. (a) Soviet PMN-2, (b) South African R2M2. *Taken from nolandmines.org and ordata.info*

Simplifying the situations, the target can be modelled as a three layer objects, inlcuding (1) the activator plate, (2) an air-filled layer, and (3) the main body, as sketched in Fig. 3.2.

Very few works have addressed the task of detecting the reflections generated by the internal components of buried landmines and determining their effects, as most trials have been performed employing devices and surrogates which imitate the outer shape of real landmines filled with a dielectric material which has a similar dielectric constant to the explosive substance.

Figure 3.2: Simplified model of anti-personnel landmines.

As a starting point, a signal having a large bandwidth is required to be able to distinguish between the various targets and to show the detailed structure of a target. Therefore, in this context it is the bandwidth of the received signal which is fundamental [176, 177, 178]. In [179], it has been found that the internal structures of penetrable objects can perturb the phase property of radar waves, therefore a distinction of objects with different internal structure can be made exploiting the phase variations induced by rough surface scattering. Unfortunately, the method allows this distinction for target located in the same homogeneous layer of soil, and buried under a flat surface. Similarly, the Authors of [180] explicitly employ the impedance discontinuity profile of a landmine in a syntactic, rather than statistical, pattern recognition scheme to discriminate landmines from clutter, underlining that these patterns are unique in the presence of clutter since they are based on the internal structure of the landmine. However, the impact is limited by the evaluation of anti-tank landmines only. Work in [181], even if with a completely different aim, gives an experimental evidence of the resonance effect of the GPR waves entering the mine and reflecting internally inside the mine.

In addition, research reported in [182, 183] both indicate that the signature resulting from minimum metal landmines is affected by the internal structure, providing modelling and approximation in order to take into account this effect in the scattering theory. Another evidence of the internal scattering is given in [184], in which a cross-polar contribution in the radar signature, quite unexpected considering cylindrical objects, is to be attributed to the presence of the detonator and other internal mine structure. What can be inferred is that identifying landmines by looking for targets with negligible cross-polar response is not to be recommended.

3.2 System design

For the purpose of enriching the information received from the target, a strategy is to employ GPR configurations with multiple components and a particular emphasis will be put on the exploitation of angular diversity. This diversity can be obtained varying the relative geometry between the system and the target, hence separately managing the transmitter and the receiver.

3.2.1 Multistatic GPR

Most of the contribution to GPR development has been directed at monostatic systems or bistatic systems with closely spaced antennas, as for the case of the previously described GPR systems. Although most of the current GPR cover wide frequency bandwidths and some of the advanced ones utilise polarimetric antennas, the quality of the acquired information and processing can still be enhanced.

The potential benefit of a multistatic system over monostatic or quasi monostatic systems is the opportunity to obtain more information on the target by taking advantage of the angular diversity from different transmitter-receiver pairs [185, 186]. Principal drawbacks are the physical limitations that could not allow a hand-held implementation. The increased complexity of these configurations is expected to pay back in an enhanced image resolution or clutter suppression [187, 188].

In recent years a remarkable advancement in the GPR field has taken place place thanks to the implementation of new multi-channel systems. Arrays have been deeply implemented for landmine detection, which was one of the first GPR applications with very specific requirements and constraints, gaining importance for their vehicle mounting capability and for forward-looking landmine detection ability, which allows long standoff distances and fast interrogation of wide areas [189]. A multi-channel array can obtain more angle-dependent scattering information, i.e., the bistatic scattering information, and thus, it is demanded to improve the capability to discriminate landmines from clutter [190]. Generally, it is understood that these acquisition schemes allow to obtain enhanced subsurface imaging.

First of all, multistatic GPR, intended here as a system in which the transmitter and the receiver are separated and independently managed, has three surveying modes (Fig. 3.3) depending on how the transmitter and receiver antenna moves:

(a) Multi-offset: both antennas move together in the direction of survey with a fixed offset, changed for each profile.
(b) Common source (receiver): the transmitter (receiver) is fixed, however, the receiver (transmitter) moves along the survey direction.
(c) Common depth or common mid point: both, the transmitter and receiver antenna, move away from a common point in opposite direction.

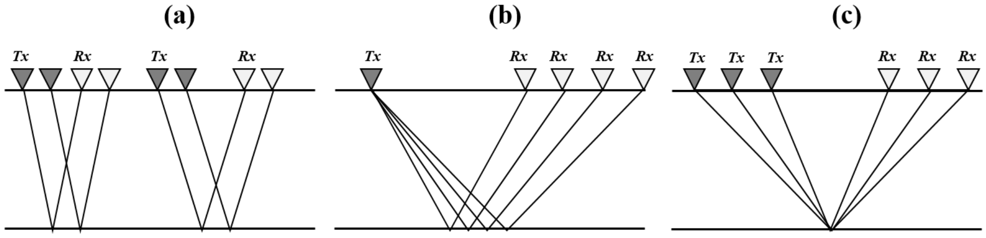

Figure 3.3: Multi-offset GPR survey. Tx and Rx represents respectively the transmitter and the receiver. (a) Multi-offset. (b) Common source.(c) Common mid point.

The expected potential of these strategies is to yield lighter weight, lower cost systems and improved performance, in terms of detection, identification and coverage, and system flexibility, as they can operate in several modes. From a logistical point of view it is quite obvious that the most efficient geometry is (a), that requires just one transmitter and receiver, followed by (b) where just one antenna is moved, and finally (c), which requires the maximum acquisition time. On the other hand, in terms of accuracy the best strategy is (c) while the less precise is (a) because is not so straightforward to follow the same path several times.

Considering the aim of the work, the advantages of the first scheme are limited by several reasons. Landmines are small objects, and their internal components are even smaller, and if one considers the width of the radiation pattern it is hard to imagine that sharp, preferential scattering directions exist, as it could be for highly reflective large planar targets. What has been found is that a change in the antennas separation could highlight internal reflections and that there could be evidence of asymmetry in the target design, but it is not possible to determine an optimum offset under which there are unique features to mark. For such a family of targets, the information gathered from a multi-offset scheme converts to the content of a single offset one. Reflections generated by the internal structure are a result of multiple reflections/transmissions events, therefore these returning waves will have a limited amplitude, bounding the effective antennas spacing. Practically, this means that from these bistatic profiles it is not possible to extract clear indications on the presence of internal scattering components, and consequently that multiple profiles are needed, with all the drawbacks that have been previously highlighted.

To provide a conceptual explanation, Fig.3.4 describes the expected impact of an offset variation applied to the characterisation of the internal structure of a buried target, comparing the two cases of a solid dielectric object and a target including an internal assembly.

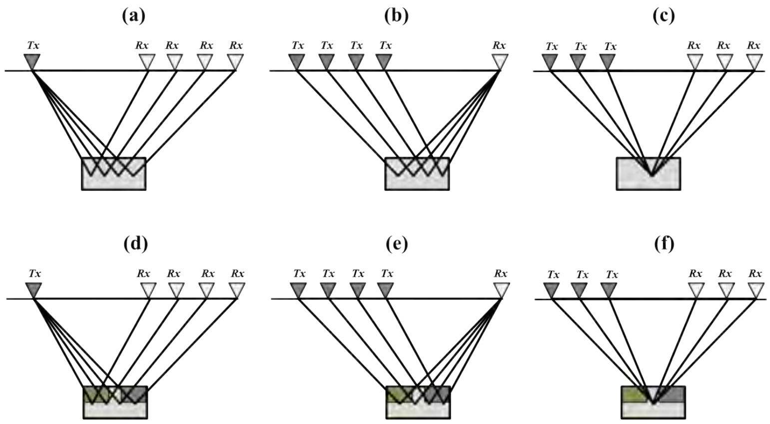

Figure 3.4: Effect of antenna separation. Solid target: (a) Common source. (b) Common receiver. (c) Common mid point. Composite target: (d) Common source. (e) Common receiver. (f) Common mid point.

As the wave propagation is defined by the ray path, a signature collected at particular incident angle will be characterised by a number of propagation phenomena which may be different for complex and composite targets. This is not supposed for a solid dielectric target, for which a change in the angle of arrival of the wave should not produce noticeable changes. Hence, these changes are highly dependent on the internal design of the target, as presented in the previous Chapter.

Regarding the terminology, the term multi-offset comprehensively includes all the geometries involving a change between the transmitter and receiver separation.

Figure 3.5 provides an example of a multi-offset radar image and the events that can be observed from its analysis.

Generally, images include three well determined events: (1) the air wave, which is the wave that travels directly from the transmitter towards the receiver, (2) the ground wave, which is the wave propagating over the surface, and (3) the reflections generated

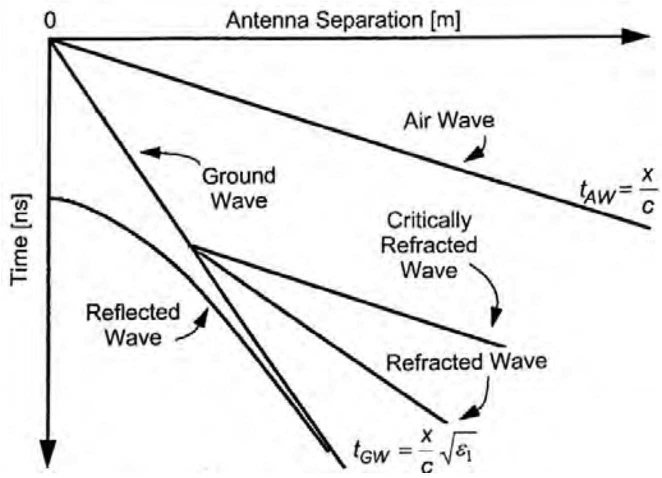

Figure 3.5: Evant recognition on a multi-offset GPR image.

by the target scattering. The gradient of the reflection events is inversely proportional to the electrical properties of the material in which the wave is propagating; therefore, for a target buried in a homogeneous medium, the latter two events have the same slope. The bistatic angle can be computed accordingly from the trigonometric relationship between the transmitter/receiver offset and the target depth.

Generally, these multi-offset strategies have been extensively employed for the velocity estimation, as they offer offer more accurate and precise estimates than hyperbola fitting methodology, to reduce random (i.e. not coherent) noises to emphasise the signal content, and to discriminate and selectively remove specific noise components. In addition, the continuous multi-offset method improves the quality of subsurface images through stacking and provides measurements of vertical and lateral velocity distributions.

However, these configurations have traditionally been employed as an obvious method of increasing the productivity rate, acquiring millions of traces in a relatively short time and with high location accuracy, rather than to implement the system as an integral array exploiting the increased capability related to inserting into the array antennas with different frequency, orientation, spacing.

Under this hypothesis, a number of works have exploited the advantages of having multiple looks at a target from a variety of antenna spacings.

Work in [191] employed numerical scattering models to compute the monostatic and bistatic image of two metallic targets (ogive and missile-like shape) to provide an imaging comparison. With different acquisition geometry and bistatic angle, it demonstrated that bistatic images could lead to a better description of the higher order scattering effects, thus depicting different target features. Similar comparison has been made in [192], where it is shown that angular diversity allows for highly resolved images from single frequency data.

In [193] a multistatic GPR array is used on a number of targets in both free space and in soil, evaluating as well the effect of surface clutter. Results show that for shallow targets a close proximity yields *SNR* ratio, while a large spacing is unsuitable for their detection. Obviously, the concept is reversed for deeper targets. In addition, a coherent sum of the collected bistatic pairs demonstrated some potential for enhancing the quality of the obtained images. The same concept is demonstrated in [194], where a target to clutter ratio can be improved combining images from different bistatic configurations and elevations. Authors in [195] used a similar same approach for testing an inversion algorithm, underlining the strong interference generated by the surface clutters.

In [196], an approach based on the combination of monostatic and bistatic systems is presented in order to lower the effect of multipath scattering. Starting from the assumption that false targets detected by the monostatic case are located at different positions from the bistatic one, a simulation with three point scatterers illustrates the benefits that can be obtained by cancelling the multipath effect using information contained in the bistatic data.

The authors of [197] presented a feature extraction scheme to obtain bistatic scattering information from a vehicle mounted GPR system with multistatic capabilities. The resulting images effectively demonstrate the symmetrical behaviour of landmines, as opposed to some clutter objects. The applied processing is based on the extraction of the seven moment invariants from a space-wavenumber processed image, which contains frequency and aspect-angle information, in order to obtain invariant properties. The assumption is that a landmine is a perfect body of revolution.

Studies in [198, 199] exploited the angular diversity for increasing the informative content of a GPR 2D image, providing at the same time a practical hardware and signal processing implementation of the proposed solution. Examples of what can be gained from multiple illumination are provided through experimental and simulated data.

Work in [200] provided a demonstration of the improved resolution that could be achieved using a multistatic array processing, in particular overcoming the influence of target radar cross sections and antenna radiation directions of monostatic 2D GPR data.

A multistatic geometry can be beneficial also for features extraction scheme, as evaluated in [201] in which an array of receivers increased the robustness of a resonance-based feature classification technique, recovering many characteristic target resonance signature. Authors in [202] applied a non-linearised image formation scheme relying on single frequency angular diversity data, hence requiring a multistatic radar system. The same factorisation method has been used in [203] to combine information gathered from a mulststatic geometry, realised in the form of multiple fixed offset. Similarly, work in [204] shows that measurements using bistatic observations can be valuable for evaluating target symmetry, but also underlines that a large and diverse collection of measures formed from different bistatic geometries are needed for a proper classification.

Independently managing the transmitter and the receiver means that interferences from the ground reflection can be properly mitigated estimating the Brewster angle and set up the system accordingly, as shown in [205, 206].

3.2.2 Polarimetric GPR

The polarisation information contained in the waves backscattered from a given target is highly related to its geometrical structure and orientation as well as to its physical properties [207]. A mono-frequency electromagnetic wave propagating in a given direction has four basic characteristics: (1) frequency, (2) amplitude, (3) phase, (4) polarisation. Polarisation refers to the locus of the electric field vector in the plane perpendicular to the direction of propagation. While the length of the vector represents the amplitude of the wave, and the rotation rate of the vector represents the frequency of the wave, polarisation refers to the orientation and shape of the pattern traced by the tip of the vector.

Three main polarisation states can be defined:

- **Linear** polarisation: the vector is confined to a plane that is parallel to the direction of propagation. It can be further divided in horizontal and vertical.
- **Elliptical** polarisation: the rotating E field follows a path that traces an elliptical pattern with time.
- **Circular** polarisation: A special case of elliptical polarisation. It can be further

divided in right and left.

Linearly polarised waves are unique because the E field does not rotate with time, therefore the only way to change its orientation in an isotropic material is to reorient the transmitting or receiving antenna. This is why in most cases, polarisation and antenna orientation terminology are alternatively employed. Hence, antenna orientation is critical for antennas that generate linearly polarised signals, but it is not as critical for antennas that generate elliptical or circular polarised signals. Finally, any linearly polarised wave can be obtained as a superposition of a left circularly polarised and a right circularly polarised wave, whose amplitude is identical. Most commercial GPR antennas are dipole or bow-tie antennas that radiate linearly polarised energy with the majority of the radiated electric field oriented along the long axis of the dipole or bow-tie.

Circular polarisation, commonly radiated through spiral antennas, has some advantages over linear polarisation in that: if a linearly polarised antenna is used, the strength of the reflected wave from an object will depend on the azimuthal position of the antenna relative to the object. Also, if the orientation of the transmitting and receiving antennas is orthogonally to reduce the mutual coupling between the two linearly polarised antennas, then the receiving antenna will hardly detect the reflected wave from the object. Another advantages of circular polarisation is that the reflected signal from the surface of the soil at oblique incidence has the opposite sense of polarisation compared to the incident wave, due to the fact that the ratio between the permittivity of soil and air is larger than one. Thus the equipment will not receive the reflected wave from the surface at oblique incidence. These advantages are unfortunately compensated by a reduced efficiency in converting the input power into radiated one.

Wave polarisation can be represented in a number of ways, usually in terms of the polarisation ellipse [208], which defines the polarisation state through the parameters of ellipticity angle, which is the ratio between the two ellipse axes, the orientation angle, corresponding to the rotation of the major axis and the horizontal one, and the polarisation sense, given by the rotation sense of the field vector. In the Poincaré sphere representation [209], the polarisation state is represented by a point in a polar coordinates system. Every point on the sphere uniquely defines a polarization state. A descriptive sketch is provided in Fig. 3.6.

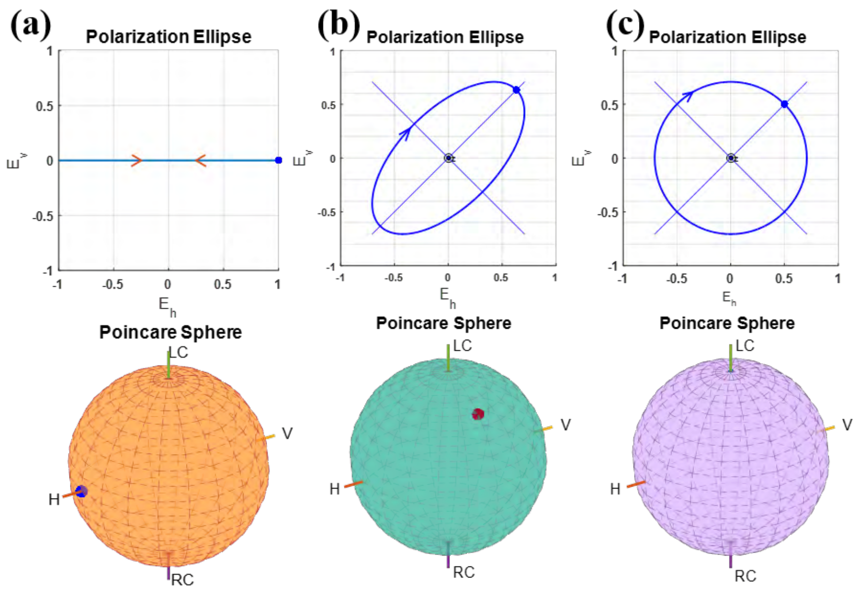

Figure 3.6: Representation of different wave polarisation state. (a) Linear horizontal polarisation. (b) Elliptical polarisation. (c) Circular polarisation.

Another useful representation is the polarisation chart, obtained by an orthogonal projection of the Poincaré sphere on its equatorial plane. Lastly, the polarisation state of waves can also be described by the Stokes vector [210].

As per the reciprocity theorem, the polarisation vector of the backscattered wave can be expressed as a function of the monostatic scattering matrix of the target [211, 212, 213] ([214, 215] for the bistatic equivalence), which represents a set of parameters for describing the symmetry, structure, torsion and helicity of a target.

Polarisation affects how a radar system sees the objects in the scene. Therefore, radar imagery collected using different polarisation combinations may provide different and complementary information [216, 217].

The advantages of using polarimetric radar systems for the characterisation of intrinsic target properties arise from two main factors: (1) the vector information contained in the target backscattered wave is retained (by reception diversity), and (2) the entire backscattering behaviour of a target can be obtained (by transmission diversity).

The benefits of considering polarisation in the GPR method are can be summarised as follows:

- Optimisation: in many cases, using a certain type of input polarisation will accomplish a given task better than any other. The shape of some targets can be inferred using a polarisation other than the conventional linear polarisation commonly used in GPR surveys.

- Discrimination: if two signals arrive at the same time, they might be impossible to separate based on just frequency, amplitude or phase. Often, however, the two waves differ or can be made to differ in polarisation. For example, data recorded using cross-polarised antennas will record almost zero direct signal, which implies less interference.
- Identification: since the shape and orientation of a scatterer on the one hand and the propagation medium on the other hand influence the polarisation, it is sometimes possible to isolate the scatterer geometry or the host medium properties by observing the polarisation characteristics of the scattered field.

When discussing wave polarisation of GPR signals, three concepts are common and important. These concepts are (1) polarisation due to antenna construction, (2) polarisation due to antenna orientation, and (3) depolarisation (or changes in polarisation) due to target orientation.

The target symmetry (shape and orientation) has an impact on the polarisation of a scattered wave, as do the incident angle of the wave, antenna separation, and the impedance contrast of the materials. A scattered wave can have the same polarisation as the incident wave, or it can be polarised differently, in which case it is said to be depolarised. It has been noted that various targets of GPR surveys, such as buried pipes and fractures, have polarisation-dependent scattering characteristics. This implies that the visibility of a subsurface scatterer in the acquired data depends on the used antenna configuration and its orientation with respect to the feature to be imaged. As a consequence, certain subsurface objects might not be imaged using a single component antenna configuration.

Antenna orientation, definition adopted for linearly polarised equipment only, is not only based on the antennas' position relative to each other but also on their orientation relative to the survey line direction. Parallel orientation of antennas allows maximising the polarisation match between them; in this case, the antennas can be arranged in broadside or end fire configuration with respect to the survey line direction, i.e., with an orientation parallel or perpendicular to the line. On the contrary, when the transmitting and receiving antennas are arranged with orthogonal orientations, they are cross-polarised and target information can be extracted based on the coupling angle [153]. Cross polarisation occurs when the target changes the polarisation of the reflected wave compared to incident one.

These configurations are sketched in Fig.3.7.

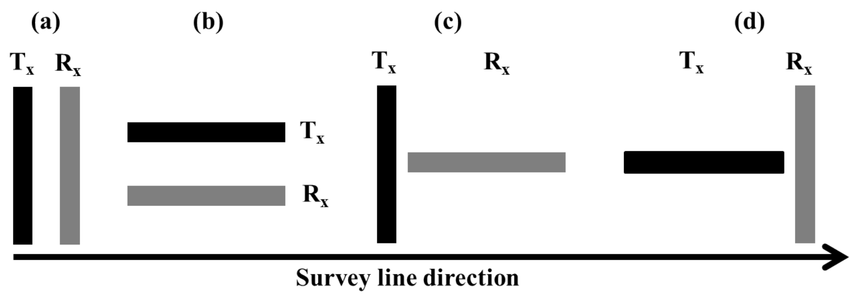

Figure 3.7: Representation of different antenna configuration for multicomponent data acquisition. (a) Co-pole, end fire. (b) Co-pole, broadside. (c)-(d) Cross-pole.

For a monostatic system, which utilises the same or at least co-located antennas for both transmit and receive functions, the two cross-polar configurations coincide, i.e. the scattering matrix is symmetrical and has only 3 independent elements.

The power of a wave scattered from an isotropic target (e.g. a sphere) is independent of the transmitter polarisation, while for linear target the polarisation of the scattered field is independent of the transmitting polarisation. For a general target, instead, both the power and polarisation of the reflected wave vary with transmitter polarisation [218]. The electromagnetic field is a vector field and the target structure is usually 3-D. Clearly, different polarisation combinations of sending/receiving antennas generate different polarimetric returns. These differences can be used for target identification purposes.

It is clear, then, that polarisation plays a fundamental role in applications such as pipe and cable detection, but also for the correct imaging of extended targets. It is also clear that the way in which the target respond to an impinging polarisation is critical in the light of wave depolarisation. Polarisation is implicit in this definition of radar cross section, and usually, it is assumed that a single polarisation is employed for both the transmitted and received fields. This assumption is not required, however, and radar cross sections can be defined for arbitrary polarisation of transmitted and received fields.

The RCS for circular polarisation is supposed to be equal to the RCS for linear polarisation if the angle between the E-field and the wire is 45 degrees, i.e., half of the RCS for parallel orientation, hence elongated targets with arbitrary orientation can be detected by GPR using either a circularly polarised antenna or two perpendicularly oriented antennas with linear polarisation.

Several detailed works on the effects of polarisation for common GPR targets have been produced. Polarisation is understood to have a significant impact for the identification of elongated objects and asymmetrical subsurface features [219, 220], and it is largely employed as a further tool that could provide additional information and features of the buried objects [221, 222, 223, 224]. However, few GPR sensors use more than one polarisation.

In [225] an FDTD solution was used to simulate the polarimetric scattering from symmetric and asymmetric targets and analytical measures were developed in order to show that symmetry features can be used to adequately separate symmetric objects from asymmetric ones. One of the main features of the technique is that it is independent of target shape, size, material, or depth. As a result, no a priori knowledge about the target or its scattering properties are required.

Authors in [226] described a polarimetric GPR which is invariant to rotations (demonstrated in [227]) to acquire quantities related to the shape and dimension of the target from the target scattering matrix. Target used was a disk brake rotor, hence the formation of the scattering matrix is facilitated.

In [228] the author offers an insight from what can be gained from polarimetric analysis of GPR backscatter signal. Assuming the target being metallic, elongated and buried at a shallow depth, simulations provide interesting results in terms of (1) length, (2) orientation and (3) radius inference. Graphs show a clear implications of the angular patterns: backscattered magnitude drop down when there is a misalignment between the antenna and the target, following the well-known trends of linear target.

Work in [229] has a similar aim, to show the influence of geometry on the fingerprints of different landmines. In particular, a comparison of landmine signature for different observation points, both vertically and laterally shifted and tilting objects is discussed. The analysed target is a M14 mine, characterized by a low metal content and a reduced dimension (40 mm height and 56 mm diameter) with a cylindrical shape. Results show a variation in the magnitude of the backscattered electric field as receiver position and orientation changes. Results illustrated that the shape of the fingerprint within the bandwidth always remains nearly the same. Differences are visible with the highest part of the spectrum, in which of course the spatial resolution is higher. It can be noticed that a tilting of the landmine significantly changes the energy trend.

Results in [230] demonstrated that the backscattered fields from a body of revolution (BOR) target excited by a vertically or horizontally polarized plane wave are characterized by a zero cross-polarisation component. Through an experimental campaign carried out with a metallic landmine surrogate, these polarimetric characteristics are proven to be valid, independently of the mine electrical properties, as long as it satisfies the BOR model.

3.3 Summary

In this Chapter literature considered relevant to the research problem has been presented and discussed. This analysis has confirmed that rather few works have addressed the task of discriminating landmines on the basis of their internal scattering contributions, and that there is a lack in understanding of the significance of these signature components and how they can improve GPR performance. Even if the presence of such reflections has been pointed out, the feature has not been exploited and researched. Moreover, despite the vast literature on radar responses of different targets, not many results are available for landmine responses. There are several reasons for this: first, available results typically deal with metal targets, while the majority of AP mines and some AT mines are dielectric objects with some metal inclusions. Second, the influence of the environment on target response is quite complicated. Finally, in a typical radar scenario, the target is situated in the far field of both the transmit and receive antennas. In typical landmine detection scenario (and often in UXO detection), the target is situated in a near field of the antenna system.

Up to now, the exploration of angular diversity in the sense of monostatic and bistatic look angles at the target has only rarely been taken into account. The majority of works on bistatic GPR configurations have focused on the evaluation of geometrical features, showing some potential but highlighting also limiting hypothesis, both concerning target modelling and acquisition scheme. Similarly, publications on polarimetric GPR largely focus on the challenge of distinguishing targets with a predominant geometry from objects showing a symmetrical structure. Theoretically, multicomponent analysis may produce a useful discrimination, however, it is currently not clear whether polarimetric information can as well be exploited for very small targets like anti-personnel landmines, and whether it could cope with inclined targets, for which the symmetrical feature will vanish.

From this review of recently published work, it can be stated that the research questions formulated in Section 1.7 and the scientific innovation summarised in Section 1.8 have not previously been addressed in the literature.

Chapter 4

GPR Design and Modelling

In theory, there is no difference between theory and practice. But, in practice, there is

Jan L. A. van de Snepscheut [231]

The objective of this Chapter is to establish a theoretical justification of the addressed problem and to provide an analytical basis for the subsequent experimental section. This Chapter covers the fundamental principles governing the GPR methodology, emphasising the differences not only between GPR and conventional radar, but also between GPR as a landmine detector and for other GPR applications.

Firstly, a succinct overview of the key concepts influencing electromagnetic wave propagation and reflection is provided and the physical issues evaluated in order to give a sense of the role played in the process. Through the radar range equation, the analysis continues considering the principal factors affecting the design of a GPR in order to illustrate those factors which need to be investigated and providing an initial estimate of the range performance of a GPR system. To examine the impact that a dynamic separation between the transmitter and the receiver has on the involved parameters, bistatic developments of the previous formulations are given as well.

As the aim of the work is to characterise a landmine in light of its internal structure, particular attention is put on the constraints in place for a landmine detection equipment, discussing the principal challenges concerning the identification of the internal scattering contributions.

In the latter part of the Chapter, a number of numerical simulations based on FDTD modelling involving the key variables affecting the imaging performance is developed and assessed in the light of the research objectives previously described.

4.1 Electromagnetic principles of GPR

The foundations of GPR lie in electromagnetic theory, of which Maxwell's equations and the electrical properties of materials are the basis, and the aim of this section is to provide the principal building block needed to work quantitatively with GPR.

4.1.1 Physics of propagation

4.1.1.1 Energy transfer

In the case of an electrically small linear antenna with a uniform current distribution,shown in Fig. 4.1, the electric and magnetic field components in free space are described in Equations 4.1 which are derived from Maxwell's equations.

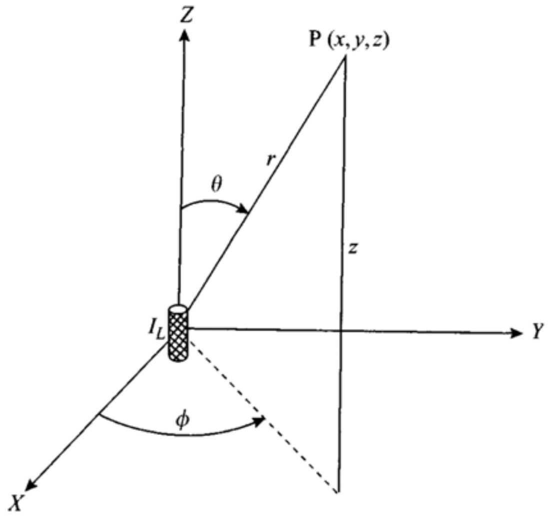

Figure 4.1: Electrically small antenna.

$$E_r = \frac{\eta_0 Idl}{4\pi} e^{-jkr} \left[\frac{2}{r^2} + \frac{2}{jkr^3} \right] \cos\theta \tag{4.1a}$$

$$E_\theta = \frac{\eta_0 Idl}{4\pi} e^{-jkr} \left[\frac{jk}{r} + \frac{1}{jkr^3} + \frac{1}{r^2} \right] \sin\theta \tag{4.1b}$$

$$H_\phi = \frac{Idl}{4\pi} e^{-jkr} \left[\frac{jk}{r} + \frac{1}{r^2} \right] \sin\theta \tag{4.1c}$$

where

dl is the length of the current element.

I is the current in the element..

η_0 is the free space impedance.

θ is the zenith angle to radial distance r.

ϕ is the azimuth angle to the radial distance r projection.

r is the distance from the element to the point of observation.

k is the wavenumber.

Three field components can be identified:

- **Inverse cube term**: quasi-stationary term or electrostatic field term. This results from the accumulation of charges at the ends of the element.
- **Inverse square term**: induction term. This represents the energy stored in the field during one quarter of a cycle and then returned to the antenna in the next. Fields do not display a spherical wavefront, thus the pattern varies with distance.
- **Inverse term**: radiation term. This term represents the flow of energy away from the conducting element of the antenna. The E and H fields support and regenerate one another as their strength decreases as the inverse square of the distance.

The regions may also be described as the near field, also called the reactive near field, the region closest to the transmitting aperture and for which the reactive field dominates over the radiative fields, the radiating near field (or Fresnel zone), in which the radiation fields dominate and where the angular field distribution depends on the distance from the transmitting antenna, and the far field (or Fraunhofer zone), where the radiation pattern is independent of the distance from the transmitting antenna [156].

At a distance $r = \lambda/2\pi$, all of these terms are equal, and this distance represents the boundary between the near fields and far fields where the contributions from the radiation, induction and the quasi-stationary terms are all of the same magnitude (Fig. 4.2).

The initial boundaries of the three regions are commonly defined as in Table 4.1.

Table 4.1: Boundaries for field region definition.

Reactive NF	Radiating NF	Radiating FF
$r = 0$	$r = \lambda/2\pi$	$r = 2D^2/\lambda$

in which D is the maximum dimension of the antenna. The last formula corresponds to a phase error (due to the curvature of the actual spherical wavefront) of no more

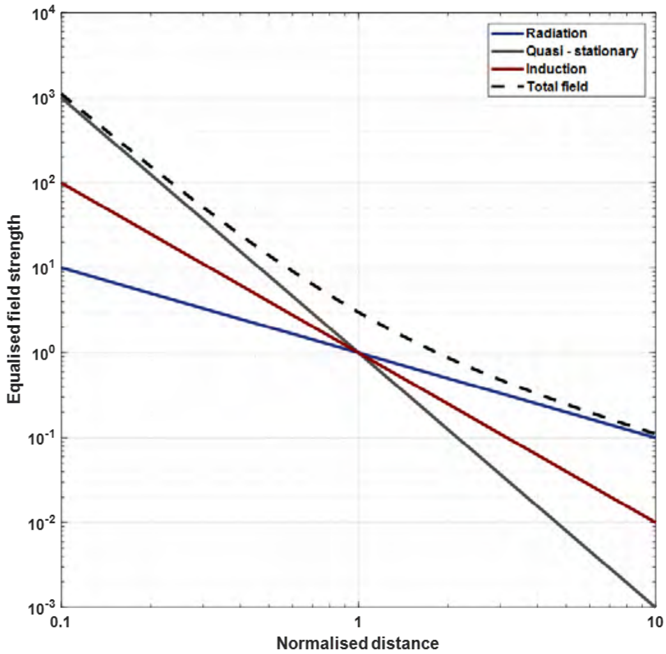

Figure 4.2: Signal level versus distance for EM field components. Distance is normalised to $r = \lambda/2\pi$

than 22.5 degrees ($\pi/8$) across the aperture. It is generally considered that the above integral formulation is not rigorous for the reactive components since the boundary conditions are undefined. Any consideration of the signal detected in a radar receiver should therefore fully account for the physical proximity of the antenna and the target [232].

The principal differences between the near field and the far field propagation behaviour can be summarised as follows:

- **Near field:**
  - E and H fields are out of phase by 90 degrees.
  - Plane wave assumption does not hold.
  - Energy decays very rapidly with distance.
  - The average energy density remains fairly constant at different distances from the antenna (localised energy fluctuations).
  - The shape of the radiation pattern may vary appreciably with distance
- **Far field:**
  - E and H fields are orthogonal to each other.
  - The fields behave as plane waves.
  - Energy decays very rapidly with distance.

- The angular distribution of the energy does not vary with distance.
- The power level decays according to the inverse square law with distance.
- The power radiated in a given direction from distinct parts of the antenna are approximately parallel.
- Radiation pattern does not change shape with distance.

Essentially GPRs operated in standoff mode are fully described by radiated field models, whereas radars operated in proximal mode may achieve better performance due to the increased contribution by the quasi-stationary and induction fields. In the case of borehole radars, the antenna actually radiates within a lossy dielectric, whereas in the case of the radar working above the surface the antenna will radiate from air into a very small section of air and then into a lossy half-space formed by the material. The interaction between the antenna and the dielectric is also significant as this may cause modification of the antenna radiation characteristics, both spatially and temporally, and should also be taken into account in the system design [233].

4.1.1.2 Wave nature of EM fields

Depending on the relative magnitude of energy loss (associated with conductivity) to energy storage (associated with permittivity and permeability), the fields may diffuse or propagate as waves (frequency-independent) [16].

With GPR, the electromagnetic fields propagate as essentially non-dispersive waves. The signal emitted travels through the material, is scattered and/or reflected by changes in impedance giving rise to events similar to the emitted signal. In other words, signal recognition is facilitated by the fact that the return signal is theoretically correlated to the emitted signal.

GPR field behaviour occurs over a finite frequency range generally referred to as the GPR plateau where velocity and attenuation are frequency independent. The GPR plateau usually occurs in the 1 MHz to 1000 MHz frequency range. At lower frequencies (diffusive field behaviour), all the wave properties are frequency-dependent, implying that there will be some variation in the velocity of propagation with frequency. Dielectrics exhibiting this phenomenon are termed dispersive, and the consequence of a propagation in a dispersive medium is that the different frequency components within a broadband radar pulse would travel at slightly different speeds, causing the pulse shape to change with time.

At higher frequencies, instead, the properties become frequency-independent, and all the frequency components travel at the same velocity and suffer the same attenuation. An impulse will travel with its shape intact, but several factors increase signal absorption such that penetration is extremely limited.

For successful GPR measurements a plateau exists where these properties become frequency independent, as shown in Fig. 4.3. The obvious success of the GPR method indicates that many applications are not subject to severe dispersion, however in some high loss materials, the plateau may not be present.

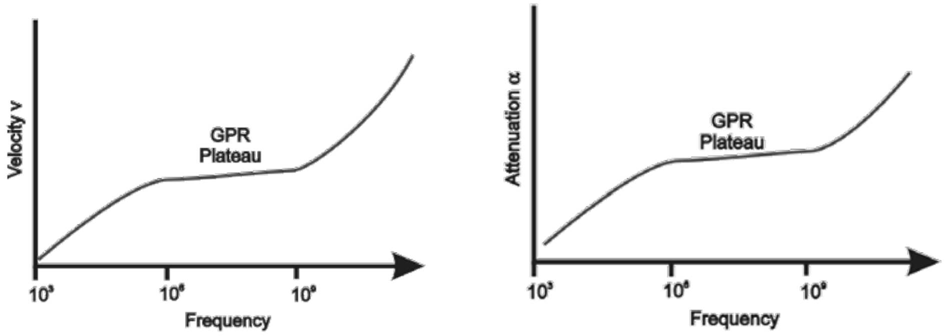

Figure 4.3: General character of EM field phase velocity and attenuation in a lossy dielectric material versus frequency.

The transition frequency between diffusion and propagation behaviour is defined as follows (Eq. 4.2):

$$f_t = \frac{\sigma}{2\pi\varepsilon} \tag{4.2}$$

This plateau may still exhibit some gradual increase in velocity and attenuation with frequency. The increase in attenuation is usually the most important as many GPR applications are close to the attenuation limit and any increase may mean the difference between success and failure of a GPR investigation. There are two primary factors which induce this increase: (1) the presence of water, which starts to absorb energy more and more strongly as frequency increases toward the water relaxation frequency (10 GHz), and (2) the scattering loss, which are frequency dependent and can become a critical factor.

The simplest solution of Maxwell's equations is the transverse electromagnetic (TEM) plane wave. The wavefronts are planar, the direction of propagation is the same everywhere, and the electric and magnetic fields are orthogonal to one another and to the direction of propagation. A wave propagating in the positive z-direction in a perfect dielectric can be described by equation 4.3

$$E_z = E_0 e^{-jkr} \tag{4.3}$$

and the velocity of propagation (Eq. 4.4) is:

$$v = \frac{1}{\sqrt{\varepsilon\mu}} = \frac{c}{\sqrt{\varepsilon_r}} \tag{4.4}$$

In a perfect dielectric no propagation losses are encountered and hence there is no consideration of the attenuation, which occurs in real dielectric. The phase constant is defined as $k = \omega/v = \omega\sqrt{\mu\varepsilon}$ (referred also to as the propagation factor for the medium), and the ratio of the electric and magnetic fields is equal to the characteristic impedance of the medium (Eq. 4.5)

$$Z = \sqrt{\frac{\mu}{\varepsilon}} \tag{4.5}$$

For nonmagnetic media, $\mu = \mu_0$, and $Z = \sqrt{\mu_0/\varepsilon}$ may be written in terms of the impedance of free space ($Z_0 = 377\Omega$) as in Eq. 4.6:

$$Z = \sqrt{\frac{\mu_0}{\varepsilon}} = \frac{Z_0}{\sqrt{\varepsilon_r}} \tag{4.6}$$

As a reference, in free space the magnetic susceptibility and electric permittivity are constants, hence they are independent of frequency and the medium is not dispersive.

4.1.1.3 GPR source near an interface

GPR sources are normally deployed close to the ground, and the radiated field can locally be considered as a planar wave impinging on the boundary at a specific incidence angle defined by geometry [234], as shown in Fig. 4.4. The signal is reflected and refracted according to Snell's law and the Fresnel coefficients.
If one examines the wavefront in the ground, it is no longer spherical, as bending occurs with differing degrees depending on the varying incidence angle.

In case of GPR surveys conducted with the source very close to the surface, which represents the most common situation, the limiting case of the source right at the interface can be considered. This case is sketched in Fig. 4.5.

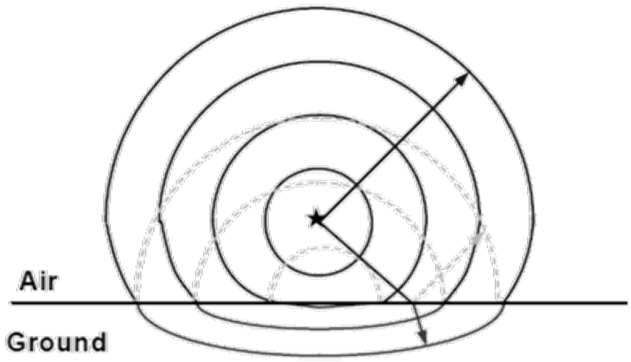

Figure 4.4: Wavefronts from a localised source located above the ground.

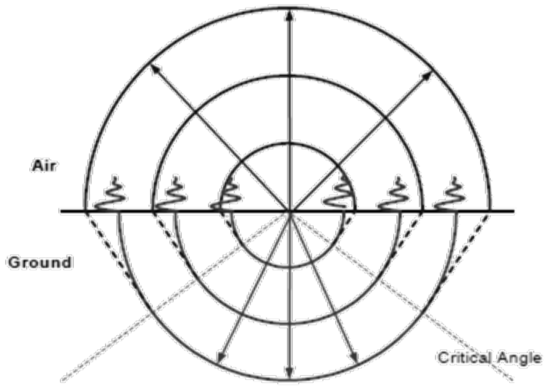

Figure 4.5: Wavefronts from a source located on the ground interface.

The incident and reflected waves in air coalesce into an upgoing spherical wave. In the ground, the transmitted signal divides into two parts, a spherical wave and a planar wavefront travelling at the critical angle, which links the direct spherical air wave and the spherical ground wave. Near the interface, the spherical ground wave extends into the air as an evanescent field. When the distance from the source is large compared to the wavelength or the pulse spatial length, these different components are clearly separate in time and space, while their identity becomes blurred for shorter distance. However, the concepts are still valid.

It can therefore be appreciated that the effect of changes in distance between the antenna and the surface cause significant variation in the resultant radiation patterns in the dielectric. In particular, when this distance is increased, the antenna field patterns are modified by a reduction in the effect of the reactive field.

As a comparison, Fig. 4.6 depicts the wavefront footprint for a dipole antenna, representing one of the most common equipment employed in GPR design.

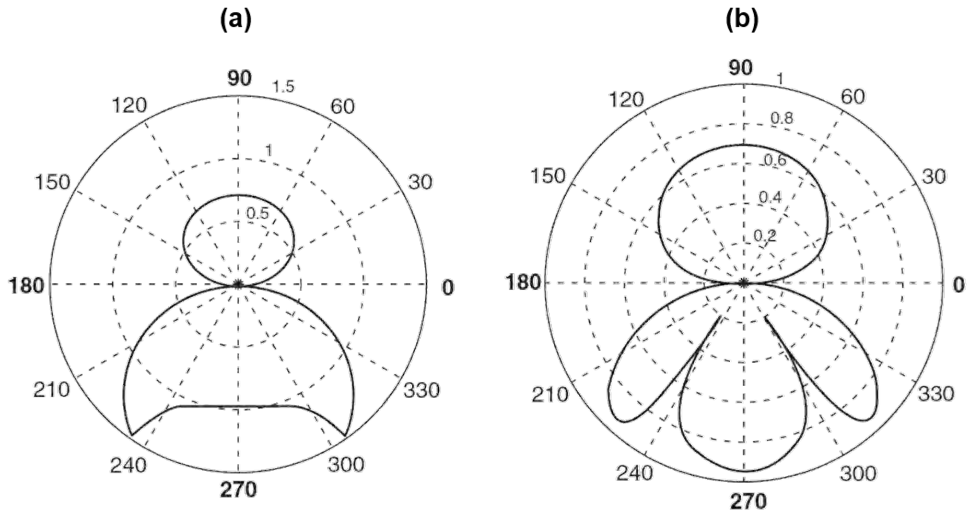

Figure 4.6: Wavefronts from a dipole antenna located on the ground interface. (a) E-field. (b) H-field.

There can be several possible paths from a transmitter to the receiver, sketched for a simple two layers model in Fig. 4.7 and characterised as follows:

1 **Direct air signal**: travelling through the air in a direct line from the transmitter to the receiver. As a result, the direct air wave is always the first signal measured by the receiver.

2 **Direct ground signal**: travelling along the surface interface at velocity v_1.

3 **Direct reflected signal**: travelling through medium 1 at a velocity v_1 and back after reflection at the interface.

4 **Critically refracted signal**: because $v_1 < v_0$ reflected waves are critically refracted at the surface. While this wave propagates along the surface interface, it will have velocity a velocity roughly the speed of light.

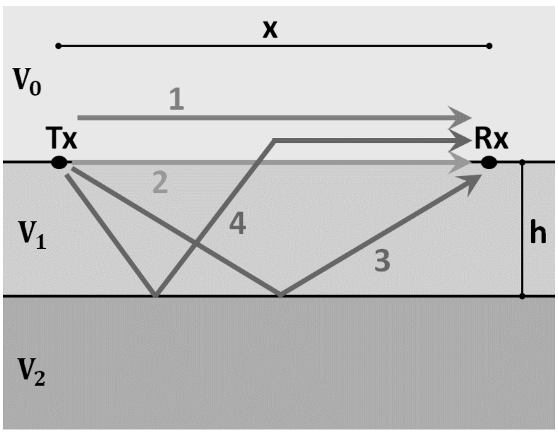

Figure 4.7: Signal paths between a transmitter and a receiver on the surface.

The relative importance of each path depends on the target depth, the separation between the transmitter and receiver and the elevation of the transmitter and receiver. Moreover, the refracted path (4) includes the refraction/reflection path and its specular reflected/refracted one, even if they can't be distinguished.

In most GPR cases, the transmitter receiver separation is small and the predominant paths are (1), (2) and (3), even if for proximal operations the direct air and ground arrival can hardly be separated from the background reflection. The signal following path (4) can have an impact if both the transmitter and receiver are a substantial distance from the target.

4.1.1.4 Reflection, refraction and transmission at interfaces

Ground penetrating radar methods normally depend on detection of reflected or scattered signal. Planar boundaries provide the simplest model for qualifying the behaviour, while the Fresnel reflection (and transmission) coefficients quantify how the amplitudes of the EM fields vary across an interface between two materials.

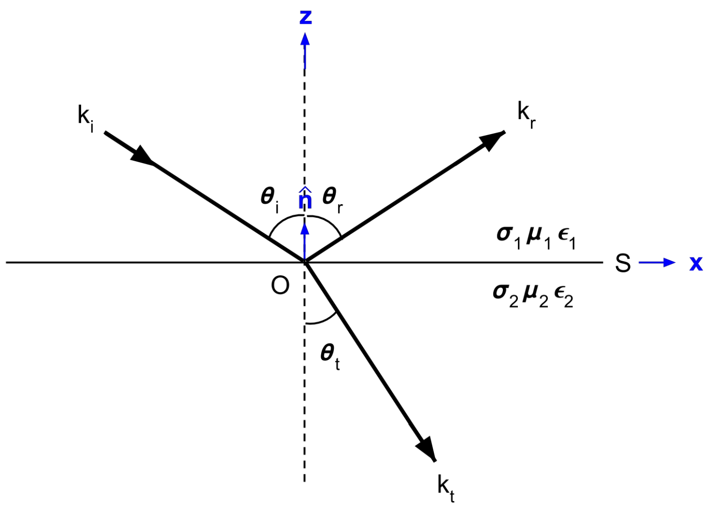

Figure 4.8: Geometry for Snell's law.

Snell's law expresses how wavefronts change direction as the fields move through materials where velocity is not constant. The concept is illustrated in Fig. 4.8, showing an EM signal incident (k_i) on the boundary between two materials of different properties (σ, μ, ε). The transmitted was experiences a change in propagation direction, thus becoming a refracted wave. Mathematically, Snell's law requires the horizontal component of the propagation vector in each material to be equal.

$$k_1 \cdot \sin\theta_1 = k_2 \cdot \sin\theta_2 \tag{4.7}$$

When the material are low loss (i.e. wave regime approximation), Snell's law takes the more simple form (Eq. 4.8):

$$\frac{\sin\theta_1}{v_1} = \frac{\sin\theta_2}{v_2} \tag{4.8}$$

In this case, the angle of incidence and refraction are directly related to the propagation velocity of EM waves within each media. When $v1 > v2$, medium 2 has a critical angle beyond which energy cannot propagate from medium 1 to 2.

The Fresnel reflection (and transmission) coefficients quantify how the amplitudes of the electromagnetic fields vary across an interface between two materials. Vector-field EM waves separate into two independent components defined by field orientation with respect to the boundary. Components are referred to as the TE (transverse electric field) and TM (transverse magnetic field), shown if Fig. 4.9.

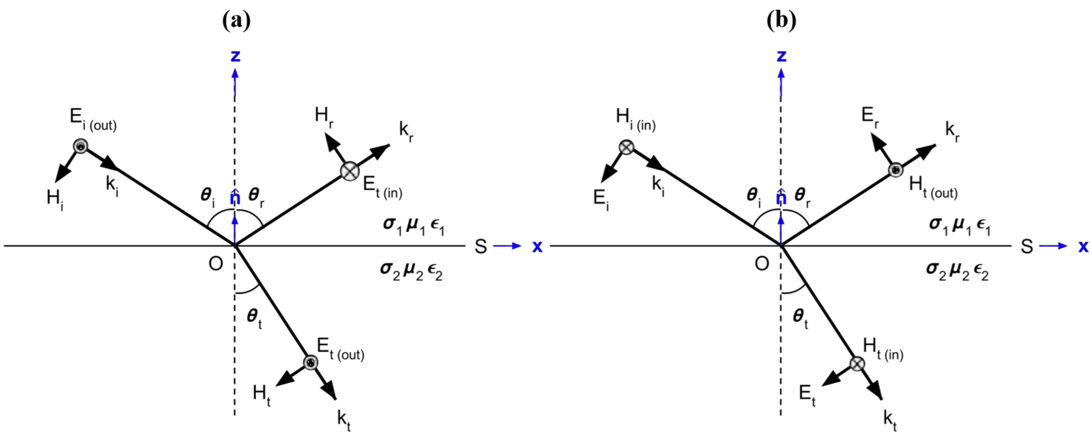

Figure 4.9: Incident wave at planar boundaries. (a) TE mode. (b) TM mode.

The incident, reflected, and transmitted field strengths are related by the following equations (4.9):

$$I_{TE} + R_{TE} \cdot I_{TE} = T_{TE} \cdot I_{TE} \tag{4.9a}$$

$$I_{TM} + R_{TM} \cdot I_{TM} = T_{TM} \cdot I_{TM} \tag{4.9b}$$

R and I are determined by requiring Snell's law to be satisfied, the electric and magnetic fields in the plane of the interface to be continuous, and the electric current and magnetic flux density crossing the interface must be equal on both sides.

The result is described by equations 4.10 and 4.11:

$$R_{TE} = \frac{Y_1 \cos\theta_1 - Y_2 \cos\theta_2}{Y_1 \cos\theta_1 + Y_2 \cos\theta_2} \tag{4.10a}$$

$$R_{TM} = \frac{Z_1 \cos\theta_1 - Z_2 \cos\theta_2}{Z_1 \cos\theta_1 - Z_2 \cos\theta_2} \tag{4.10b}$$

$$T_{TE} = 1 + R_{TE} \tag{4.11a}$$

$$T_{TM} = 1 + R_{TM} \tag{4.11b}$$

where Z_i and Y_i are the impedances and admittances of the $i-th$ material. The critical factor is that an EM impedance contrast must exist for there to be a response.

When the EM wave is vertically incident on the interface ($\theta_1 = \theta_2 = 0$), there is no distinction between a TE and a TM wave, and the TE and TM reflection coefficients become identical (for the field components). For non-vertical incidence, the coefficients are different.

In a non-conducting medium such as dry soil, and when considering only a single frequency of radiation, the above expressions may be simplified and rewritten as (Eq. 4.12:

$$R = \frac{\sqrt{\varepsilon_{r2}} - \sqrt{\varepsilon_{r1}}}{\sqrt{\varepsilon_{r2}} + \sqrt{\varepsilon_{r1}}} \tag{4.12a}$$

$$T = \frac{2\sqrt{\varepsilon_{r2}}}{\sqrt{\varepsilon_{r2}} + \sqrt{\varepsilon_{r1}}} \tag{4.12b}$$

where ε_r is the relative permittivity of the medium.

From these results, the following considerations should be pointed out:

- If the impedance contrast is small most of the incident wave is transmitted through the interface, and viceversa.
- The reflection magnitude becomes larger at large angles.
- The TM reflection coefficient can show a null or a reduction to a minimum as the angle of incidence increases. The angle of the minimum is known as the Brewster

angle, where maximum transmission occurs.

- For TE waves, the admittance must decrease at the interface for Brewster angle to exist, while for TM waves the impedance must decrease crossing the interface.
- When the waves are travelling from a low velocity to higher velocity medium, the magnitude of the reflection coefficients becomes unity for angles greater that the critical angles. The waves are totally reflected but fields do exist in the other material but behave as evanescent signals which decay exponentially with distance from the interface.
- The sign of the reflection coefficients can be either positive or negative and determines whether the reflected wave experiences a reverse in polarity. As a result, the polarity of reflected signal to determine whether the impedance of the first layer is greater than or less than the below one.

The normal incidence reflection coefficients for some air-dielectric interfaces are provided in Fig. 4.10.

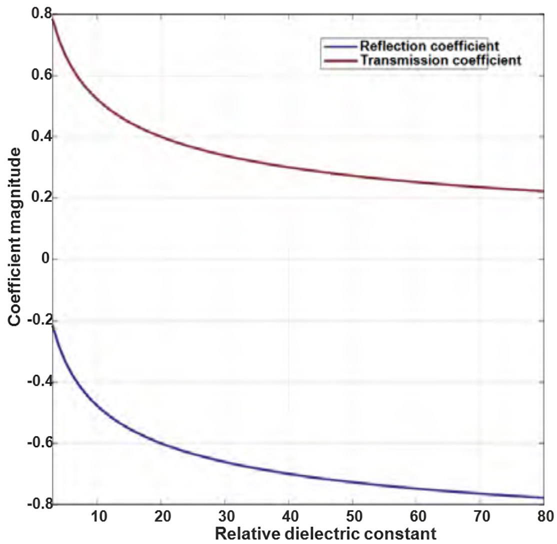

Figure 4.10: Reflection and Transmission coefficients for normal incidence as a function of material dielectric.

4.1.2 Propagation in a dielectric

The signal pulse consists of an electromagnetic wave which oscillates at a particular frequency, and as it propagates through the subsurface, it is distorted due to the distribution of subsurface electromagnetic properties $(\sigma, \mu, \varepsilon)$.

Electromagnetic waves propagating through natural media experience losses, to both the electric (E) and magnetic (H) fields [67]. This causes attenuation of the original electromagnetic wave. For most materials of interest, the magnetic response is weak and need not be considered as a complex quantity, unlike the permittivity and conductivity.

The propagation of a plane wave along the z-direction, perpendicular to the surface, in a homogeneous medium is governed by the wave equation (Eq. 4.13):

$$\frac{\partial^2 E}{\partial^2 z^2} = -\omega^2 \mu \varepsilon E \tag{4.13}$$

where

$E = \Re\left\{E_0 e^{j\omega t}\right\}$ is the sinusoidal time varying electric field vector (V/m), with E_0 the amplitude of the electric field vector (V/m).

ω is the angular frequency (rad/s).

z is the distance along the propagation direction (m).

μ is the magnetic permeability.

$\varepsilon = \varepsilon' - j\varepsilon''$ is the complex permittivity (F/m).

$\sigma = \sigma' - j\sigma''$ is the complex conductivity (Ω/m).

Electrical conductivity characterises free charge movement (creating electric current) when an electric field is present, as resistance to charge flow leads to energy dissipation. Dielectric permittivity instead characterises displacement of charge constrained in a material structure to the presence of an electric field. Charge displacement results in energy storage in the material. The real component, ε', represents the energy stored through electrical polarisation (relative permittivity), and the imaginary component, ε'' represents a measure of energy loss associated with both conductivity and frequency.

The solution of Maxwell's equations for a wave propagating within a homogeneous medium describes an EM field which is affected by an amplitude decay dependent on distance (Eq. 4.14):

$$E = E_0 e^{-jkz} \tag{4.14}$$

with propagation constant (Eq. 4.15):

$$k = \omega\sqrt{\mu\varepsilon(1 - j\tan\delta)} \tag{4.15}$$

in which the loss tangent $\tan\delta = \frac{\sigma' + \omega\varepsilon''}{\omega\varepsilon' - \sigma''}$, sometimes expressed as a dimensionless factor $\frac{\varepsilon''}{\varepsilon'}$, can be interpreted as the ratio between the conduction current density to the displacement current density. In the case of a material that relatively lossless, it may be reasonable to consider that the loss tangent constant over the GPR frequency range. However, for materials that are wet and lossy such an approximation is invalid.

If the real and the imaginary parts of jk are separated, the attenuation parameter α and the phase parameter β are described by Eq. 4.16:

$$\alpha = \omega\sqrt{\left[\frac{\mu\varepsilon}{2}\right]\sqrt{1+(\tan\delta)^2}-1} \tag{4.16a}$$

$$\beta = \omega\sqrt{\left[\frac{\mu\varepsilon}{2}\right]\sqrt{1+(\tan\delta)^2}+1} \tag{4.16b}$$

Therefore, Eq. 4.14 can be rewritten as:

$$E(z) = E_0 e^{-\alpha z} e^{-j\beta z} \tag{4.17}$$

The amplitude of the GPR pulse decreases as it propagates in the material medium, and the pulse shape is distorted because of the nonlinear phase term βz. The first exponential term represents the attenuation of the plane wave in a lossy medium. The rate is specified by α, the attenuation constant, and the second exponential term represents the propagation, controlled by the phase constant β. From the first exponential function it is seen that at a distance $z = 1/\alpha$ the attenuation is $1/e$. This distance is known as the skin depth and theoretically provides an indication of the penetration depth of the GPR system.

Attenuation defines the continuous loss of amplitude a wave experiences as it propagates through a particular medium. Considering typical GPR scenario, a few constrictions can be assumed. In most soils the relative magnetic permeability is equal to one and will thereby be neglected. In the frequency range of common georadar applications (10 MHz to a few GHz), the imaginary part of the electrical conductivity can be ignored and the real part is assumed to be frequency independent and equal to the DC conductivity.

It can be seen from the above expressions that the attenuation constant of a material is, to a first order, linearly related (in dB/m) to frequency (Fig. 4.11), and in a second instance to the square root of the permittivity of the material.

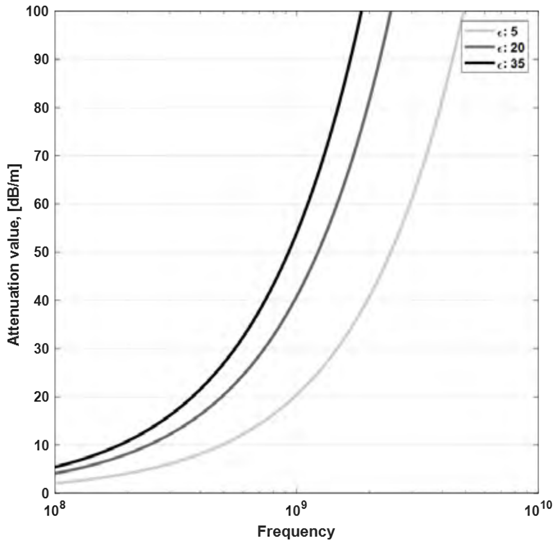

Figure 4.11: Material attenuation as a function of frequency and relative dielectric constant.

Applying the wave regime approximation, the expression for the material attenuation in Eq. 4.16 becomes:

$$\alpha = \frac{\sigma}{2}\sqrt{\frac{\mu}{\varepsilon}} \tag{4.18}$$

This essentially underlines that the higher the conductivity of the material, the faster the wave will dissipate into the ground.

Empirically derived forms such as Topp's relationship [235] and variations of Archie's law have long demonstrated the relationship between permittivity, electrical conductivity, and volumetric water content for soils [236, 237]. Because of high rates of signal attenuation, penetration depths are greatly reduced in soils that have high electrical conductivity, parameters which increases with increasing water, soluble salt, and/or clay contents. As a general rule, the permittivity at zero volumetric water content is in the range $3-4$ and conductivity is usually very small. As water is added to the mix, the permittivity and conductivity rise until the porosity of the material reaches its maximum saturation, dictating the maximum permittivity and conductivity of the mixture.

The velocity of electromagnetic wave propagation in a medium with electrical parameters as described in Eq. 4.13, and considering nonmagnetic material ($\mu_r = 1$), is expressed as:

$$v = c\left\{\frac{\varepsilon' - \frac{\sigma''}{\omega}}{2\varepsilon_0}\left[\sqrt{1+\left(\frac{\varepsilon'' + \frac{\sigma}{\omega}}{\varepsilon' - \frac{\sigma}{\omega}}\right)^2}+1\right]\right\}^{-\frac{1}{2}} \tag{4.19}$$

Considering ω large compared to σ' and σ'', the expression becomes:

$$v = c\left\{\frac{\varepsilon'}{2\varepsilon_0}\left[\sqrt{1+(\tan\delta)^2}+1\right]\right\}^{-\frac{1}{2}} \tag{4.20}$$

The velocity of propagation is also slowed by an increase of loss tangent as well as relative dielectric constant, however $\tan\delta$ must be significantly greater than 1 for any slowing to occur. The effect is shown in Fig. 4.12(a).

Under this approximation (ε'' is small compared to ε'), Eq. 4.20 can be approximated as:

$$v = \frac{c}{\sqrt{\frac{\varepsilon'}{\varepsilon_0}}} = \frac{c}{\sqrt{\varepsilon_r}} \tag{4.21}$$

The propagation velocity decreases with increasing relative permittivity (Fig. 4.12(b)), and the wavelength within the material also decreases as the velocity of propagation slows.

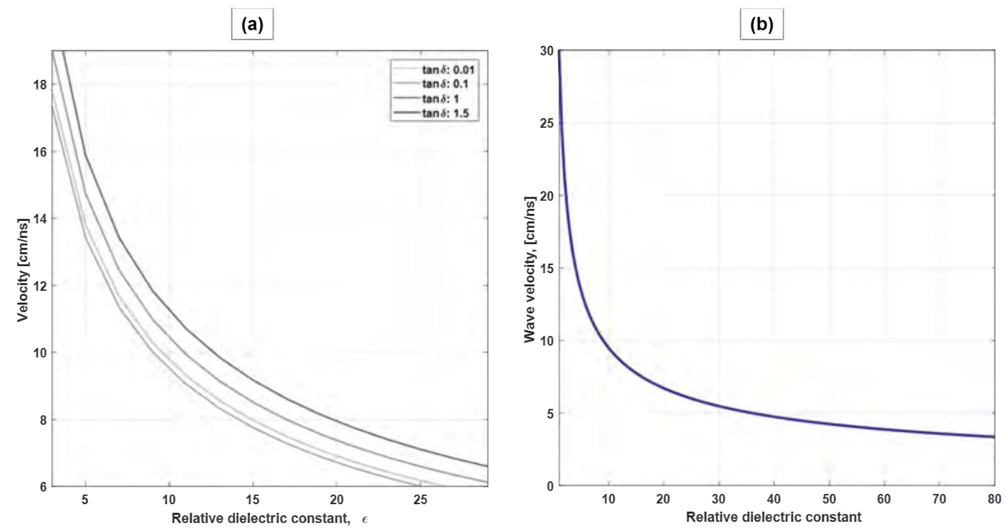

Figure 4.12: Effects on wave velocity of (a) loss tangent, and (b) relative dielectric constant.

From the general equation for propagation velocity, we see that as $\sigma \to \infty$, the propagation velocity goes to zero, meaning that the wave cannot propagate through extremely conductive objects. Because of this, when a wave reaches the interface between the Earth and a highly conductive object, the wave is completely reflected regardless of the incident angle.

4.1.2.1 Properties of lossy dielectric materials

Unfortunately, there is no simple model to describe the variations of permittivity and conductivity for the great variety of soils and rocks that can be encountered in GPR surveying. This, to a great extent, is a result of the formation of soils and rocks as mixtures of a number of simpler substances which each have different influences on the electromagnetic fields.

The determination of the dielectric properties of earth materials remains largely experimental. Rocks, soils and concrete are complex materials composed of many different minerals in widely varying proportions, and their dielectric parameters may differ greatly even within materials, which are nominally similar. Most earth materials contain moisture, usually with some measure of salinity. Since the relative permittivity of water is of the order of 80, even small amounts of moisture cause a significant increase of the relative permittivity of the material. The influence of moisture content upon the dielectric properties of earth materials is significant and is well documented in the literature.

Table 4.2 provides typical dielectric constant and electrical conductivity values for common materials encountered using GPR.

Table 4.2: Typical electromagnetic properties for common geological materials at 100 MHz.

Material	Dielectric constant	Electrical conductivity (mS/m)
Air	1	0
Sea water	80	30000
Fresh water	80	0.5
Distilled water	80	0.01
Ice	3-4	0.01
Limestone	4-8	0.5-2
Sand, dry	3-5	0.01
Sand, wet	20-30	0.1-1
Silts	5-30	1-100
Clay	5-40	2-1000

Notice how water has both the highest and lowest conductivity - and hence attenuation rate - depending upon salinity. This is why the presence and composition of water is the single most significant contributor to the dielectric properties of the material, and consequently to GPR performance. Clay is also a very important factor, with only a small amount of clay contributing to significantly decreased GPR performance.

Among the methods of classifying soils, the clearest way is probably the textural triangle, shown in Fig. 4.13, which represents all possible combinations of soil separately.

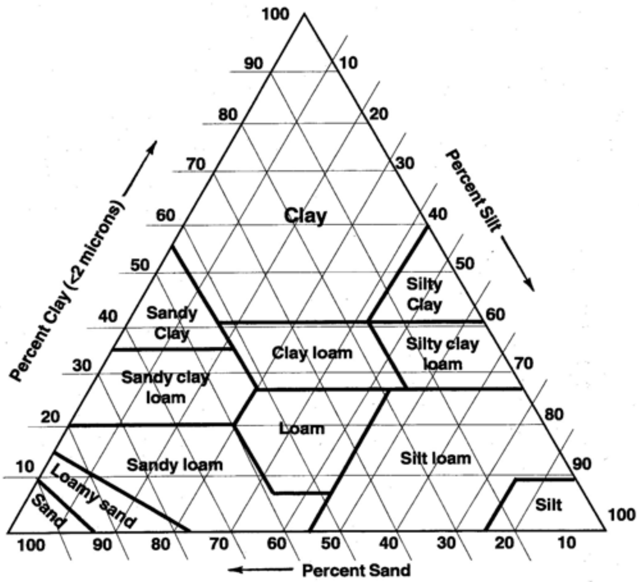

Figure 4.13: Soil textural triangle.

Following this classification, some useful soil mixture can be described (Table 4.3): in which it is once again evident that the permittivity of subsurface materials can vary

Table 4.3: Typical electromagnetic properties for common soil mixtures at 100 MHz.

Material	Dielectric constant	Electrical conductivity (mS/m)
Sandy, dry	4-6	0.1-100
Sandy, wet	15-30	10-100
Loamy, dry	4-6	0.1-1
Loamy, wet	10-20	10-100
Clayey, dry	4-6	0.1-100
Clayey, wet	10-15	100-1000

dramatically, especially in presence of free and bound water. Finally, recalling Table 4.4 describe the dielectric properties of landmine constituents, from which it is easily understandable why detection of zero metal landmines is a very challenging task [238].

Table 4.4: Relative dielectric constant of landmine constituents.

Material	Relative dielectric constant ε_r
Neoprene rubber	6-9
Bakelite	3-5
Polycarbonate	2.9-3.5
Polyethylene	2-2.5
Epoxy resin	3-4
TNT	2.7
PETN	2.72
Comp B (RDX TNT)	2.9
Tetryl	2.9
Semtex (RDX PETN)	3
Comp C-4 (RDX)	3.14
Nytroglycerine	19

Scattering from mines is reduced by a larger factor because of reduced dielectric contrast between the mine material and the surrounding soil, so that in wet sandy soils, minimum metal mines are more readily detected than in dry conditions [239, 240]. Examples of detection performance depending on soil characteristics and environmental factors can be found in [241, 242]. As an electromagnetic subsurface imaging technique, GPR is highly sensitive to soil heterogeneity and anisotropy, thus soil texture should be considered as well [243, 244].

4.2 System design

GPR concept and design differs significantly from conventional radar primarily because of the short range of the targets, which is of the orders of metres, and the lossy propagation media for the EM waves, for which the attenuation and the inhomogeneous nature of the earth become a dominant factor for GPR.

In addition, the target dimensions sought with GPR are of a different order of magnitude than the ones which are usually detected with atmospheric radar, and they are in all case stationary.

4.2.1 GPR range equation

GPR system performance is also governed fundamentally by the radar range equation, but some additional losses have to be introduced, i.e. the transmission loss at the air-ground interface, transmission losses associated with any mismatch in the ground (different layers in the ground) and propagation loss in the ground.

The modified GPR equation can be written as:

$$P_{rx} = \frac{P_{tx}\varepsilon_{tx}G_{tx}A_{rx}G_{rx}\varepsilon_{rx}\sigma_{RCS}}{(4\pi z^2)^2} \cdot \left(Z_{tx} \cdot e^{-2\alpha z} \cdot e^{-2\alpha z} \cdot Z_{rx}\right) \tag{4.22}$$

in which:

P_{tx} is the transmitted power.

$\varepsilon_{tx}, \varepsilon_{rx}$ are the transmitter and receiver antenna efficiency.

G_{tx}, G_{rx} are the transmitter and receiver antenna gain.

A_{rx} is the receiver antenna effective area.

σ_{RCS} is the target cross section.

z is the distance of target from transmitter (assumed equal to the one from the receiver).

Z_{tx}, Z_{rx} are the coupling losses.

α is the attenuation coefficient of the material.

A schematic diagram of the different variables of the radar equation is provided in Fig. 4.14.

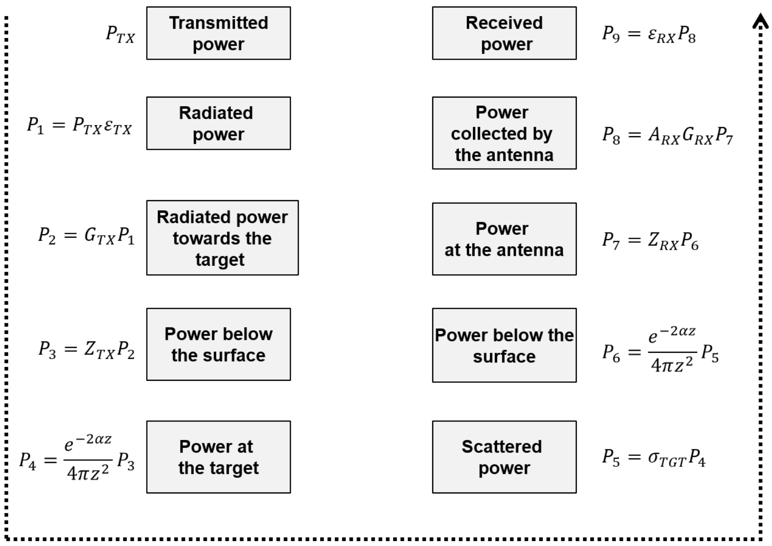

Figure 4.14: Block diagram of the GPR range equation.

The strength of the received signal depends on the radar cross section of the target and the losses encountered by the radar signal as it couples into the ground, propagates from the transmitter, reflects from the target and returns to the receiver. The processes producing losses are sketched in Fig. 4.15.

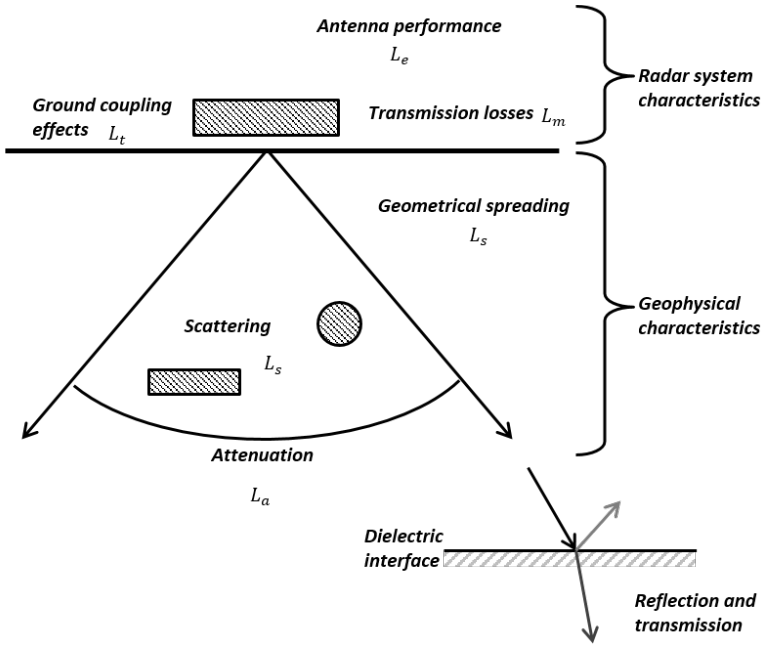

Figure 4.15: Processes that lead to reduction in signal strength.

All the parameters are detailed in the following sections.

4.2.1.1 Antenna efficiency and mismatch

Antenna efficiency relates to the fact that all practical antennas suffer from losses. The antenna efficiency is a measure of the power available for radiation as a proportion of the power applied to the antenna, while the antenna mismatch loss is a measure of how well the antenna is matched to the transmitter.

4.2.1.2 Coupling losses

The proximity of the antenna to the ground means that it is necessary to consider the coefficients of reflection and transmission as the wave passes through the dielectric to the target, described by the Fresnel equations. According to this, at the boundary between two media, some energy will be reflected and the remainder transmitted.

The ground has a frequency dependent characteristics impedance which lies in the range of 50 to 200 Ω, whereas most antennas are designed to radiate into free space (impedance of 377 Ω). The variability of the ground impedance is a primary source of loading and mismatch. For proximal operation, the efficiency of the coupling process is generally high, but this is not the case for standoff radar systems since, where lossy materials are involved, complex angles of refraction may occur. Note also that the transmission coefficients further suppose that the interface is flat and in the far-field of the antennas. In practice these two assumptions are not always respected.

4.2.1.3 Spreading losses

Spreading losses are related to the decay of energy due to the distribution of the energy on the front, as the energy of the wavefront is spread over an increasingly larger area.

In conventional radar, the target is in the far field of the antenna and the spreading loss is proportional to the inverse fourth power of distance provided that the target is a point source. In many situations relating to ground penetrating radar the target is in the near field and Fresnel zone and the relationship is no longer valid.

The nature of the target influences the magnitude of the received signal. Considerably more backscattered energy will be returned from planar reflector at a given depth compared with other target types exhibiting similar dielectric contrasts. Therefore, the following adjustments should be considered when evaluating the parameter:

- Point scatterer: inverse fourth power.
- Line reflector: inverse cube.
- Planar reflecting surface: inverse square

4.2.1.4 Scattering losses

At any change in material properties, some propagating energy is scattered. Scattering is a function of the contrast in material properties at a boundary, the spatial scale of the contrast, the angle of the propagating wave to the boundary, the polarisation of the wave, and the wavelength of the propagating wave. The scattered energy behaves as if it were reradiated from another antenna at the interface.

Many of the targets being searched for by subsurface radar methods are non-metallic, so their scattering cross-section is dependent upon the properties of the surrounding dielectric medium. The physical shape of the target will influence the frequency and polarisation of the backscattered wave and can be used as a means of preferential detection.

The RCS seen by radar also depends on whether the radar is monostatic or bistatic, in which case the bistatic RCS must be considered.

Scattering losses are problematic for GPR because they reduce the amplitudes of useful signals while increasing extraneous noise, especially for cluttered environments. Several sources of scattering are:

- Irregular surface shape of larger buried objects.
- Rocky soils, which are a large contributor to the scattering of GPR signals.
- Gas bubbles trapped in ice.
- Clutter made up of small buried objects

In the case of a medium with a large number of scatterers which size is smaller than the wavelength, the scattering is described as the reflection of the wave in deviated trajectories in a random and not expected direction. This effect is similar in the case of incident waves on large rough surface.

4.2.1.5 Attenuation losses

Since attenuation is exponential with distance, there is always a finite depth of exploration. The properties of the ground, such as soil type and water content, affect the path loss, and the path loss is not always a linear function of depth. To overcome path losses and increase range, the operating frequency can be lowered, but this reduces bandwidth, which is directly proportional to resolution. The best way to visualise these losses is by considering the ground as a low-pass filter, with parameters depending on the soil characteristics, i.e. the texture of soil, the density and the moisture content. Essentially, ground attenuation has the effect of placing a window across the aperture.

A typical range of loss for various materials at 100 MHz and 1 GHz is shown in Table 4.5:

Table 4.5: Attenuation properties of common materials at 100 MHz and 1 GHz.

Material	100 MHz Attenuation dB/m	1 GHz Attenuation dB/m
Sea water	100	1000
Fresh water	0.1	1
Ice	0.1-5	1-50
Loamy, wet	1-60	10-600
Sandy, dry	0.01-2	0.1-20
Clayey, wet	5-300	50-3000

In the table the linear dependency that exists between attenuation and frequency is evident.

4.2.2 Bistatic GPR corrections

Separating the transmitter and the receiver means that in what has been described above, an additional variable needs to be included and its effect on Eq. 4.22 evaluated.

In particular, the principal variations moving from a rigid platform to a bistatic one are related to (1) the experienced attenuation due to the different path travelled by the wave, and (2) the target scattering modelling, as in this case the angle of incidence differs from the direction of the receiver.

4.2.2.1 Attenuation

The difference in the geometry of the problem is clearly inferable comparing the distance from the target corresponding to the shortest travel time, i.e. when the receiver is directly located above the target. For a monostatic system, its equal to twice the target depth, as the transmitter and the receiver are collocated. Employing a bistatic system, instead, means that only the receiver is located in the optimum location, and therefore the distance calculation needs to count also for the target-transmitter distance. The larger is the offset, the longer is the ray path of the reflections and the attenuation of EM waves may reduce the amplitude of the wave field below the sensitivity threshold of the receiving antenna. If the ground attenuation is high, the signals may die out before the maximum separation is reached.

Considering a target at 10 cm below the surface, Fig. 4.16 compares the experienced attenuation by a monostatic and a bistatic configuration for different material properties. It is evident that due to the increased path length the suffered attenuation is notably higher for the bistatic case, thus limiting the maximum allowable separation.

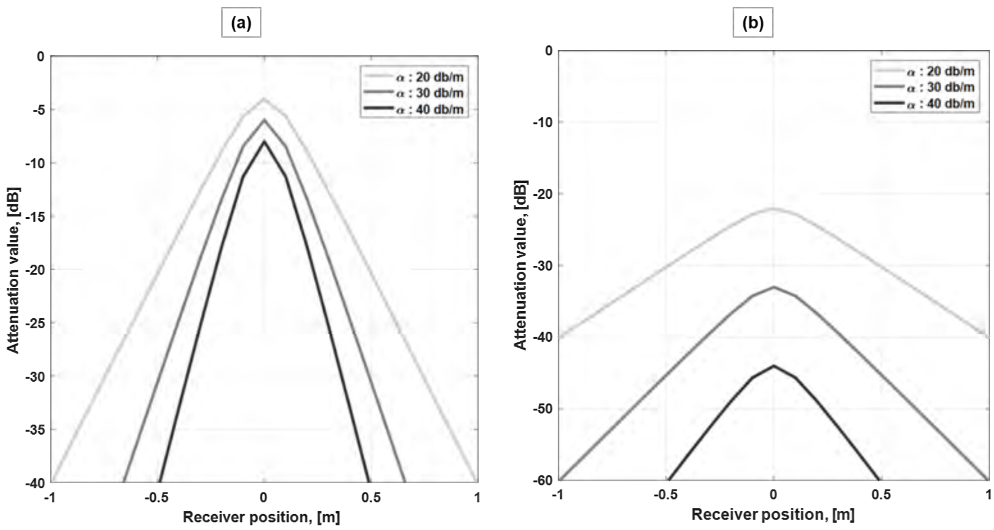

Figure 4.16: Modelled attenuation for (a) monostatic, and (b) bistatic system.

Essentially, this means that the dynamic range of the signals to be handled is reduced, because of the defined minimum range from the radar equation. As for the depth performance, the soil variability does not allow an accurate estimate of the maximum separation or of the optimum antenna separation for a unique target characterisation.

4.2.2.2 Target scattering

Bistatic scattering is subject to greater variability than the monostatic case, because there are more variables associated with the geometry, in particular as its definition additionally should include the dependency from the antenna separation. Although numerous mathematical formulations have been developed for retrieving the bistatic RCS from its monostatic equivalent, mostly based on the equivalence theorem, such methods have a number of assumptions that for GPR applications can't be met, especially for complex targets and for objects whose dimension is close to the wavelength.

Moreover, when the antenna offset is large compared to the depth of the targets, the small spread approximation (SSA) cannot be considered valid anymore and the reflection traveltimes cannot be approximated by simple hyperbolas [143].

These considerations apply obviously to every source of scattering, including clutter sources and scattering generated by anisotropic and heterogeneous soils. In addition, for air launched systems, the terrain roughness may represent another aspect to be considered.

4.3 GPR design for landmine internal structure detection

There are three principal differences in GPR system design between conventional GPR sensors and GPR sensors for landmine detection. First, the latter require a down-range resolution in the order of a few centimetres (in ground) to distinguish between reflection from a buried landmine and reflection from the air–ground interface. A down-range resolution of the same order is also required to distinguish between reflections from the top and from the bottom of a landmine, which is needed for target classification. Second, to avoid triggering of surface-laid or shallowly buried landmines, the antenna system of a landmine detection GPR sensor should be elevated above the ground. For a handheld system, the minimal elevation of the antenna system is of the order of a few centimetres, while for a vehicle-based sensor, such an elevation is typically several decimetres. Third, the requirement for GPR to support classification of detected targets requires considerably higher stability and accuracy of the reflected field measurements than that offered by conventional systems.

The variety of environmental conditions in which mines can be found is enormous. Minefields are not only ordered rows of landmines in flat deserts but can also be found among the debris of collapsed buildings and post-conflict urban and rural environments. The complexity of the framework brings several issues when evaluating the parameter of a GPR system for landmine detection.

There are three main parameters which influence frequency selection:

- Required resolution.
- Clutter limitations.
- Required penetration.

There is a trade-off between spatial resolution, depth of penetration and system portability. To overcome signal losses and increase range, the operating frequency can be lowered, but this reduces bandwidth, which is directly proportional to the resolution. High resolution is generally a desirable parameter, but a high resolution means a high clutter level. Hence this trade-off is one of the major challenges. Additionally, antenna size increases as the frequency decreases. For most of the currently employed GPR system, the solution has been found by choosing a central frequency in the range 500 MHz-3 GHz.

GPR, as well as many other EM techniques, is commonly operated very close to the surface, therefore it is possible that the far field assumptions may not hold. The propagation regions, which depend on the covered distance in wavelength, need now to be calculated considering the effective frequency that is propagating.

Fig. 4.17 presents the near field boundary for a number of frequencies and with varying dielectric properties of the subsurface.
It can be seen that for an average soil dielectric of 9 and a frequency range of 0.5 GHz to 2 GHz, the near field condition is dominant up to a distance of approximately 15 cm, from which it is evident that the target may very often be situated in this region, rather than in the far field one. Therefore, any consideration of the signal detected should fully account for the physical proximity of the antenna and target.

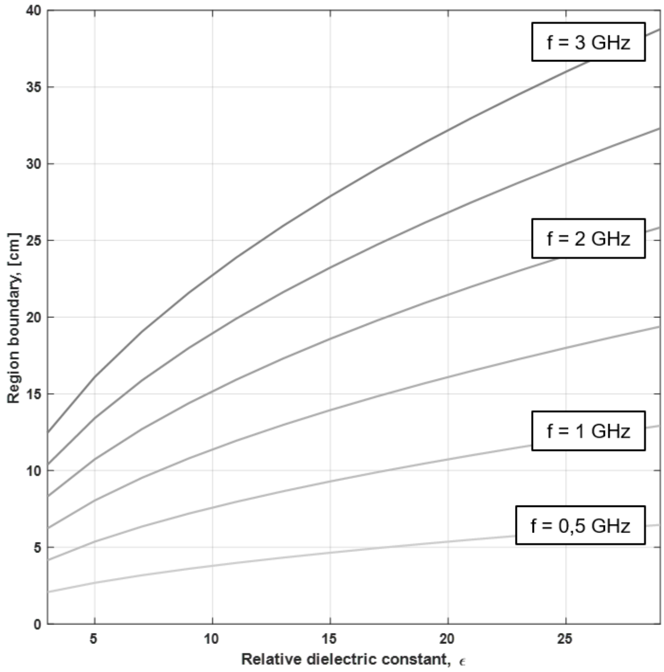

Figure 4.17: Near field boundaries for varying frequencies and dielectric.

First of all, propagation losses decrease at lower rates depending on the landmine dimensions for near field boundary conditions, and hence targets closer than that distance will have increased field contributions, resulting in greater signal levels from targets very close to the antenna (when in proximal operations). As soon as the antenna is moved further away the signal levels return to those of the induction fields. These considerations suggest that antennas for GPR applications should be designed to operate within the near field distance to optimise the received signal levels.

In addition, the boundary between the two regions is actually hard to predict and define, because of the small scale variability of the soil electrical properties. The RCS is usually defined in the far field. In this case, it is an intrinsic value of the object under test, totally independent of the radar antenna orientation and of the range of the radar from the target. These properties hold as long as the antennas maintain a sufficient distance from the object so that the transmitted wave appear locally planar at the object surface and the scattered waves appear locally planar at the receiver. For the much shorter ranges involved with GPR, the near-field case presents an object that has a significant angular extension as seen from the antenna. In this situation, there are ambiguities in defining its expression.

Several works have addressed the issue of converting a far field RCS to a near field one, but still the unpredictable electrical properties of the subsurface may frustrate the attempts.

4.3.1 Detection of the landmine internal structure

Detecting the internal structure of a landmine means detecting a signal that is repeatedly reflected and transmitted as shown in Fig. 4.18(a).

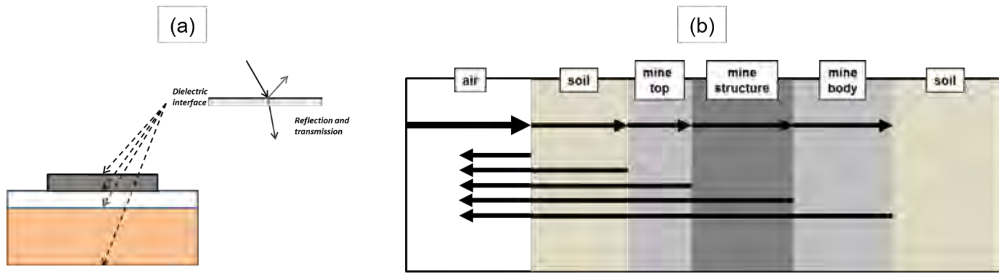

Figure 4.18: Addressed scenario. (a) Schematic diagram, and (b) transmission line scheme. Dimensions are deliberately exaggerated.

Moreover, it should be taken into account that the scattering event generated by the internal structure should reach the receiver antenna with enough strength to be detected (Fig. 4.18(b)). It is inherent that a suitable resolution is needed for a reliable detection and identification, otherwise some of the components might be missed. This will be evaluated later in this Chapter.

From Fig. 4.18(b) it is also possible to visualise why a bistatic approach could lead to a better signature characterisation. Each interface that is depicted has its own scattering characteristic, in terms of transmission and reflection angles, therefore a system capable of exploiting the angular diversity can offer significant advantages.

4.4 System modelling

Of all the current research areas in GPR, numerical modelling is arguably one of the most popular, with increasing numbers of publications containing some form of numerical modelling in their content.

Advancing beyond the stage of detecting underground features using GPR into trying to extract specific information about the nature, type, size, location and other characteristics of GPR targets, one runs into difficulties.

GPR modelling is critical for the following reasons:

- Understanding of physical behaviour and quantifying response.

- Providing performance requirements for design of measuring instruments.
- Predicting response and sensitivity to parameter changes.
- Optimising survey design.
- Enabling interpretation at a variety of levels of complexity.
- Facilitating mathematical inversion and quantification of interpretation uniqueness.

In summary, modelling underpins translation of geophysical observations into useful information (knowledge).

The extraction of such information from GPR data is not often a simple process, mainly due to the complexity of the factors involved in the GPR detection mechanism. Interpretation of GPR data can be assisted and improved with the aid of a model which will provide a close approximation to the response of GPR to subsurface targets and it will provide the means of studying the effects of the lossy environment, in which they are located, on the GPR signals.

In general, electromagnetic simulations are very helpful for achieving an in-depth understanding of the underlying physical concepts, because it is possible to study the effect of different parameters of the GPR system systematically.

The sophistication, size, and accuracy of GPR models have accelerated over the last years as computational resources have improved and become more accessible. All this, has made numerical modelling a useful and widely appealed approach to the GPR problem.

4.4.1 Computational methods comparison

GPR geometry can be studied from a simple single frequency evaluation of path losses to complete 3D time domain descriptions of each physical layer of GPR and its environment.

Under the condition that EM waves propagate in the high frequency regime, such that displacement currents dominate, and that the electrical conductivity of the subsurface medium is sufficiently small, one can consider that EM wave propagation within the subsurface has kinematic properties similar to rays, hence being along ray paths defined by Snell's law. Under these circumstances, GPR waveforms can be simply and effectively simulated based on the ray theory. Reflection and transmission coefficients are defined from the dielectric permittivity contrasts at each interface. This allows to study GPR issues by geometrical ray theory.

The formal mathematical representation of the electromagnetic fields, which is used to build the modelling procedure, could be directly Maxwell's equations in differential or integral forms, or equivalently the vector wave equations, or any other formulations directly related to Maxwell's equations or the vector wave equations. The choice of a differential or an integral formulation leads to numerical methods known as differential equation methods (DE) or integral equation methods (IE) respectively.

Equally important in the formulation stage of the problem is the decision about the domain of the formulation. When time is explicitly present as a variable, the numerical methods are characterized as time domain methods (TD) whereas, if a time harmonic variation of the electromagnetic fields is assumed, the numerical methods are characterised as frequency domain methods (FD).

In general, time domain methods are most suited for problems when the transient response is of interest, whilst frequency domain techniques are mainly used when the steady-state response is required. Clearly, since most GPR systems employ signals of wide bandwidth and operate in the time domain, a time domain model will be more suitable than a frequency domain one. This will save in computational effort since the transient solution will be calculated directly instead of having to calculate the response of the same model for a number of frequencies and then use an inverse Fourier transformation to obtain the required time domain response.

The choice of a differential equation based model instead of an integral equation approach is justified in general by the ability of the first method to handle inhomogeneous problems more efficiently than the latter one. Moreover, since a half space Green's function is not available in closed form, an IE approach will not result in a more computationally efficient model. Overall the simplicity of a DE model makes it more appealing when compared with the more complicated IE methodology.

The most basic model is that of the Transmission Line Matrix method (TLM), which is essentially a computer implementation of an electrical network model used for the solution of an electromagnetic field problem. This electrical network is constructed as a mesh of orthogonal two-wire transmission lines. Each layer is modelled as an equivalent impedance and the propagation of voltage and current pulses in the

TLM network simulate the propagation of electric and magnetic fields in the actual electromagnetic problem. Moreover, the constitutive parameters of the media present in the electromagnetic problem are simulated by transmission line parameters.

The Method of Moments (MoM) [245] is a frequency domain method which discretises the surface of the source to solve current density or charge density. Once these are known, the radiated or scattered fields can be found using the standard radiation integrals. These integral equations can be used for both radiation and scattering problems. And since MoM involves expanding the currents, which are restricted to a finite domain, instead of the fields, which may extend to infinite, it is convenient for open domains. The MoM technique essentially transforms a general operator into a matrix equation which can be solved easily on a computer. However, for many problems, the technique is significantly computationally less efficient than volume-discretisation methods, as it usually gives rise to fully populated matrices. This means that the storage requirements and computational time will tend to grow according to the square of the problem size.

The Finite Difference Time Domain (FDTD) [246] approach is a numerical method which provides a solution to Maxwell's equations, expressed in differential form, in the time domain. The method is based on the discretisation of the partial derivatives in Maxwell's equations using central differencing. The resulting difference equations are used in a time marching iterative procedure to obtain the required solution. The strength of FDTD modelling is its ability to calculate the response of the system over a wide range of frequencies from a single simulation.

4.4.1.1 Assumptions and approximations of models

According to George E.P. Box, FSR [247]:

> "Is the model true?". If "truth" is to be the "whole truth" the answer must be "No". The only question of interest is "Is the model illuminating and useful?"

Although varied in their individual approaches, they all attempt to simulate the propagation of the GPR wave from the surface downwards with the emphasis on the interaction of the electromagnetic wave with the subsurface materials. Therefore, the ability of realistically represents the true 3D geometry and structure of both subsurface targets and the GPR antennae becomes of vital importance.

Analytical modelling can be applied under simplified hypotheses on the nature of the problem, resulting in problem specific solution. For example, the aforementioned radar equation enables an estimate of the received signal level and related detection performance, but it has significant weaknesses in that most GPR systems are operating in the near field and in bistatic mode, whereas the model assumes a far field model.

On the other side, more sophisticated numerical modelling can deal with the complex geometry and its boundary conditions, but they often suffer from low computational efficiency leading to difficulty in real time implementation.

In constructing a GPR model in two and three dimensions, some assumptions are necessary. These mainly result from the need to keep the amount of computational resources, required by the model, to a manageable level and to facilitate the study of the important features of the GPR response to a target, without cluttering the solution with details which can obscure the fundamental response. However, the approach followed should ideally be easily extendable and able to handle more ”complicated” GPR modelling scenarios if required. This trade-off between sophistication and usefulness is strongly bounded to the problem to be solved.

4.4.2 Finite Difference Time Domain scheme

The FDTD technique has become one of the most common modelling methods particularly due to the increase in accessible and inexpensive computational resources. There are different FDTD formulations, but there are a number of key common elements [248].

The FDTD approach to the numerical solution of Maxwell's equations is to discretise both the space and time continua. Therefore, the choice of cell size $(\Delta x, \Delta y, \Delta z)$ is critical when employing the FDTD technique - it must be small enough to permit accurate results at the highest frequency of interest, and yet be large enough to keep resource requirements manageable. For instance, the higher the permittivity or conductivity, the shorter the wavelength at a given frequency and the smaller the cell size required.

To understand why the cell must be smaller than one wavelength, consider that at any particular time step the FDTD grid is a discrete spatial sample of the field distribution. From the Nyquist sampling theorem, there must be at least two samples per spatial period (wavelength) in order for the spatial information to be adequately sampled. Because the smallest wavelength may not be precisely determined, more than two samples per wavelength are required. In addition, another important factor is the error associated with numerically induced dispersion, inherent in the discretisation process. Contrary to the real world where electromagnetic waves propagate with the same velocity irrespectively of their direction and frequency (assuming no dispersive media and far field conditions), waves of different frequencies will propagate at slightly different velocity through the grid, causing a dispersion error. Another cell size consideration is that the important characteristics of the problem geometry must be accurately modelled [249].

Hence, the FDTD model represents a discretised version of the real problem and is of limited size and its building block of this discretised FDTD grid is the Yee cell [250], illustrated in Fig. 4.19.

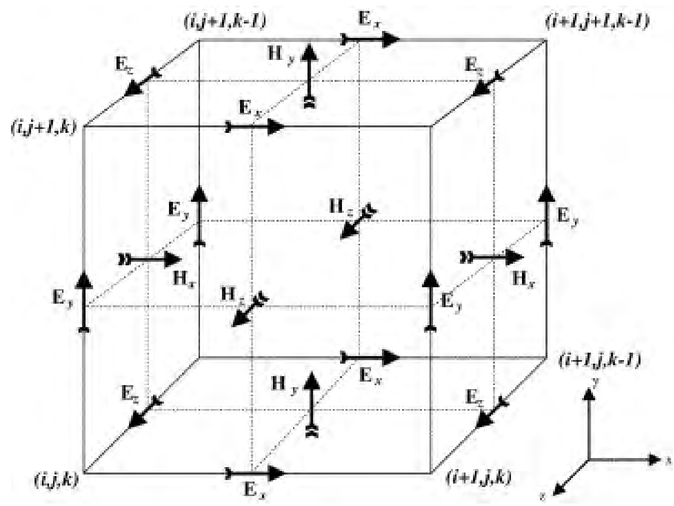

Figure 4.19: The Yee cell.

By assigning appropriate constitutive parameters to the locations of the electromagnetic field components complex shaped targets can be included easily in the models. However, objects with curved boundaries are represented using a staircase approximation, which may cause significant errors.

The numerical solution is obtained directly in the time domain by using a discretised version of Maxwell's curl equations that are applied in each FDTD cell in an iterative fashion. In each iteration the electromagnetic fields advance in the FDTD grid and each iteration corresponds to an elapsed simulated time of Δt. The price to pay for obtaining a solution directly in the time domain using the FDTD method is that the spatial and temporal discretisation steps can't be assigned independently. As the FDTD is a conditionally stable numerical process, the maximum time step is bounded by the values of $\Delta x, \Delta y, \Delta z$ and determined by the Courant stability condition [251] (Eq. 4.23):

$$\Delta t \leq \frac{1}{c\sqrt{\frac{1}{\Delta x^2} + \frac{1}{\Delta y^2} + \frac{1}{\Delta x^z}}} \tag{4.23}$$

where c is the speed of light in the medium. The stability condition for the 2D case is easily obtained by letting $\Delta z \rightarrow \infty$. Smaller steps do not generally result in computational accuracy improvements, while larger ones result in instability. In fact, when the equality holds, the discretised wave most closely approximates the actual wave propagation, and grid dispersion errors are minimised. However, exceptions to this occur. Even if the stability step is set by the speed of light in free space, and hence by the maximum velocity of propagation in any medium, for conducting materials stable calculations may require time steps smaller than the Courant limit, as well as for nonlinear materials.

The nature of the GPR forward problem classifies it as an initial value open boundary problem. That means that in order to obtain a solution one has to define an initial and allow for the resulting fields to propagate through space reaching a zero value at infinity because there is usually no specific boundary limiting the problem's geometry where the electromagnetic fields can take a predetermined value.

Therefore, one of the most challenging issues in modelling open boundary problems, such as GPR, is the truncation of the computational domain at a finite distance from sources and targets where the values of the electromagnetic fields cannot be calculated directly by the numerical method applied inside the model. Hence, an approximate condition known as absorbing boundary condition (ABC) is applied at a sufficient distance from the source to truncate and therefore limit the computational space [252]. The role of this ABC is to absorb any waves impinging on it, hence simulating an unbounded space. The only reflections which will originate at the truncation boundaries are due to imperfections of the ABCs and in general are of very small amplitude compared with the reflections from target inside the model. Clearly, the computational space limited by the ABCs should contain all important features of the model such as sources and output points and targets, as shown in Fig. 4.20.

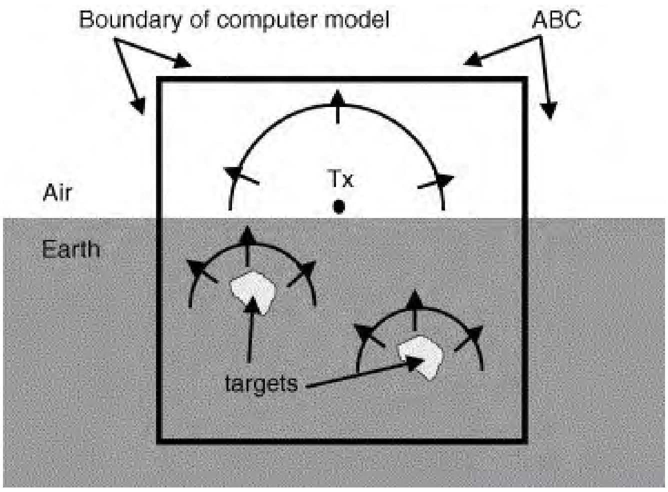

Figure 4.20: FDTD view of the model's space.

The FDTD method offers many advantages as an electromagnetic modelling tool over other numerical techniques in that :

- The solution is obtained with a sequential procedure and is very well suited for computer implementation.
- The method is very general and simple in nature, its implementation is robust and could handle complex problems.
- The formulation is entirely in the time domain and therefore is particularly suited to transient problems. A frequency domain approach would require the solution procedure to be repeated for a large number of frequencies in order to be able to perform a Fourier transformation.
- It can incorporate material property changes without the need to alter the mathematical description of the scheme.
- It can include arbitrary, 3D subsurface geometries, complex material features and sophisticated antenna designs by the use of different grid types and layouts.
- It does not require the solution of Green's functions.

In summary, the strengths of the FDTD method are that it is a simple, fully explicit, general, and robust technique. To this list can be added the advantage of computational efficiency for large problems in comparison with other techniques such as method of moments, especially when broadband results are required. The main weakness is due to the fact that the entire computational domain must be discretised which can require extensive computational resources.

4.4.2.1 Software description

The FDTD solver used in this section is gprMax, which is an open-source software that simulates electromagnetic wave propagation for numerical modelling of GPR, available at http://www.gprmax.com. gprMax was firstly introduced in 1996 and designed for modelling GPR but can also be used to model electromagnetic wave propagation for many other applications [253]. gprMax is principally written in Python 3 with performance-critical parts written in Cython. It includes a CPU-based solver parallelised using OpenMP, and a GPU-based solver written using the NVIDIA CUDA programming model. gprMax uses a text-based input file in which users specify all of the parameters for a simulation, e.g., model size, discretisation, time window, geometry, materials, and excitation, via pre-defined commands [254].

Compared to some widespread commercial software, such as the computer-aided design (CAD) tool CST Microwave Studio Computer Simulation Technology (CST, http://www.cst.com), gprMax provides similar performance and sufficient features for GPR simulation. In addition, although a CAD-based GUI is useful for creating single simulations it becomes increasingly cumbersome for a series of simulations or where simulations contain heterogeneities. Embedding the python script into a model enables more flexibility, automation and extensity. gprMax allows anisotropic objects to be modelled in a simulation, as well as dispersive materials and soil topography modelling, which may be difficult to replicate through a CAD environment. Another feature to be considered is the fact that in CST the near field response can be obtained only through the inclusion of a realistic antenna model, which may become overly expensive.

4.4.3 Forward modelling

A number of simulations have been carried out to get a preliminary insight of the effects that the presence of a components within the target has on the radar signature, at the same time to provide a basis for the following experimental campaigns.

A 2D simulation is achieved by specifying a computational domain that has only a single cell dimension in one direction (that direction is considered the infinite direction), solving the transverse-magnetic mode with respect to the z-direction (TMz). In this case a theoretical Hertzian dipole source fed with a Ricker waveform with amplitude equalling 1 V is used to simulate the GPR antenna. The corresponding radiation pattern shape, which is not a function of the radial distance, is a circular section toroid shaped and symmetrical about the axis of the dipole.

The simulation parameters are detailed in Table 4.6:

Table 4.6: Model set-up

Parameter	Value
Spatial discretisation ($\Delta x, \Delta y, \Delta z$)	0.1 - 0.05 - 0.1 cm
Domain size	50 x 80 cm
Number of cells	8e5
Antenna separation	6 cm
Time window	12 ns
Time step (Δt)	0.0015 ns
Number of iterations	8045

In this scenario, a landmine-like target is modelled including both the activator or pressure plate and the internal structure, commonly sketched as a thin air layer located between the activator and the main body of the mine. The target is 8 cm wide and 6 cm height. The relative dielectric for the activator is 7, while the explosive is considered to have a dielectric of 3. The soil is simulated as a homogeneous material.

The configuration is pictured in Fig. 4.21. The two points above the soil are the transmitter and receiver antenna that are polarised orthogonal to the plane of the page (z polarity)

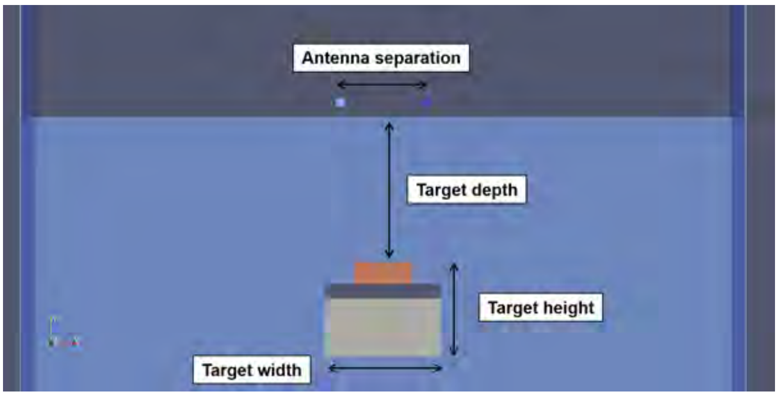

Figure 4.21: Geometry of the gprMax model.

This section will consider the effects of a range of key parameters to show their impact on the detection performance. These variables include the bandwidth of the excitation source, its height above the ground, the physical design of the object and the soil attenuation. The range of variables is listed in Table 4.7.

Table 4.7: Simulation variables

Parameter	Value
Source bandwidth	0.5 - 1 - 1.5 - 2 - 2.5 - 3 GHz
Source height	1 - 6 - 11 - 16 - 21 cm
Internal air layer	0 - 1 - 2 - 3 cm
Pressure pad	1.5 - 2.5 cm
Target depth	5 - 15 - 25 cm
Soil texture	low loss - high loss

The aim of such a process is to give evidence of the impact that the characteristics of the excitation, environment and target have on the resulting signature.

4.4.3.1 Bandwidth evaluation

As previously anticipated, a proper signature characterisation is only possible when the achievable resolution is high enough to separate each component of the modelled landmine-like target. Therefore, the first set of simulations involves the assessment of the bandwidth boundary for being able to detect the internal components of a mine. In the section the fractional bandwidth is considered to be 1, therefore the terms ”central frequency” and ”bandwidth” are interchangeable.

The same scenario which has been previously described is employed, and the source frequency is varied according to Table 4.7. Modelled soil is a sand-like material with a relative dielectric of 4.5, while the target is located 10 cm below the surface. With such a configuration, the velocity dispersion error is less than 1% and the wavelength is sampled by 12 cells, obeying the rule of thumb of a tenth of the wavelength.

The computed time domain signatures of a landmine-like target with varying bandwidth are shown in Fig. 4.22.

First of all, it can be noted that a low frequency source does not allow the separation of the mine reflection from the background one, impeding the detection of very shallow targets. This effect is also a consequence of the soil texture, as the ground reflection pattern depends on the dielectric properties of the subsurface. Instead, a wider bandwidth is capable of discriminating even thinner layers.

The late signal perturbation visible in the radar signatures can be associated with multiple reflection events generated by the ground ringing, as they appear as highly attenuated and delayed replica of the target response.

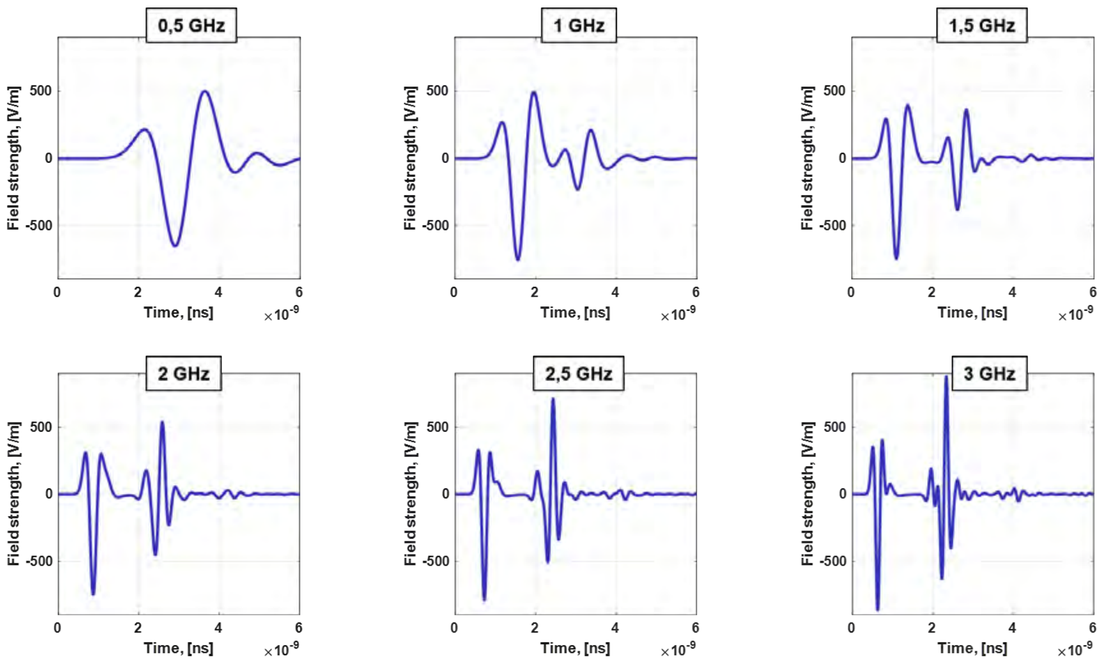

Figure 4.22: Time domain signature of a buried landmine with varying source bandwidth.

These considerations are evident after a background subtraction, shown in Fig. 4.23.

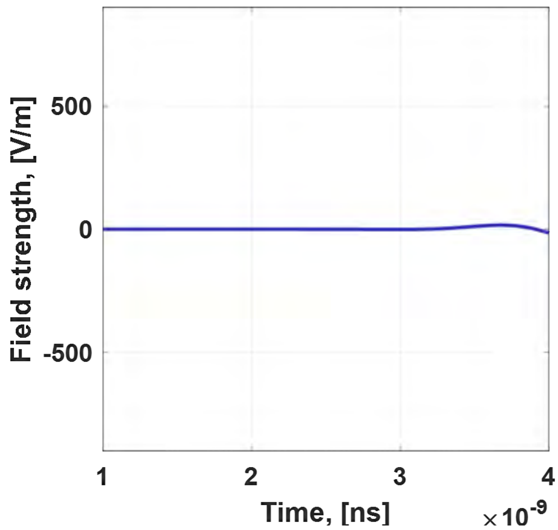

Figure 4.23: Simulated response from a 500 MHz bandwidth source after background subtraction.

As long as the bandwidth does not reach 2 GHz, the target is detected as a single reflection, due to an insufficient resolution of the different landmine components. At this boundary, highlighted in Fig. 4.24, three separate events can be identified: the upper part of the landmine (marked A in Fig. 4.24), a sharp reflection after it (marked B in Fig. 4.24) and a weak response indicating the bottom of the target (marked C in

Fig. 4.24).

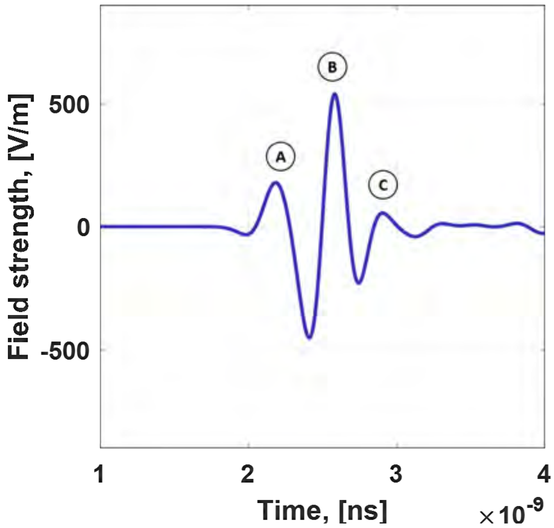

Figure 4.24: Simulated response from a 2 GHz bandwidth source after background subtraction.

The reflection belonging to the bottom of the target appears as a very weak reflection due to (1) the limited impedance contrast between the explosive ($\varepsilon_r = 3$) and the sandy soil ($\varepsilon_r = 4.5$), and (2) the reduced signal amplitude caused by the strong earlier neoprene/air interface reflection.

A wider bandwidth is not only able to describe the complexity of the target, but is also capable of fully resolving the upper activator pad, due to the improved resolution of the wave. In this case the resulting radar signature includes the reflections generated by both the top and the bottom of the layer (shaded region in Fig. 4.25).

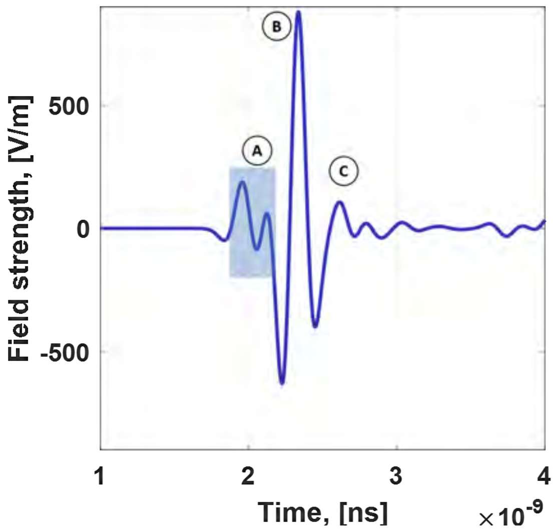

Figure 4.25: Simulated response from a 3 GHz bandwidth source after background subtraction.

Moreover, the signature confirms the considerations made on the characteristics of the bottom reflection, as it can be seen that the resulting reflections shown appear closely similar. Due to its high velocity characteristic, a correct geometrical reconstruction of the air layer would be hardly achievable, as its thickness would probably be consistently larger than the resolution performance.

A useful way to visualise what has been described and for a better understanding of the physical reasons beyond the results is the representation of the propagating wavefield, shown in Fig. 4.30. for different bandwidth. Each snapshot has been numerically computed at the same time instant.

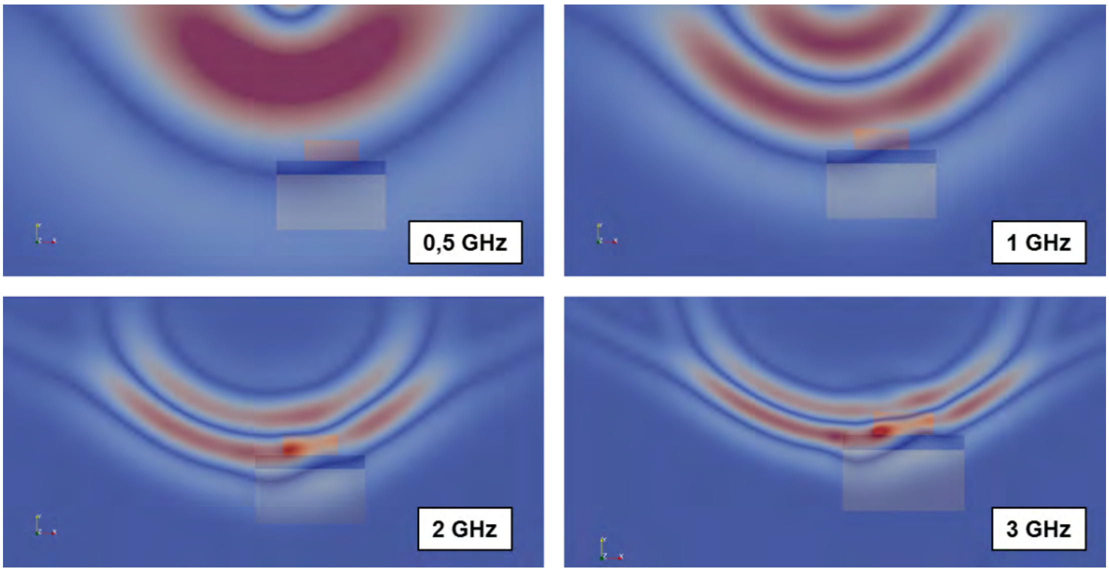

Figure 4.26: Snapshots of the E field with varying bandwidth.

The wider the bandwidth, the shorter the wavelength and hence the shorter the distance between two subsequent wavefronts. The consequence is what has been described before, the inability of narrow bandwidth of discriminating between closely spaced features. This is evident if one looks at the modification of the pattern of the wavefront produced by the target.

4.4.3.2 Antenna height

As previously discussed, the antenna height above the ground is a critical factor, both concerning the design of the GPR platform and the quality of the collected data. Recalling the described concept, it is clear that a stand-off radar system might represent a reasonable choice when surveying a minefield, but the impact of elevating the antennas on the reflected signal strength must be evaluated.

Considering a central frequency of 2 GHz, the source has been progressively elevated from the ground according to Table 4.7, in order to assess the influence of the parameters on the target radar signature. As before, a fixed scenario has been maintained, in therm of soil properties and target depth.

The resulting signatures, plotted in the A-scan mode and normalised by the maximum value of the closest situation (height of 1 cm) are presented in Fig. 4.27.

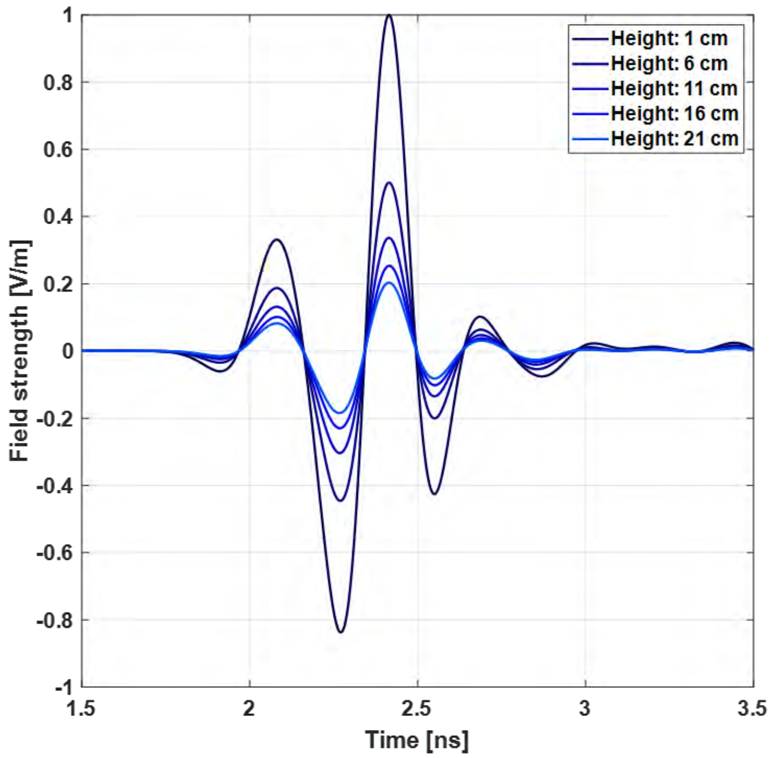

Figure 4.27: Time domain signature of a buried landmine with varying source height above the ground.

All the graphs show that the target response reduces as the height of the antenna is increased, with the most significant losses occurring in the first steps, i.e. just detaching the antenna from the ground. In this region, approximately, half of the amplitude is lost, as described in Fig. 4.28.

Obviously, the reflection generated by the bottom of the landmine, which is the weakest contribution, is marginally affected by the loss of strength as it occurs after the air interface, boundary causing a marked signal reflection, thus even in favourable conditions the amount of energy reaching the bottom of the target is limited.

Then, the signal strength suffers a less pronounced reduction, but still the limited amplitude may lead to a signal below the sensitivity of the system.

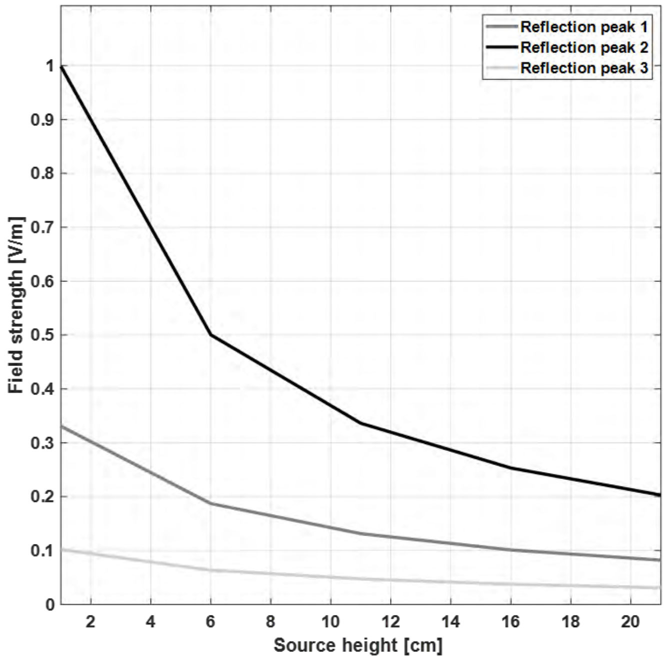

Figure 4.28: Comparison between reflection peaks magnitude and source height

It is clear that for high loss propagation environment these patterns and signal reductions will be emphasised, as well as when increasing the depth of the mine as the path attenuation will become higher.

However, the internal scattering contribution remains a clearly detectable event, even if its prominence vanishes with the antenna elevation, as it can be noticed that the spread among the reflection peaks is visibly reduced. This concept is described in Fig. 4.29.

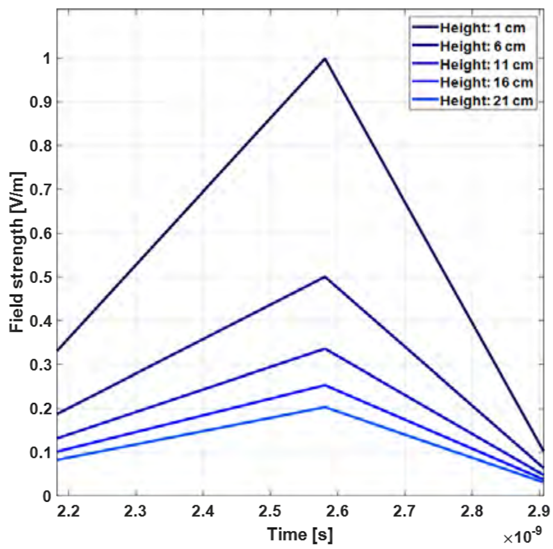

Figure 4.29: Comparison between reflection peaks spread.

Consequently, the information is that the nearer to the ground the source is, the stronger the reflected signal will be.

4.4.3.3 Target parameters evaluation

From the previous analysis, it can be assumed that a close proximity with the ground and a minimum bandwidth of 2 GHz are requisite to ensure a proper internal structure detection. The logical step ahead is to evaluate the target physical parameters that may modify the signature of the target and weight their impact on its pattern. Nominal values are listed in Table 4.8.

Table 4.8: Target design: model set up

Parameter	Value
Source bandwidth	2 GHz
Source height	1 cm
Soil relative dielectric	4.5
Target depth	10 cm

For a proper assessment of the results when altering the target design, its total vertical size has been maintained.

Air layer effect The first step is an investigation of the weight of the effect of the internal air layer on the target signature. The principal reason is to prove the importance of employing objects closely resembling the real devices, and not simpler surrogates.

The analysis compares a solid, homogeneous mine-like target and one with a progressively thicker air layer (Fig. 4.30).

From the graph it is possible to make the following considerations:

- A solid dielectric target shows the top and bottom reflection only, without any variations in the signature. The low signal level is due to the small contrast between the target and the surrounding soil.
- The presence of the internal air gap produces a significant modification of the pattern of the signature.
- Increasing the thickness of the air layer does not alter the shape, but contributes to the magnitude of the internal reflection peak.

When the thickness of the air layer becomes relevant, a variation in the temporal extension of the target can be noted, due to the propagation in a faster medium. However, as

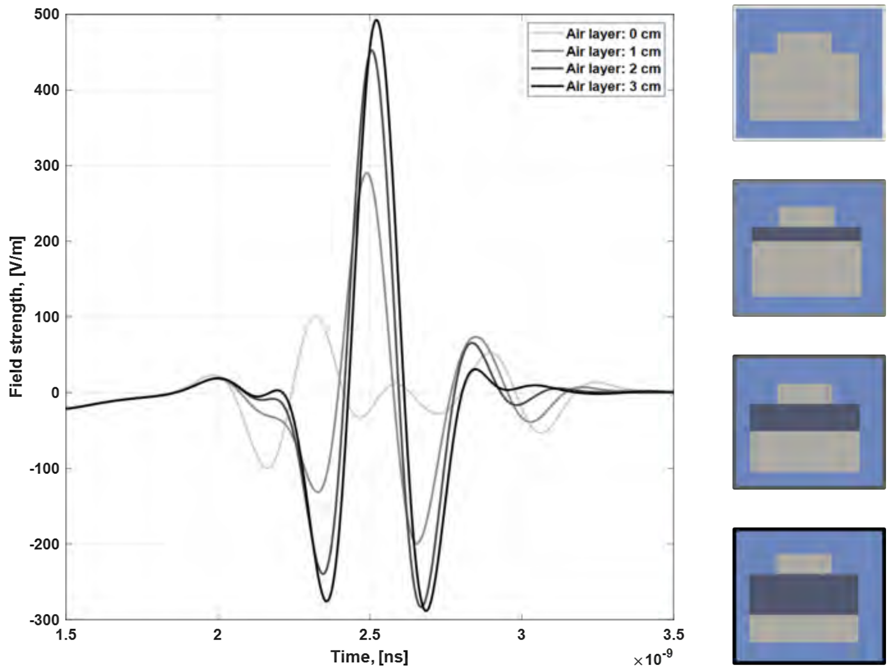

Figure 4.30: Comparison between internal air layer thickness.

the velocity of propagation in the air layer is high, even a 3 cm layer is not completely resolvable, due an insufficient vertical resolution.

These considerations confirm that the presence of the air layer is beneficial for the detection of minimum metal landmines with GPR, as the reflection generated by this layer are clearly stronger than the other components of the target signature.

Activator plate effect The second aspect that has been analysed is the effect produced by the upper activator plate. What is expected is (1) a stronger reflection due to a higher impedance contrast, and (2) a different signature shape, probably resembling the one previously obtained, as the lower boundary of the activator plate coincides with the upper boundary of the air gap.

The comparison between a solid target and the described one is provided in Fig. 4.31.

The graph confirms what was expected, in particular regarding the variation in the signature shape. Moreover, in this case the target response is longer in time, due to the fact that the wave travels through a slower material. Finally, it is worth noting that in this case the reflected wave experiences a reverse in polarity compared to the correspondent homogeneous target, as a consequence of the change in the sign of the reflection coefficients. It can be also noticed

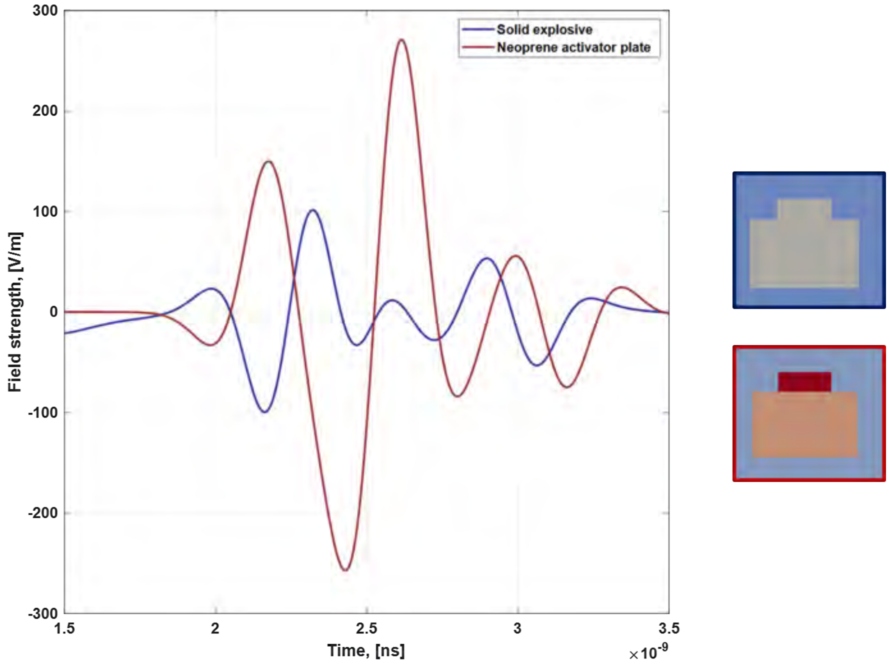

Figure 4.31: Comparison between presence and absence of the activator plate.

As the vertical resolution is related to the size of the feature compared to the wavelength, a wider activator enables the wave to generate a reflection for both the top and the bottom of the layer, as shown in Fig.4.32.

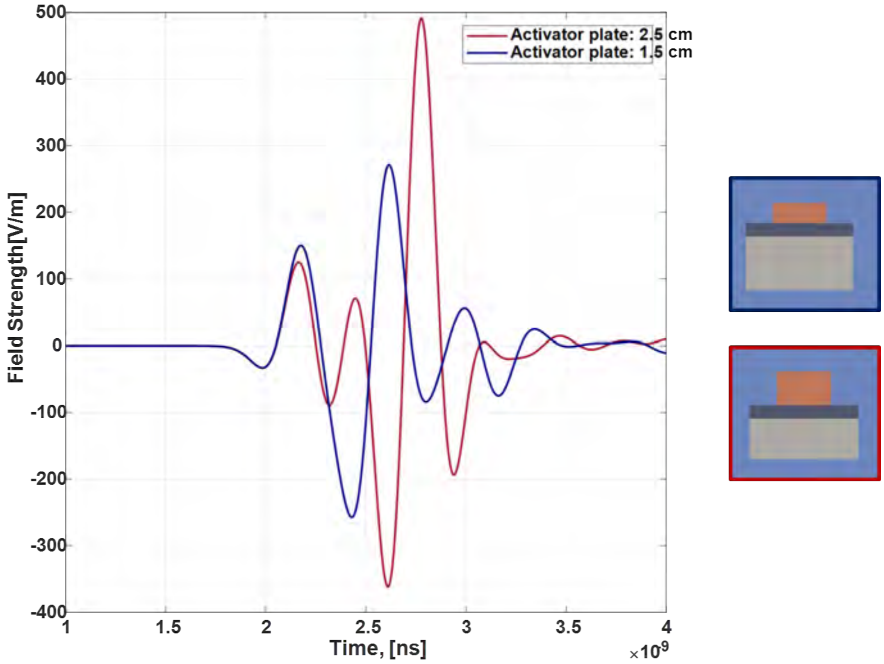

Figure 4.32: Comparison between activator plate thickness.

Except for this, no additional modifications are produced by a thicker activator plate.

Combined effect The last results may cast some doubts on whether the additional reflection visible in Fig. 4.32 is generated by the air layer or by the activator plate. To remove any uncertainties, the combined effect of these parameters has been evaluated. In particular, the activator plate size is kept constant, while the air layer is progressively increased to verify the responsible of the internal peak. Results are shown in Fig. 4.33.

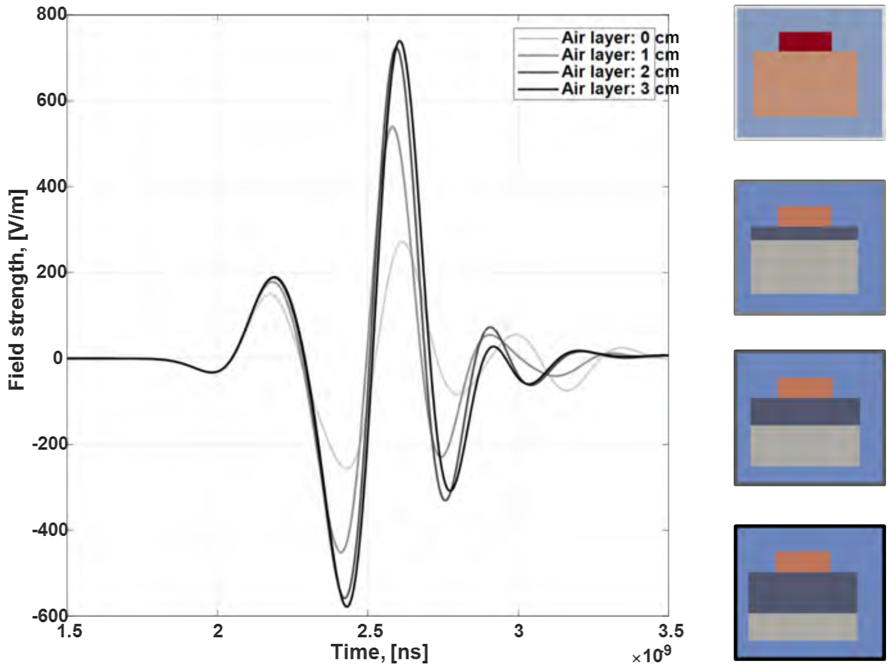

Figure 4.33: Comparison between internal air layer and activator plate.

The resulting signatures show that the two effects are indeed almost coincident, but a significant difference in the magnitude of the reflection exists. Whichever way one considers the result, it is evident the need for a precise and accurate target design.

As before, the representation of the propagating field for the full landmine model and for a solid object is provided in Fig. 4.34, in which a set of 0.1 ns snapshots has been extracted starting from 1 ns to 3 ns.

Two main aspects can be highlighted: (1) the strongest reflection is generated by the air layer, and (2) the effects on the shape of the wavefront. In particular, the modifications are a function of the layer permittivity and size, therefore a complex shape variation can be noted. Conversely, the propagation through a homogeneous dielectric target does not affect the spherical pattern in the same complicated way, as can be seen in the right-column frames.

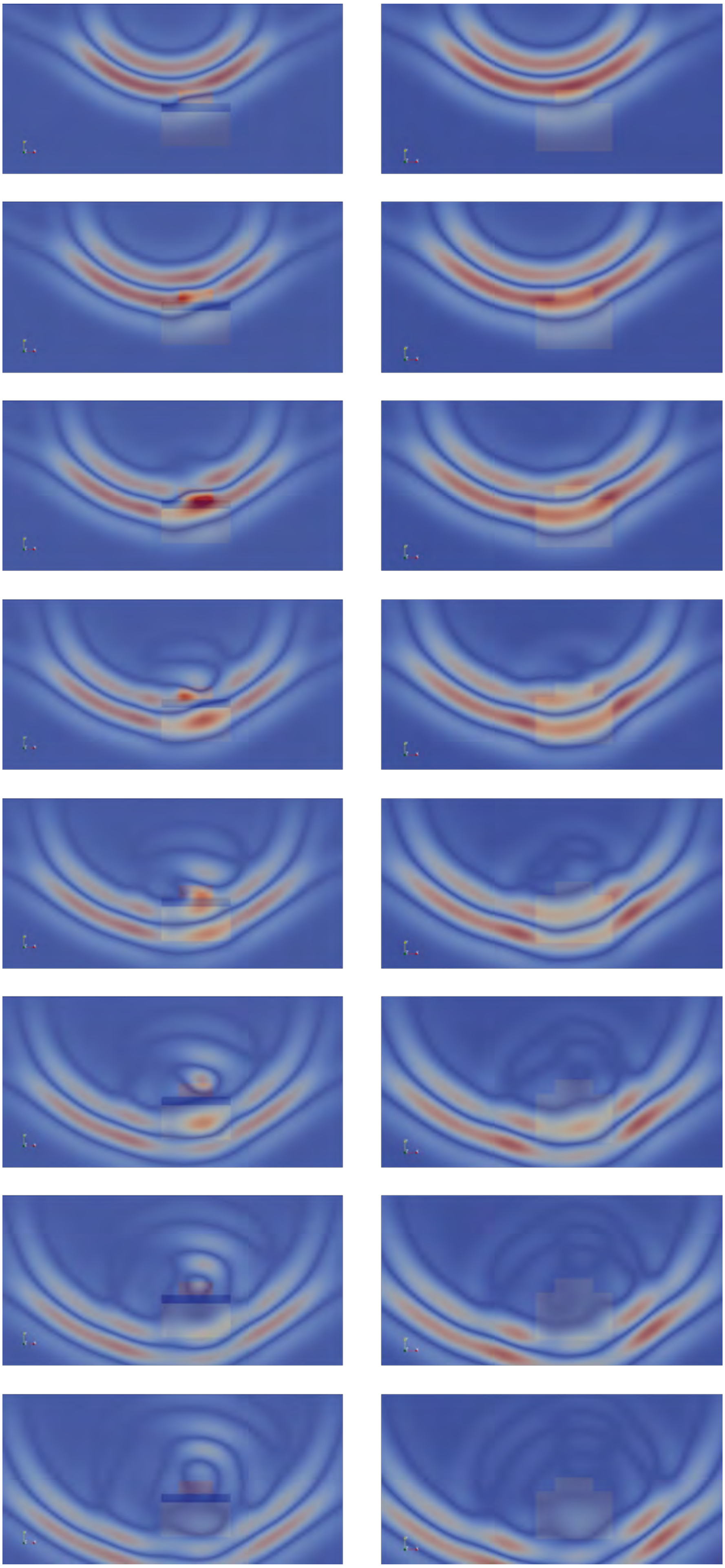

Figure 4.34: Snapshots of the E field for a landmine-like target (right column) and a solid object (left column).

4.4.3.4 Target depth and soil impact evaluation

Having demonstrated the impact that the target design has on its signature, the last section is dedicated to a brief assessment of the extensibility of the approach, investigating the effect of the target depth and soil attenuation characteristics.

To verify the reliability of the strategy two different scenarios have been simulated. The first one describes a highly beneficial situation in which a landmine is covered by a sandy material with an attenuation of approximately 10 dB/m, while the unfavourable case is described by a high attenuation soil, represented by a material with a higher moisture level and a higher clay content, with attenuation coefficient of 30 dB/m. The two situations represent two representative environments in the landmine contamination framework. Details of the soil properties are given in Table 4.9.

Table 4.9: Target design: model set up

Parameter	Value
Soil dielectric (ε)	Low loss: 4.5 High loss: 20
Soil conductivity (σ)	Low loss: 0.01 S/m High loss: 0.05 S/m

There were three guiding principles behind this design decision. Firstly, the choice of the geophysical parameters determining the heterogeneity of the target may be hard to define. Secondly, modelling a heterogeneous/nonlinear/dispersive material would bring additional variables at that point would need a deeper exploitation. Lastly, a complex environment makes the interpretation of the resulting signatures difficult, as it will be hard to clearly separate and characterise the effects of soil attenuation and scattering losses.

The soil effect is essentially of placing a window across the aperture, trimming the spectrum and deteriorating the maximum resolution, which is dependent on the maximum propagating frequency. Therefore, as the strategy is to determine the nature of a buried object whether or not there are scattering contributions from the internal structure, it is more useful and noteworthy to test if the internal reflections previously characterised appear also for a more hostile environment.

Three depths have been investigated covering the typical range of antipersonnel landmine location. In particular, a shallower situation in which the target is buried at 5 cm, a depth close to the UN standard requirement (15 cm) and a third one in which a deeply buried mine has been considered (25 cm). Fig. 4.35 shows the geometry of the model.

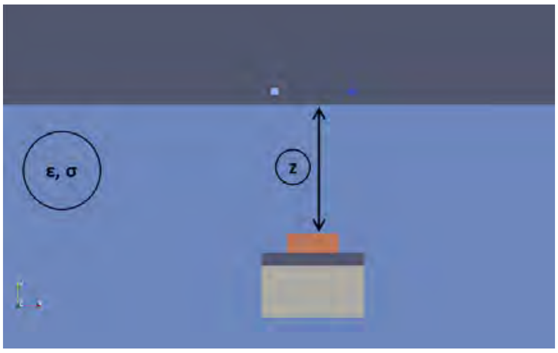

Figure 4.35: Geometry of the gprMax model.

Results from the low loss scenario, characterised by an attenuation factor of approximately 10 dB/m, are provided in Fig. 4.36.

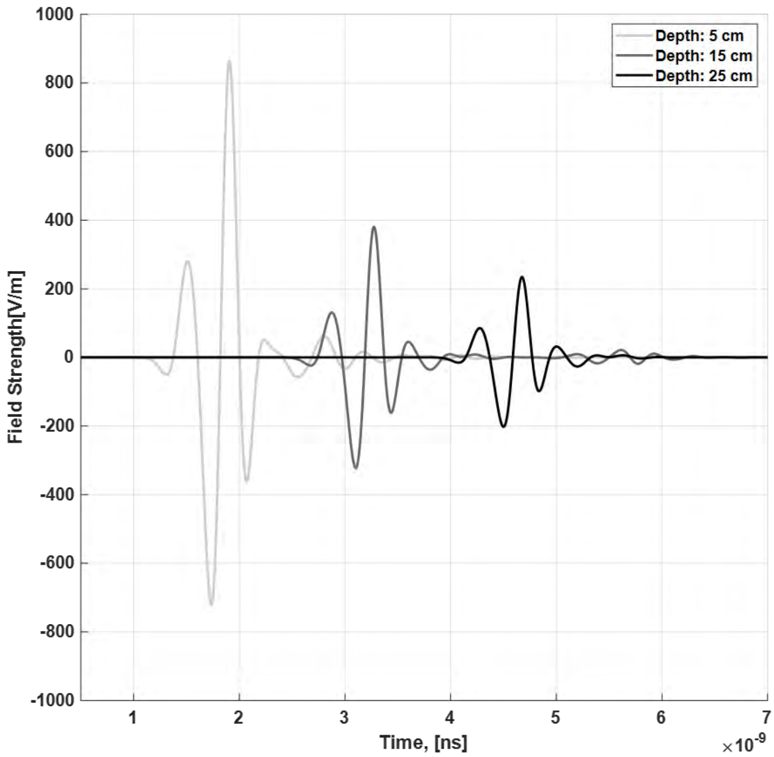

Figure 4.36: Comparison between landmine depths for a low loss scenario (α = 10 dB/m).

As expected, all the simulated signatures show the internal air layer reflection, regardless the burial depth, and their correlation is very high, as no significant modification of the shape are visible. The trends of the signal are in agreement with the well-known exponential decay related to the attenuation coefficient.

Results from the simulation of a soil with a higher attenuation coefficient (approximately 40 dB/m) are illustrated in Fig. 4.37.

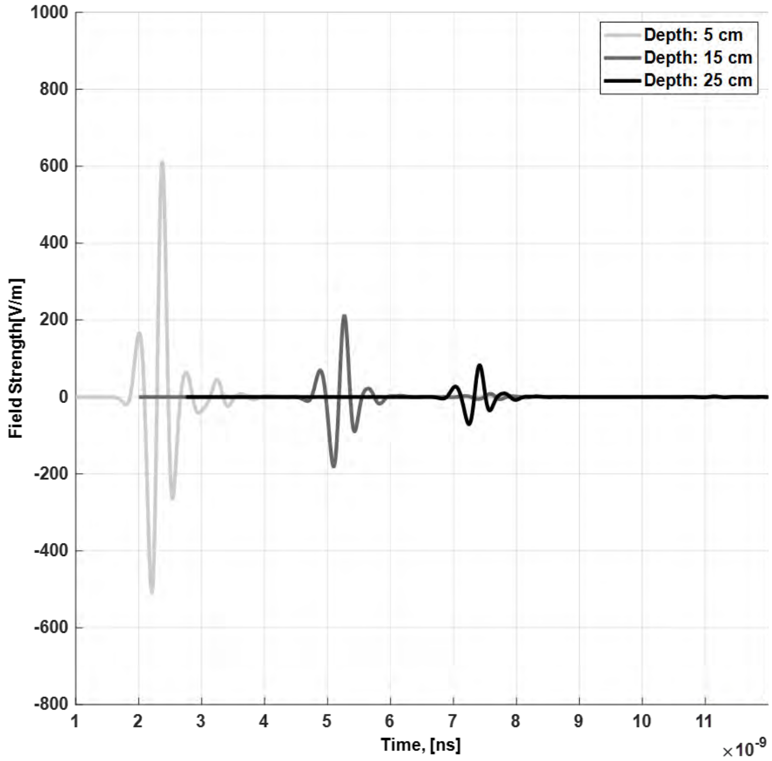

Figure 4.37: Comparison between landmine depths for a high loss scenario (α = 40 dB/m).

In this case, the following considerations can be pointed out:

- The amplitude of the signatures is significantly lower and the decrease rate is sharper than the previous case, in agreement with the ratio between the attenuation value. In addition, the homogeneous texture of the modelled soil produces a signature qualitatively similar to the one computed in Fig. Fig. 4.36.
- The internal air layer reflection appears to be the only visible contribution, due to the loss of resolution produced by the soil texture. Theoretically, the scattering from the layer is consistently visible regardless the target depth, and particularly the deeper mine almost shows the air layer contribution only, demonstrating once again that it plays a fundamental role for the detection.

The critical condition is that the limiting factor of detectability is the dynamic range of the receiver. Therefore, it has been proved true that the internal air layer emerges also in high loss soil situation and for deeply buried mine, but it is also true that the detection of this contribution depends on exceeding the noise figure threshold of the GPR system.

4.5 Summary

In this Chapter, the fundamental EM relations which are the governing equations of the GPR forward problem have been presented, as well as a basilar assessment of the parameters affecting the range performance of a GPR system. The dependencies within the main variables have been exploited in detail.

A comparison between a monostatic system and a bistatic one has been included to appraise the advantages that the inclusion of an additional variable (the antenna separation) may have or not on the system performance. In particular, the principal modifications are related to the target scattering and the experienced attenuation. Following the same concept, a brief section has discussed the issues that a GPR system should face when employed for demining operations, both in terms of system design and operational context.

From the examination of simple modelling scenarios, the effects of the GPR parameters, target design and soil properties on the GPR responses have been examined. Apart from the assumption involved in considering an infinitesimal source, there are no other simplifications in the modelling procedure. Therefore, all the EM phenomena are taken into account by the model.

In particular, given a suitable bandwidth (at least 2 GHz) and a close proximity to the ground, the reflections generated by the internal components of the landmine can be clearly identified, and the favourable conditions are consistent with the range of frequencies typically employed. Further, results from numerical experiments have revealed that the target design (external and internal) significantly alters the target radar signature, both in terms of magnitude and pattern, highlighting the importance of this aspect. Finally, results from the soil effects suggest that the detection of the internal structure is possible even for a deep target in high loss environment, provided that there is enough dynamic range for the system to record the reflection.

Chapter 5

Methodology and Results

Landmines do not distinguish the foot of a combatant from that of a playing child. Land mines do not recognize ceasefires or peace agreements.

G. Strada, 1996, [7]

This Chapter presents the results of the field campaign carried out for the purpose of the study. As described in depth in the research scope, the internal components of a landmine are expected to act as multiple scattering elements with a certain radiation pattern, therefore their effect should be evident and may be highlighted exploiting the angular domain of the problem.

The adopted strategy moves progressively from a preliminary evaluation of the magnitude of these contributions in a single mono-dimensional radar signature and in a 2D GPR profile, towards a full 3D imaging methodology, capable of overcoming unfavourable geometries and asymmetric target design, the two main issues that arose from the initial measurements.

Defining the productiveness of a GPR survey as trade-off between the level of information gathered from the data and the acquisition effort, whether survey time or deployment, it is clear that ideally a survey should collect as much information as possible, as quickly (or easily) as possible. Under this perspective, the Chapter ends presenting the radar results obtained from two different bistatic geometries, each of them with advantages and limitations, but both having the capacity of providing an equivalent level of information at the same time lowering the acquisition effort.

A detailed description of the employed targets and the experimental settings for each campaign are provided, together with a summary of major findings for each section.

5.1 Target description

The radar signature of a landmine is highly dependent on the materials used to make the external and internal components as well as the chemical properties of the explosive content. Landmines are objects which are difficult to obtain and replicate to carry out a measurement campaign and therefore it was the first priority to obtain properly constructed inert landmines to ensure the collection of landmine signatures as close as possible to those of a real live device.

Three representative landmines, provided by the Defence Academy of the UK, were used: a Soviet PFM-1, an Italian SB-33 and an Italian VS-50. These were complete with all their external and internal components and were filled with a high explosive simulant commonly used to train UK Ammunition Technical Officers. As the purpose of the research is to evaluate the effects of the internal structure on the radar signature, the correspondent VS-50 simulant mine provided by *Fenix Insight* was also tested. The surrogate is moulded from the actual mines in a resilient epoxy resin, accurately resembling in appearance the real target but without the internal assemblies. Dimensions and characteristics are provided in Table 5.1.

Table 5.1: Experimental targets description.

Target	Shape	Dimensions [cm]	Outer material	Metal content
PFM-1	Maple seed	120 x 60 x 20	Polythene	Medium
SB-33	Cylindrical	8.5 x 3	Polycarbonate	Low
VS-50	Cylindrical	9 x 4.5	Plastic	Low

A photograph of the three landmines and the surrogate is displayed in Fig. 5.1.

The VS-50 is an anti-personnel mine which consists of a circular plastic body with vertical ribs moulded into the circumference. The VS-50 landmine consists mainly of three sections: a main body containing the explosive charge, a section comprising the fuze and the arming mechanism, covered with a plastic cap, and the upper par including the neoprene pressure pad. It is a minimal metal mine, with a ribbed, waterproof and blast resistant plastic case. The mine incorporates an anti-shock feature which will

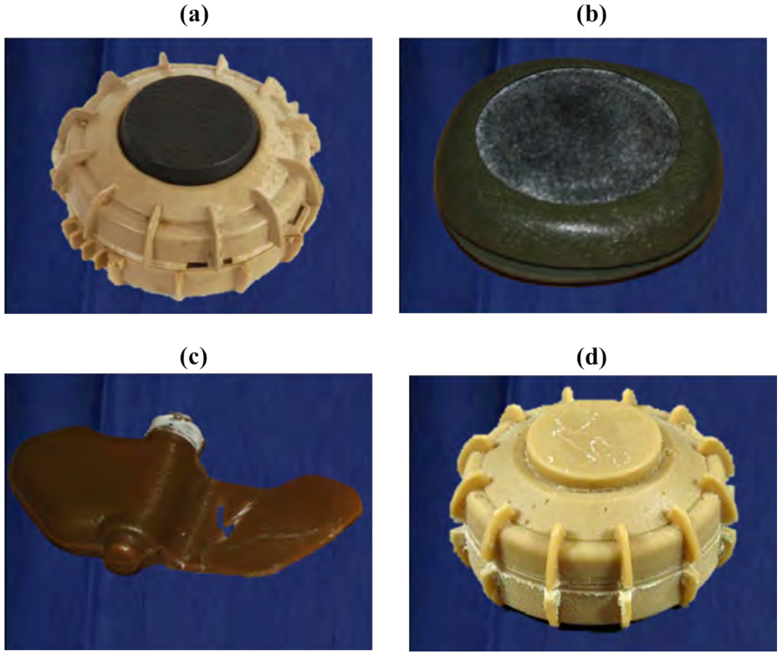

Figure 5.1: Picture of the employed devices. (a) Inert Italian VS-50. (b) Inert Italian SB-33. (c) Inert Soviet PFM-1. (d) VS-50 surrogate.

reduce the effectiveness of landmine countermeasure techniques such as fuel air explosives and explosive line charges. A downward force of approximately 10 kg for a minimum of tenth of seconds is needed for the landmine activation. The middle section includes the air pressure delay mechanism, composed of an anti-shock bladder to block the detonation if the force on the pressure pad is of insufficient duration. The assembly has the additional consequence of allowing the mine to be scattered by a ground vehicle or by helicopter-carried dispensers. It can therefore be regarded as a blast resistant mine. A picture of the internal components of the landmine is provided in Fig. 5.2. Recorded copies of the mine were produced in Iran, Egypt and Singapore.

The SB-33 landmine is made of glass reinforced plastic, with the top surface carrying a neoprene flexible pressure cap, to ensure minimal deterioration of the mine casing. It has a unique irregular shape to aid concealment and impede visual detection. Its asymmetric internal structure includes a cylindrical stab-fuze assembly in the middle of the target, just below the pressure note, and a void section on a side, covering only a portion of the main body. This sector allows a locking collar to rotate until the striker is released, flipping into the detonator. As for the VS-50, a sudden pressure, such as that generated by mine clearance machines, causes the striker to lock only the rotating collar in position for the duration of the pressure, preventing the mine from

Figure 5.2: VS-50 landmine, component details. *Taken from ordata.info*.

detonating.

The disassembled landmine is shown in Fig. 5.3, in which one can clearly see that the metal content is minimum. Variants of this mine have been produced by Argentina, Greece, Portugal and Spain.

Figure 5.3: SB-33 landmine, component details. *Taken from ordata.info*.

The structure of the PFM-1 (also known as *Green Parrot* from its NATO reporting name, or also butterfly mine) is such that the landmine cannot be easily opened and hence it was not possible to take a picture of its internal components. The device is a reverse-engineered copy of the US BLU-43, a scatterable air-dropped anti-personnel landmine designed during the Vietnam War. The mine is essentially a plastic bag containing liquid explosive attached to a cylindrical detonator, activating when a deformation of the soft plastic skin of the mine forces the arming plunger to strike the detonator (a single press of 5 kg or more will make it function). This mine is designed to float to the ground on plastic wings, usually air delivered, hence its nickname.

The surrogate is fundamentally a solid explosive with a representative metallic content (mild steel pin). The four devices have been selected to investigate targets with different complexity, both internal and external.

To prove the electromagnetic consistency of the filling material, its dielectric properties were characterised by a coaxial probe measurement [255]. The same technique was used for characterising the epoxy resin employed for the landmine surrogate.

Results of the dielectric measurements are provided in Fig. 5.4. On average, the dielectric constant of the explosive simulant was around 2.95, while a value of 3.0 was found for the resin.

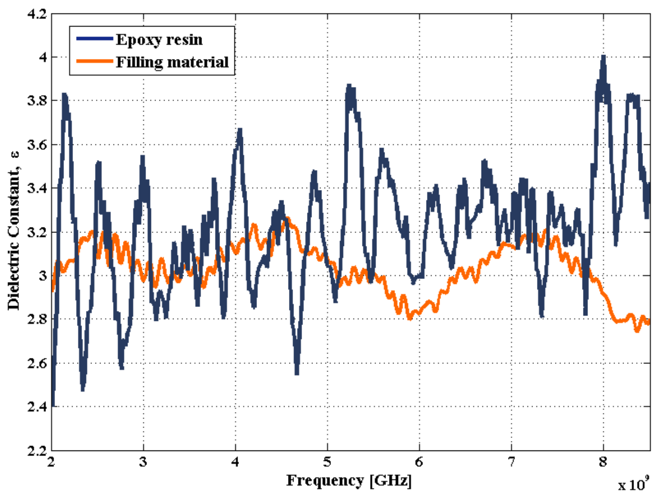

Figure 5.4: Materials dielectric characterisation.

The high variability of the results is a consequence of the uneven surface (and hence possible presence of air gaps) of the sample and its limited size. Considering the values of the commonly used explosive listed in Table 4.4, both the materials are sufficiently accurate for a reliable investigation.

5.2 Evidence of the internal structure: radar signature

First of all, it is necessary to understand the characteristics of mines, in terms of their shapes, case material and explosives, and their relative radar signature.The following section describes the preliminary analysis carried out to validate the research question and to provide an initial evaluation of the radar capabilities of detecting the internal reflections of the target.

5.2.1 Off the ground measurements

A set of free space radar signatures have been acquired in controlled conditions at the Defence Academy of the UK. Effects of polarisation and target inclination angle have been evaluated for off the ground landmines to exploit the landmine signature variations with acquisition geometries in the most favourable conditions.

Data were collected using a MS46322A Anritsu VNA transmitting a stepped frequency waveform with a bandwidth of 3.5 GHz from 5 to 8.5 GHz, with a frequency step of 0.4375 MHz. The dynamic range of the system is 115 dB, while the transmitted power was set to -20 dBm. Time domain data was obtained by Inverse Fast Fourier Transform (IFFT), applying zero padding to the complex frequency domain data to calculate the time domain signals. The obtained data are therefore the results from the convolution of the antenna impulse response and the target response.

No windowing functions have been applied to preserve the maximum achievable resolution. The Hilbert transform was then applied to the signal to get the envelope of the reflected signal from the object.

In addition, an experimental characterisation of the antenna effects (impulse response and transfer function) has been carried out to verify the linear phase frequency response and the constant amplitude over the operational bandwidth. This evaluation has been performed by analysing the reflection from a metal flat plate located a sufficient distance from the antennas plane.

Although the frequency band employed would allow very limited soil penetration for subsurface imaging, it was selected to obtain a typical value of the ratio between common propagating wavelengths in the ground and the size of the landmine. A central frequency of 6.5 GHz corresponds to a wavelength λ of 4.6 cm in free space, and this value of the wavelength can be used to compute a hypothetical downshifted system for typical soil characteristics.

In particular, a 4.6 cm wavelength corresponds to a system with a central frequency of 2.4-3.2 GHz in dry sandy or loamy soil (ε_r:4-7) and 1.5-2.4 GHz in wet soils (ε_r: 9-20). Considering that mostly GPR equipment employed in demining operations works in a frequency range from 1 to 3 GHz, the achieved equivalence corresponds to a realistic operational configuration.

Another consideration is that air is a less dense material with a very low absorption rate, compared with typical encountered soils. This will lead to a better characterisation of the signature features, as all the expected multiple reflections coming from the different assemblies of the target will likely be effectively recorded. The effects on polarisation are such that the soil will have an impact in the presence of several heterogeneities, but homogeneous soil will not alter the wave polarisation characteristics.

Two identical horn antennas in quasi monostatic configuration and parallel polarisation were mounted on a LinearX precision turntable to collect polarimetric range profiles with a 5-degree rotation step over 180 degrees. The turntable was mounted on the vertical face of a L-shaped metallic frame to ensure a perpendicular alignment with respect to the ground. The antennas were arranged to transmit and receive with the same polarisation and rotating the turntable allowed measurements of the targets with different polarisation angles (i.e different angles of the incident linear E-field with respect to the landmine). Fig. 5.5 shows the antenna geometry.

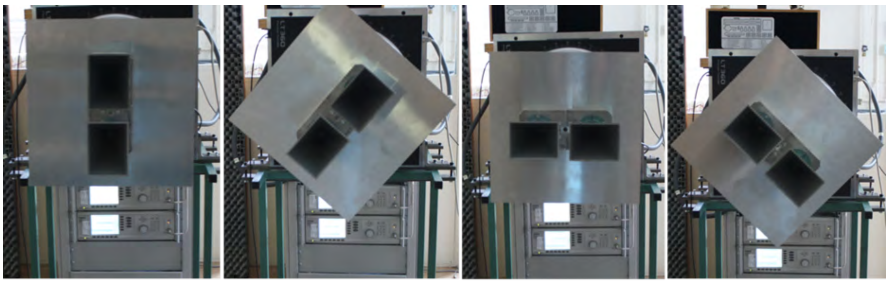

Figure 5.5: Measurements details. From left to right: starting polarisation (HH), 45 degrees orientation, Orthogonal polarisation (VV), 135 degrees inclined orientation.

A summary of the experimental activity is provided in Table 5.2.

The landmines under test were placed at a distance of approximately 170 cm from the antenna plane on a styrofoam cone (Fig. 5.6). The styrofoam material was used due to its low reflection properties to minimise the impact of the stand.

Table 5.2: Off the ground acquisition parameters and set up.

Parameter	Value
Frequency range [GHz]	5 - 8.5
Frequency step, Δf [MHz]	0.4375
Central wavelength [cm]	4.6
Angular range [deg]	0 - 180
Antenna dimension [cm]	9 x 12
Antenna offset [cm]	9
Antenna gain [dB]	16.5

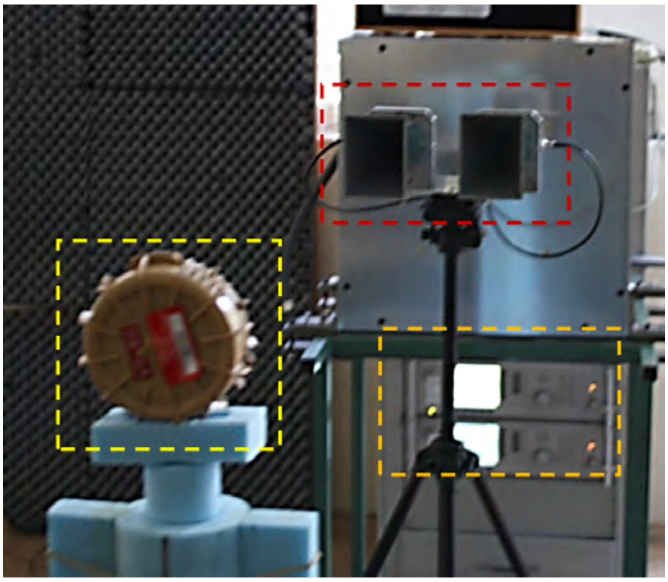

Figure 5.6: Experimental set up with the two horns connected to the VNA and facing the landmine under test on the stand.

Results for all targets are analysed in detail at two different aspect angles to further quantify the impact of target inclination on the signature. The geometry is shown in Fig. 5.7. The choice of evaluating the radar signature at different target angle is motivated by the fact that being a composite target with a number of internal scatterers, landmine response could provide different features and characteristics. In a large variety of environments, landmines may have been subject to alterations, such as landslips and flooding, which may have modified the geometry and orientation of the buried target.

To obtain the reflected signal from the object, a measurement of the background was taken to remove all stationary clutter from the target signature. Considering the non-optimal measurements environment, the placement of the target was accurately evaluated to ensure its spatial separability from room interference.

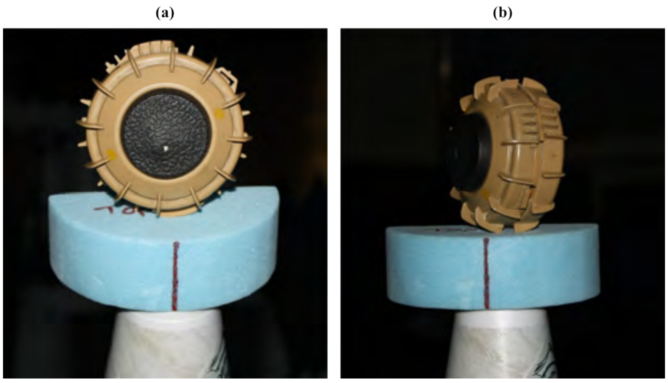

Figure 5.7: Target aspect angles. (a) 0 degrees. (b) 45 degrees.

Analysis of the measurements environment is provided in Fig. 5.8, in which it can be seen that (1) interference generated from the room and multipath effects are very limited, in both range and magnitude, except for the strong reflections generated by the front wall (approximately 6 metres distant), and that (2) these events show an almost stationary and constant behaviour over the different antenna orientations, ensuring an accurate background whitening step.

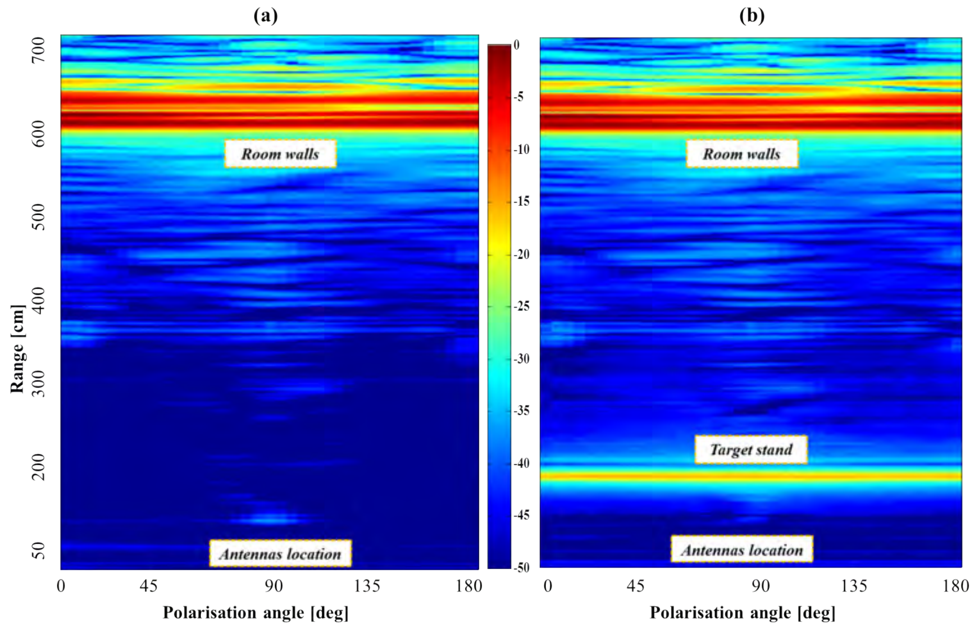

Figure 5.8: Background quality analysis. (a) Background only. (b) Target stand inclusion.

Finally, as an additional figure of merit the acquisition set-up was tested against a metallic sphere with a radius of 3 cm, as shown in Fig. 5.9.

Resolving the canonical radar equation provided in Eq. 4.22 for the considered set-up and employed equipment, and assuming a target RCS of roughly -25 dB (given by a

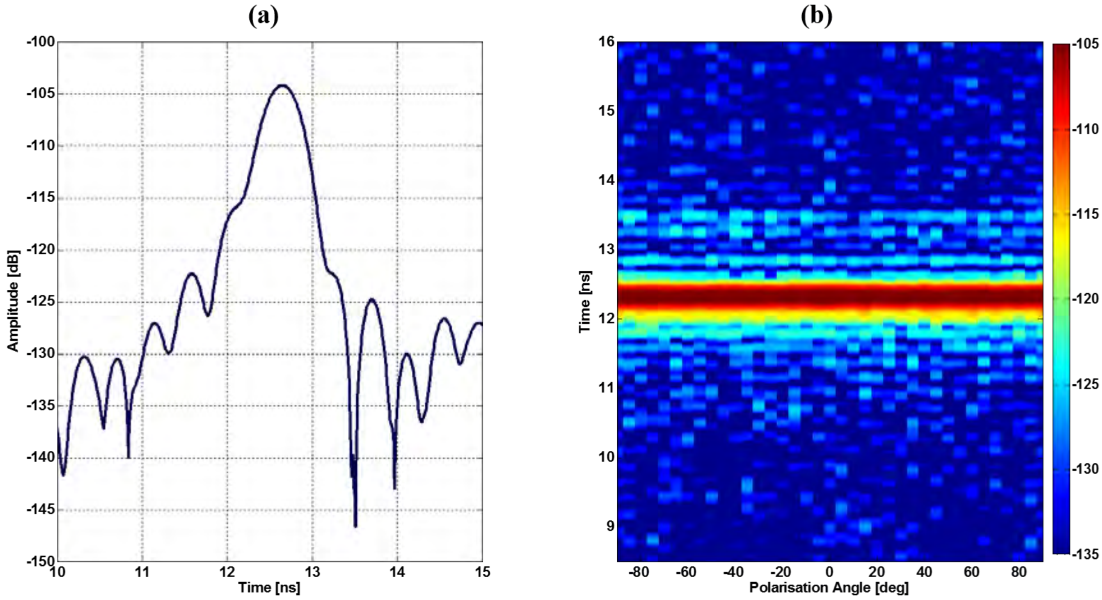

Figure 5.9: Measurement set-up quality analysis. (a) Target 1D signature. (b) Target polarimetric profile.

radius of 3 cm), the received signal level would theoretically be around -102 dB, which is in close agreement with the amplitude of the main peak of Fig. 5.9(a), nearly -104 dB. Further on, the polarimetric analysis, Fig. 5.9, shows that no significant variations occur when changing the antenna orientation, as the amplitude values of both the main peak and the sidelobes are consistent throughout the whole angular space.

As the aim of this section is to provide a qualitative evaluation of the target response depending on its geometrical properties and orientation, the recorded time domain signatures of the inclined target (i.e. 45 degrees) have been normalised with respect to the maximum value of the aligned configuration (i.e. 0 degrees).

However, as a reduction of the signal level is expected when the target does not perfectly face the antennas plane as a consequence of the different projected RCS seen by the system, the magnitude of this amplitude difference is provided as well.

For the two described aspect angle, Fig. 5.10 presents the 1D time domain signature of the PFM-1 landmine.

Due to the simple design and absence of complex internal structure, the radar response of the PFM-1 landmine is mainly represented by a single reflection peak, regardless the relative geometry. Considering the physical design of the target, this contribution to its signature arises from the cylindrical detonator assembly, as the stabiliser wing is hardly contributing due to its limited size.

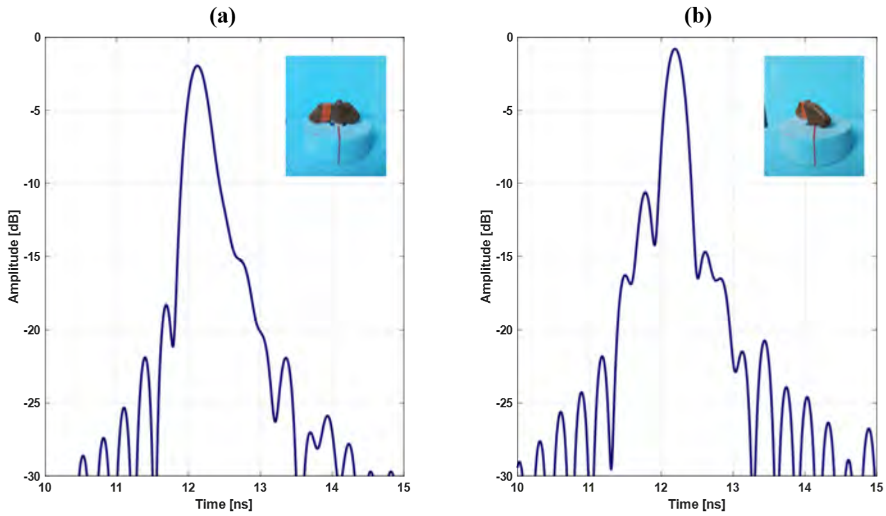

Figure 5.10: PFM-1 landmine signature, 1D signature. (a) 0 degrees. (b) 45 degrees.

In Fig. 5.11 the radar response of the SB-33, as a function of the aspect angle is displayed.

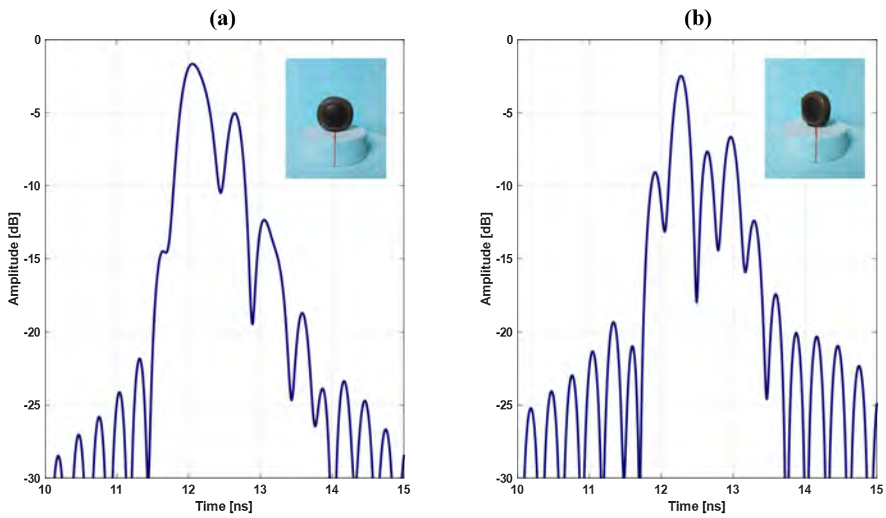

Figure 5.11: SB-33 landmine signature, 1D signature. (a) 0 degrees. (b) 45 degrees.

When the target includes an internal design, the structure of the device significantly complicates its signature, in which several contributions can be highlighted. When the target is lying horizontally (Fig. 5.11(a)), the effects of the target complexity becomes evident, as an internal reflection is clearly visible, due to a combination of the reflections generated by the detonator and the void sector located aside of it. The presence of internal assemblies becomes even clearer when the target is inclined (Fig. 5.11(b)), as several multiple reflections are identifiable.

The response of the real inert VS-50 is presented in Fig. 5.12.

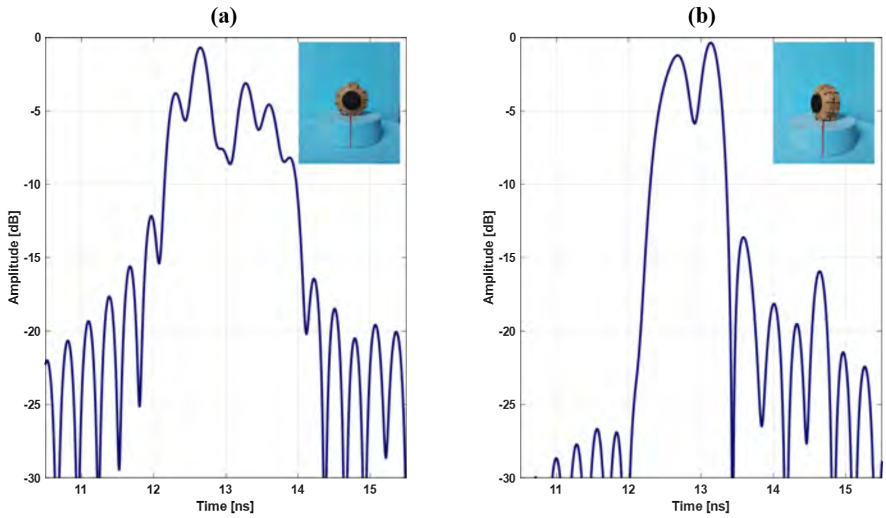

Figure 5.12: VS-50 landmine signature, 1D signature. (a) 0 degrees. (b) 45 degrees.

Also in this case the internal structure of the landmine is clearly visible when the target is aligned with the antenna plane (Fig. 5.12(a)), as multiple reflections can be detected. Further on, it can be noted a close similarity with the numerical results obtained with a 3GHz bandwidth (Fig. 4.23) previously analysed.

While the first peaks could be identified with the activator plate response, fully resolved thanks to a suitable resolution, the second interface belongs to a scattering contribution generated by some internal assembly. Considering the landmine design, the responsible for this scattering contribution is the air gap layer behind the activator plate. The last peak is due to the bottom of the landmine. These considerations are no longer valid when the target is inclined: Fig. 5.12(b) shows only two reflections, belonging to the top and bottom of the landmine, generated by a combination of the air layer and the landmine main body. The increasing magnitude of the internal reflections are related to the parabolic effect of convex surface, which tends to focus the radar beam back to the antenna.

A final comment is related to the relevant amplitude of the range sidelobes which might be a results of small variations in the target stand position during the measurements, causing the background subtraction step not to completely cancel them out. The periodicity feature is then a result of the IFFT algorithm.

To give a quantitative evidence of the possible energy losses due to a target misalignment, Table 5.3 details the recorded amplitude strength of the three targets for both configuration.

Table 5.3: Reflections strength variability with inclination angle.

Target	Aligned configuration	Inclined configuration	Amplitude loss
PFM-1	-114.63 dB	-123.42	7.79 dB
SB-33	-117.91 dB	-121.37	3.46 dB
VS-50	-117.35 dB	-118.96	1.61 dB

The reduced scattering contribution recorded for the inclined PFM-1 landmine is a consequence of (1) a smaller projected RCS, limiting the target scattering, and (2) reduced target scattering directed towards the receiver. These considerations are supported by the fact that the recorded amplitude of the tilted PFM-1 is lower than the one observed for the other landmines. For the VS-50 model, instead, the regularity of the air layer limits the impact of a target rotation, as it still represents the more relevant contribution to the target signature. In this case, almost no differences can be observed and this hypothesis is . As presumable from the geometry of its internal structure geometry, a change in the aspect angle of the SB-33 landmine leads to a more pronounced amplitude gap, compared to the VS-50.

The effect of antenna polarisation on the PFM-1 mine as a function of aspect angle is presented in Fig. 5.13. Each signature has been normalised to its own maximum value to help the comparison process and displayed as range profiles in the time domain.

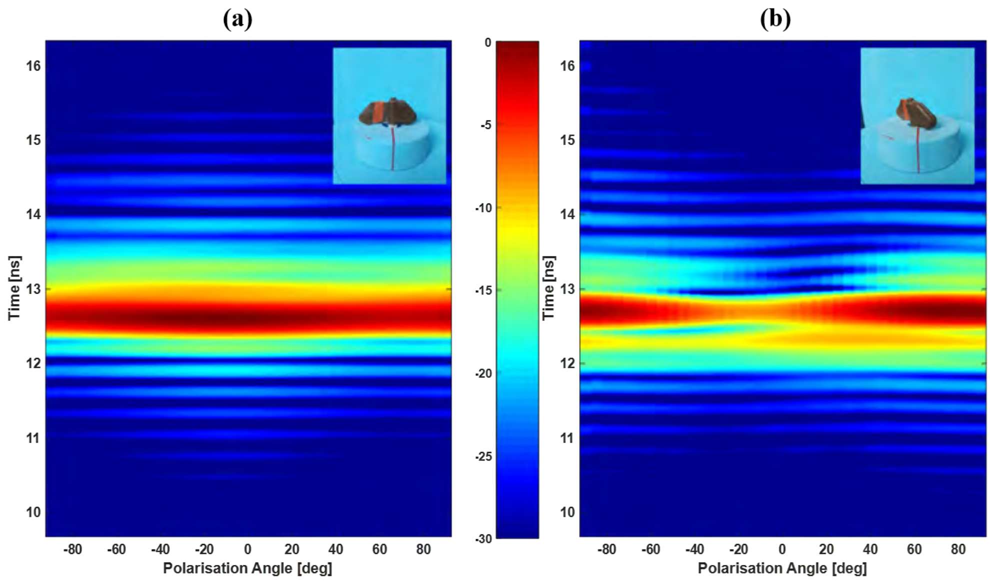

Figure 5.13: PFM-1 polarimetric profiles. (a) 0 degrees. (b) 45 degrees.

As expected, the polarimetric behaviour of the target is almost constant due to its relatively simple structure. There is a main scattering contribution in the range of the target which is overall regular also with aspect angle. When the target is inclined (Fig. 5.13(b)) the effects of antenna polarisation become slightly evident from some weak variations due to the different illumination of the target. However, on average the polarimetric analysis shows high levels of correlation.

The polarimetric profiles for the SB-33 mine are presented in Fig. 5.14.

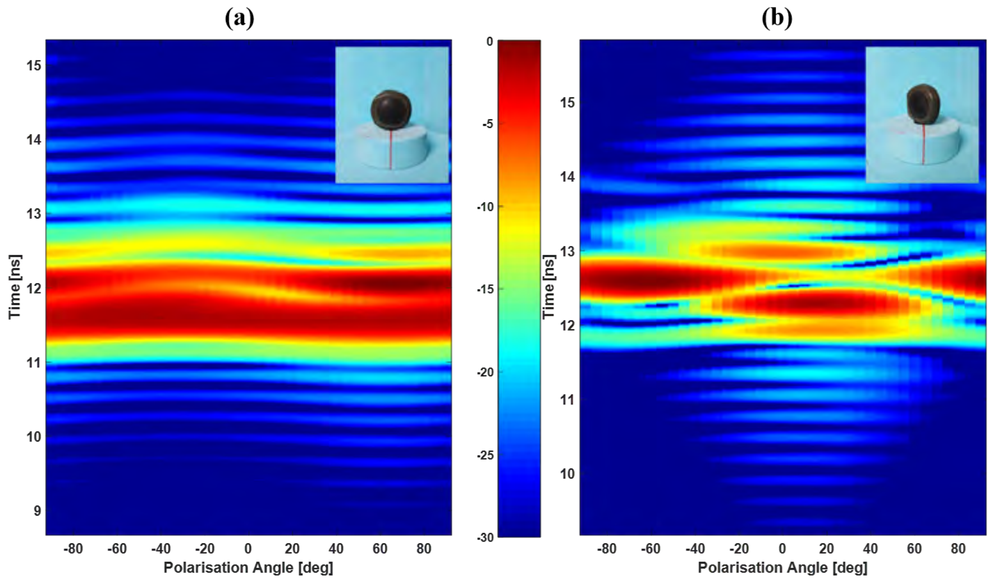

Figure 5.14: SB-33 polarimetric profiles. (a) 0 degrees. (b) 45 degrees.

Just from the first view, it is clear how the internal structure of the landmine impacts the polarimetric response. In all the frames the signatures decorrelate very fast from angle to angle. The SB-33 has a larger physical dimension than the PFM-1, hence it is quite obvious that its response when the target is placed at no inclination angle (Fig. 5.14(a)) will be thicker in space, but what is to be noticed is that the main contributions is not constant, but some variations in the magnitude of the peaks occur. This feature is a suggestion of the presence of inner assemblies which gives rise to multiple reflections. The effect is even more evident when the target creates an angle towards the antenna plane (Fig. 5.14(b)) in which both reflection distribution and magnitude vary significantly with polarisation angle. This is a first demonstration that to gather reliable information regardless the relative geometry of the target, a set of signature is needed, rather than a single trace. What is to be noticed is that at certain angles the contributions from the internal assemblies (the cylindrical detonator and the void sector) lose their singular identity and the resulting signature does not include a number of single reflections but a mixture of them. In practice, this means that even changing the orientation of the antennas, one can run the risk of wrongly determining the nature of the buried anomaly.

Figure 5.15 presents the acquired profiles for the VS-50 mine.

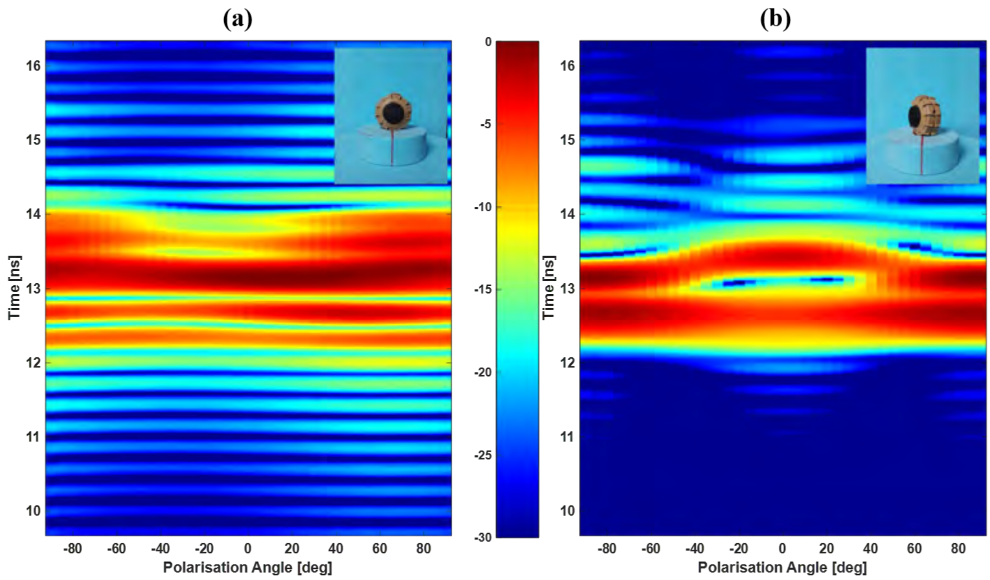

Figure 5.15: VS-50 polarimetric profiles. (a) 0 degrees. (b) 45 degrees.

The same considerations made for the SB-33 mine hold here, as the internal structure affects the polarimetric trend in a clear and noticeable way. The profile in Fig. 5.15(a) is less heterogeneous compared to its SB-33 equivalent due to the presence, just below the activator plate, of a large number of air gaps, which modify the signature and balance out the illumination changes. When these gaps are not dominant over the signature, when the target is rotated, Fig. 5.15(b), the profiles return to describe a more complex polarisation dependent behaviour.

5.2.2 Buried targets measurements

To validate the highlighted features in a more realistic setting, the same acquisitions were carried out burying the landmines in a sand pit. The test bed, located at the Defence Academy of the United Kingdom, Shrivenham, is a confined bay composed of several quadrants, Fig. 5.16(a), and filled with a sharp sand material characterised by a very low clay content and a gritty texture (Fig. 5.16(b)). The material is representative of several mine-affected regions of the world.

Figure 5.16: Defence Academy test bay overview. (a) Overview. (b) Highlight on the filling material.

From a radar perspective, the conditions were favourable, as the material was relatively homogeneous and free of clutter, with an average particle size of less than half centimetre. A background-only profile is shown in Fig. 5.17(a).

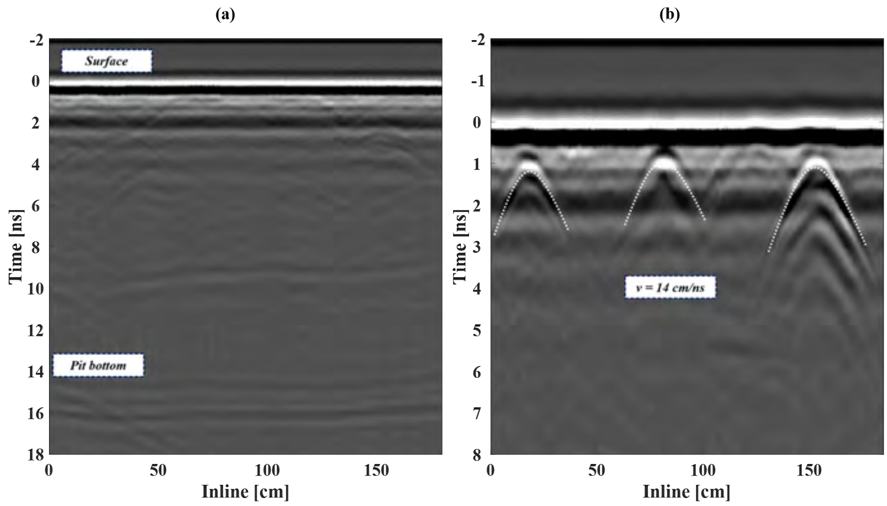

Figure 5.17: Defence Academy test bay soil properties. (a) Background profile. (b) Estimated wave velocity.

Despite the environment humidity, the sand maintained a velocity, computed from hyperbola fitting in Fig. 5.17(b), of 14 cm/ns and a consequential relative dielectric constant of 4.5. Soil attenuation properties are such that it is possible to detect the bottom of the pit, approximately at a depth of 120 cm, with an attenuation coefficient around 10 dB/m.

The equipment employed was an IDS Aladdin (IDS Georadar srl) georadar platform, a shielded ground coupled dipole antenna, spaced 6 cm, with a central frequency and bandwidth of 2 GHz. These parameters bring a minimum wavelength of 4.5 cm, therefore a consistency with the free space measurements has been successfully achieved, in terms of wavelength to target size ratio. Obviously, the existing difference between the two employed bandwidths exists and will affect the overall resolution capability.

The equipment is composed by two pairs of orthogonally polarised dipole antennas, as shown in Fig. 5.18(a), located such that the reflection centre corresponds for both couples and coincides with the geometrical centre of the unit.

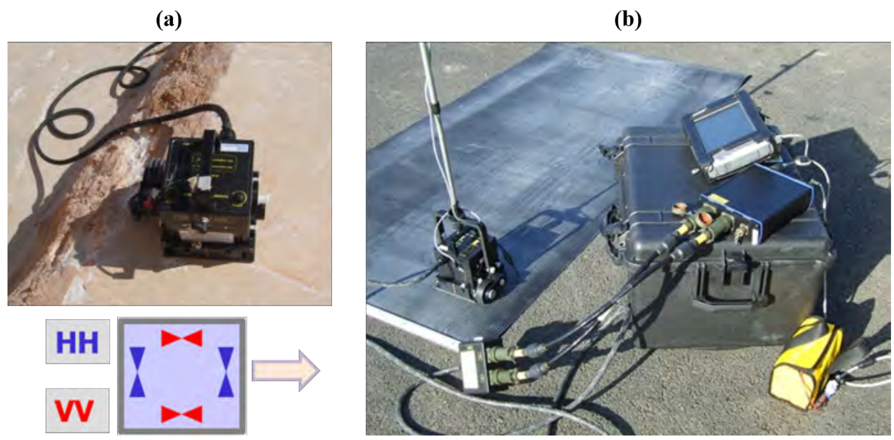

Figure 5.18: Employed GPR equipment. (a) GPR scheme. (b) Complete platform.

The radiation characteristics, i.e. the emitted waveform and the radiated spectrum are shown in Fig. 5.19(a) and (b) respectively.

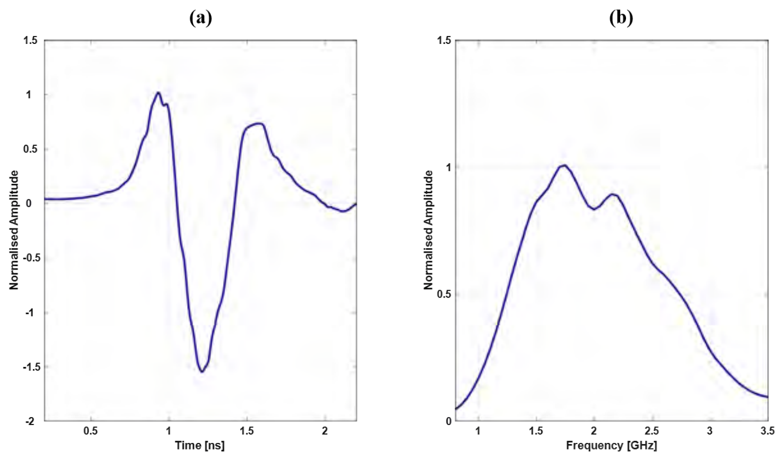

Figure 5.19: GPR equipment radiation characteristics. (a) Emitted waveform. (b) Emitted spectrum.

The sensor head, which is essentially a passive component weighting approximately 2 kg and with a size of 12 by 12 cm, is connected to a central unit (Fig. 5.18(b)) responsible for the generation, transmission and reception of the signal.

To perform an accurate platform rotation a mechanical turntable was placed below the antenna Fig. 5.20.

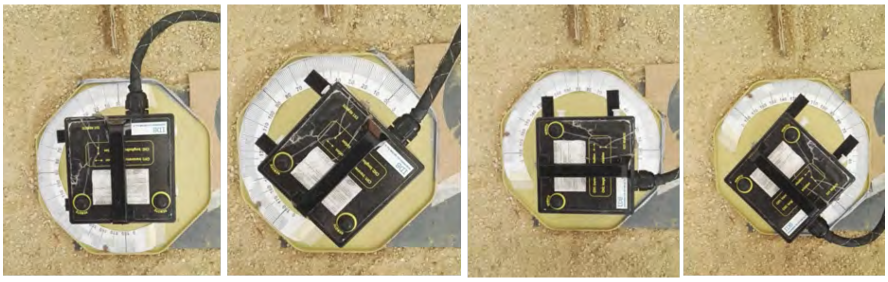

Figure 5.20: Measurements details. From left to right: starting polarisation (HH), 45 degrees orientation, Orthogonal polarisation (VV), 135 degrees inclined orientation.

The three targets were buried at a depth of approximately 13 cm, which represents the standardised clearance depth for humanitarian demining operations.

Data were collected with the reflection centre of the antenna right in the middle of the target and following the previous strategy: a 180 degrees rotation, with an angular sampling of 5 degrees, and targets buried at two different inclination angles (Fig. 5.22). The experimental setup is detailed in Table 5.4 and Fig. 5.21.

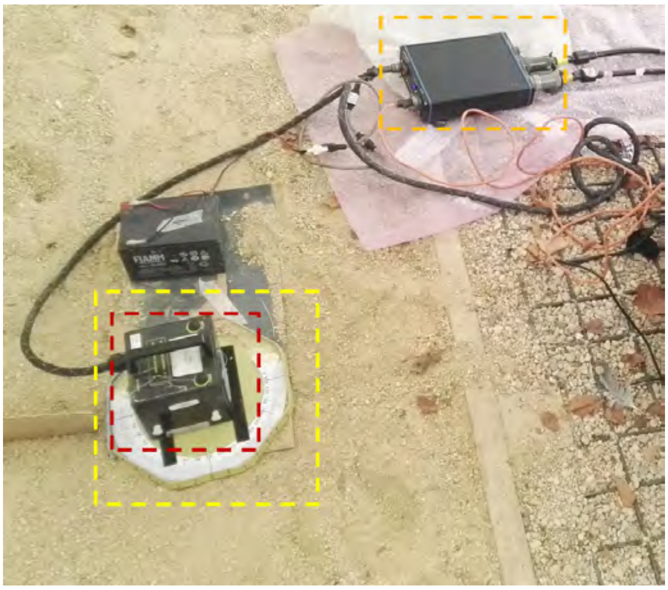

Figure 5.21: Experimental set up with the GPR equipment and the mechanical turntable below the platform.

The processing chain applied to the data consisted of a linear frequency filtering and a spherical exponential compensation gain function, matched to the soil characteristics, to recover the amplitude losses.

Table 5.4: Sand pit acquisition parameters and set up.

Parameter	Value
Frequency range [GHz]	1 - 3
Frequency sampling, $1/\Delta t$ [GHz]	17
Central/Minimum wavelength [cm]	7 / 4.5
Angular range [deg]	0 - 180
Time window, ΔT [ns]	20
Antenna offset [cm]	6

(a) (b)

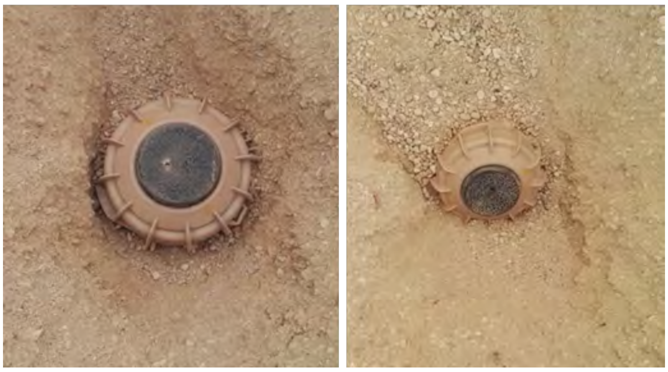

Figure 5.22: Target aspect angles. (a) 0 degrees. (b) 45 degrees.

The A-scan signature of the PFM-1 landmine is provided in Fig. 5.23. Considering the design of the device, the radar signature is dominated by the scattering produced by the cylindrical fuze, represented by the narrow high amplitude peak. The same component is responsible for the reflection recorded when the target is inclined, even if more than a single contribution is visible. These multiple reflections are probably due to a ringing effect generated by the metallic part of the landmine.

Figure 5.24 shows the collected signature of the SB-33 landmine. In this case, a very close correspondence with the free space results has been achieved, for both the inclination angles. Despite the propagation through a lossy material, the effects of the inner design of the target is recognisable as an additional reflection occurring after the first peak, though its relative amplitude is significantly lower (especially compared to the results in Fig. 5.11). The higher amplitude of the internal reflections of Fig. 5.24(b) is due to the higher contrast with the air gap inside the landmine.

Finally, results from the VS-50 investigation are shown in Fig. 5.25

A notable close correlation with the laboratory experiments can be highlighted, thanks to the regular design of the landmine, especially for the inclined configuration

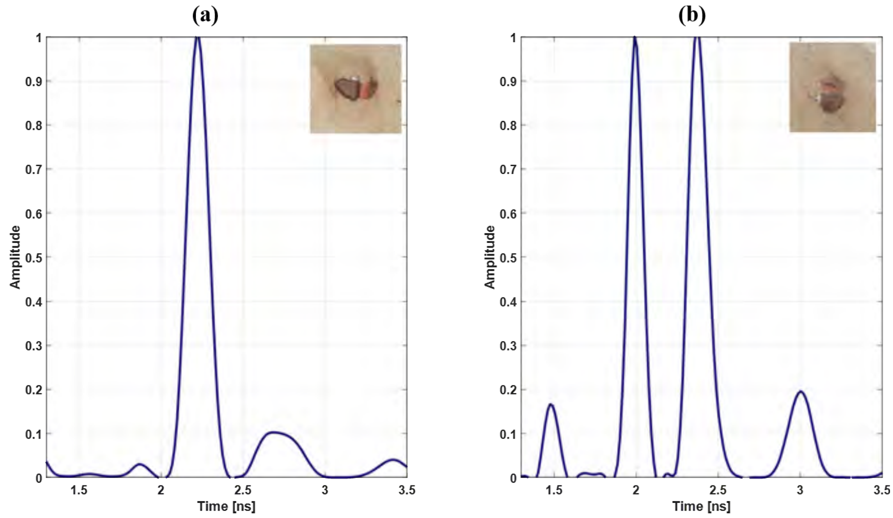

Figure 5.23: PFM-1 landmine signature, horizontal polarisation. (a) 0 degrees. (b) 45 degrees.

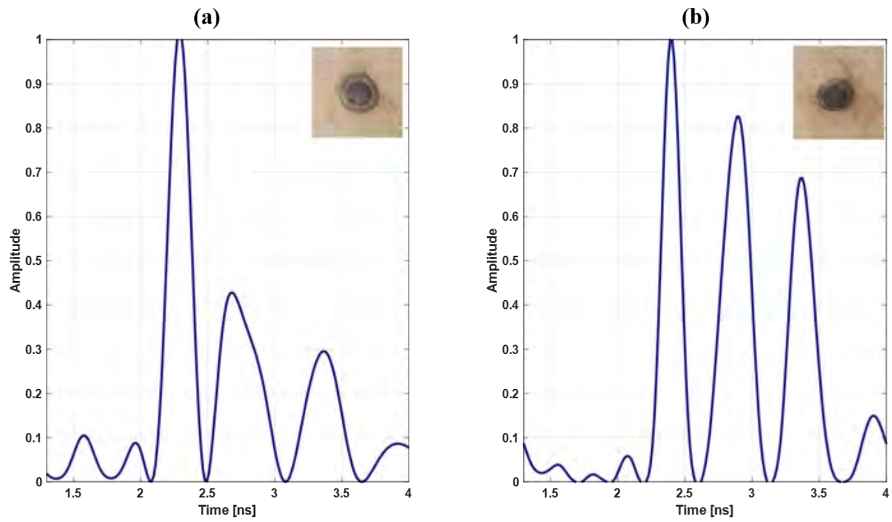

Figure 5.24: SB-33 landmine signature, horizontal polarisation. (a) 0 degrees. (b) 45 degrees.

in which case, consistently with what has been individuated in Fig. 5.12(b), the effect of the air layer vanishes.

As before, the validity of the feature has been addressed through a set of polarimetric measurements. The PFM-1 landmine results, depending on the antenna orientation and aspect angle are shown in Fig. 5.26.

As expected, due to the soil absorption the signature presents lower information content than the free space equivalent (Fig. 5.13), but the overall trend is consistent between the two experiments. A single reflection is detectable when the target is placed at an aspect angle of 0 degrees, and the same trend can be highlighted between the two trials. In particular, the response of the cylindrical fuze to a change in the antenna

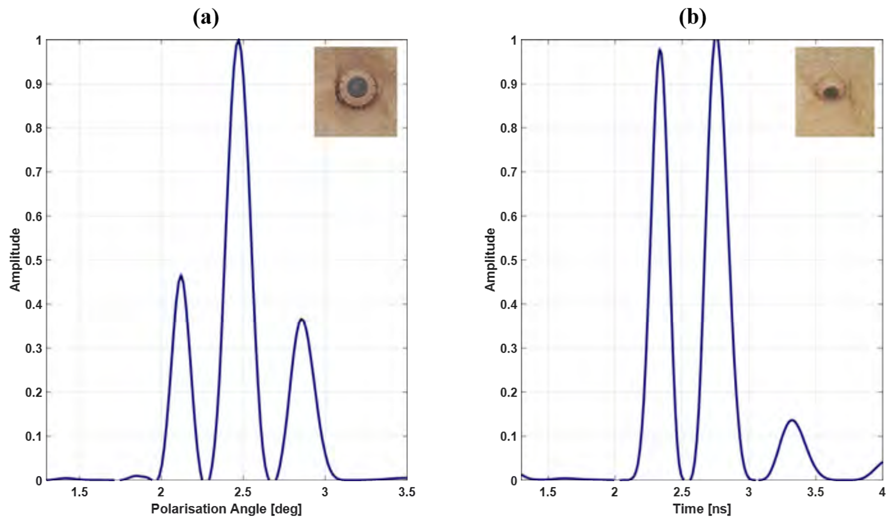

Figure 5.25: VS-50 landmine signature, horizontal polarisation. (a) 0 degrees. (b) 45 degrees.

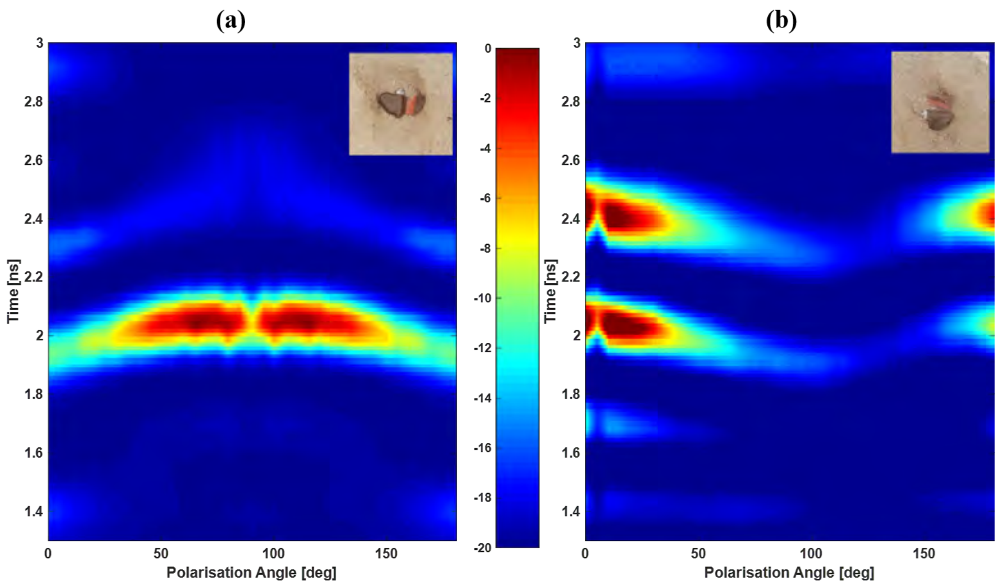

Figure 5.26: PFM-1 polarimetric profiles. (a) 0 degrees. (b) 45 degrees.

orientation follows the polarimetric behaviour of linear metallic targets. The difference from the free space measurements is likely be a consequence of the larger pattern of the dipole antennas, which is dominated by the presence of the metallic assembly. When the target is rotated, Fig. 5.26(b), two events can be clearly identified, confirming the hint made from the mono-dimensional data on the ringing effect. This consideration is based on the fact that the two events follow almost exactly the same pattern, which would be unusual in case of two different scattering contributions. A consistent trend with the free space trial can be noticed, as the signature intensity decreases in the range 45 to 90 degrees.

Figure 5.27 describes the results from the analysis of the SB-33 device.

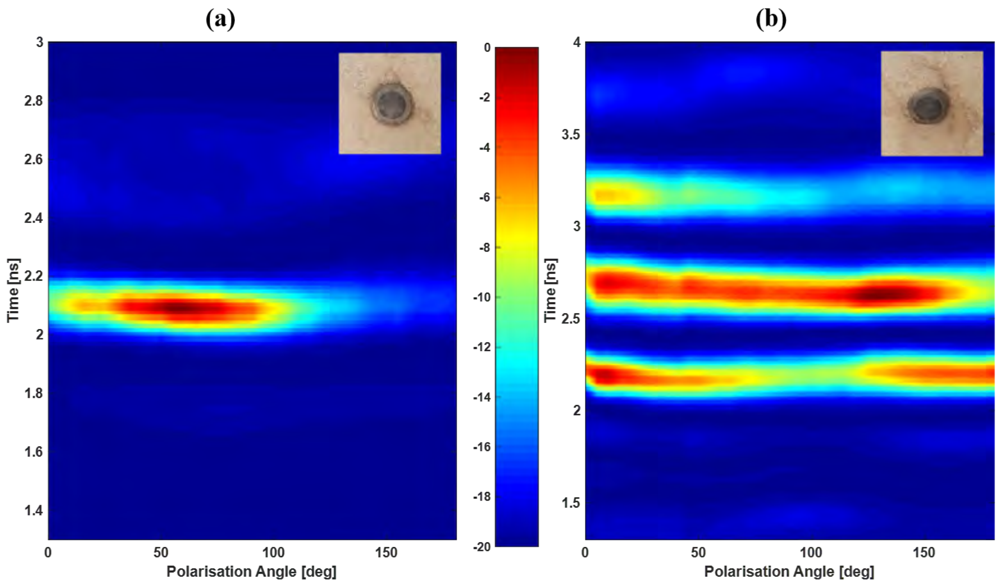

Figure 5.27: SB-33 polarimetric profiles. (a) 0 degrees. (b) 45 degrees.

The same consideration can be outlined for the second device, characterised with a highly heterogeneous and composite design, with some exceptions. A single reflection is visible when the target is oriented at 0 degrees towards the antennas, with nothing related to the internal structure. As evident also in Fig. 5.14(a), the bulk of the contribution is located in the 0 to 90 degrees range. A rotation of the target produces a richer response, as three well-defined events have been recorded. These belong to the upper surface, probably to the air gaps inside the landmine or the fuze assemblies (refer to Fig. 5.3 for the structure of the SB-33) and the bottom reflection, respectively. The latter reflection, obviously, has almost half of the magnitude of the other two, with the air interface being the higher and more stable one. These multiple scattering was visible when measuring the target in air (Fig. 5.14(b)), even if the presence of the internal reflections and a wider pattern complicated the identification of the three events.

Polarimetric profiles of the VS-50 are presented in Fig. 5.28.

The investigated device has an internal design (Fig. 5.2) characterised by the presence of a homogeneous layer of air gaps just below the activator plate: this is clearly visible when it is directly below the GPR platform as the stronger reflection in Fig. 5.28(a). In an opposite way to the signature of the SB-33, in this case the number of detectable interfaces is higher for an aspect angle of 0 degrees than with for the inclined configuration. This is due to the fact that the air layer is located in the upper part of the

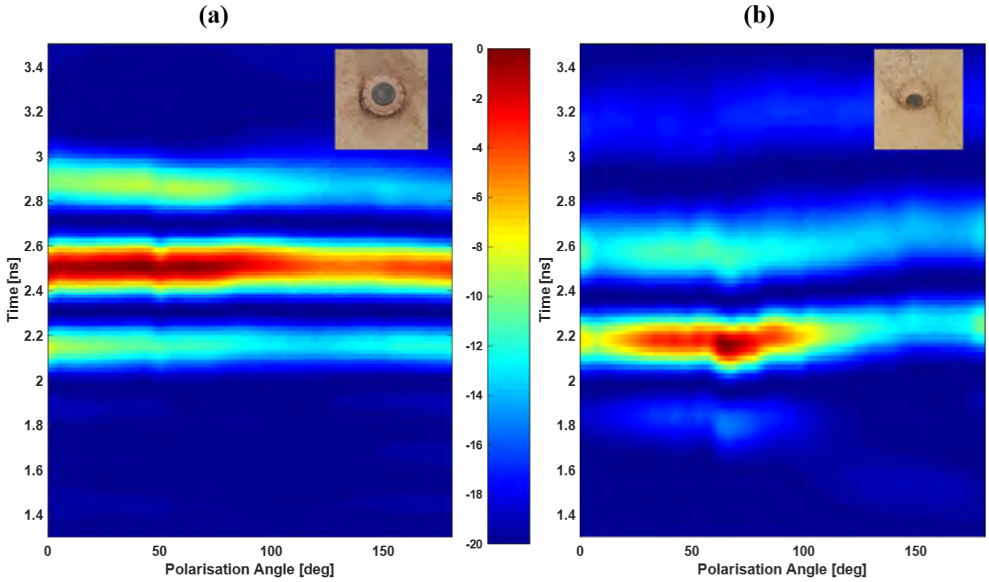

Figure 5.28: VS-50 polarimetric profiles. (a) 0 degrees. (b) 45 degrees.

target, thus becoming of secondary importance when the target is rotated. The SB-33, instead, has a bulk of air located beneath the target, hence still predominant even when the landmine is inclined.

5.2.3 Comments

The preliminary analysis carried out in this section has demonstrated two main points:

- Scattering phenomena generated by the internal assemblies of the target do have a noticeable effect on the target radar signature, thus demonstrating that the presence of such features can be properly recorded. There is also a consistent behaviour comparing the radar results and the actual design of the landmine.
- Internal components do not behave as the other parts of the mine, thus a change in the illumination pattern orientation is sufficient to highlight these phenomena, providing deeper information on the investigated object.

From a radar detection perspective, the presence of internal assemblies is beneficial as these mines, and zero metal mines in general, contain significant air gaps to allow movement behind the pressure plate. This affects to some degrees their strength and the features of their signature. For this reason, the possibility of detecting internal reflections or scattering from multiple assemblies could represent an important key point for target discrimination.

Effects of aspect angle on reflections distribution have been evaluated and proved to be a further element to exploit. The results have shown that both the internal structure and the outer design give a varying contribution to the overall response, depending on the geometry relative to the antennas.

The VS-50 landmine, which includes a number of air gaps creating a thin, homogeneous layer in the upper part of the device, is a clear demonstration of the effects of target inclination: these voids are predominant when facing the antennas, while a rotation of the target will cause the layer to play a secondary role and vanishing.

The situation changes when investigating buried targets, as the absorption effects significantly alter the level of details and information gathered by the signature analysis.

A comparable trend was found, as the spatial distribution and location of the main reflections were consistent between the two trials. Differences have been noticed in the density of the reflections for the soil buried targets. While in free space the impact of internal assemblies and structures on the signature was clearly visible and easy to characterise, burying the target into a lossy ground allowed nothing but the strongest reflections to be successfully collected at the surface. Internal reflections are still detectable for the VS-50 and the SB-33, due to the presence of a relatively large air gap inside the structure but only in favourable geometrical conditions.

Finally, the comparison between the numerical simulations and the experimental results shows a close agreement, as shown in Fig. 5.29.

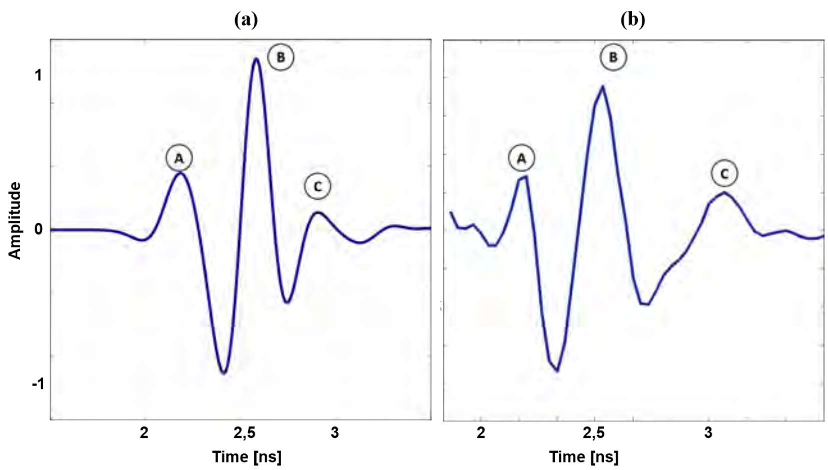

Figure 5.29: Comparison of simulation and measurement. (a) Numerical result. (b) Experimental result.

From the two graphs the similarity between the two results is visible, as the temporal occurrence of the reflections and their pattern are highly correlated.

5.3 Evidence of the internal structure: radar profiles

The analysis of the mono-dimensional signatures have shown some deficiency in detecting the internal scattering contributions, in particular for targets presenting an irregular structure, as for the case of the SB-33. Consequently, even if results have proven to be reliable, confidence must be augmented, and the logical option for obtaining a higher information content is to increase the dimensionality of the problem, i.e. exploiting also the spatial dimension.

5.3.1 Trials description

A set of GPR profiles has been acquired in the test pit at the Defence Academy (Fig. 5.16) employing the same GPR equipment, with the three landmines buried at 13 cm and facing the surface and the GPR profile crossing the middle of the target (Fig. 5.30).

Figure 5.30: 2D GPR profiles, acquisition details. Profiles location is indicated with the dotted arrow.

In this case, to guarantee a precise profile collection, a soft pad, the PSG (Pad System for Georadar) was placed below the radar equipment, as shown in Fig. 5.31(a). The surface of the pad is designed with parallel tracks that are a few millimetres high, so that the GPR antenna can slide over them ensuring a constant antenna orientation during the whole survey. The same pattern is attached to the bottom of the GPR platform so that it could be easily slotted in the tracks (Fig. 5.31(b)).

The acquisition is controlled by an odometric wheel directly connected to the sensor, Fig. 5.31(c), equally constrained in the pad tracks.

The pad plays the additional role of compensating smooth surface topography in order to maintain the equipment always in contact with the surface. Table 5.5 lists the acquisition parameters.

A pictorial description of the survey is provided in Fig. 5.32.

(a) (b) (c)

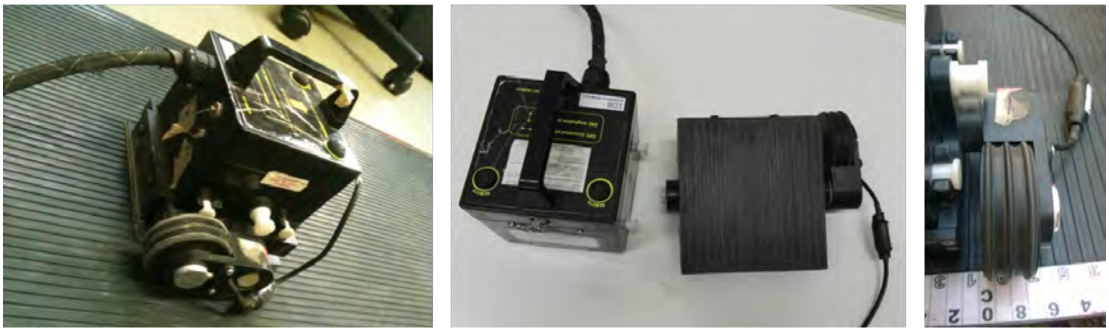

Figure 5.31: 2D GPR profiles, acquisition configuration. (a) GPR platform and survey pad. (b) GPR platform bottom. (c) Odometric wheel.

Table 5.5: 2D GPR acquisition parameters and set up.

Parameter	Value
Frequency range [GHz]	1 - 3
Frequency sampling, $1/\Delta t$ [GHz]	17
Inline sampling, Δx [cm]	0.4
Time window, ΔT [ns]	20
Profile length [cm]	50
Profile length [samples]	125

Considering the nature of the targets and what has been found characterising their signature, internal reflections are supposed to plainly appear only for the VS-50 landmine, while no evidence for the PFM-1. The SB-33 represents the principal ambiguity, as it has an asymmetric structure and its signature (Fig. 5.24(a)) does not presents any contribution from its internal design.

GPR profile obtained from the PFM-1 landmine is shown in Fig. 5.33

As expected, the acquired scan of the target is characterised by a single hyperbola (marked A), confirming what was previously highlighted. In addition, as the responsible of this reflection is the metallic detonator assembly, a ringing event is visible (marked B) as a delayed version of the main contribution, closely resembling its pattern as has been pointed out in the previous section.

Figure 5.34 presents the B-scan results for the VS-50 device.

In this case there is a clear indication of the presence of the internal structure: after the reflection generated by the top of the landmine, marked A, the effect of the void ring covering the main body of the landmine is an additional hyperbola with a thicker shape and higher amplitude (marked B). The last event, marked C, is the bottom of the target.

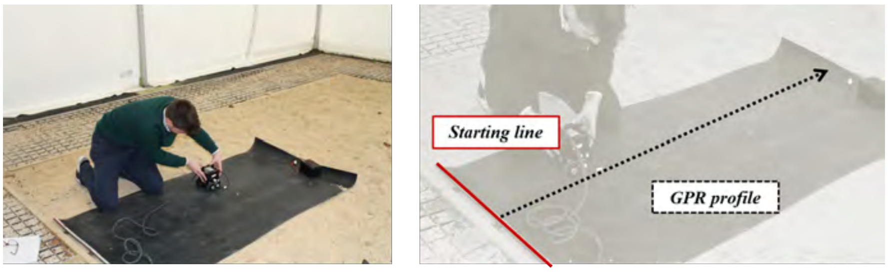

Figure 5.32: 2D GPR profiles, acquisition photographs.

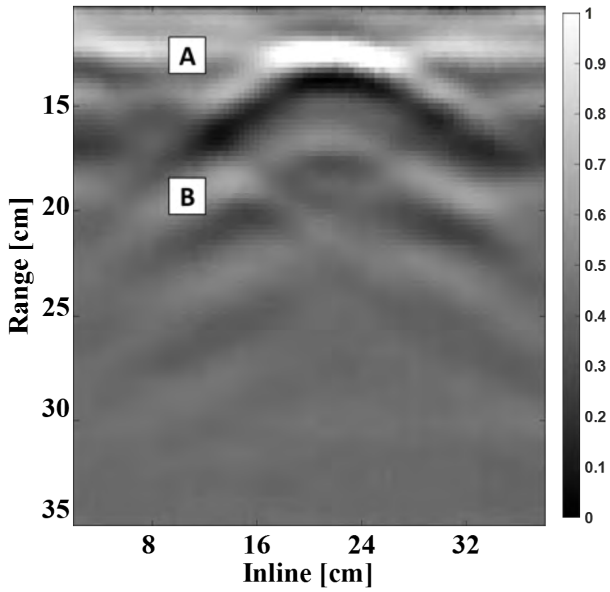

Figure 5.33: 2D GPR profiles, PFM-1 landmine.

For such a design, a single profile is sufficient for identifying the target and to recognise its internal design.

Finally, the profile acquired over the SB-33 is displayed in Fig. 5.35.

In this case a single reflection event is detectable (marked A) and no hypothesis can be made on the presence of internal assemblies, in contrast to what is the actual design of the device. The non uniform internal design therefore produces a radar results which would provide a misleading basis for identifying the target, as no information on the internal structure is evident. Whilst the outcome validate the results obtained from the signature characterisation previously made, it can be concluded that a single profile is not able to provide reliable performance. Compared to the previous case, the diffraction curve which appears on the radar profile does not present a perfect hyperbolic pattern due to a more flattened shape of the SB-33 landmine.

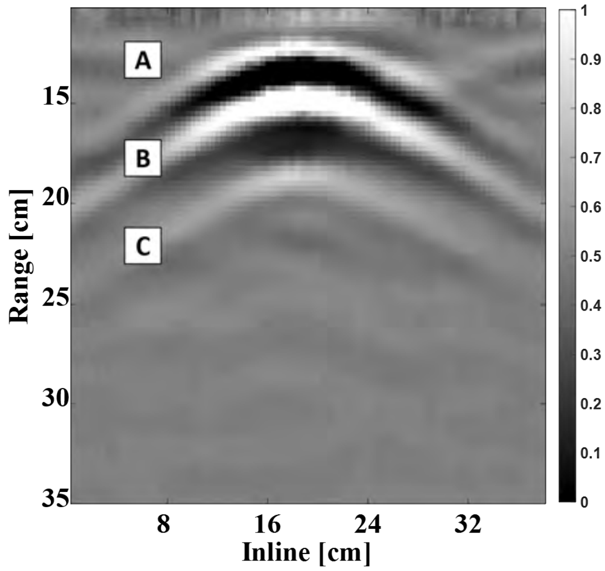

Figure 5.34: 2D GPR profiles, VS-50 landmine.

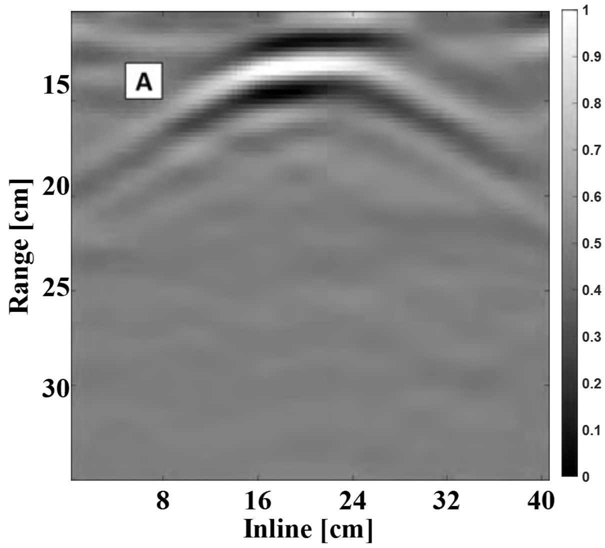

Figure 5.35: 2D GPR profiles, SB-33 landmine.

5.3.2 Validation of results

To confirm the highlighted features and to ensure that the detected additional reflections effectively represent the target internal structure, the VS-50 surrogate shown in Fig. 5.1(d) was also investigated. As described, the main difference between the two objects is that the surrogate does not include any internal assemblies, while the dielectric properties are closely correlated.

This essentially means that, being the survey scenario equal, any possible disagreements in the GPR results can be associated to a dissimilarity in the internal design of the device, as the outcomes would otherwise be closely comparable.

The two GPR profiles are presented in Fig. 5.36. The profiles have been normalised by the joint maximum value.

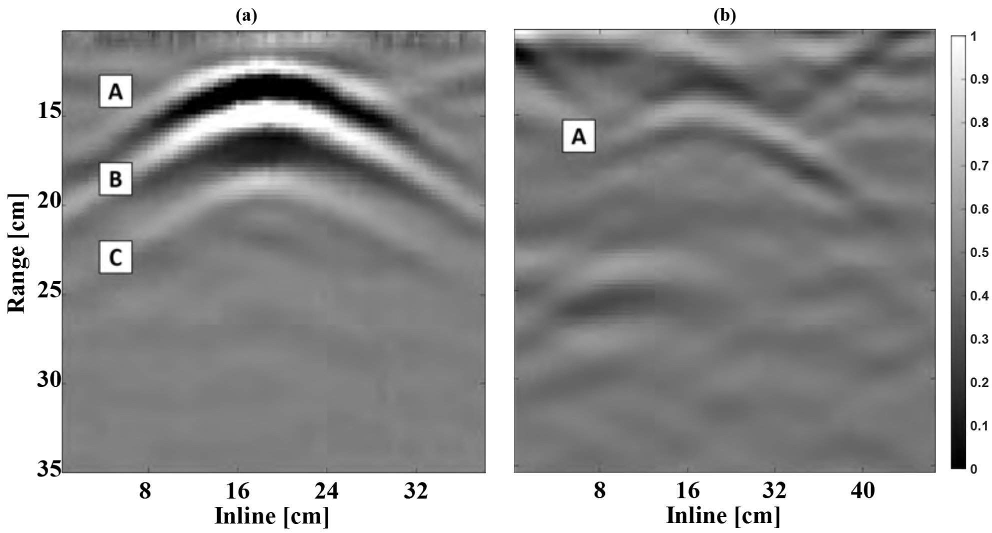

Figure 5.36: 2D GPR profile, target comparison. (a) Inert VS-50. (b) Surrogate VS-50.

First of all, it can be noticed that the magnitude of the response of the inert VS-50 is higher than its surrogate. This is due to the neoprene pressure pad which has a dielectric constant of approximately 9, while for the resin the value is roughly 3, producing a stronger impedance contrast. Secondly, and most important, the two results validate the suggested target characterisation, as it is evident the additional reflection generated by the internal air layer, feature which does not appear in the surrogate target (as expected).

In addition, as one of the critical limitation of the 1D signature is detecting the internal contribution when the target is not horizontally laying, a 2D profile has been acquired changing the inclination angle of the target to assess the robustness of the method. Resulting radargram is shown in Fig. 5.37

It can be seen that it is still possible to recognise the internal structure contribution, clearly with a different pattern and shape. Hence, this restriction can be overcome by increasing the dimensionality of the problem.

5.3.3 Comments

The analysis of the GPR profiles and the latter comparison with the target surrogate have first of all confirmed the hypothesis and suppositions made when characterising

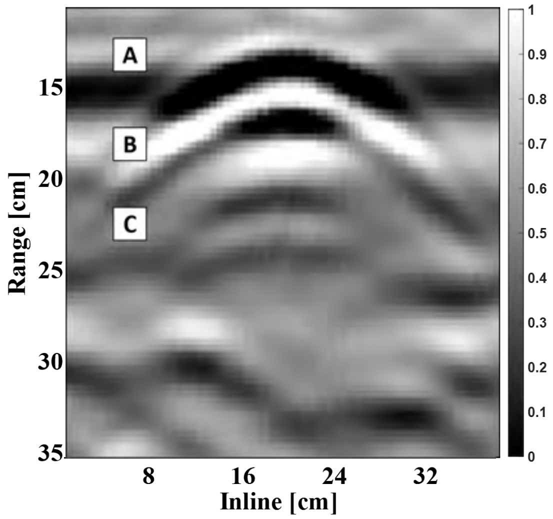

Figure 5.37: 2D GPR profile, inclined VS-50.

the multiple reflections visible in the A-scan signature response: these scattering components are induced by the presence of the air layer inside the target, providing a more readable proof of the suppositions.

Concerning the information content, it may be said that, compared to what can be extracted from the target signature, there is little benefit in acquiring a 2D profile as it still suffers from not producing consistent performance. The case of the SB-33 landmine is explicative: when the internal structure of the target has a non uniform shape, the single profile might not be able to clearly image its scattering contribution.

5.4 Evidence of the internal structure: radar images

Following the outcome of the previous campaign, to mitigate the recognition challenge a properly sampled 3-D dataset is needed, allowing the extraction of advanced physical and geometrical information of the buried target, as well as eliminating ambiguities due to challenging target properties. As a consequence, only the two inert landmines that include a structure, i.e. the SB-33 and the VS-50 have been evaluated, together with the VS-50 surrogate to further validate the results.

5.4.1 Trials descriptions

To ensure a proper data density and regularity, in order to obtain unaliased 3-D subsurface images, acquisitions were carried out once again employing the PSG. As a result of the acquisition set-up, the collected profiles (Fig. 5.38) have been linearly interpolated to create the subsurface volume.

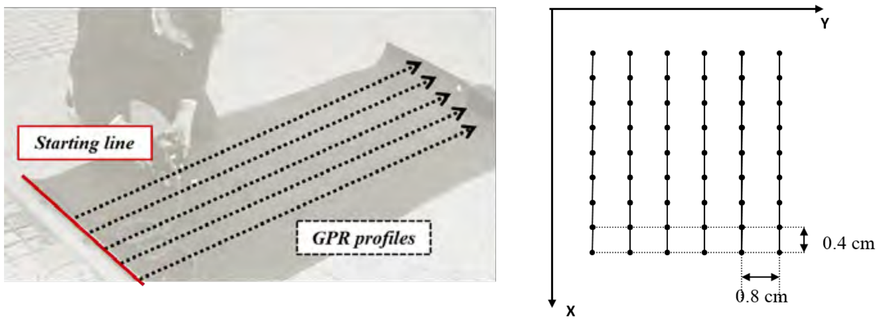

Figure 5.38: 3D GPR, acquisition details.

The two inert landmines and the surrogate were acquired simultaneously, buried at approximately 13 cm and horizontally laying. Acquisition parameters and data details are listed in Table 5.6.

Table 5.6: 3D GPR acquisition parameters and set up.

Parameter	Value
Frequency range [GHz]	1 - 3
Frequency sampling, $1/\Delta t$ [GHz]	17
Inline sampling, Δx [cm]	0.4
Crossline sampling, Δy [cm]	0.8
Time window, ΔT [ns]	20
Acquired area [cm]	80 x 80
Acquired area [samples]	200 x 100

Results are shown in terms of a set of time slices, essentially a series of C-scans of the volume taken at a specified time instant (Fig. 5.39). This allows an easy investigation of the target reflections. Except for a time calibration to correct for jitter effects, a linear filtering operation to remove out-of-band noise and a spatial window, no other processing steps were applied to the data.

The time difference between subsequent slices is approximately 0.05 ns, given the frequency sampling of 17 GHz, which corresponds to a range difference of 0.65 cm. Obviously, this value can be computed only for a propagation in a homogeneous material, otherwise the relationship cannot be verified as the conversion becomes non linear. For this reason, the time indication provided on the presented time slices only represents their temporal occurrence.

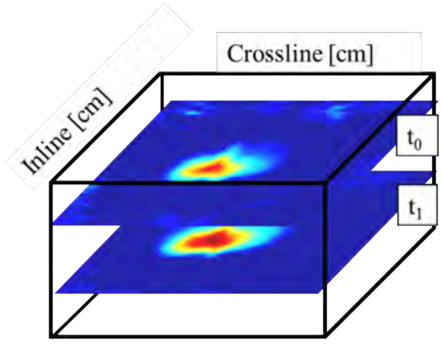

Figure 5.39: Radar time slice extraction.

Amplitude of the slices is displayed in a blue-yellow-red colourmap and normalised by the overall maximum value to the range [0-1].

GPR slices for the inert SB-33 landmine are provided in Fig. 5.40.

From a preliminary analysis, several considerations can be pointed out and, depending on the considered slices, it can be confirmed the capability of GPR of sensing the presence of internal reflections, as the collected frames exhibit different features which may be associated to distinct scattering events. What would have been expected from a solid objects would be a homogeneous pattern, net of absorption effects, and a close agreement between the thickness of the target and the number of slices including the target contributions.

Analysing the slices included within the target boundaries, represented by the first reflection generated by the pressure plate and the bottom of the landmine, Fig. 5.41 shows the selected sections.

If one analyses the two slices within the top (pressure plate contribution, Fig. 5.41(a) and the bottom (bottom cover contribution, Fig. 5.41(d) of the target, valuable information can be gathered.

The slice of Fig. 5.41(b) shows a uniform high reflectivity area centred on the middle of the target, indicating a regular scattering element smaller than the target and located in the centre of it. The hint on the contour of the feature arises from the fact that the maxima of the reflections are concentrated in a single location, with the amplitudes gradually decreasing following the typical hyperbolic behaviour.

Instead, the reflections distribution of Fig. 5.41(c) identifies a semi-circular shape, possibly generated by a number of scattering events near the outer border of the target. As before, the suggestion of an extended scattering element, rather than a single point

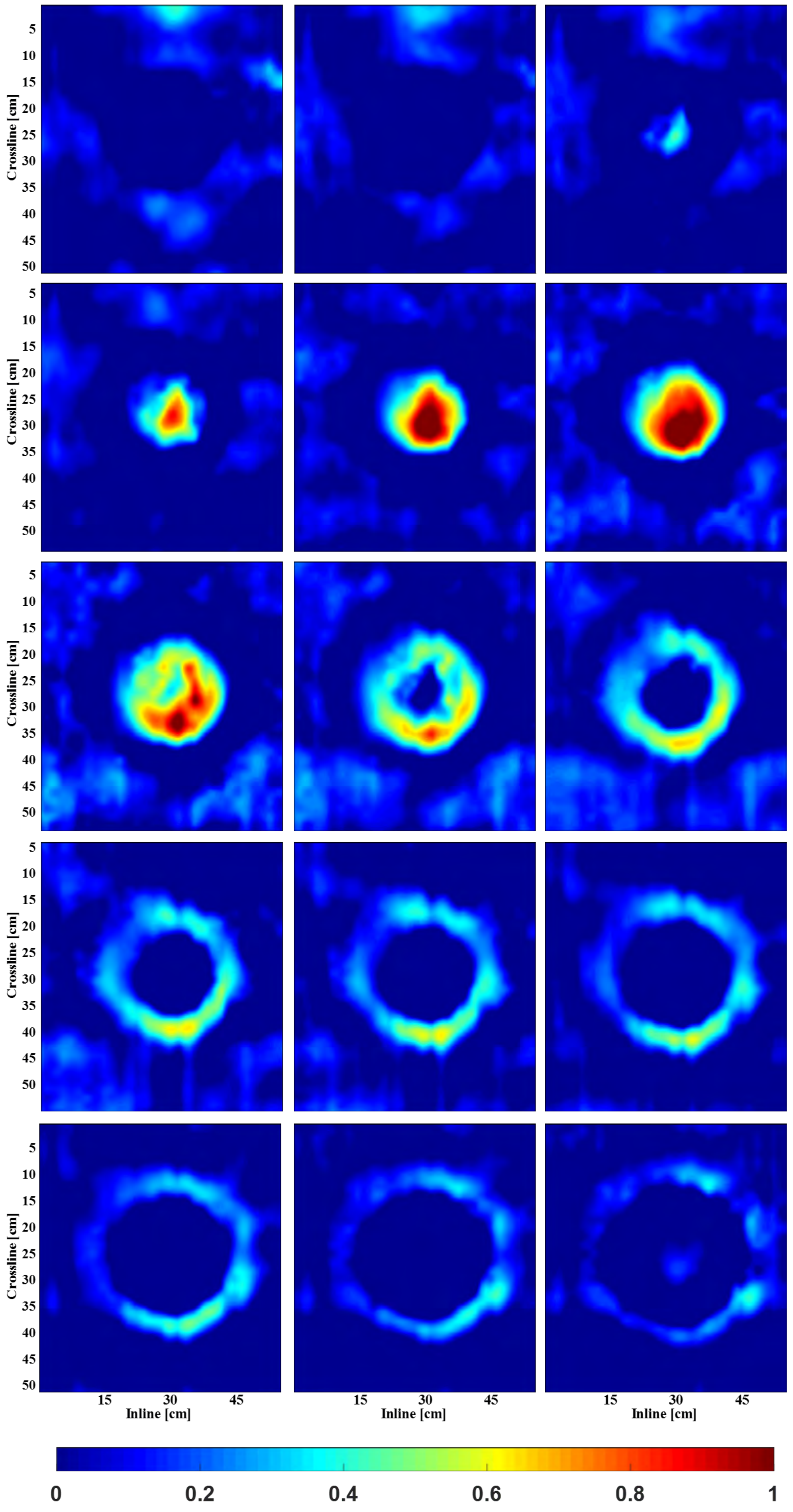

Figure 5.40: Inert SB-33 landmine time slices. Order from left to right, top to bottom.

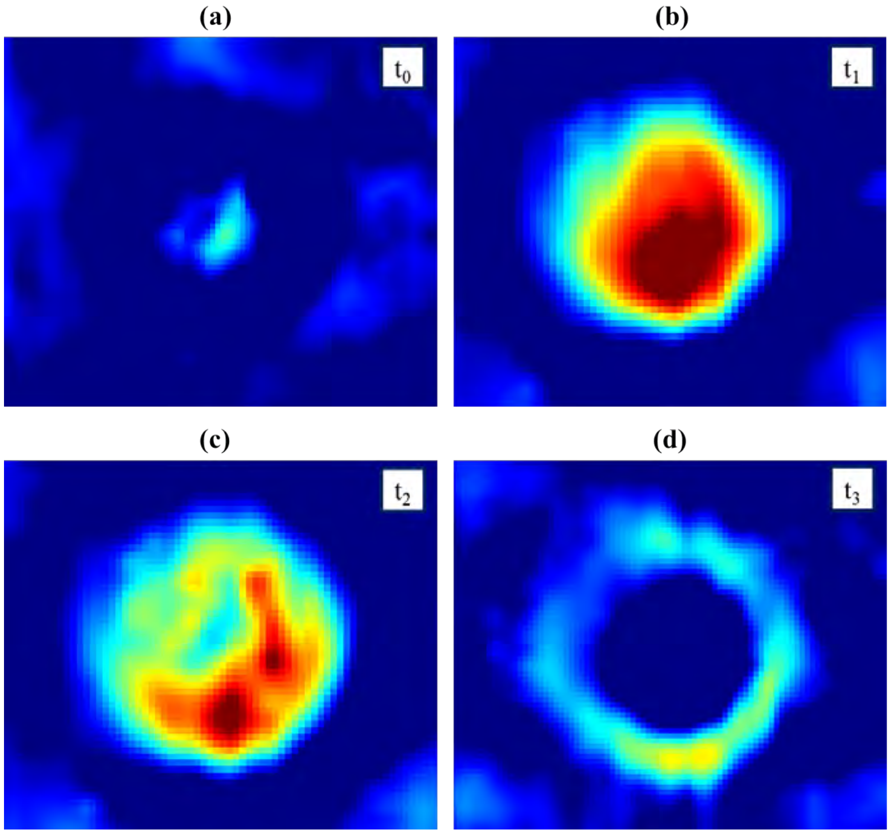

Figure 5.41: Inert SB-33 landmine time slices, internal structure highlight. (a) Upper section - pressure pad. (b) - (c) Internal structure. (d) Bottom part.

scatterer, comes from the analysis of the amplitude pattern.

Essentially, the internal structure of the detected target, as hinted from the raw radar data, can be considered consisting of a central element, possibly regular, and a scattering region embracing it and covering a rounded sector of the landmine. This is consistent with the design of the SB-33 and, recalling the previous results, the fact that this feature is located in a certain area of the target makes the internal structure hard to detect in a single 2D radar profile.

To further validate these comments and to better identify the described features, an overlay of the radar slices and the optical picture of the landmine is shown in Fig. 5.42.

The central scattering feature highlighted in the radar slice is confirmed to be the fuze and striker assembly, which has a cylindrical shape and contains the entire metal content of the landmine, motivating also the high radar reflectivity. The radar anomaly of Fig. 5.41(c) fits particularly well with the void quarter of the landmine, positioned aside of the fuze and encompassing it, both in terms of location and shape. Finally, the

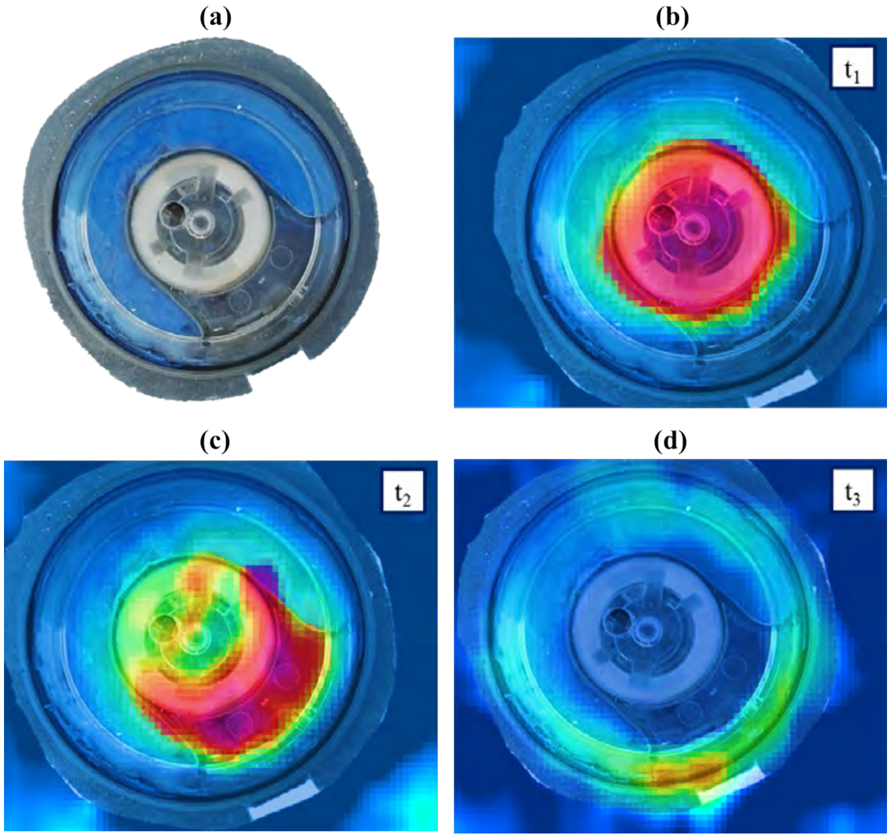

Figure 5.42: Optical overlay of the radar results, inert SB-33 landmine. (a) Upper section - pressure pad. (b) - (c) Internal structure. (d) Bottom part.

overlay provides also a further correspondence for the circular evidence of Fig. 5.41(d), which was initially associated only to the bottom cover of the landmine. Superimposing the two images, one can note that the bolder part represents the detonator capsules, which is essentially a void cylinder.

Figure 5.43 presents the collected radar slices for the inert VS-50.

In this case, the overall pattern of the slices is different, as (1) the main target contributions are described by a higher number of slices, compared to the SB-33, and (2) the contribution seems to disappear for a couple of slices and then appears again before the end of the target, suggesting the presence of a highly reflective layer occurring after the top of the landmine. As before, Fig. 5.44 presents a highlight of the target slices.

The neoprene activator plate is clearly identifiable with the early reflections (Fig. 5.44(a)), as well as the bottom of the landmine (Fig. 5.44(d)) as the last collected reflections. Regarding the pressure plate, it can be noticed a significant amplitude difference between Fig. 5.44(a) and Fig. 5.41(a), despite being moulded from the same material: this is due to its higher density and thickness, which also justifies the fact that in this

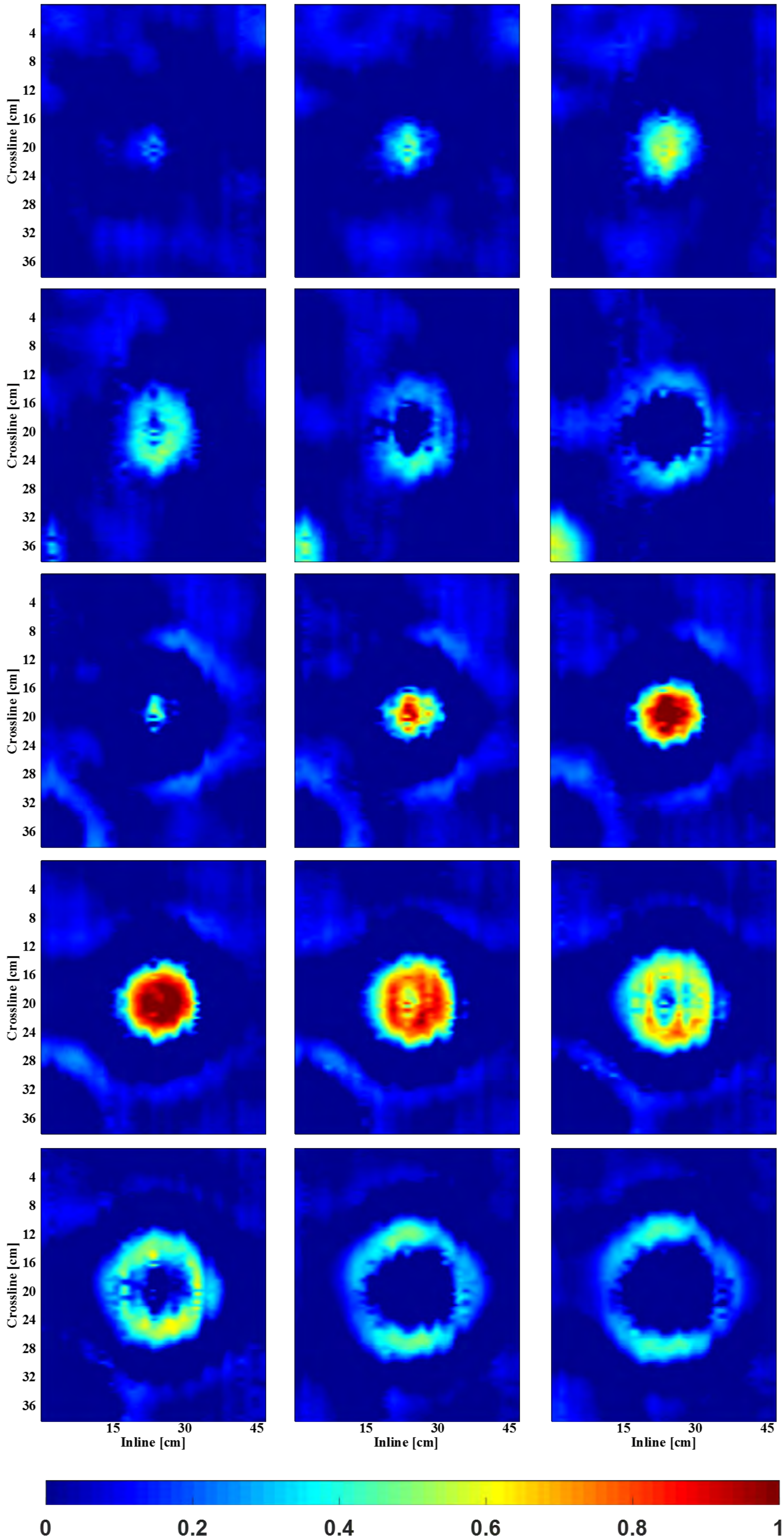

Figure 5.43: Inert VS-50 landmine time slices. Order from left to right, top to bottom.

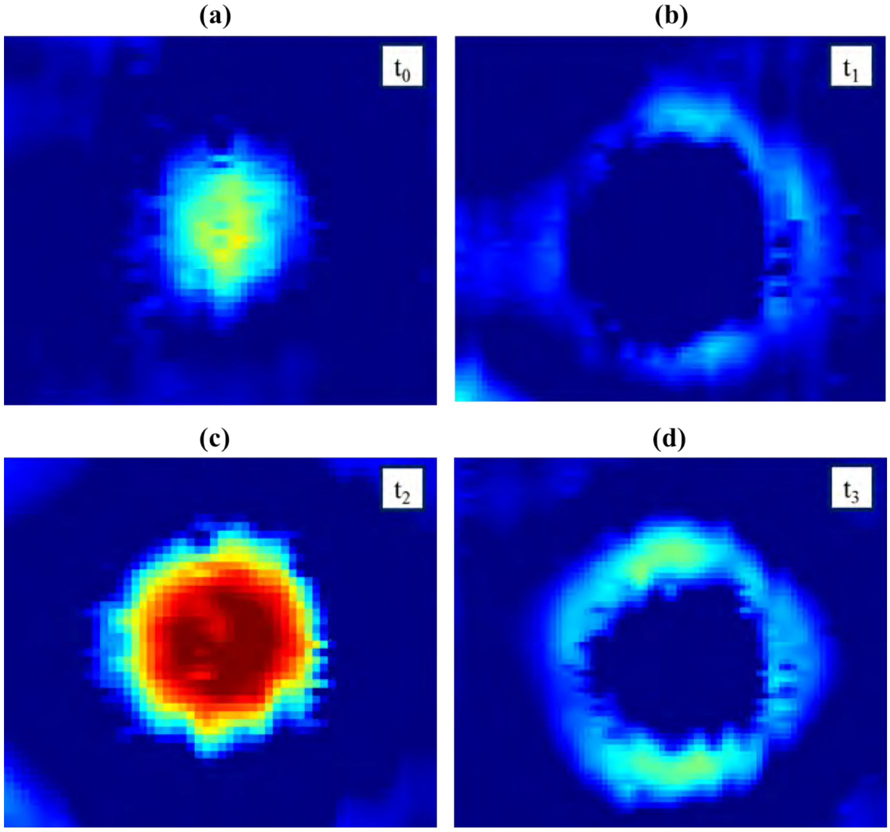

Figure 5.44: Inert VS-50 landmine time slices, internal structure highlight. (a) Upper section - pressure pad. (b) - (c) Internal structure. (d) Bottom part.

case it can be completely resolved (Fig. 5.44(b)).

What is worthy of note is the detection of a highly reflective area beneath these boundaries, with a slightly larger extension compared to the pressure pad contribution. As this layer lies within the target volume, and it has different characteristics (shape and amplitude) compared to the first frame, it can be considered as a contribution generated by the internal structure of the landmine, recalling also the landmine physical structure and what has been found analysing the 2D profile.

This conclusion arises from two main considerations: (1) the amplitude of the reflections is higher than the previous ensemble, suggesting a higher dielectric contrast, and (2) the spatial extension is relatively regular with an amplitudes distribution almost uniform. Both hints are consistent with the air layer below the activation plate, representing the blast resistant assembly. Obviously, the dimension of each air hole is not sufficiently large for the equipment to be able to individually contour the single contributions.

The effects of the sectioned void ring can be recognised through a comparison with Fig. 5.41(c). The two slices both described the effect of an air gap, but if for the SB-33 the pattern is more homogeneous, the slice extracted from the VS-50 shows a more milled pattern. This different appearance can be related to the fact that in the first case there is a single empty area while the latter scattering contribution is generated by a combination of multiple scattering.

The optical overlay is shown in Fig. 5.45.

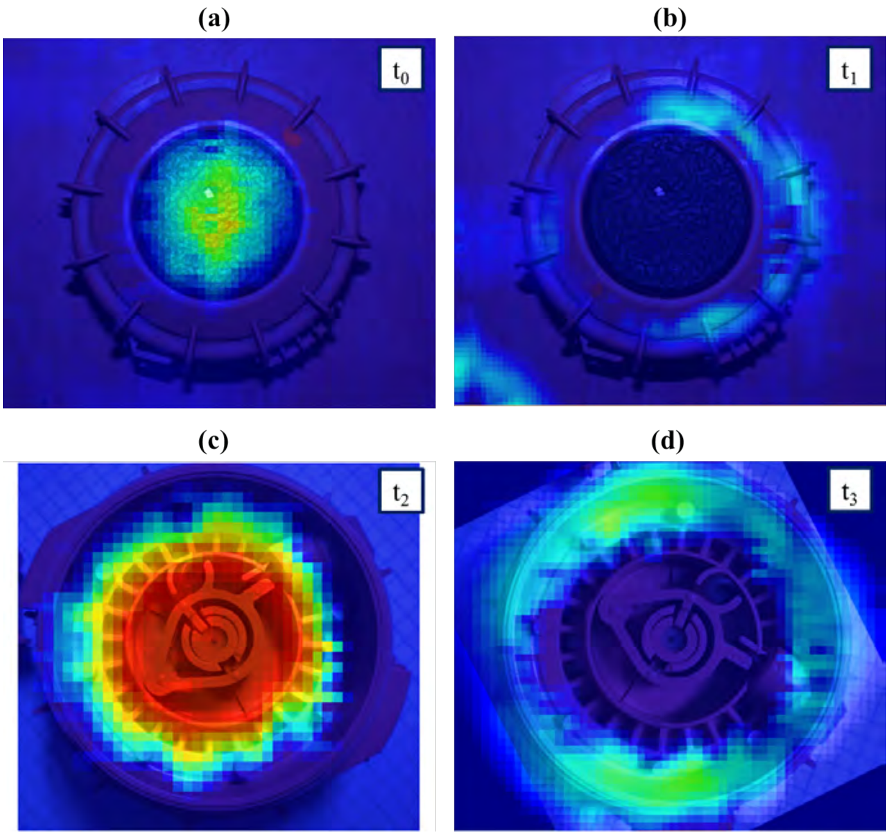

Figure 5.45: Optical overlay of the radar results, inert VS-50 landmine. (a) Upper section - pressure pad. (b) - (c) Internal structure. (d) Bottom part.

Thanks to a more regular design, in this case the overlay is clearly more readable and the previous considerations can be easily verified. What can be noted is the correlation between the last frame, Fig. 5.44(d), with the outer part of the mine base. It should additionally be noted that there is a precise equivalence between the physical dimensions of the landmine sections and the extension of the radar reflections.

5.4.2 Validation of results

Following a similar structure, the obtained results have been verified through the comparison with the VS-50 landmine surrogate, shown in Fig. 5.1(d). What is expected from the surrogate is an ensemble of radar images in all respects consistent with the real inert objects and characterised by a homogeneous behaviour from slice to slice, with no multiple and/or internal reflections.

In addition, also the absence of the rubber activator plate in the target surrogate might have an impact on its radar response, as modelled in the previous Chapter and pointed out above.

The correspondent slices collected from the VS-50 surrogate are presented in Fig. 5.46.

Coherently with the previous considerations, the target exhibits a homogeneous behaviour throughout its volume, without any evidence of contributions from internal reflections. The comparison validates the hypothesis made on the nature of the reflections of Fig. 5.44(c) as the only differences between the two employed targets lies in the air layer below the activator plate.

As a figure of merit of the achieved resolution performance, and as a demonstration of the effect of the pressure pad, a correspondence between the inert VS-50 and its surrogate equivalent cannot be found considering the target extension, as the latter appears in a fewer number of slices. This is due to the neoprene pad which is a material with a velocity which is approximately 60% slower than the surrogate resin. Considering a relative dielectric constant of 3 for the epoxy resin of the surrogate, which produces a range difference between slices of approximately 1 cm, and six as the number of slices embracing the target volume, the estimated height is very close to the physical one (5 cm).

Figure 5.47 and Fig. 5.48 show the focus on the target depth slices and the optical overlay, respectively.

A valuable consideration that rises from the comparison between the two targets is that in comparison with an air gap, a small metal inclusion has a very weak effect on the target response. Therefore, the presence of an air gap notably facilitates the detection of buried plastic cased landmines with GPR.

Finally, to provide a qualitative comparison among the investigated targets, the ensemble of the characterised GPR depth slices have been arranged in a 3D volume visualisation, Fig. 5.49.

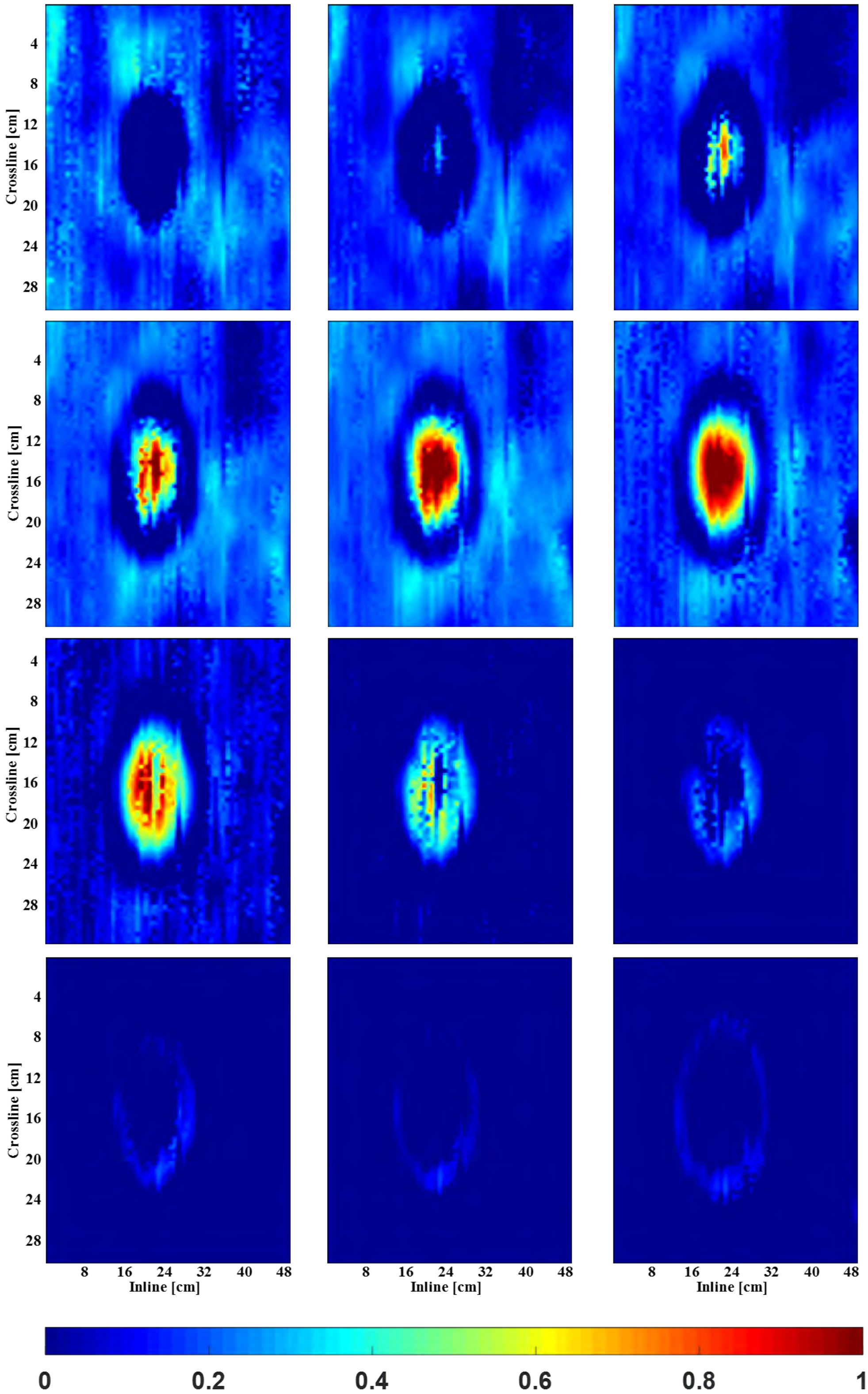

Figure 5.46: Surrogate VS-50 landmine time slices. Order from left to right, top to bottom.

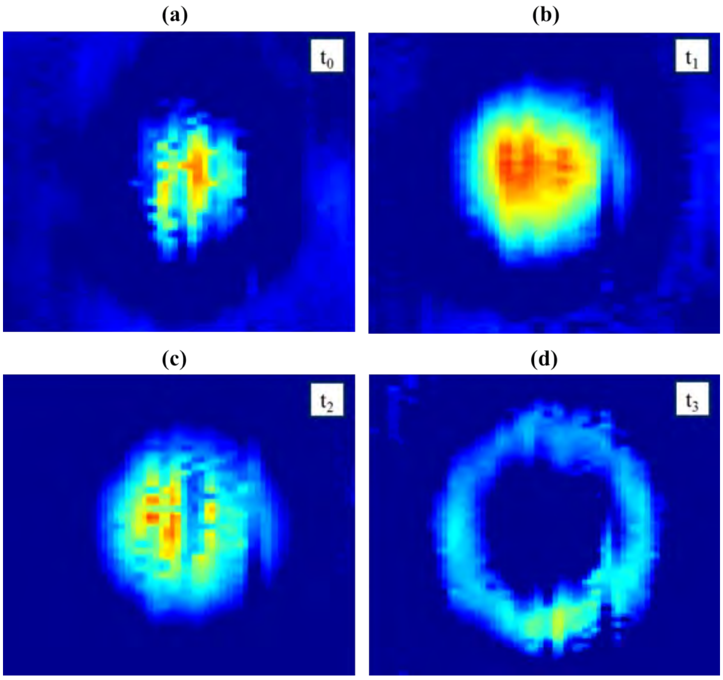

Figure 5.47: Surrogate VS-50 landmine time slices, internal contributions highlight. (a) Upper section - pressure pad. (b) - (c) Internal structure. (d) Bottom part.

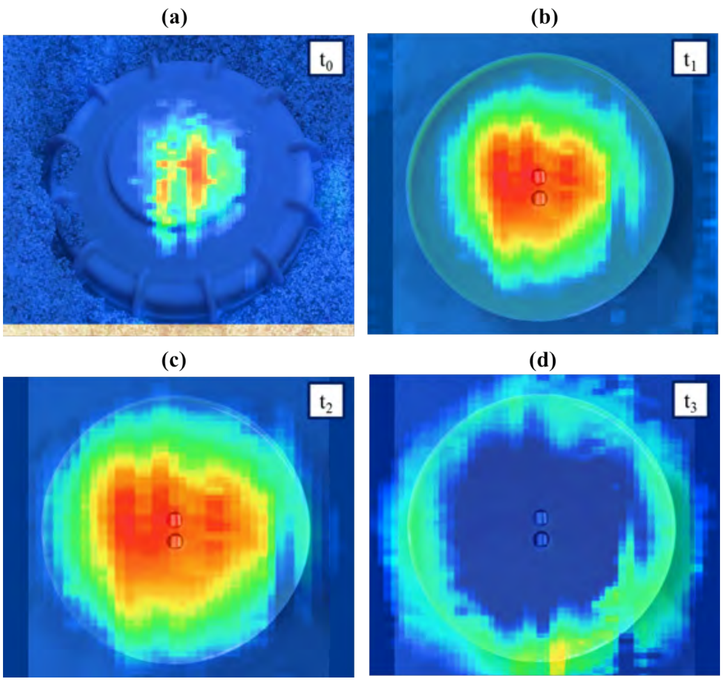

Figure 5.48: Optical overlay of the radar results, surrogate VS-50 landmine. (a) Upper section - pressure pad. (b) - (c) Internal structure. (d) Bottom part.

5.4.3 Constraints on GPR imaging

The quality of the produced images comes at the price of acquiring very dense and regular data. Even if it may be expected that the structure of the VS-50 could still be

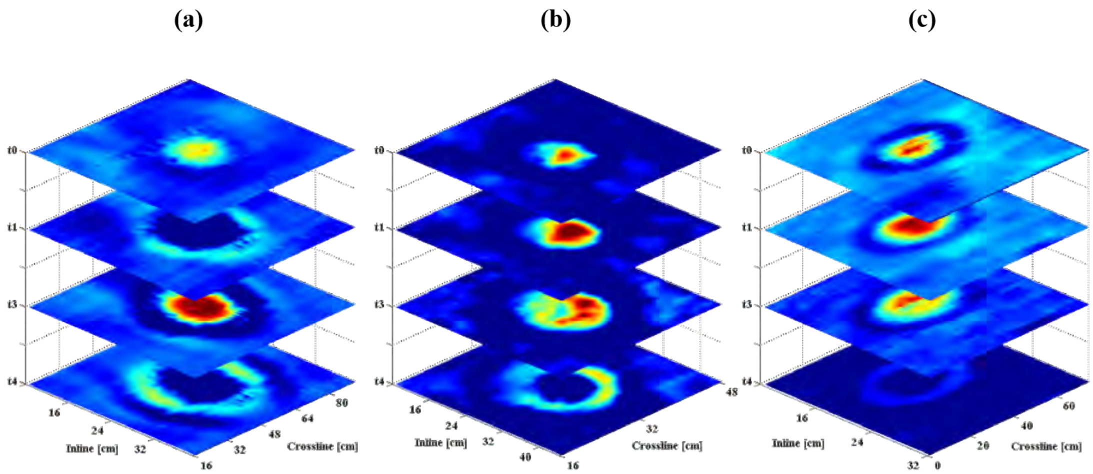

Figure 5.49: 3D visualisation of the radar depth slices. (a) Inert SB-33. (b) Inert VS-50. (c) Surrogate VS-50.

imaged also from degraded data, this will be definitely untrue for the SB-33.

The need for autonomous devices with higher mobility is a continuous research topic for GPR applied to landmine detection. However, to obtain a clear and readable image, a 3-D GPR acquisition should be carried out, meaning that precise and fine spatial samplings are needed. This logically affects the positioning devices, as it has to operate synchronously with the GPR and its accuracy should be definitely less than the GPR sample spacing.

Strictly theoretically, there is a bound beyond which the acquired data will be corrupted and aliased, making the acquisition ineffective. As described in the first Chapter, data gathered with an inline and crossline distance of $\lambda/4$ provide the maximum available information level. When the spacing of acquisition points is greater than the Nyquist interval, one can expect a distortion of the quality and an increase in the number of artefacts in the final image. In particular, data will not adequately define diffraction tails or steeply inclined reflectors. If one includes also the fact that the volume should be acquired with a very high accuracy, it will be easy to understand why the 3D GPR technology is still far from being widespread.

The quarter-wavelength criterion represents the most restrictive requirement, corresponding to the most unfavourable situation when a very shallow target is struck laterally by a surface wave. In such a hypothesis, the signature of the target is represented by two steep lines departing from the location of the target, the inclination being inversely proportional to the medium velocity. Instead, when the object is buried it will appear as a diffraction hyperbola (Fig. 5.50).

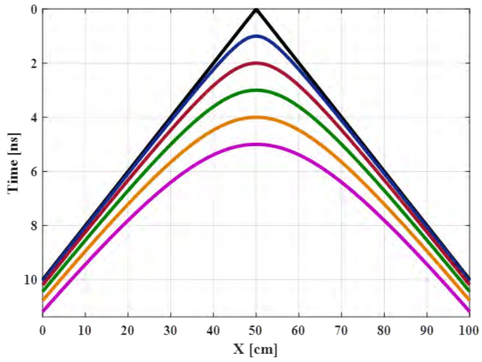

Figure 5.50: Diffraction curves expected on a radar profile.

The following experiments have been performed in order to quantify the level of data sparsity that allows a proper target reconstruction. The dataset employed was acquired at the former Multi-Sensor Mine-Signature (MsMs, Fig. 5.51(a)) test site, located at the European Commission's Joint Research Centre (JRC), Ispra, Italy. The main peculiarity of the site was that for each material plot, an ensemble of targets were buried at different depths. The investigated target was a large anti-personnel landmine (diameter of 11 cm) surrogate and the burial depth of the selected target was 5 cm and 15 cm. The target, visible in Fig. 5.51(b), is designed to resemble mines in respect of their signatures and is moulded in silicone rubber. A low loss loamy material, with a relative dielectric $\varepsilon = 4$ and a resulting velocity of 15 cm/ns has been investigated.

(a) **(b)**

Figure 5.51: JRC test site details. (a) Test lane. (b) Investigated target, blue circled.

A 3D volume was collected using a shielded 1-GHz RAMAC/GPR equipment, manufactured by Mala Geoscience, and employing the pad system previously described (Fig. 5.52). The antenna consists of two bow-tie dipoles oriented perpendicular to the survey direction and separated 9 cm. Details on the acquired data and the acquisition parameters are provided in Table 5.7.

Figure 5.52: JRC acquisition details.

Table 5.7: Data sparsity acquisition parameters and set up.

Parameter	Value
Frequency range [GHz]	0.5 - 1.5
Frequency sampling, $1/\Delta t$ [GHz]	11
Central wavelength [cm]	15
Inline sampling, Δx [cm]	0.8
Crossline sampling, Δy [cm]	0.8
Time window, ΔT [ns]	15
Antenna offset [cm]	9

Considering a maximum frequency of 1.5 GHz, the dielectric properties of the soil gives a quarter wavelength criterion equal to 2.5 cm.

Initially the data were collected with very dense spatial sampling, then they were progressively decimated by the same factor in the inline and crossline directions to obtain the minimum acceptable data density to preserve the features of the target. As the aim of the campaign was to investigate the maximum allowable sample distance to preserve a proper geometrical reconstruction, the processing chain included also a data migration step, performed via hyperbola focusing. A sketch of the methodology is provided in Fig. 5.53.

Also in this case, results are shown through depth slices. Collected scans for the landmine buried at 5 cm are shown in Fig. 5.54.

As expected, the necessary sampling rate to ensure a proper target reconstruction

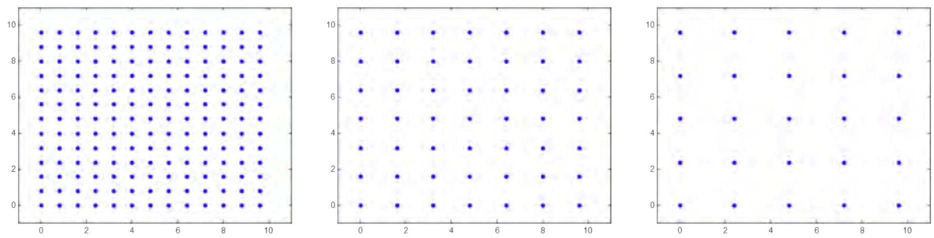

Figure 5.53: Data sparsity analysis: grid decimation example.

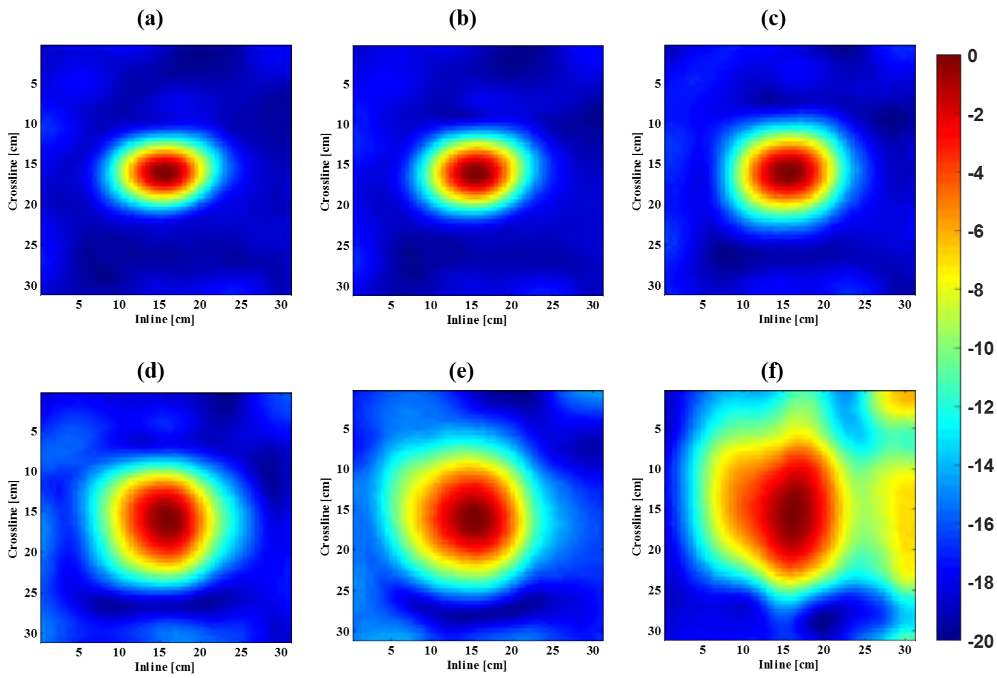

Figure 5.54: Decimation results, landmines at 5 cm. Grid spacing: (a) 1.6 cm. (b) 3.2 cm. (c) 4.8 cm. (d) 6.4 cm. (e) 8 cm. (f) 12 cm.

is sparser than the commonly adopted quarter wavelength. The distance between subsequent samples can be relaxed of an approximate percentage of 20%, Fig. 5.54(b).

Due to frequency dispersion effects of the medium that cause a downshift of the central frequency, the target is still detectable even beyond the defined limit, but the degradation of the resolution is evident. In addition, one should consider also a further quality decay produced by noise and soil effects, which in this case are both negligible. From Fig. 5.54(c) onward, a change in the geometrical reconstruction of the target shape can be noticed.

Applying the same methodology to a deeper target, buried at 15 cm, the difference between the Nyquist criterion and the actual grid spacing increases (Fig. 5.55).

In this case, the same information content can be obtained with a grid spacing

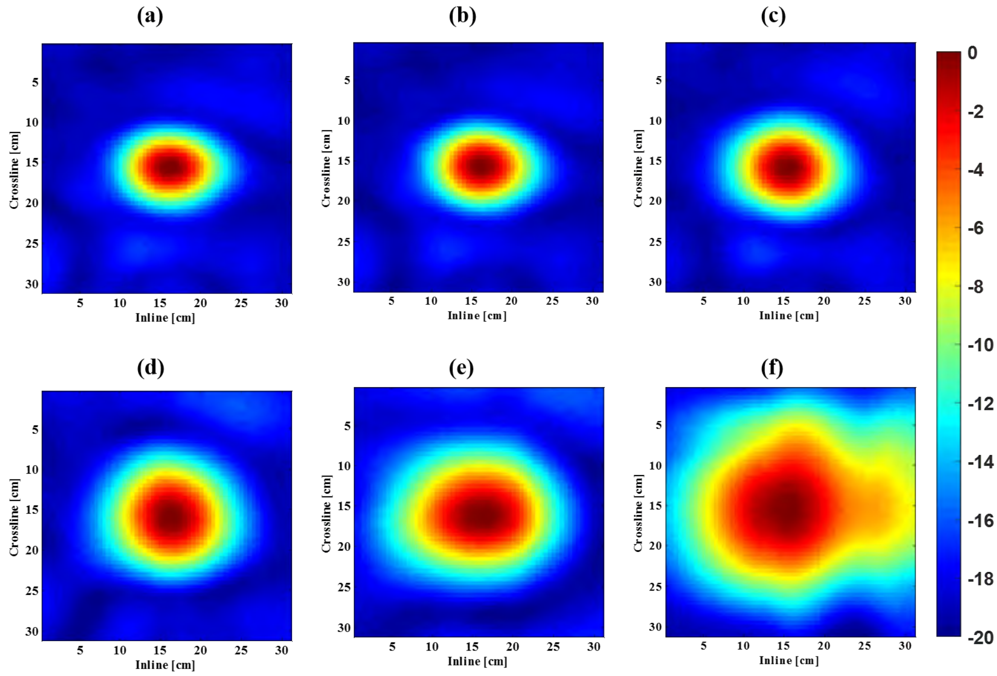

Figure 5.55: Decimation results, landmines at 15 cm. Grid spacing: (a) 1.6 cm. (b) 3.2 cm. (c) 4.8 cm. (d) 6.4 cm. (e) 8 cm. (f) 12 cm.

which is almost two times the $\lambda/4$ criterion, Fig. 5.55(c). As before, the geometrical focusing is still capable of retrieving the target properties even with a very sparse grid, but the shape is unacceptably corrupted.

Obviously, with no *a priori* information on the buried target, it is reasonable to consider the most restrictive case.

Addressing the second requirement of 3D GPR acquisition, a positioning error was introduced by substituting the acquired linear sample with a neighbouring trace according to a random criterion. As the purpose of the experimentation is to appraise the maximum affordable positioning error, the data were decimated following the outcomes of the density reduction step to obtain the maximum acceptable sample interval and to create the worst possible scenario.

The synthetic positioning error, introduced on raw data (before the migration process) to effectively simulate a degraded acquisition, was computed by substituting the acquired sample (the nominal one) with an adjacent sample according to a definite but random criterion. The irregular grid has been created by randomly generating for each nominal sample a numeric flag indicating the axis and direction of the sample to replace the existing one. The chosen statistical distribution is a random uniform distribution, with a seed probability of 0.20 for each ill-positioned trace (4 in total) and 0.20 for the nominal sample (Fig. 5.56(a)). The histogram of the distribution sequence is shown in Fig. 5.56(b).

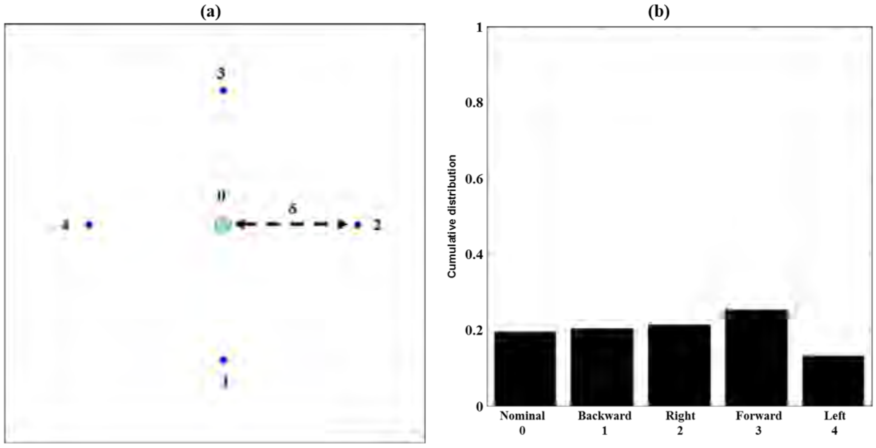

Figure 5.56: Regularity degradation. (a) Sample replacement scheme. (b) Random distribution for traces substitution.

It can be seen from the sample distribution that for each nominal sample, there is an equal probability of replacing it with the forward, backward, leftward, and rightward neighbour or maintain the correct one. Such a distribution was chosen to simulate the most unpredictable situation in which: 1) the accuracy degradation is not polarized along a preferential direction and 2) no prediction of the possible spatial distribution of the acquisition error can be made in advance.

The same error distribution was applied considering a different error radius (δ in Fig. 5.56(a)), which defines the distance with respect to the nominal position of the sample to be substituted, according to the mentioned geometry. Values for the radius are listed in Table 5.8.

Table 5.8: Data sparsity acquisition parameters and set up.

Target depth	Radius, δ	Distance from the nominal sample
5/15 cm	1	0.8 cm
	2	1.6 cm
	3	2.4 cm
	4	3.2 cm
	5	4 cm

A sketch of the resulting irregular grid is shown in Fig. 5.57.

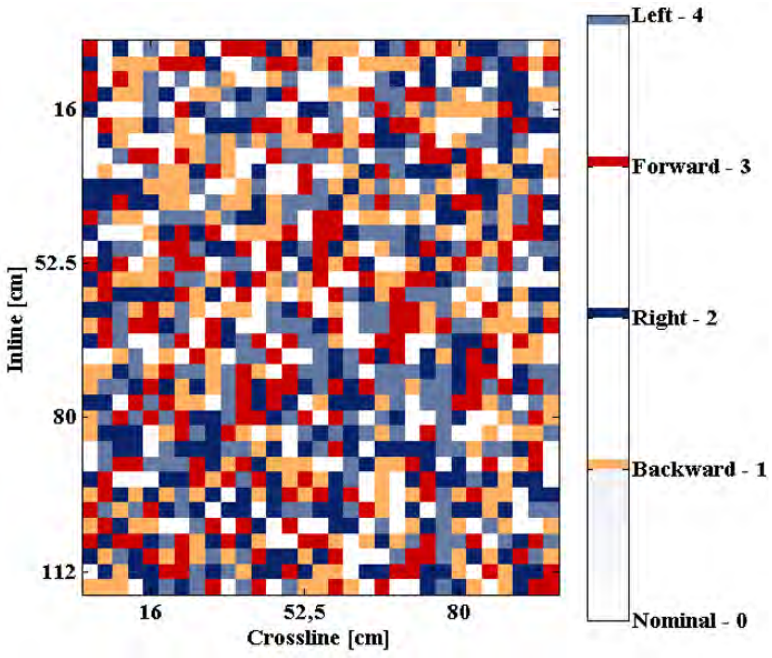

Figure 5.57: Synthetic acquired grid after irregularity superimposition

Processed slices for the landmine buried at 5 cm with varying error radius are presented in Fig. 5.58. Amplitude is displayed in a blue–yellow–red colour map and normalized in the range [0–1] with respect to each relative maximum value.

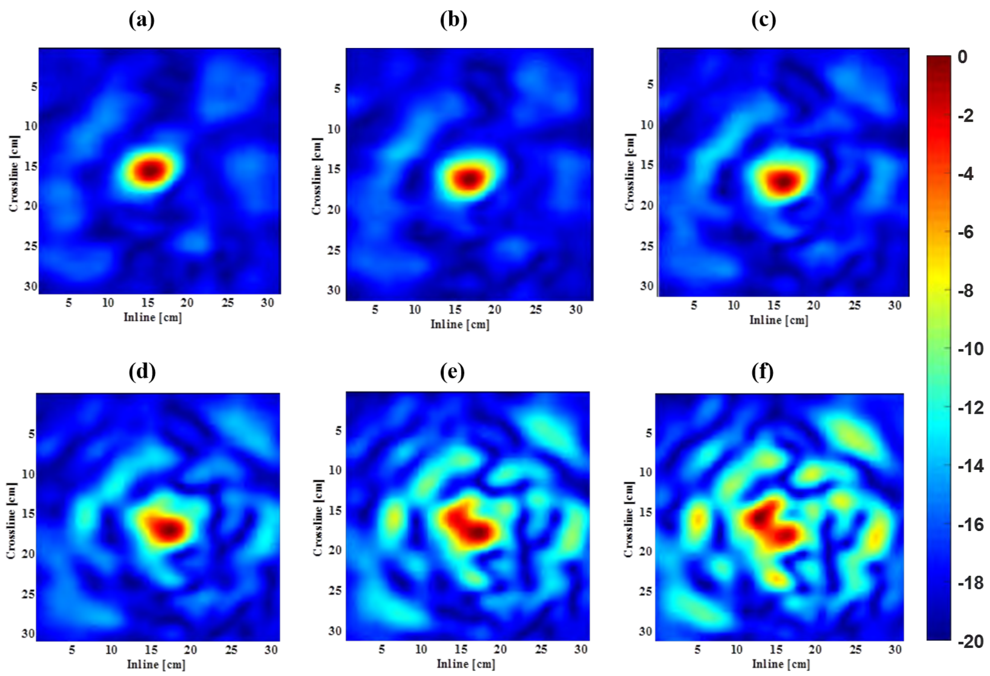

Figure 5.58: Irregularity results, landmines at 5 cm. Error radius δ: (a) 0 cm. (b) 0.8 cm. (c) 1.6 cm. (d) 2.4 cm. (e) 3.2 cm. (f) 4.0 cm.

Considering that the first frame, Fig. 5.58(a), is the original regular data, it can be seen that a pronounced degradation of the focusing performance arises from Fig. 5.58(c) onward, giving a maximum error radius of 1.6 cm. This value corresponds to half of the linear sample distance, suggesting that as long as the trace is included in the boundaries of the same information cell, no loss of information occurs and the reconstruction process is capable of correctly retrieving the spatial information.

Increasing the magnitude of inaccuracy causes processing artifacts faults which reduce the image quality. Obviously, the target is still detectable, thanks to the homogeneity of the host material, but the noise level could decrease the confidence in the recognition process.

Figure 5.58 presents the correspondent results for the deeper target.

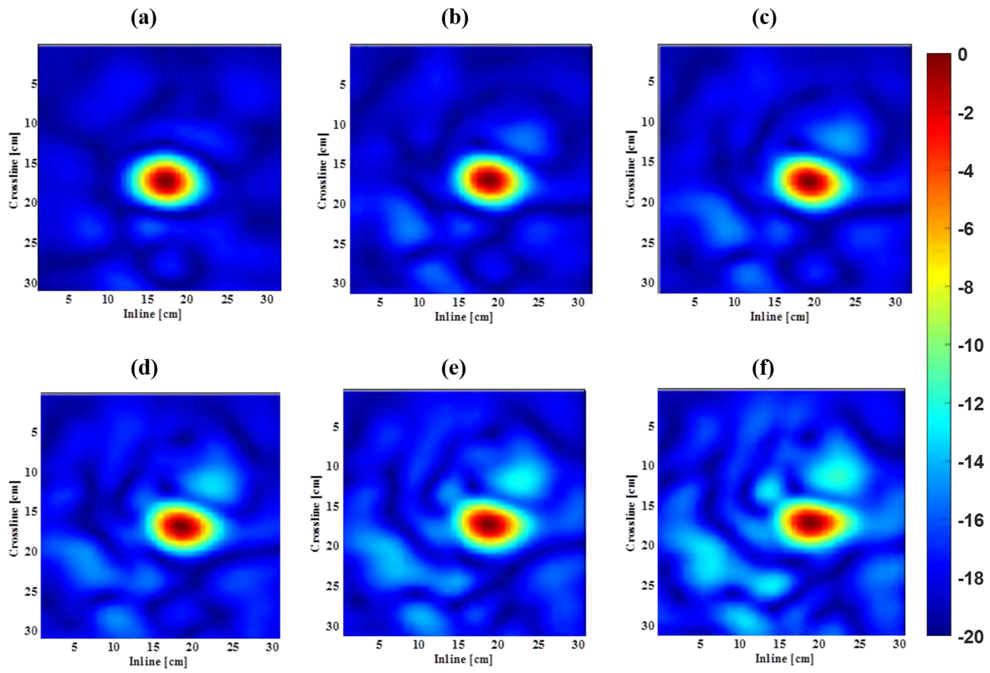

Figure 5.59: Irregularity results, landmines at 15 cm. Error radius δ: (a) 0 cm. (b) 1.6 cm. (c) 2.4 cm. (d) 3.2 cm. (e) 4.0 cm. (f) 4.8 cm.

In this case, given a maximum sampling distance of 4.8 cm, the radius beyond which the resolution starts to deteriorate is equal to 2.4 cm (Fig. 5.59(c)), confirming the outcomes found for the shallower target. Following the previous considerations, the target can be identified in each of the slices of Fig. 5.59, even without hints on the presence of a target, but a degradation in the shape of the reconstructed landmine and in the focusing performance is clearly noticeable.

To quantitatively assess the effect of the magnitude of the positioning error, the correlation between the regularly acquired slice and the irregular ones has been computed. The analysis of the images correlation for both the investigated targets is provided in Fig. 5.60.

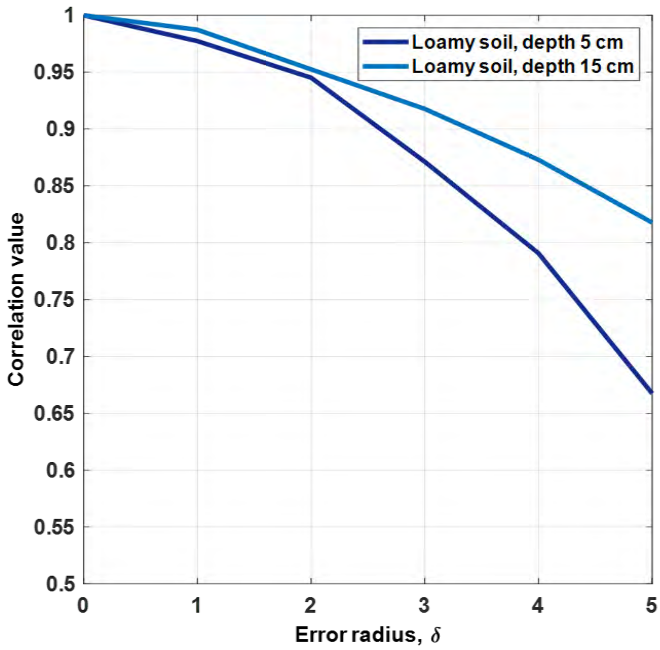

Figure 5.60: Irregularity results, image correlation analysis.

For the deeper target, given a larger affordable spacing, the ultimate limit of the irregularity corresponds to a radius of 2.4 cm, consistent with the spacing of 4.8 cm of the regular data. This is identifiable as an increase of the inclination of curve after a radius of 3. The same applies to the shallower target, for which the limit is definitely more evident. No significant losses of accuracy are evident elsewhere.

5.4.4 Comments

The set of extracted slices has allowed a precise and detailed definition of the internal composition of the targets, considering also the absence of data processing. Such a resolution means that the frequency content of the collected data, especially its higher portion, has been preserved, and this performance has been achieved mostly through the employment of a ground coupled GPR system, but also thanks to the low frequency absorption effects of the surrounding material. Obviously, the presence of inhomogeneities, multiple clutter scattering or soil texture variations, will dampen the collected energy and complicate a proper recording of these reflections.

The collected high resolution GPR slices showed that the internal design of the landmine can be properly imaged and characterised, confirming the applicability of the approach. The internal assemblies of the landmines under test were identified with a high degree of confidence, even from raw radar data. In addition, the superimposition of the radar slice to the picture of the unscrewed target provided a very close correspondence between the radar images and the actual structure, both in terms of anomalies location and spatial extension accuracy.

A notable conclusion is that the achieved precision can be a significant value for target recognition algorithm based on image matching. Furthermore, this capability may overcome the need for extensive data collection, as the level of accuracy is such that the correlation can be performed even with sketches and diagrams.

Another valuable consideration stems from the comparison between the inert VS-50 and its surrogate, and it is the evidence that for the detection an air gap has a predominant effect over a small metal inclusion.

However, this quality does not come without a price. Profiles spacing in the order of couple of centimetres maximum are usually adopted to ensure a proper target reconstruction and to avoid artefacts in the subsurface image. Considering that landmine detection and removal is a time-consuming business, and that the survey time is directly related to the data density, a decrease in the number of collected points will result in a shortening of the acquisition time. In addition, another challenging task given a high spatial sampling rate is a consequently high accuracy in linear samples positioning.

These two requirements may run the risk of not being fulfilled in particular situations, as for examples the presence of obstacles or obstructions and an uneven surface topography.

The evaluation of the maximum affordable grid spacing and sample regularity, both intentionally altered creating a sparse acquisition grid, has shown that, even for small targets such landmines, there is space for reducing amount of data that need to be collected to maintain a suitable level of resolution. The experimental results taken together highlight that the same reconstruction performance that can be obtained with an uneven and coarser sampling grid, lowering the demanding and challenging requirements of samples precision.

5.5 Bistatic characterisation of landmine signature

The results generated by the 3D survey can comprehensibly justify the adoption of such strategy, as the produced images speak for themselves, but in the light of increasing the efficiency of GPR technology, a way to provide the same level of information but reducing the effort for data acquisition should be evaluated.

Easily understandable, the alternative methodology should go through a dimensionality reduction, as otherwise there will be no advantages, considering the clarity of the imaging results. At the same time, it should be as independent as possible to the geometrical variables, such as landmines inclination angle and internal design, as a deviation from a standard set-up could affect the detection performance.

As described in the research scope, a possible strategy that could gather the same level of information is the collection of a set of signatures changing the separation between the transmitter and the receiver, i.e. exploiting the angular domain of the problem.

The following section describes the related experimental campaign carried out to investigate the potential of a bistatic approach for buried target characterisation and identification.

5.5.1 Trials descriptions

A set of bistatic signatures from the three different inert landmines and the target surrogate has been acquired in the test sand pit located at the Defence Academy (Fig. 5.16) following the same arrangement of the previous experimental campaigns.

The GPR equipment employed for the measurements consisted of the IDS Aladdin radar and an additional IDS THRHF radar, both provided by IDS Georadar srl. The two impulsed devices carry dipole antennas spaced at 6 cm with a central frequency and a bandwidth of 2 GHz and 3 GHz, respectively, pictured in Fig. 5.61. The two antennas were connected to the same central unit to allow a separate and synchronised configuration. The lower frequency equipment was chosen as a receiver to maintain uniformity with the previous campaigns and to take advantage of the finer sensitivity of the higher frequency equipment components.

To investigate the capability of a bistatic geometry to match the information content produced by a high resolution image, two different schemes have been evaluated,

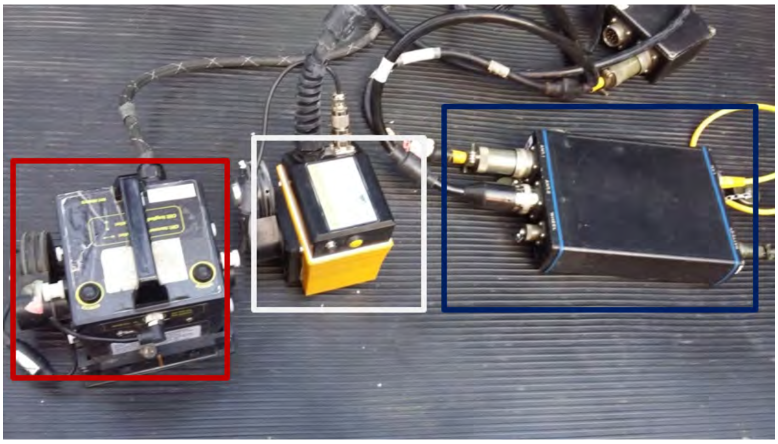

Figure 5.61: Bistatic characterisation, equipment details. From left to right: 2 GHz equipment, 3 GHz equipment and central unit.

respectively the common receiver (CR) and the common mid point (CMP) scheme. The choice of a common receiver, rather than a common source method was made for convenience only, as the two acquisition strategies are reciprocal. Photographs of the acquisition are provided in Fig. 5.62.

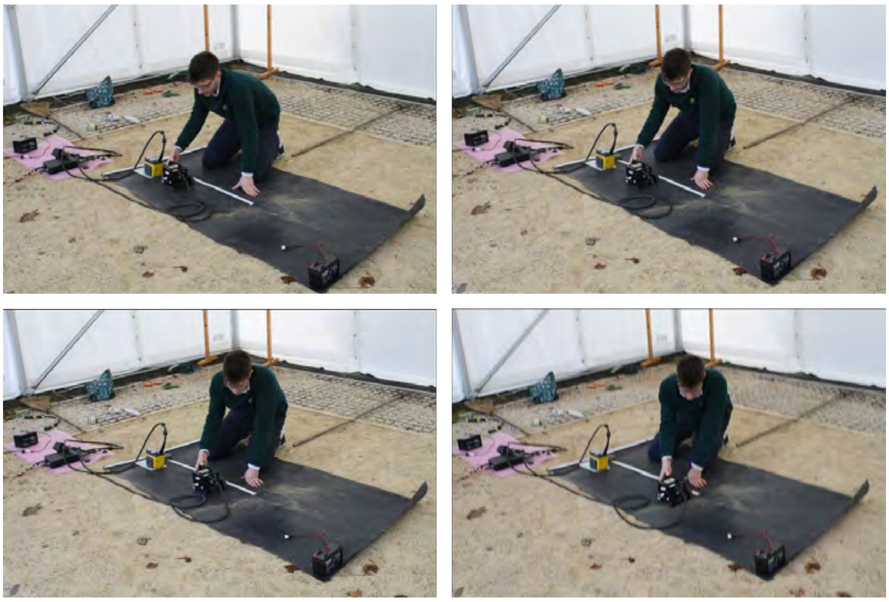

Figure 5.62: Bistatic characterisation, acquisition photographs.

A series of CR profiles were acquired each time moving the receiver toward the target, as sketched in Fig. 5.63, so that also the CMP signature could be extracted from the data. This was made in order to avoid possible variations in the measurement set-up and consequential loss of consistency among all the results provided in the work. To guarantee precise profile matching and accurate acquisition, the soft pad was placed between the radar equipment and the soil.

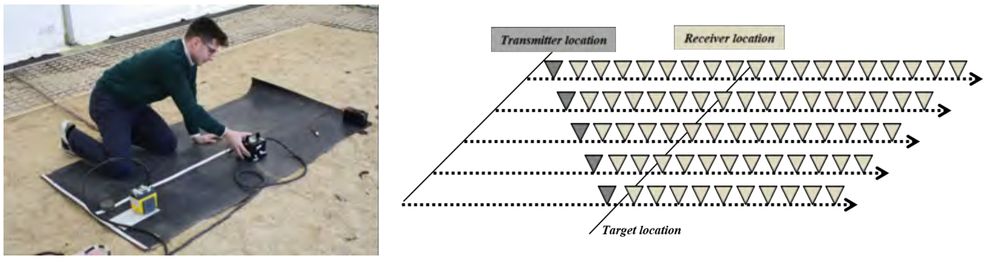

Figure 5.63: Bistatic characterisation, common source acquisition scheme.

Starting with both the equipment located at a distance of approximately 30 cm from the target location, the transmitter was moved at a 0.4 cm step, controlled by the odometric wheel attached to its side, until reaching a sufficient distance to consider the target contribution vanished. Then, the receiver was advanced by 1 cm and the scheme was replicated. The last collected profile corresponds to the receiver located exactly over the target. Generally, no significant differences are expected between the two techniques in terms of gathered information, even if some logistical advantages and disadvantages are evident, as described in Chapter 1.

The process of arranging the CMP sounding from a set of CR profiles is illustrated in Fig. 5.64.

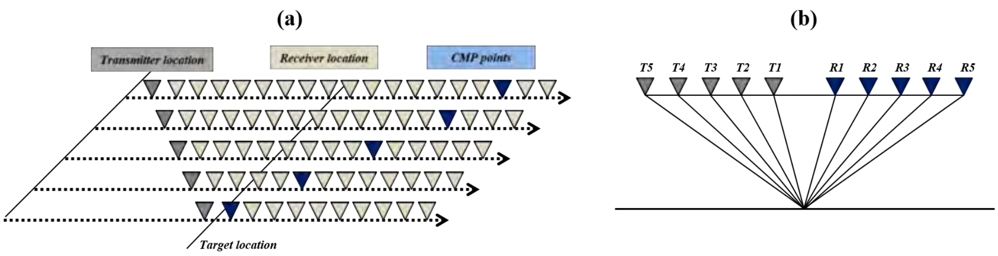

Figure 5.64: CMP signature extraction.

Acquisition parameters and data details are summarised in Table 5.9.

Bistatic signatures of landmines are presented in the commonly employed range versus offset format, which provides a very clear illustration of eventual amplitude variations with offset. In this case, to preserve integrity and to provide a proper comparison, the only processing step computed on the data consisted in the frequency filtering.

The results of the bistatic characterisation of the PFM-1 landmine is provided in Fig. 5.65, for both the described geometries.

Table 5.9: Bistatic acquisition parameters and set up.

Parameter	Value
Frequency range [GHz]	Transmitter: 1-3, Receiver 1.5 - 4.5
Frequency sampling, $1/\Delta t$ [GHz]	17
CR inline sampling, Δx [cm]	0.4
CR profile length [cm]	50
CR profile number	30
CMP offset sampling, Δ_{off} [cm]	1
CMP offset range [cm]	6 - 33
Time window, ΔT [ns]	30

The two results show similar content, though some differences, especially in the quality of the output are visible. A single reflection is visible (marked A), with a spatial extension directly linked to the physical dimension of the target, and no further events are detectable. Considering the high amplitude and the constant behaviour, the reflection can be attributed to the metallic detonator, confirming what has been found in the signature analysis. Given the nature of the target, this was expected. In addition, both frames show the ghost replica of the target generated by the earlier strong reflection, as previously pointed out.

The situation should change when the illuminated target includes internal assemblies, as controlling the incident angle of the wave and the vertical position of the reflection plane, the antenna separation might better highlight the additional internal scattering feature.

The CR profile and the CMP profile of the VS-50 are shown in Fig. 5.66(a) and (b) respectively.

In this case, three events are detectable, and these have almost the same spatial extension. While the upper and lower reflections are due to the top and the bottom of the landmine (marked A and C, respectively), the middle one is generated from the internal scattering point. Its constant trend over the separation range means that as long as the target is illuminated, this components will contribute to the radar signature. Considering the design of the target and the previous results on the target signature analysis, the detected reflections can be associated with the activation mechanism behind the pressure plate, which covers the whole landmine extension. This contribution is the same recognised from the 3D campaign as a homogeneous, high amplitude reflections

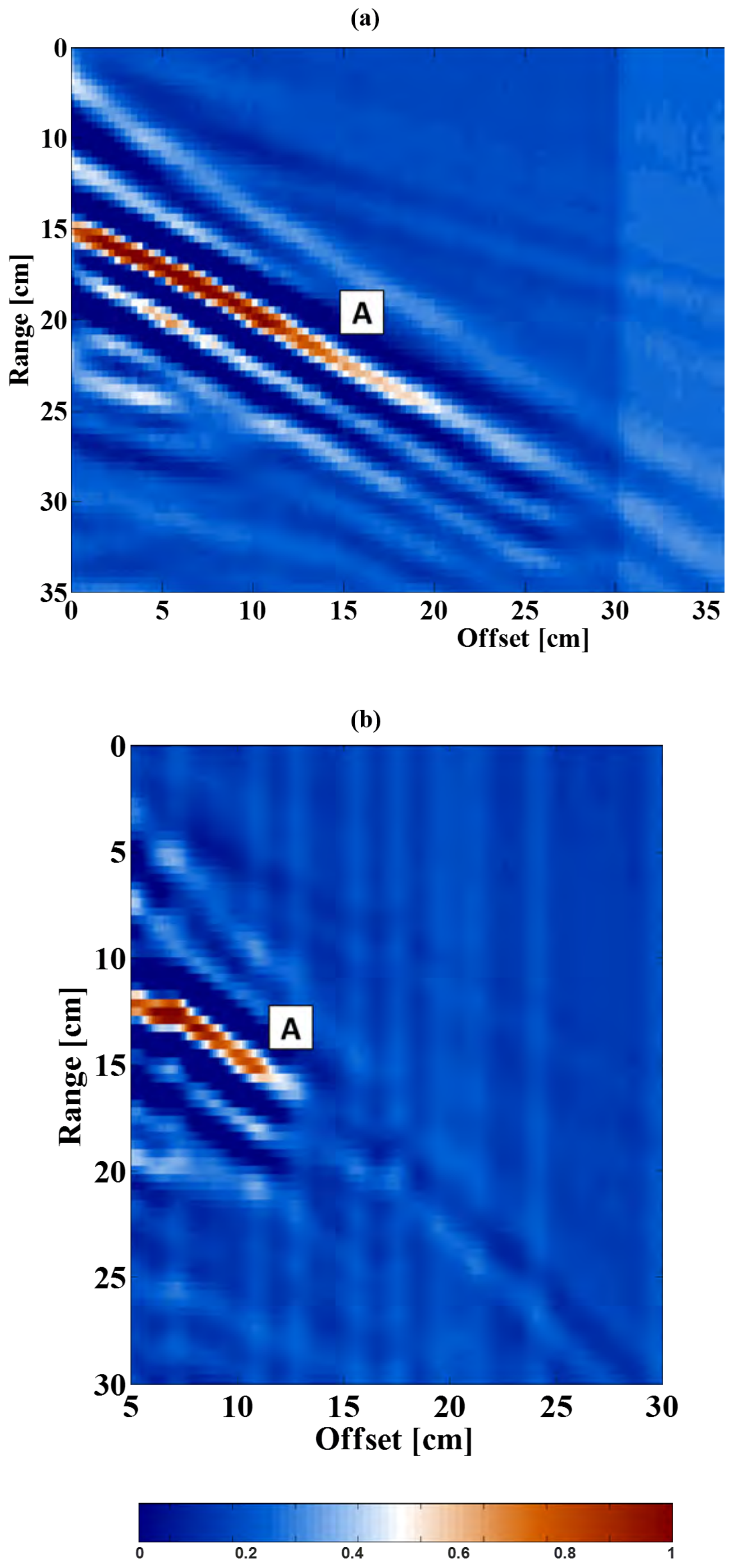

Figure 5.65: Inert PFM-1, bistatic characterisation. (a) CR profile. (b) CMP profile.

occurring below the early recordings of the target.

Fig. 5.67 presents an interpretative diagram for a better identification of the feature.

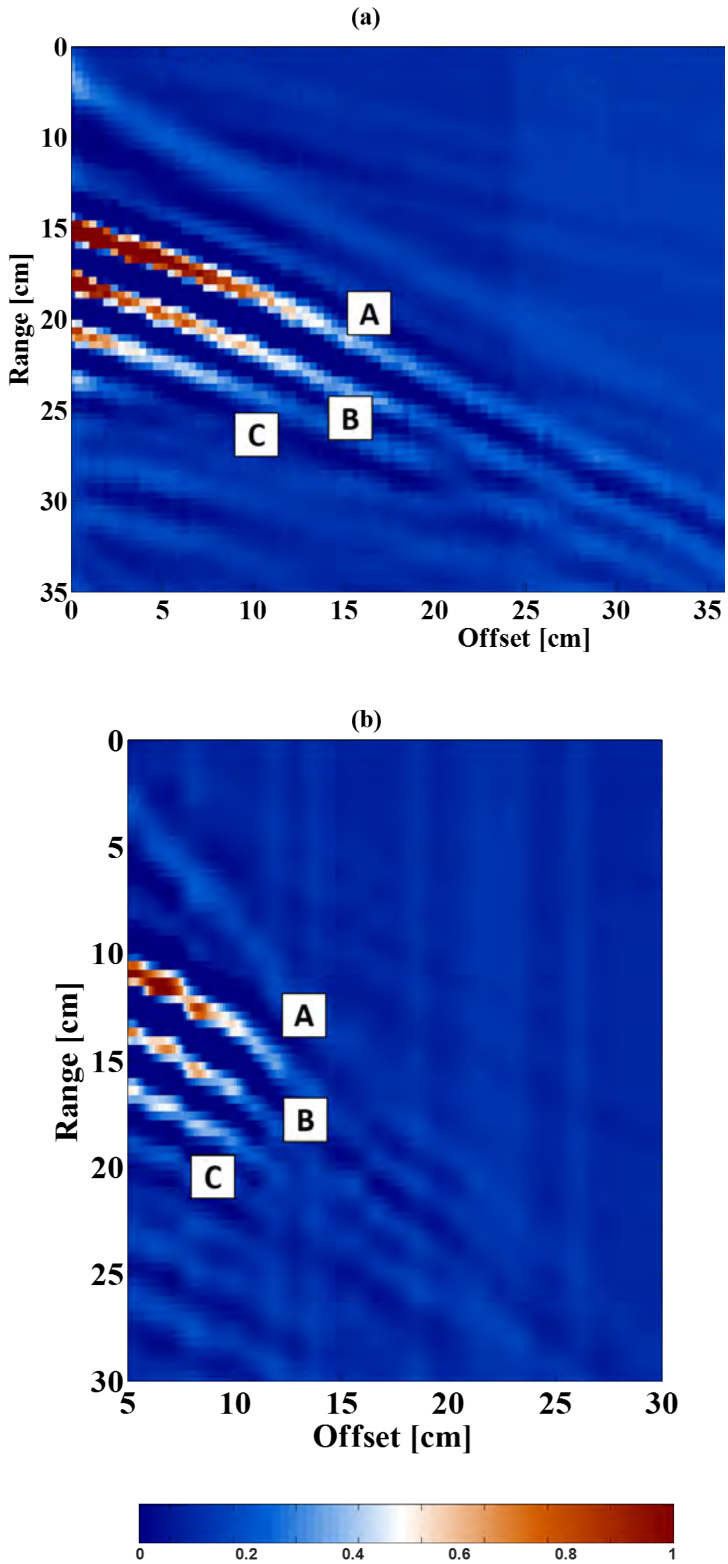

Figure 5.66: Inert VS-50, bistatic characterisation. (a) CR profile. (b) CMP profile.

The last investigated landmine is the SB-33, which presents an irregular internal design, including different components with different shapes. Its range versus offset

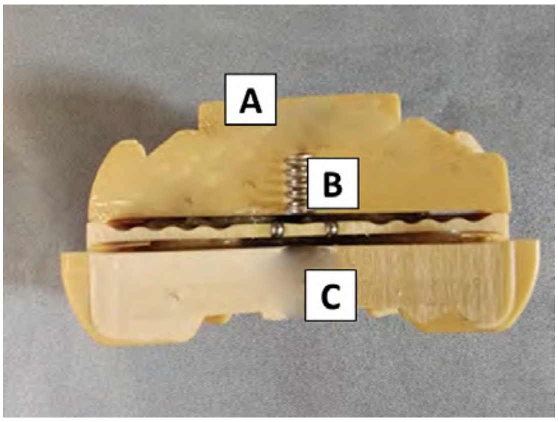

Figure 5.67: Inert VS-50, bistatic signature. Interpretative diagram.

results for both acquisition methodologies are provided in Fig. 5.68.

In a similar manner to the VS-50, more than one reflection is evident, therefore a preliminary indication of a target with a composite structure can be obtained. However, the middle reflection (marked B) is spatially longer than the top (marked A) and bottom one (marked D), demonstrating that the scattering event is not homogeneous over the target space. This reflection is due to the void located aside the detonator (identifiable with reflection C) which is located in a particular section of the target. In this case, the advantage of a bistatic approach is clearly visible, as this reflection is stronger under a particular angular range, differently from the other reflections.

If one considers the results presented in Fig. 5.11, this results represents a notable improvement. A descriptive cutaway is presented in Fig. 5.69

The last aspect is related to the target size. The diffraction hyperbola generated in a raw monostatic radar image depends mostly on the target size, orientation and depth, as well as the surrounding soil properties. Hence, a measure of the target actual extension is hard to guess from its hyperbolic representation. Progressively separating the transmitter and the receiver, instead, at some point will cause the target to leave the illumination region of the antennas. Substantially, the acquisition procedure reduces the hyperbola tails extension, as both the equipment are moving away from the target centre, and limits the collected target contributions. Taking as a reference the first or the last contribution from the target, i.e. the top or the bottom reflection, the target size can be easily inferred with a certain level of accuracy even from raw data.

Proof of this is provided in Fig. 5.70. Estimation accuracy can be evaluated by a comparison with the actual dimensions (Table 5.1).

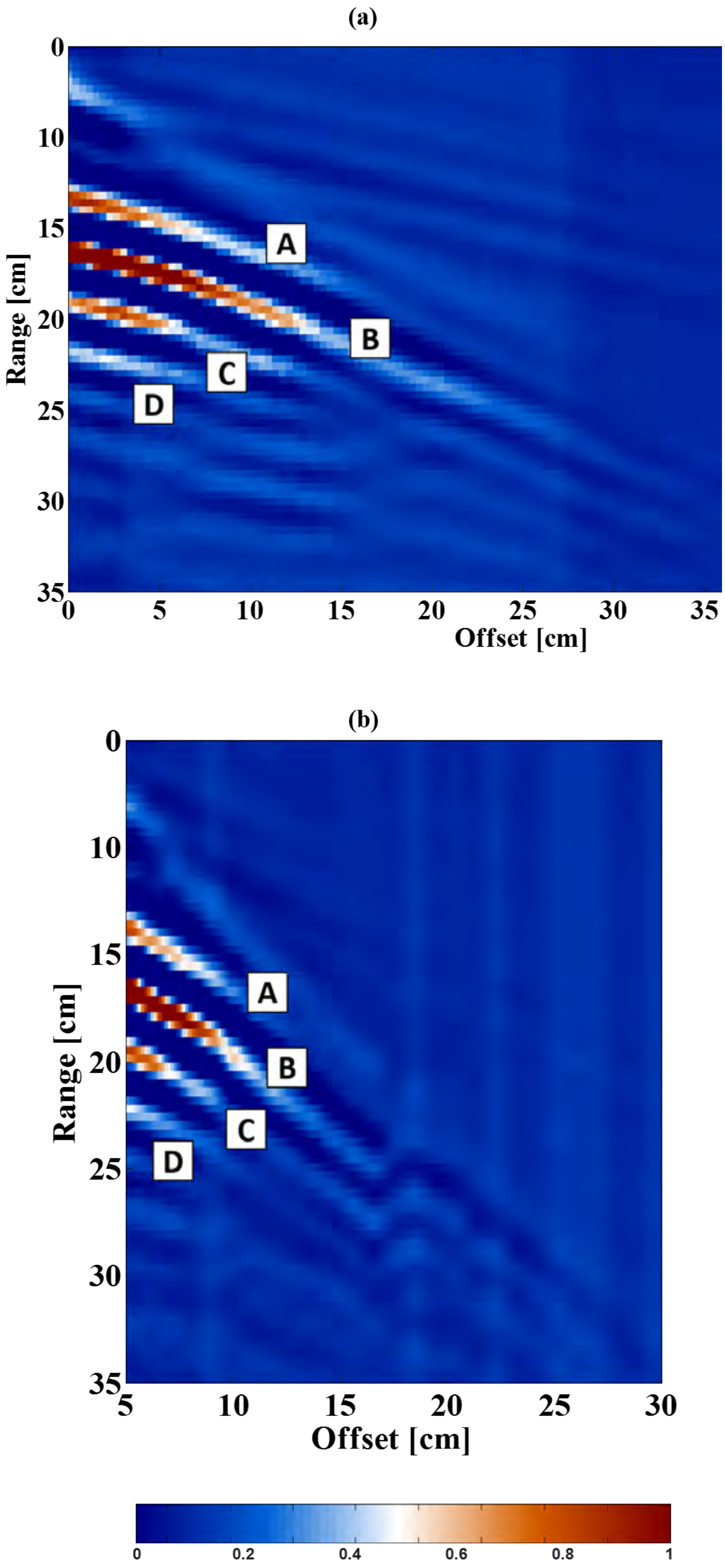

Figure 5.68: Inert SB-33, bistatic characterisation. (a) CR profile. (b) CMP profile.

This feature represents probably the principal difference between the two bistatic methodologies, as it is evident the better accuracy achieved with a CMP scheme.

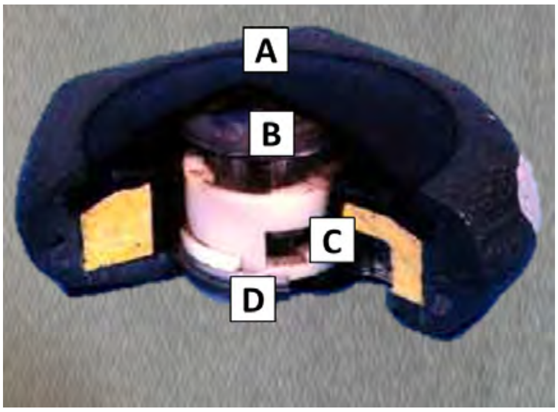

Figure 5.69: Inert SB-33, bistatic signature. Interpretative diagram.

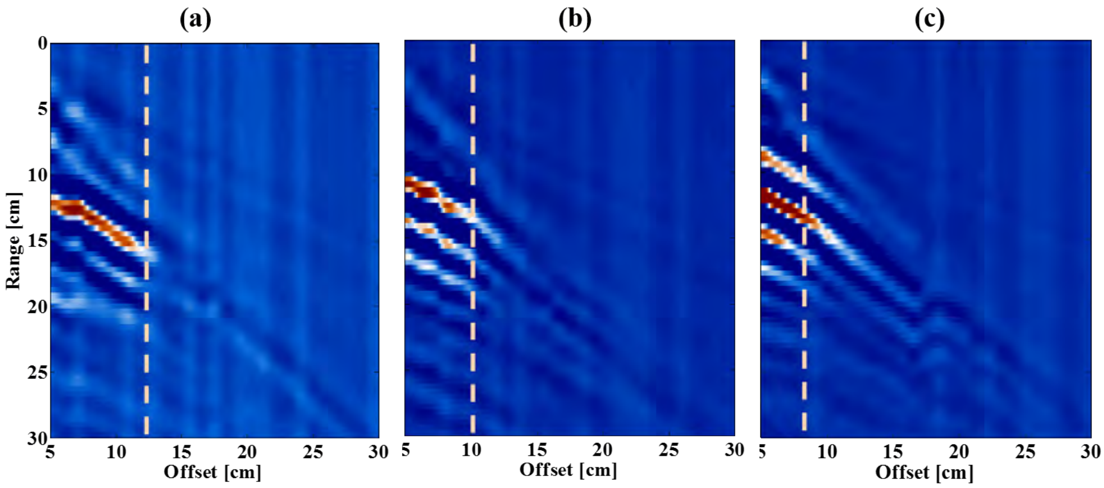

Figure 5.70: Target size estimation. (a) Inert PFM-1. (b) Inert SB-33. (c) Inert VS-50.

5.5.2 Validation of results

As before, the surrogate VS-50 was investigated to prove the methodology. Recalling the previously made considerations, the bistatic signature of the surrogate should be almost constant regardless the bistatic angle, as (1) no internal structure is included, and (2) the metallic content does not provide a detectable contribution.

Due to the unavailability of the test site at the Defence Academy, the following acquisitions have been carried out in a conventional sand pit. Although a different texture and a higher level of humidity, the two materials have proved to show very similar propagation characteristics.

As no meaningful differences have been noticed between the two bistatic strategies, for validation purpose only the CMP signature of the landmine surrogate will be presented and commented. The collected signatures are described in Fig. 5.71.

As can be noticed, a single reflection (marked A) appears, with a spatial duration

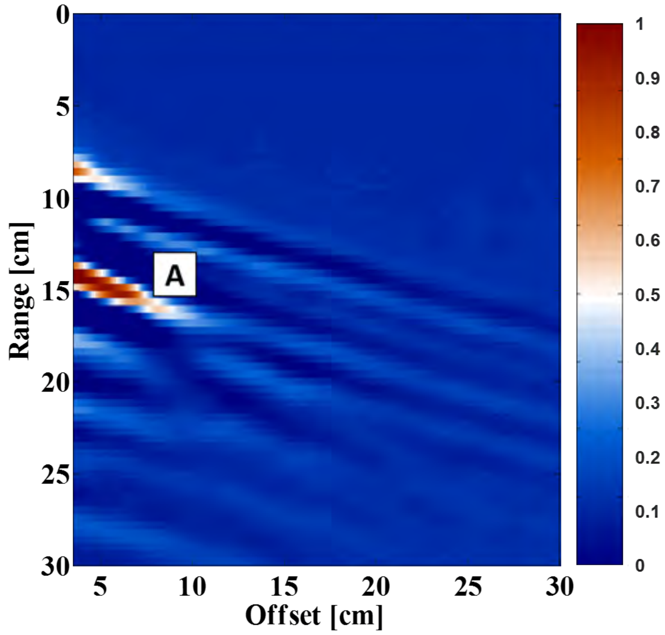

Figure 5.71: Surrogate VS-50, CMP signature.

approximately equal to the target size and very close to its inert counterpart. Also in this case, the metal inclusion does not impact the signature.

Finally, recalling one of the limitations highlighted for the 1D signature analysis, to assess the reliability of the performance of a bistatic approach, an additional investigation has been performed changing the target inclination angle, variable that has a notable impact on the detection of the internal reflection.

Results from the inclined inert VS-50 and surrogate are shown in Fig. 5.72(a) and Fig. 5.72(b) respectively.

The collected CMP signatures demonstrate that the effect of the internal structure is robust to the target inclination, as all the three events previously detected (Fig. 5.66) are still identifiable, even though the reflections no longer appear constant, due to the change in the relative geometry. Compared to Fig. 5.12 and Fig. 5.25, it is evident the improved performance as in the mentioned situations, the internal scattering contribution was not detected. On the contrary, no significant variations are visible for the surrogate. In conclusion, no internal reflections are missed and no misleading reflections are produced.

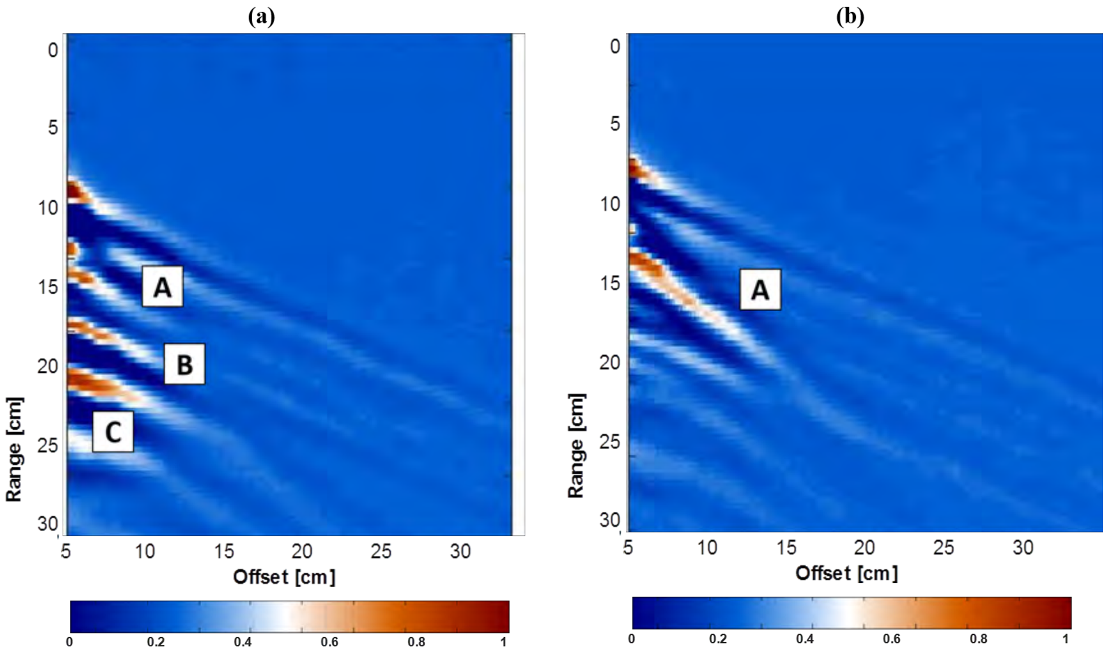

Figure 5.72: Bistatic signature comparison, inclined targets. (a) Inert VS-50. (b) Surrogate VS-50.

5.5.3 Comments

From a target characterisation perspective, the outcomes have demonstrated that a bistatic acquisition methodology could yield as much information as a time consuming 3D GPR campaign, with the great advantage of being less expensive and demanding.

In particular, when the target does not include any internal assemblies, as for the PFM-1 landmine, no additional reflections are detectable, while when the object is characterised by a more complex design the contributions of these components are identifiable and a clear match to the actual design can be supposed.

Data have been acquired through two different bistatic geometries to provide a comprehensive evaluation of the technique. In particular, a common receiver (CR) and a common mid point (CMP) scheme were employed, using two different GPR equipment connected to the same central unit to ensure synchronisation.

The two proposed schemes were both able to properly characterise the investigated target, without significant differences between the acquisition geometries. This aspect is probably due to the width of the antenna pattern combined with the reduced dimension of the internal components of the landmine. The discriminant properties is related to the acquisition logistic only.

The results from the three devices under investigation have shown that, despite a reduction in the dimensionality of the data, a close agreement between the physical structure of the internal assemblies and the radar imaging is maintained, especially considering the spatial extension of the reflections. In addition, what has been inferred from the bistatic results is consistent and analogous to what was previously suggested from the analysis of the 3D experimental campaign outcomes, demonstrating that the same information content was successfully achieved and that such details are sufficiently informative to ensure a correct target characterisation. Finally, a benefit of such an acquisition scheme was found to be a precise estimation of the buried target dimension. For all the three objects a close correspondence with the physical size was reached.

Even if the intelligibility of these results is lower than the immediate understanding gathered from the radar images, it should be take into account that in this case the identified features have been extracted from a single profile, therefore the performance and suitability of the methodology should be compared to the 2D results previously presented.

Following the same analysis scheme, the method was validated employing the VS-50 surrogate, for which the same considerations apply. In addition, the methodology has been tested also in the case of an inclined target, proved to be a critical variable and a source of missing detection. Also in this case, a bistatic approach shows reliable performance and robustness to variations in the geometry of the scenario.

5.6 Summary

The content of this Chapter can be strictly summarised through two main concepts:

- The GPR methodology is capable of recognising and extracting the internal scattering contribution from the target radar signature.
- Survey strategies significantly impact the robustness and interpretability of the results, as well as the detection performance.

In particular, a single 1D signature suffers from not being consistent when there is a change in the target inclination angle and when the internal design of the device is irregular, and even the inclusion of the polarimetric variables does not ensure reliable outcomes. Increasing the dimensionality of the problem, hence acquiring a 2D GPR profile of the object, can solve the issue of adverse geometries but it is not able to properly characterise targets with complex internal structure.

If one expresses the efficacy of a GPR survey as a ratio between the amount of information that can be extracted from the data and the acquisition effort (time or resources as well), the two approaches that ensure an exhaustive detection, i.e. a 3D survey and a bistatic one, follow distinctive strategies and it is plainly inferable that a time consuming acquisition is justifiable only if the produced results bring a remarkable information content.

Even if this relation cannot be mathematically expressed, as it is not possible to define a unique connection among all the involved parameters, some considerations can be developed.

As previously stated, the choice of performing a 3D acquisition produces clear and straightforward information for the characterisation of the buried target, but the time required for the data collection cannot be neglected. As a general rule, a long acquisition time could be acceptable; however, a time consuming survey means that resources, from power consumption to equipment usage and human attention, are required. Data dimension, i.e. the volume in terms of number of inline and crossline profiles of the acquired data, means resources as well. If for traditional GPR applications these parameters could be easily reached and handled, in this framework they play an important role for determining the suitability of a surveying technology.

The information level brought by the results is closely related to the quality of the acquisition phase, as no processing step can solve the loss of information due to erroneous data collection. But in this case data processing and interpretation are activities that do not necessarily have to be performed during the acquisition process (i.e. there are no constraints on real time and on field data processing). For that reason, the key point is to be able to gather all the possible information in whatever form.

It is clear, therefore, that the GPR imaging approach tends to solve the ratio by maximising the interpretation ability while sidelining the acquisition phase. On the contrary, the bistatic characterisation strategy renounces to an evident readability in order to minimise the data collection expenses.

Chapter 6

Concept for a bistatic system

I believe it is possible for ordinary people to achieve extraordinary things.

Jody Williams, 2006, [44]

Following the outcomes of the research, several considerations can be pointed out in the light of the development of a GPR system for landmine detection.

First of all, as described in the previous Chapter, a preliminary distinction should be made depending on the desired output. If the scope is to produce a high resolution image of the subsurface, the fulfilment of the spatial sampling requirements would be needed. Recalling the provided definition of system efficacy, conveniently defined as a ratio between the information content of the data and the survey effort, in this case the ratio is optimised by increasing the information content. However, the acquisition effort still represents an obstacle. Mechanical scanner with automated data acquisition can reduce the amount of labour that is needed to acquire the data, but the total acquisition time is still limited by the performance of the radar and the time needed to reposition it. Even if the acquisition time is not as critical as the detection capability, this value becomes unacceptably high if one considers that this effort is required regardless the presence of not of a buried anomaly.

A bistatic survey strategy, instead, has proven to be able to overcome the problem of a time consuming survey, maintaining the same conceptual level of information of a 3D one. In particular, the strategy has demonstrated its valuable contributions providing information not only on the presence of internal reflections, which is a matter of resolution rather than acquisition geometry, but also showing a suitability for characterising the design of the landmine structure. Moreover, all that can be extracted is evident in a single profile, therefore the acquisition effort can significantly benefit from the strategy. In this case, the time needed for the data recording depends on the desired data stacking only.

It is evident that following this strategy, the previously defined efficacy ratio is optimised by significantly reducing the survey time, accepting a less straightforward result, in terms of immediate understanding. It is furthermore clear that, to achieve an adequately time-saving performance, a certain amount of mechatronic and automation is needed. Finally, the system needs to be designed as much autonomous as possible, to improve the safety of personnel along with efficiency, productivity and flexibility.

This Chapter will firstly introduce motivations behind the development of landmine detection equipment, covering both technological and economical issues and then a conceptual idea for an efficient and affordable bistatic GPR for landmine detection, following the field trials experience and the obtained results. Clearly, the adoption of a dense bistatic acquisition scheme precludes the use of an hand held platform, as (1) such an equipment will hardly support the sensor head, (2) it will be hard to maintain the same set-up for all the survey, and finally (3) the weight of the equipment could negatively impact the performance of a human-based survey. Therefore, an automatic scanning platform may be the most reasonable choice. The benefits of mounting a mine detector on a remotely controlled vehicle must be balanced against the added cost and possible reduction in efficiency. A cost analysis should be conducted to determine to what extent remotely controlled vehicles are justified and evaluate their suitability for the application.

6.1 Motivations and platforms

Critics often present the ”man with hand-tools” as an unsophisticated cave-man technology. In fact, it is more sophisticated than any artificial device yet available. No matter how many millions of dollars are thrown at robotics, it will be a very long time before machines equal the sophisticated array of data gathering and processing equipment that is a human being.

The common belief is that the solution for increasing the impact of mine clearance activities lies in building a better sensor. Assume then that a sensor is capable of producing a 99% accuracy rate and it is then fixed to a hand held device as is done with the metal detector. The most significant accomplishment then is the speed needed to determine whether a mine exists or not.

Unfortunately, it is still a dangerous operation for the deminer that uses the hand held sensor. In 2017, there were 60 casualties among deminers in 14 countries (18 deminers were killed and 42 injured), a decrease from 2016, when there were 102 casualties identified (Fig. 6.1 (a)). On an average, 99 casualties among deminers per year have been recorded since 1999 [256]. Even if these numbers might seem limited, they are still unacceptably far from zero, and the statistics do not seem to indicate a decrease in the number of incidents.

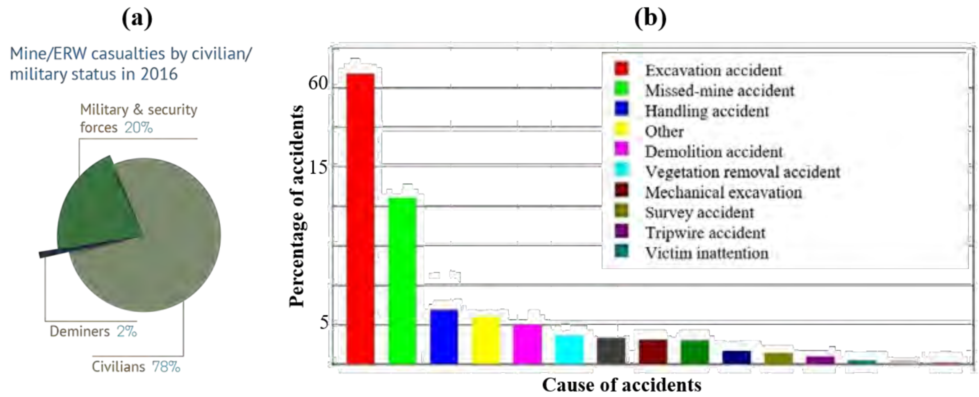

Figure 6.1: Humanitarian operations casualties statistics. (a) Casualty demographics reported in 2017 [10]. (b) Accidents classification (2000-2005), *Courtesy of nolandmines.com*

The ratio of accident classification during demining operations, shown in Fig. 6.1, gives the following insights: the most common activity by a long way is excavation, either investigating a metal detector signal or conducting area excavation by removing the ground surface. The next most common accidents are missed mine accidents when a deminer steps on a missed mine or pressure sensitive munition. Then, far below this are handing accidents which occur when moving, disarming or destroying a mine.

Even with training, mine disposal experts expect that for every 5,000 mines cleared, one worker will be killed and two workers will be injured by accidental explosions. Thus, it would be fair to say that having an unmanned platform to carry the sensor and use it would be ideal for this problem.

Dirty, dangerous and dull tasks, all of which are found in landmine detection, can be greatly aided by remotely operated platform. It is very desirable to remove the operator from the vicinity of the landmine and from the repetitive, boring operations that lead to loss of attention and potential injury. An ability to automatically detect mines over large areas would make a significant contribution to military and humanitarian demining. Such a capability could be used to delimit suspected mined areas, conduct mine clearance, or assist in quality assurance operations. Equally important is to identify areas that are not affected by landmines as these permit direct productive land use. A considerable area of the total mine suspected area is not mine contaminated or only to a small extent.

Conversely, the methods most commonly used in manual demining today are based on handheld detectors, a successful approach that has changed little in the last sixty years. An operator sweeps a landmine detector from side to side as the operator moves forward to cover ground (Fig. 6.2). The detector head is held close to the surface, at a suitable height without hitting the ground or any objects on it. If required, the operator can pass the detector head a number of times, in a number of directions, over the same piece of ground to confirm the detection.

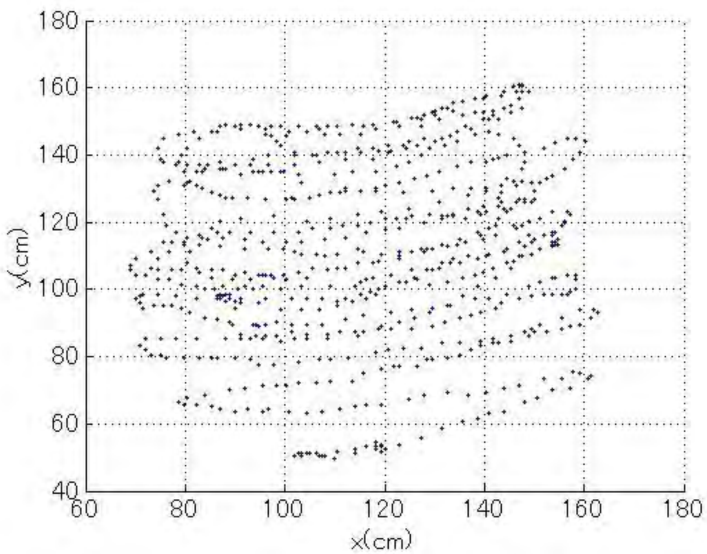

Figure 6.2: Example of manual area sweeping. *Taken from [100].*

The operator can vary the width of sweep to suit a particular situation, and is usually not limited by terrain. Unfortunately, the manual method is slow, hazardous, manpower-intensive, and stressful to the operator who, as a result, can perform this task only for short periods at a time, with a highly variable proficiency. In addition, exploiting multiple looks and precisely repeated overpasses of a target is difficult in a hand-held system without sensitive and bulky instrumentation which adds to the burden placed on the operator.

The implementation of a GPR sensor in a handheld system is restricted by weight (typically in the range 2 to 5 kg) and size as the ground is surveyed manually. Generally, a handheld system includes a relatively simple GPR with a single pair of transmit-receive antennas and relatively simple data processing, along with a metal detector coil.

The main alternative to the handheld devices are the vehicle-mounted ones, which can be mounted on various types of vehicles and may be used where the terrain allows the movement of the carriers. Clearly, there is a logical tendency on developing stand-off systems which can spot the presence of a buried objects from safe distance, up to tens of metres. However, GPR performance suffers from not being in proximity of the surface and there are several constraints that need to be taken care before designing any vehicle-mounted system which makes the system expensive.

GPR of this type are divided into the two groups: downward-looking devices and forward-looking ones. The latter is obviously preferable operationally as it removes the need for the vehicle to have overpass capability. There is theoretically a restriction on system performance for forward looking radar considering that at incidence angles less than the Brewster angle and for vertical polarisation, transmission losses at the ground interface are relatively small, but at larger incidence angles the losses increase more rapidly. Therefore a radar looking forward will no longer be able to detect buried targets in the ground. Conversely, there is potentially no such restriction on the other configuration. Examples of vehicle mounted GPR equipment are shown in Fig. 6.3 (*Courtesy of respective owners*).

Arrays are typically between 1 and 4 m in width and can operate at speeds up to tens of km/h. In general, vehicle based GPR systems allow for higher quality of the acquired data and much higher processing power than that in handheld systems. As the interpretation of the 2D GPR images is not trivial, the use of 3D processing and visualization techniques in landmine detection has been widely increased thanks to the employment of GPR arrays.

To date, vehicle based systems concentrate on anti-tank landmines because it is

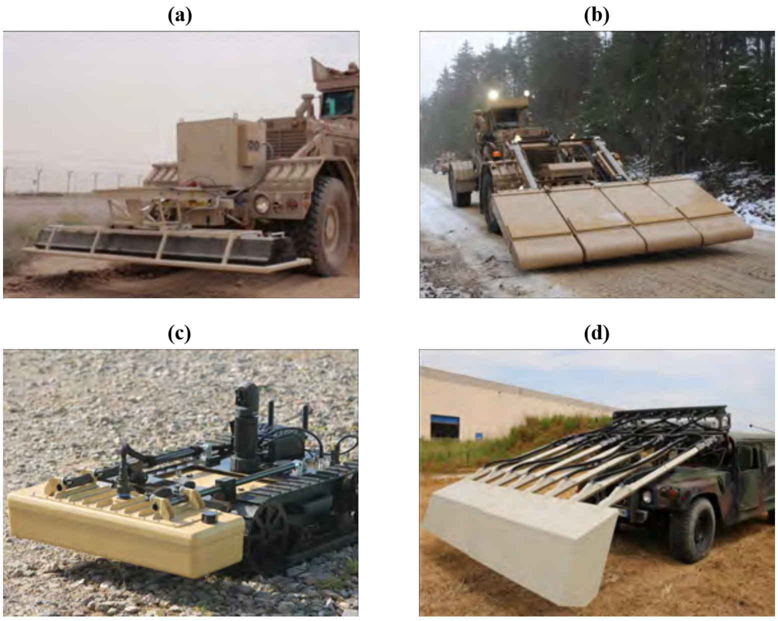

Figure 6.3: Examples of vehicle mounted GPR systems. (a) 3D-Radar DX. (b) Niitek VISOR. (c) Cobham AMULET. (d) Ingegneria dei Sistemi MINERVA.

difficult to achieve appropriate cross range resolution at realistic budgets. A further aspect to be considered is the antenna element spacing, as this needs to be adequate to provide proper resolution of the investigated target, as the effect of spatial undersampling on the radar image degrades the image quality. Moreover, as the array elements are generally fixed in position, changes in ground topography affect the path propagation and influence the collected signals. As an example, the Wichmann/NIITEK GPR system currently employed by the US Army adopts a channel spacing of approximately 5 cm.

Several attempts have been made to detect minefields from airborne platforms [257], employing both airships (as for the MINESEEKER, [258, 259]) and unmanned aerial vehicles (UAVs, see for example the TIRAMISU project [260]).

Small, lightweight UAVs (less than 3 kg) are being introduced for airborne Synthetic Aperture Radar (SAR)-based terrain observation, avoiding the need of large aircrafts, especially for monitoring small size areas. Improvements in UAV technology have made possible the development of UAV-assisted landmine detection systems, as they exhibit disruptive advantages such as:

- Higher scanning speed compared to existing solutions in the market based on autonomous robots.

(a) (b)

Figure 6.4: Examples of airborne GPR systems. (a) A-60 airship equipped with camera and radar detector. *Courtesy of Mineseeker foundation.* (b) Multicopter Microdrones equipped with camera and infrared detector. *Courtesy of TIRAMISU.*

- The possibility of inspection of remote areas, inaccessible with other systems.
- Higher safety throughout the scanning process, since contact with soil is avoided.

While range resolution is given by the radar bandwidth, cross-range resolution is limited by by positioning and georeferring accuracy [261]. As a consequence, these systems have been proved to be effective for detecting buried targets larger than 25-30 cm, and/or exhibiting significant contrast with the medium (e.g. metallic targets buried in clay or sand) [262]. In addition, as the aperture of any airborne sensor is not sufficient to detect AP mines, the resultant radar image, which is the convolution of the antenna footprint with the target cross-section, might not be able to detect targets with small radar cross-section.

Logically, these efficiency and performance limitations have strongly affected the usage of airborne GPR technology.

Drones are currently employed for their high resolution imagery, as they can efficiently assist the post-release development monitoring and demining operations planning. In addition, the capability of generating digital surface models can be useful in determining suitable access routes for demining machines. Hyperspectral imaging is another application employing aerial platforms, with the aim of detecting different temperature variations pattern in order to spot the presence of landmines. It is clear that both purposes are mostly related to surface or above ground object detection.

Detecting and removing landmines seem to be a perfect application for ground robots. Having an effective mine detection technology demands to develop mechanised and robotised solutions properly sized with suitable modularised structure and well adapted to local conditions of minefields can notably improve operations efficiency and flexibility. Such intelligent machines can speed the clearance process when used in combination with mine detection tools. A robotised solution is useful in quickly verifying that an area is clear of landmines. Essentially, these systems emulate the downward-looking vehicle mounted GPR approach, where a vehicle is often replaced with an accurate scanning platform. The popularity of the approach is explained by the fact that if technically feasible it represents the best possible conditions from the radar point of view.

Robots have been suggested for the problem of landmine detection but has been met with controversy, the principal issue related to a general lack of awareness of the problem, that has led in the majority of cases to inappropriate solutions that never make it to the minefield. Most robotic equipment thus far developed have been extremely expensive: expensive to build, to run and to maintain. Another reason for lack of successful solutions is the complexity of the machine. Finally, one should always consider the deminers understandable demand for complete safety and coverage, and at least a significant confidence in the technology on which their lives depend.

As can be hinted, the problem is mainly the delivery of technology, rather than the technology itself.

Although less mature than hand-held detectors, vehicle-based, remotely-controlled (either stand-alone or combined) detection systems are able to provide wider coverage and reduce risks for human safety. Examples of developed prototypes are shown in Fig. 6.5.

There have been important advances related to technology for mine detection and removal over the past decades, even though none of the current robotics platforms seem to have reached production on a larger scale (except for military EOD/IEDD tasks).

6.2 Concerns regarding technology

There are a number of concerns regarding the development and use of technology for humanitarian demining operations. In particular, the most can be outlined as follows:

- **Cost**: Many people involved in humanitarian mine action are ambivalent about the use and development of more mine action technology. While they appreciate the benefits that accrue, particularly in the areas of speed and safety, a common

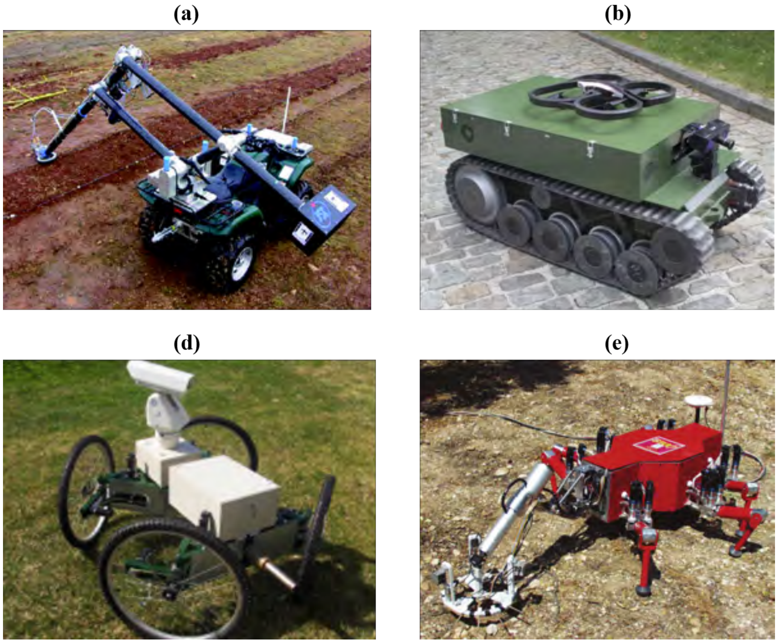

Figure 6.5: Example of robotic platform for humanitarian demining. (a) Gryphon (Tokyo Institute of Technology). (b) tEODor (Royal Military Academy of Belgium). (c)ARES (University of Lisbon). (d) SILO-6 (DYLEMA project).

feeling is that if all the R&D money spent on developing new technologies were simply applied to existing methods, then more mines would have been cleared in a shorter time. In addition, it is apparent that it is mostly NGOs who tend to question the cost/benefit balance of technology. The NGOs' attitudes may be influenced by the fact that they are concerned about decreasing funding available for their operations and see technology R&D as competition for those funds.

- **Socio-economic impact**: Receptivity to the use of technology in particular countries may be affected by the place of demining in local economies. The people using these tools and performing demining tasks are for the most part locally engaged, and considering that many countries where demining is currently being undertaken have economies severely stressed by recent conflict, a steady paying job, even an inherently dangerous one, is a desirable commodity. Hence, some NGOs may hesitate to introduce new technologies.

As with any environment there is a significant demand for incremental improvements to existing technology. As demining organisations gain experience, they inevitably identify ways to do things better, both in terms of practices and use of technology. However, an important limitation on this demand is the cost-benefit analysis of the incremental improvement. The issue is how the cost of the new/improved piece of equipment compares with the marginal improvement (rate of demining, safety, accuracy) that can be expected by employing it. Finally, radical advancements can be supposed in a few key areas of demining operations, such as area reduction and close-in mine detection.

This suggests that technology already developed that demonstrates a capacity to help demining teams work more quickly and efficiently has a chance of being used, subject to the constraints of this market. It also suggests that the development of new technology to address humanitarian demining may find itself without a market, unless it can be developed quickly.

The humanitarian market for metal detectors is estimated to be annually around $10 million, with an average sales price of $2,500 per unit. Non-governmental organisations in the field of demining have limited budgets to purchase new technology, which sets the bar for the sales price for new detectors. The market is also too small to support the high costs of developing advanced technologies [263, 264]. Therefore, a basic comparison of these costs can be polarised by the fact that, being mostly carried out with locally employed people, the actual cost per day for demining operations is visibly lower than the cost needed for the development and deployment of new technologies. However, if one considers the total life time of the equipment, the costs directly and indirectly related to the manual operations might probably be higher.

6.3 Sensor fusion

As a general rule, the system must have the capability that far fewer of the fragments of metal need to be excavated and the level of confidence in the overall process must be so high that larger fragments are left in the ground, but every mine is detected and disposed of. Recalling that the so called false alarms arise from physical features in the ground that are not caused by noise but clutter, it is clear that the ongoing software challenge is to devise algorithms that enable mines to be distinguished from other non-mine targets that are detected by the first stage of processing. According to the GICHD, in many cases up to 98% of an area said to be mined is in fact mine-free. For instance, between 1992 and 1998, humanitarian demining in Cambodia excavated over 200 million items, less than 0.3% of which were antipersonnel mines or other explosive devices.

Sensor fusion methods have been well researched for landmine detection in the last few decades in order to improve demining operations. Most sensor fused systems for AP landmine detection comprise the MD and GPR, representing the most mature solution in terms of technology development, and in some cases consist of a third sensor which is commonly an IR imaging sensor or some form of camera. Metal detector and GPR are not strictly orthogonal sensors, as they both give the largest response signal in the presence of metal in the ground. But with the GPR one can observe that buried objects may cause certain signatures, which can be traced over a certain depth range. These are caused by reverberations of radar waves inside the object, due to air gaps, pronounced contrasts in permittivity or metallic parts.

As an example, performance improvements of the VMR3 Minehound compared to single MD equipment are shown in Fig. 6.6.

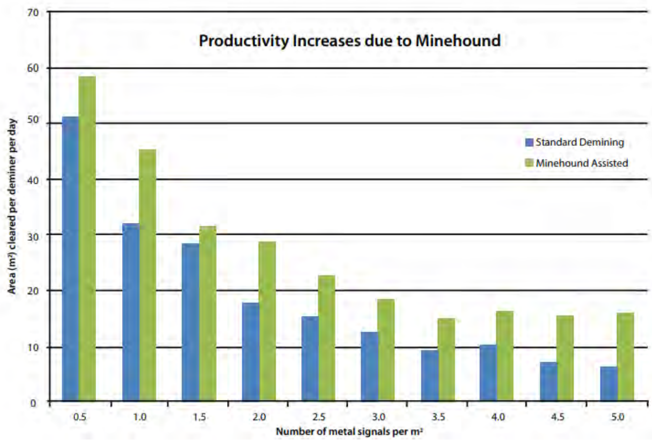

Figure 6.6: Productivity increases due to dual sensor equipment compared to MD only. *Taken from [265].*

As reported in several field verifications [101], using a metal detector as a primary detector and using GPR to check all the alarms produced by the metal detector can have a dramatic impact on false alarm rates. A low-cost GPR could have significant impact as a confirmation tool, while being within the budgets of most humanitarian organisations. A low-cost, dual-sensor metal detector and GPR, or a low-cost standalone GPR, would improve productivity within a year or two of widespread implementation. This improved productivity and reduction in person hours needed to clear contaminated minefields would cover the cost of the initial investment. Over the years, this would reduce the cost per cleared square metre.

Finally, the incorporation of metal detection allows the new work to build upon what has gone before.

6.4 Conceptual design

From what has been desribed in the previous Chapters, the logical implementation of a bistatic GPR takes the form of antenna arrays, in which each channel can be configured in order to acquire a bistatic signature of the detected target. Clearly, this means that the primary constraints are related to the physical system geometry:

- **Maximum offset**: how wide the array should be to ensure all contributions from the target are collected.
- **Maximum sampling**: how wide the spacing between channels should be to ensure all information from the target are collected.

The first item is basically a matter of soil attenuation (i.e. the maximum achievable bistatic range), and target dimension (i.e. the maximum spatial extension of the object radar contributions). Following the results of the field trials, one might consider the equipment size to be approximately 50 cm, allowing an effective recording of sufficiently extended and dense bistatic signatures. Moreover, these range of sizes can be suitable for unmanned platforms mounting.

The latter feature represents a more complex item to be addressed, as it is a compromise between the Nyquist sampling requirements and the effective physical (and electrical) dimension of the antenna elements, as in this case, the channel spacing corresponds to the offset sampling. A fixed array therefore would require a large number of elements, which themselves might be larger than the required spacing, causing the resulting equipment to be excessively under sampled. Even if interpolation can help, usually the minimum separation between the receiving and transmitting antennas has to be equal to the maximum size of the antenna, in order to limit the unwanted electromagnetic interaction between them.

In particular, to take into account the reduction in the bistatic signature extension when the target is inclined (as shown in Fig. 5.72), the maximum tolerable spacing might be in the order of a centimetre. To date, minimum spacing of massive array systems is not less than 5 cm, reaching tens of cm for large scale applications.

To visually evaluate the effects of reducing the CMP profile density is shown in Fig. 6.7, in which the previously obtained results for the VS-50 landmine have been decimated to synthetise a sparser sampling.

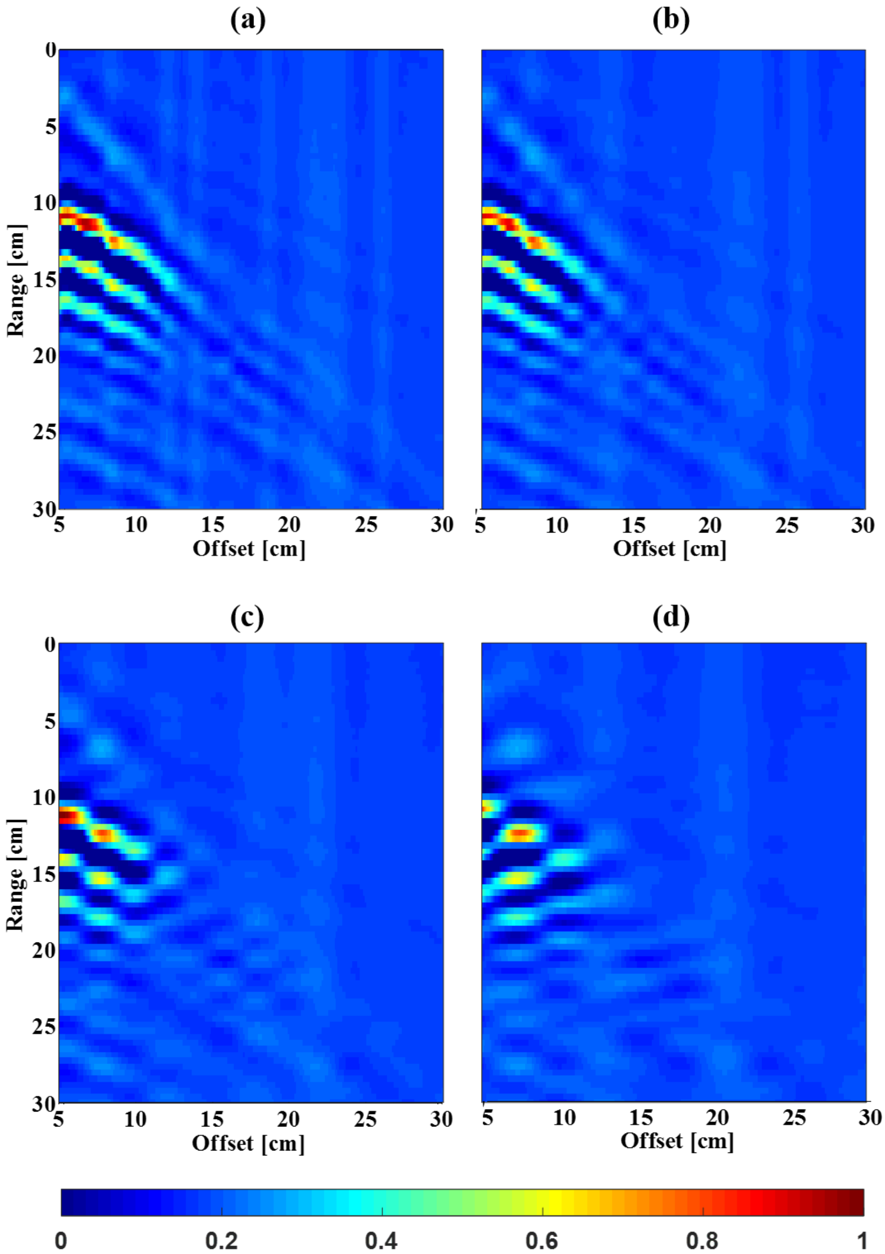

Figure 6.7: Effects of offset sampling on landmine signature. (a) Sampling 1 cm. (b) Sampling 1.5 cm. (c) Sampling 2 cm. (d) Sampling 2.5 cm.

It is evident the effects of reducing the number of collected bistatic signatures, as there is a severe loss of information when the spacing is higher than 2 cm. Practically, this means that there are limited possibilities in reducing the data density. In addition, it should be considered that the field experiments were carried out in favourable conditions, therefore the visible degradation may increase in case of more complex conditions.

A centimetric-spaced equipment can be ideally achieved by a reconfigurable system, in which a large number of very closely spaced elements can be dynamically activated and deactivated. However, even mitigated, the risk of having unwanted cross talk and mutual interference still exists. In addition, accurate synchronisation might become harder to obtain.

The idea behind the conceptualisation a bistatic equipment can be found in the strategy adopted for the experimentation, i.e. having two different GPR equipment independently managed. It is clear that in this case, if the aim is to implement an autonomous platform, a key parameter is to maintain a reduced weight.

A raw diagram of the described equipment and concept is provided in Fig. 6.8.

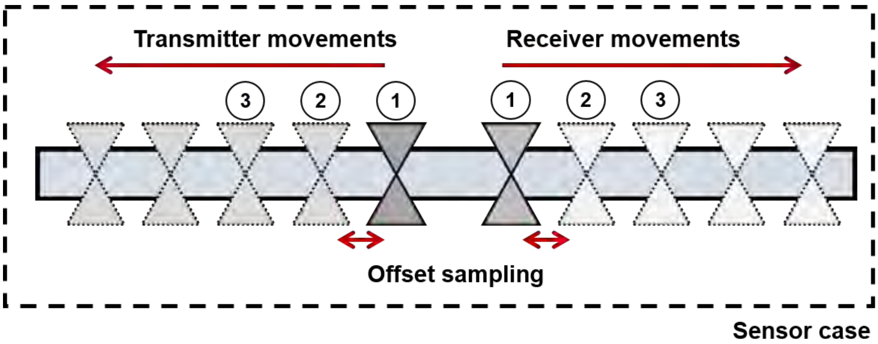

Figure 6.8: Raw diagram of automatic bistatic scanning GPR.

This essentially means that the bistatic data recording would require some sort of electro-mechanical components to systematically and precisely increase the distance between the transmitter and the receiver and to perform the series of periodic motion simultaneously. This mechanical effort is balanced by the fact that a single equipment has to be included in the sensor head, reducing the electronic and computational complexity of the system. The principal requirement is that the sensor head shall include only passive elements to keep a low weight and facilitate its mobility. In this way, the weight would not exceed the typical values for hand held equipment.

The employment of multiple and separated rows of elements to avoid the inclusion of automation will negatively impact the physical dimension of the equipment, as it would be wider and larger to accommodate the required number of channels.

Two assumptions are accepted in almost every landmine detection operations: the need of very high frequencies and the necessity of keeping the antennas away from the terrain surface. The first assumption is motivated by the goal of being able to classify the targets according to their accurate geometric reconstruction, while the second assumption is a standard accepted approach for safety reasons. For effective operation, particularly at the highest frequencies, it has been shown that it is highly desirable to have the radar antennas in close proximity to the ground. Reactive coupling and system sensitivity is rapidly lost as the antenna is raised, but it is also potentially dangerous to search a minefield with the antenna resting on the surface.

Following these considerations, one of the critical points is whether the platform should be in direct contact with the surface or whether it can be operated at a stand-off distance. In this case, the discriminant feature is the possibility of detecting the internal reflections of the target.

An experimental evaluation of the height effects on the detection performance of GPR has been performed, to verify also the numerical results shown in Fig. 4.29 in which it seemed that the reflections generated by the internal air layer appears in the radar signature for the first tens of centimetres.

In particular, a series of coincident 2D profiles have been acquired over the representative VS-50 landmine, each time inserting a styrofoam tiles between the radar and the soil surface to change the antenna height above the soil. Details are provided in Table 6.1.

Table 6.1: Antena height evaluation parameters and set up.

Parameter	Value
Frequency range [GHz]	1 - 3
Frequency sampling, $1/\Delta t$ [GHz]	17
Inline sampling Δx [cm]	0.4
Time window, ΔT [ns]	15
Antenna offset [cm]	6
Antenna height [cm]	5 - 10 - 15

The landmine was buried at a depth of 13 cm as previously made, horizontally laying. Photographs of the acquisition are shown in Fig. 6.9.

To highlight the target contribution, in this case a background removal step was applied to the data [266]. In particular, the subtraction has been applied through the application of SVD algorithm and eigenvalues/eigenvectors suppression, in order to selectively removes the flat horizontal reflections from the GPR profiles [267]. The

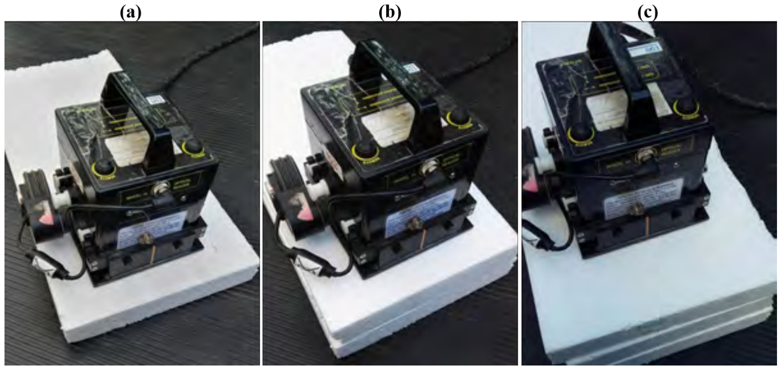

Figure 6.9: Antenna height evaluation, acquisition details. (a) Survey setup. (b) Height 10 cm. (c) Height 15 cm.

resulting GPR profiles are presented in Fig. 6.10.

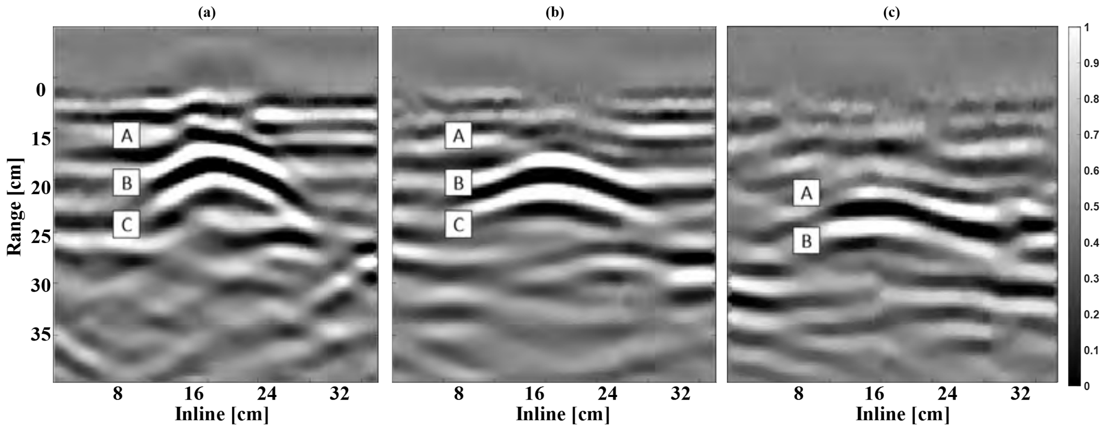

Figure 6.10: Antenna height evaluation results. (a) Height 5 cm. (b) Height 10 cm. (c) Height 15 cm.

Disregarding negligible topography variations and surface clutter, the landmine internal structure can be retrieved up to 10 cm, beyond which its scattering contribution becomes hard to recognise. In particular, Fig. 6.10(c) further demonstrates that the effects of air gaps located within the landmine is beneficial for its detection, as it can be noticed that the principal contribution detectable is the internal layer, rather than the top of the landmine. This is in agreement with the numerical results, showing the same pattern.

From a practical point of view, this represents a valuable advantage, as it means that the GPR equipment can achieve comparable performance even not in contact with the surface. For comparison purposes, the Proper Lane Sweep technique (PLS), requires the sensor head height not to exceed 5 cm. Moreover, possible interferences generated by closely located structures due to the wide pattern of the antennas are reduced due to the limited height of the platform.

However, these results might suggest that a ground based system is nearly the only feasible solution, as a UAV would need to fly at a very low altitude to allow a proper radiation performance, feature closely bounded to the environmental factors and that may impact the scan accuracy and imaging performance. In addition, it should be taken into account the payload limitations of such platforms employed at low altitude.

A parallel advantage of this solution is that it would be also suitable for vehicle mounting integration

The last aspect to be considered is the acquisition step. Since landmine clearance personnel are concerned about not triggering the landmine, the scan pattern is often erratic, lowering the quality of the results and impeding a physical implementation of the described methodology in a hand-held system. Suitable performance of the currently employed platforms are obtained only when experienced operators are performing the survey, and it is well-known that operators skills decay with time, issue that vanishes when the task is carried out by a mechanical infrastructure. Mechanical infrastructure does not tire like humans, provided they have enough power, and their performance is not affected by psychological tension and trauma. In addition, the accidental triggering of landmines is minimised due to the mechanical capability of the system of adjusting the sensor head elevation to maintain a constant height above the ground. Finally, the operator can actually stand in a 100% safe position.

The data acquisition step represents the bottleneck of the problem, as described in detail in the previous sections, as target characterisation and potentially target identification both rely on very dense and accurate data.

The main question is therefore how to define a sufficiently sparse grid to ensure detection and maintain efficiency at the same time.

To increase the efficiency, the following considerations can be made: it has been demonstrated that detection of the diffraction hyperbola can be obtained also with a sparser acquisition grid, therefore the acquisition strategy can be configured so that most of the resources are concentrated when there is a precise need and evidence, i.e. when a target is detected and located, saving time and resources from non-contaminated areas (which represent the predominant situation). In addition, it should be take into account that the tougher barrier is the spacing between the parallel profiles, i.e. the crossline direction (Δy), while the inline one (Δx) could be easily managed, therefore the data sampling along this dimension does not significantly impact the acquisition effort.

The acquisition strategy can be analysed considering the antenna radiation pattern and the target size. In particular, most landmines may be classified with a size of approximately 10 cm, while the majority of GPR equipment, to maintain a practical size, employs wideband dipole antennas having a wide radiation pattern. As the radiation pattern can only be characterised taking into account the soil dielectric properties, which may be difficult to exploit, the optimum grid spacing can be estimated considering the the target size only and the need of having at least one profile located inside the target.

With a reliable estimation of the parameter and of the wave propagation characteristics, it would be possible in theory to dynamically adjust the grid spacing to the soil dielectric properties, further increasing the efficiency of the system.

From these considerations, it is clear that the maximum crossline spacing cannot exceed 10 cm, otherwise there is the risk of being inadequately sparse, as shown in Fig. 6.11.

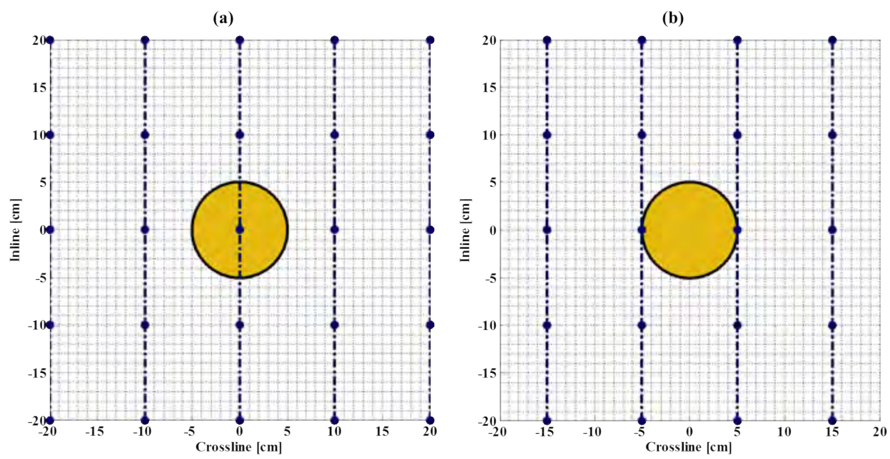

Figure 6.11: Optimum sampling mesh analysis, $\Delta y = 10$ cm. (a) Target axis profile. (b) Target edge profile.

It is clear that ideally a spacing of 10 cm will be sufficient for detecting the diffraction hyperbola, even in the less favourable condition, as in such case there are two profiles crossing the target. However, this choice would require a very accurate acquisition to ensure that even when the profile is located on the border of the target the target would still be detected. The effects of being close to the target edges is depicted in Fig. 6.12.

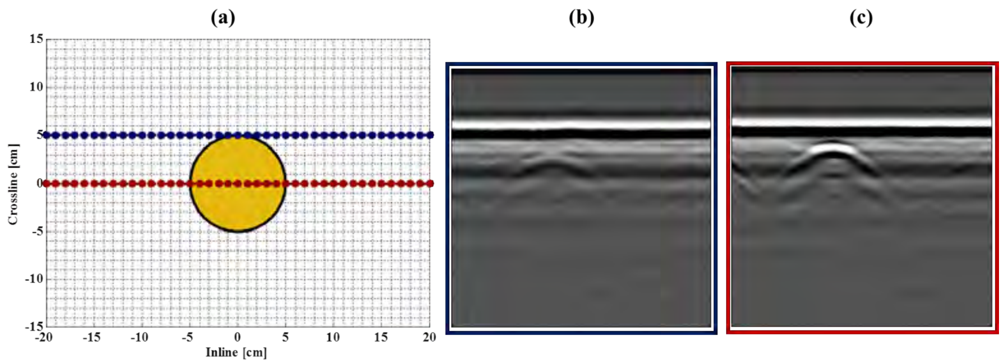

Figure 6.12: Radar profile collection, effects of profile location. (a) Profile location. (b) Target edge profile. (c) Target axis profile.

It is implicit that when including the width of the radiation pattern, a profile located on the border will include an increased scattering contribution from the target, reducing the risk of missing it. On the other side, it must be considered that uneven soil topography and surface obstacles and/or clutter may reduce the profile location accuracy during the survey.

Reducing the spacing between parallel profiles brings a more conservative situations, described in Fig.6.13.

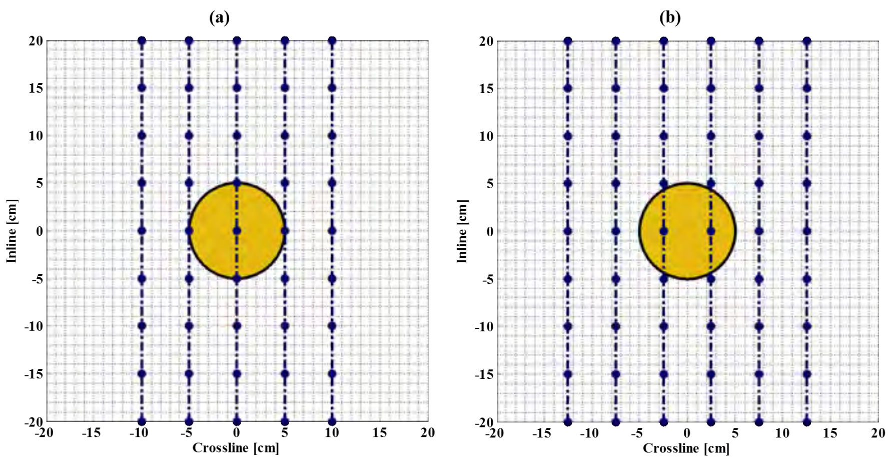

Figure 6.13: Optimum sampling mesh analysis, $\Delta y = 5$ cm. (a) Target axis profile. (b) Target edge profile.

In this case, it can be seen that there is a higher probability of acquiring a profile crossing the target, therefore this scheme might be capable of better manage smaller and/or non-symmetrical targets, as well as inclined objects (which have a reduced radar signature).

Still, it is reasonable to reduce the total amount of data to be collected, i.e. inline direction, but it must be taken into account that a highly oversampled acquisition might not produce a clear hyperbola in the radar profile, therefore the detection step would be based on a single signal, which clearly yields less information. A comparison between the two output is shown in Fig. 6.14, in which a conservative spacing of 1 cm is taken as a proper parameter.

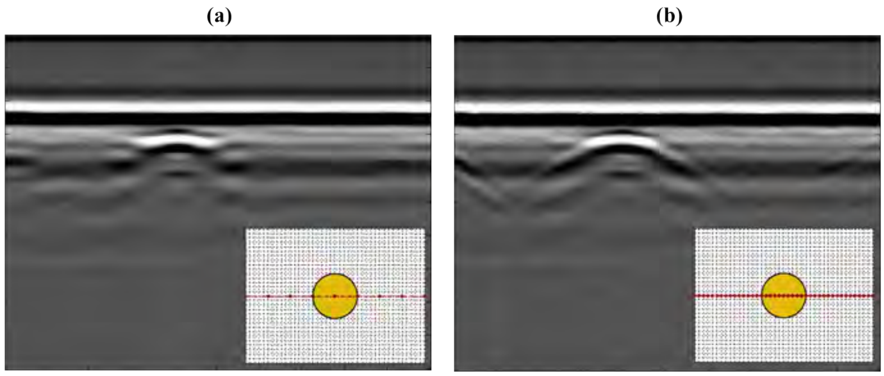

Figure 6.14: Data collection, effects of inline sampling on detection decision. (a) $\Delta x = 5$ cm. (b) $\Delta x = 1$ cm

As can be seen, even with a sample spacing of 5 cm the resulting image still shows an hyperbolic pattern, but it is expected that a less cooperative soil will degrade the results, making the interpretation of the profile of Fig. 6.14(a) less intuitive.

When the system detects an hyperbola in the GPR image, through an automatic detection scheme or via human supervision, as well as through a combination of sensors response, the platform should search for the apex of the target in the neighbourhood of the profile to pick up the optimal geometry. This location can be easily found by acquiring an orthogonal GPR scan from the apex of the individuated hyperbola, obviously along the orthogonal direction along (the crossline one). This additional effort put in place for positioning the equipment precisely over the centre of the target is required to ensure a proper CMP profile collection. Then, the bistatic signatures collection can be performed, and the detected buried anomaly can be classified according to the collected results.

Search flow can be described as follows:

- **Area reduction** through a sparse survey to reduce the impact of non-contaminated sectors.

- **Target detection** from the GPR profile and surrounding regions.
- **Target characterisation** through a bistatic scheme.

Finally, it was described that the effects of the internal scattering are somehow independent of the antenna polarisation, in the sense that its contributions is visible regardless the antenna orientation, hence there are no preferential directions to follow for the acquisition of the bistatic signatures.

6.4.1 Considerations on dual sensor equipment

Following the considerations of the previous Sections, an efficient way of performing the survey can be employing a combined GPR platform and a metal detector unit. In this way the metal detector can operate as a trigger for a GPR acquisition, taking into account also that there are still many metal mines and just a number of landmines are completely free of it. Therefore, in case of no alarms, the acquisition can be sparser, while once something is found by the MD unit, the GPR system will take control of the process and impose a more dense acquisition. Strictly theoretically, this way of surveying allows both methodology, the 3D imaging and the 2D bistatic, to be accomplished.

The use of an additional sensor as a trigger for the GPR survey could provide at the same time supplementary features that can be a valuable inclusion for the identification and recognition step. In addition, electing the MD rather than the GPR as the trigger for the acquisition also overcome the sampling issue of the radar sensor and the geometrical constraints for the hyperbola formation. Clearly, in situations in which the MD might become inefficient, the hierarchy can be inverted, thus promoting the GPR survey as the principal. In addition, the capability of MD sensors to accurately locate the target center of mass can bring additional advantage in the detection phase.

The great advantage of including the additional MD unit is however compensated by the increasing platform complexity, as a supplemental mounting and/or scanning platform need to be integrated. On a general perspective, there are mainly two possibilities:

- Robotic arm sweeping the terrain, equivalent to the operations carried out by a human operator.
- Multi-channel array, equivalent to the GPR array commonly mounted on vehicles.

Clearly, the effort required by the first option is the electro-mechanical structure that can allow for a precise sweep of the area in front of the platform, while the second solution forces the inclusion of an additional equipment with relevant physical dimensions (order of metres).

6.5 Summary

Conventional methods for demining operations works, but their efficiency and safety should be improved taking advantage of the evolving technology. To facilitate machine-based sensing in place of manual sensing, the intuitive way to ensure a precise area scanning, continuous operations and to allow efficient operations is to employ an autonomous and/or mechanical platform. Given the framework of application and the demanding constraints, the only probable solution is the development of a ground based equipment, due to the described limitations of aerial platforms.

This solution has the advantages of (1) being flexible, as it can be intended also for vehicle mounting, (2) maintaining a size and weight suitable for terrain robotic platforms, and (3) increasing the efficiency in area survey.

In several studies it has been noticed that a large amount of time is spent in surveying non contaminated areas, hence the first addressed feature has been the resources saving when there is no need of, meaning that the acquisition strategy will follow the sparsest scheme as possible in order to ensure the detection of the target.

To achieve the desired bistatic characterisation of the target, starting from the experimental trials experience, an electro-mechanical array is delineated, as the needed signature density almost preclude the use of a fixed system due to elements spacing constraints. This implementation substitutes the two single GPR platforms to maintain a reduced physical size.

The introduction of such a platform in the humanitarian demining market is clearly dependent from the cost of production and development, but it is clear that on a lifetime scale consideration, these costs can challenge the current expenses.

Even if representing an acceptable compromise, the only parameter that does not match the current hand-held operations is the sweep velocity, which would be slower (tens of cm/s maximum) employing the designed platform. The reasons for this are mainly related to the motion planning in case of rugged topography and obstacle avoidance.

Finally, the inclusion of an additional sensor, in particular a metal detector unit, might notably increase the performance of the equipment and improve the productivity, clearly with the associated costs of inserting an additional sensor in the platform.

Chapter 7

Conclusions and future work

Collectively we have the knowledge, skill, and resources to achieve it, so let's make future generations proud.

Prince Harry of Wales KCVO, 2017, [268]

This thesis has addressed the challenge of characterising buried targets to enhance the performance of GPR as a landmine detection methodology. A key to improve performance is to identify, understand and extract the features of the landmine radar signature so that a discriminant plane between the landmine and clutter targets can be identified. A discriminant properties is expected to be the presence, in the target radar response, of scattering components that can most likely be attributed to the presence of the detonator and other internal mine structure. This feature can be ascribed only to man-made objects, thus, considering the variety of targets commonly found in a minefield scenario, its presence could be beneficial for removing a number of misleading detections.

A landmine may be characterised by a number of scattering centres, each with its own angular radiation pattern, in particular when the plastic content of the internal structure is high. Most landmines may be considered as multiple layered dielectric cylinders that interact with each other to produce multiple reflections.

The challenge is therefore to be able to effectively sense these internal reflections to achieve improved discrimination.

The first key aspect is the availability of representative inert landmines for the experimentation. As landmines are objects that are difficult to replicate, and given the research scope, it is essential that properly constructed inert landmines are used for research and development, otherwise the results could be significantly affected or misleading. The employed devices were complete with all their external and internal components and were filled with a high explosive simulant commonly used to train the UK Ammunition Technical Officers; the substance has the same electrical and chemical properties of commonly employed explosive materials.

The impact that the internal assemblies of the landmine have on the resulting radar signature has been evaluated through a series of experimental campaigns, aiming at (1) confirming the validity of the research question, and (2) evaluating a suitable way to highlight these contributions and improve the efficiency of GPR.

In particular, the aim of this research has been to establish to what extent GPR technique is suitable for providing information on the design and composition of a buried target and the impact that a bistatic strategy may have on the characterisation and identification process. Considering that when a dielectric target is illuminated by an electromagnetic wave, energy is partially transmitted through the target, a variation in the transmitter and receiver separation will illuminate a different internal section of the target, which will scatter the energy accordingly to the features of that particular section. Therefore, it is expected to be able to highlight targets with composite structure and internal assemblies.

The novelty of this work arises from the demonstration of the valuable contribution that the internal structure yields to the radar results and the potential that a bistatic approach shows for target discrimination and identification.

7.1 Summary of findings

Investigation of radar signatures in the form of simulations and measurements has increased the understanding of the scattering mechanisms induced by the internal components of landmines.

The preliminary numerical analysis has shown that, at least theoretically, the presence of internal assemblies can be detected and recognise as an additional scattering contribution. This potential has been investigated considering design parameters (mainly system bandwidth and frequency) that are common to the majority of GPR equipment employed in demining operations to maintain a realistic operational configuration. In addition, the reliability of these scattering events has been tested by changing both target geometrical properties and soil attenuation characteristics, assessments which have shown that the internal structure information can be retrieved even for deeper targets and in case of unfavourable propagation conditions.

Off the ground targets investigation showed a relatively strong multiple reflections that appears beneath the target space, confirming the outcomes of the numerical simulations and additionally highlight the importance of the relative geometry between the target and the antennas plane not only for the their detection but also for their recognition. This includes the antenna orientation, i.e. polarisation, and target inclination angle. Even if the experimental set up would hardly be suitable for a proper ground survey, as the employed frequencies would allow a very limited soil penetration, the results maintain a certain level of reliability due to a consistent central wavelength to target size ratio and a realistic bandwidth. The only phenomenon that the results did not consider, for obvious reasons, is the absorption due to the propagation in free space. However, for the purpose of this initial investigation the effect could be neglected.

The methodology has been replicated burying the targets in a sharp sand pit and employing a GPR platform already on the market, and the results confirmed what was found in the previous experiments. Effects of soil, even if in controlled conditions, appears as a reduction in the number detectable reflections, as only the prominent one were able to reach the receiver antenna. However, the scattering contributions can be easily identified. Despite the different propagation environments, a high degree of correlation has been achieved.

Analysis of the collected signatures demonstrated that the expected reflections generated by the detonator and other internal mine structure are detectable, thus providing a first hint on the significance that this feature can bear. In addition, as the internal components have their own radiation pattern, a change in the antenna orientation provides a clearer marking of their presence, as a solid dielectric object will show no variations.

A single, mono-dimensional scan, unfortunately, has the limitation of being dependent on the target aspect angle. As well, as landmines may not be perfectly symmetric a bi-dimensional profiles may not be able to properly characterise the internal components. Example of this can be found considering the two employed devices: if for the VS-50 landmine the structure covers the entire target extension, the SB-33 shows some assemblies located in a precise sector of the landmine. Hence, their detection but especially their characterisation can be unreliable.

A logical step ahead can be increasing the dimensionality of the problem, hence evaluating the imaging performance of a 2D profile. Also in this case the results have shown some improvements, especially for inclined targets (VS-50 example), but they still present the critical limitation of not being able to properly delineate the structure for irregular targets (SB-33 example).

Therefore, a 3D acquisition is needed to extract valuable information on the spatial extent of the internal design of a landmine.

A set of dense and regular 3D GPR acquisition have been carried out, under the same set up of the previous experiments to maintain consistency. The produced images exhibit a very close correlation with the actual design of the investigated targets, confirming the ability of GPR to image and to precisely delineate the internal features of a landmine. In addition, the shortcomings highlighted from the 1D signatures and the 2D profiles are significantly mitigated. The overlay of the radar slices and the photograph of the target further demonstrates this capability. The innovative aspect of this section is that it is possible to produce images closely matched with the physical design of the landmine. To validate these outcomes, a surrogate of the VS-50 landmine has been investigated as well. The surrogate is accurately moulded from the actual landmine but it is substantially a solid explosive, with just a representative metallic inclusion. Furthermore, in comparison with an air gap, a small metal inclusion has a very weak effect on the target response. Therefore, the presence of an air gap notably facilitates the detection of buried plastic cased landmines with GPR.

Although not strictly within the scope of this work, results suggested the use of inert (otherwise known as neutralised) landmines for releasing the potential of GPR of detecting the internal structure of a target.

A discussion on the requirements for a proper 3D imaging has been provided as well, highlighting the demanding constraints on the density, i.e. the maximum affordable sample spacing, and the regularity, i.e. the precision in samples positioning, that the acquisition grid should have. Even if a relaxation is possible, the need for a sub-wavelength sampling still represents an obstacle for an effective employment of 3D methodologies.

This considerations gave birth to the main theme of the thesis, whether a bistatic approach could provide the same level of information but with a lower acquisition effort.

The chosen methodologies for the bistatic acquisition were a common receiver, fixing the receiver and moving the transmitter only, and a common mid point scheme, in which both the transmitter and receiver antenna move away from a common point in opposite direction. With the target located in the common point, both strategies allow to investigate the target internally, layer by layer, with little differences between them. The resulting bistatic signatures clearly show the potential of the approach, as information on the presence of internal assemblies can be extracted, and details on the complexity of such internal design can be easily obtained. Considering the investigated targets and their design, a consistent pattern has been found in case of regular structure (VS-50 example), while a more complex reflections pattern was generated by the irregular device (SB-33 example). This benefit becomes even more important considering that a demanding 3D volume is no longer needed. As before, the corresponding surrogate has been exploited as well to validate the outcomes. Bistatic characterisation has been proposed in the case of an inclined targets, showing robustness and consistency.

Based on the experimental results, a conceptual design of a possible bistatic GPR platform has been provided, highlighting advantages and limitations compared to the actually way of area scanning. In particular, two main aspects have been considered: (1) operator safety, and (2) acquisition efficiency. Clearly, the first aspect is of notable importance given the application and therefore the equipment must allow the the operator to stand in a 100% safe position. This can be achieved by designing an unmanned or a remotely controlled GPR platform, with all the consequences that arise, in terms of cost and complexity. The latter item has been addressed by considering that the landmine density per square metre can be very low, thus the system should save time and resources from non-contaminated areas (which represent the predominant situation). This can be achieved by following the sparsest grid as possible in order to ensure detection. The need for a dense bistatic characterisation logically not only precludes the use of an hand held platform, but also brings the need for electro-mechanical components to simultaneously perform the series of periodic motion. Considerations on a possible MD-GPR sensor combination have been provided as well. The described architecture represents a suggestion to increase the efficiency, reliability and safety of demining operation where such an infrastructure can be employed.

7.2 Future work

This thesis has resulted in some key achievements summarised in the previous section. However, it has also opened up many possibilities for further work and improvements.

First of all, only three types of landmines have been investigated in this thesis. Even though it would not be practical to exploit all the devices spread around the world, a further step could be to increase its number in the light of a common landmine signature database. A significant advantage for its development might come from the high degree of correlation found between the numerical solutions and experimental trials, features which may suggest that the catalogue development can take advantage of the (ideally) infinite modelling possibilities. It has been found that for a given minefield, the possible number of different landmine models is limited, therefore this information can be used to infer a representative list of high priority targets to extend the work made in this thesis.

Similarly, other variables that strongly influence GPR efficacy are the soil conditions and electromagnetic properties, as GPR detection performance can bounce from optimal to unacceptably low depending on the propagation characteristics of the soil. Further validation of the proposed technique should be carried out in less favourable terrain conditions, in terms of texture homogeneity and absorption coefficients. It has been shown that the scattering contribution of the internal air layer is robust to the lossy attributes of the surrounding medium, thanks to a strong impedance contrast, but this must be verified considering the detection threshold of the system. As indicated for the landmine models, mine contamination has reached a worldwide scale, therefore also for this attribute, a prioritisation of the terrain models should be made.

It has been shown that the detection of internal components is somehow independent of antenna orientation, i.e. they scatter randomly, but only for co-polar configuration, therefore a detailed analysis of the radar signatures in the cross-polarisation domain could bring further indications of the presence of these components. In addition, the acquisition of both cross-polar and co-polar data allows for a fully polarimetric analysis of the target, reducing the number of unknown of the problem and increase the accuracy of the results.

In this work, two regular geometries have been examined and evaluated. However, separating the transmitter and the receiver, and independently managing their operations can ideally produce an unlimited number of possible combinations. This practically means that there is plenty of space for investigating more complex acquisition geometries and survey methodology. Nevertheless, it must be taken into account that landmines are shallow targets, with a possibly weak RCS and with reduced dimensions. This means that the maximum separation between the antennas is limited, soil absorption included, as well the possibility of deploying elaborated acquisition geometries. The suggested autonomous platform, even if only a conceptual design, is firstly limited by these factors: close proximity to the ground, methodical area sweeping and regular relative geometry between the transmitter(s) and the receiver(s). Unleashing the true potential of a fully independent bistatic and polarimetric GPR system would clearly be of remarkable importance, even if the trade-off between the achievable results and the system complexity would then be a critical argument.

The aim of the work has been focused only to demonstrate the feasibility of determining the nature of a target from its internal structure contribution, therefore, concerning the possible dedicated processing schemes, there are several possible expansion of the work. The use of information on the internal structure of a target has been restricted to characterisation only, using the prior information on the buried target, but significant advantages can be achieved if employed in blind target recognition and identification scheme.

First of all, the majority of the current recognition algorithms are mostly based on the extraction of features related to the physical properties, i.e. dielectric characteristics or geometrical design, without accounting for the contributions from the internal structure. While there are a large number of useful automatic detection schemes for GPR data analysis, robust recognition and identification remain a challenge as the scale of the problem severely impacts the performance of certain features, lowering their discriminant properties. The capability of extracting the scattering contribution generated by the internal structure of a target, instead, it is theoretically independent of the boundary conditions of the problem, therefore representing a robust and valuable feature to rely on.

It has been demonstrated that this landmine feature brings quite a discriminant information on the nature of the target, hence a processing scheme driven by the presence of multiple reflection in the target signature need to be developed to fully exploit this GPR capability. As it has been showed, the potential level of accuracy may lead to identify the landmine model, as each family of landmines can be thought of being characterised by a similar structure. The close correspondence with the optical image further suggests also that a diagram, rather than a number of expensive experimental campaign, can be employed for finding the proper template match. This aspect is particularly important, as robustness of automatic recognition/identification schemes strongly relies on the amount of data available for training and learning, and overcoming the necessity of extensive data acquisition can fasten the development.

Bibliography

[1] Croll M. *The History of Landmines*. Leo Cooper, 1998.

[2] The New York Times. http://www.nytimes.com/2018/03/07/opinion/the-danger-underfoot.html.

[3] United Nations Information Center. http://www.cinu.org.mx/temas/asun_hum/minas.htm.

[4] Vines A. and Thompson H. Beyond the mine ban: Eradicating a lethal legacy. Technical report, Research Institute for the Study of Conflict and Terrorism, London, 1999.

[5] Landmine and Cluster Munition Monitor. http://www.the-monitor.org/.

[6] Wurst J. Ten million tragedies, one step at a time. *Bulletin of the Atomic Scientists*, 49(6):14–21, 1993.

[7] Strada G. The horror of land mines. http://www.scientificamerican.com/article/the-horror-of-land-mines/, April 1996.

[8] United Nations International Children's Emergency Fund. http://www.unicef.org/press-releases/220000-children-threatened-by-mines-other-explosive-weapons-eastern-ukraine.

[9] United Nations. Convention on the prohibition of the use, stockpiling, production and transfer of anti-personnel mines and on their de-

struction. http://www.icbl.org/en-gb/the-treaty/treaty-in-detail/treaty-text.aspx, September 1997.

[10] International Campaign to Ban Landmines. http://www.icbl.org/.

[11] Geneva International Centre for Humanitarian Demining. http://www.gichd.org/resources/publications/.

[12] Turk A.S., Hocaoglu K.A., and Vertiy A.A. *Subsurface Sensing*. John Wiley & Sons, 2011.

[13] Blagden P.M. Kuwait: Mine clearing after iraqi invasion. *Army Quarterly & Defence Journal*, 126(1):4–12, 1996.

[14] International Standards for Humanitarian Mine Clearance Operations. http://www.un.org/Depts/mine/Standard/glossary.htm.

[15] Daniels D.J. *Ground Penetrating Radar*. Wiley Online Library, 2005.

[16] Jol H.M. *Ground Penetrating Radar Theory and Applications*. Elsevier Science, 2008.

[17] Bello R. Literature review on landmines and detection methods. *Frontiers in Science*, 3(1):27–42, 2013.

[18] Gonzalez-Huici M.A., Catapano I., and Soldovieri F. A comparative study of gpr reconstruction approaches for landmine detection. *IEEE Journal of Selected Topics in Applied Earth Observations and Remote Sensing*, 7(12):4869–4878, 2014.

[19] Mendez-Rial R., Uschkerat U., Rial F.I., and Gonzalez-Huici M.A. Evaluation of landmine detection performance applying two different algorithms to gpr field data. In *Detection and Sensing of Mines, Explosive Objects, and Obscured Targets XVIII*, volume 8709, pages 8709 – 8709 – 10, 2013.

[20] Slob E., Sato M., and Olhoeft G. Surface and borehole ground-penetrating-radar developments. *GEOPHYSICS*, 75(5):75A103–75A120, 2010.

[21] Watson F.M. *Better imaging for landmine detection: an exploration of 3D full-wave inversion for ground-penetrating radar.* PhD thesis, The University of Manchester, 2016.

[22] Claerbout J.F. *Imaging the Earth's Interior*. Blackwell Publishers, 1985.

[23] Tarantola A. *Inverse problem theory and methods for model parameter estimation*. SIAM, 2005.

[24] Huxley A. *Ends and Means: An Inquiry into the Nature of Ideals*. Harper & Brothers, 1937.

[25] Roberts S. and Williams J. *After the Guns Fall Silent: The Enduring Legacy of Landmines*. Vietnam Veterans of America Foundation, 1995.

[26] New York Times. `http://www.nytimes.com/2017/09/06/world/americas/bangladesh-rohingya-land-mines.html`.

[27] Human Rights Watch. `http://www.hrw.org/news/2017/09/23/burma-landmines-deadly-fleeing-rohingya`.

[28] The Telegraph. `http://www.telegraph.co.uk/news/worldnews/europe/hungary/11867291/Fear-of-landmines-as-Hungarys-iron-curtain-forces-migrants-to-consider-new-routes.html`.

[29] The New York Times. `http://www.nytimes.com/1993/08/09/world/four-us-soldiers-are-killed-by-mine-in-somali-capital.html`.

[30] UNAMA. `http://unama.unmissions.org/unama-condemns-series-bombings-nangarhar-targeting-civilians-and-schools`.

[31] Ejercito Nacional. `http://www.ejercito.mil.co/?idcategoria=437712`.

[32] United Nations International statistical resources. `http://research.un.org/en/mines/statistics`.

[33] United Nations Mine Action. `http://www.mineaction.org/`.

[34] The Irrawaddy. `http://www.irrawaddy.com/news/burma/3-civilians-reportedly-killed-landmines-shan-state-june.html`.

[35] Reuters. `http://www.reuters.com/article/us-colombia-landmines/colombia-aims-to-rid-country-of-landmines-by-2021-govt-idUSKBN15T2FM`.

[36] Sloan C.E.E. *Mine Warfare on Land*. Brassey's Defence, 1986.

[37] Monin L. *The Devil's Gardens: The Story of Landmines*. Random House, 2011.

[38] Maslen S. *Anti-personnel Mines Under Humanitarian Law: A View from the Vanishing Point*. Clarendon paperbacks. Intersentia, 2001.

[39] BBC News. `http://www.bbc.com/news/world-europe-40200305`.

[40] VV.AA. *Issues in Peace and Conflict Studies: Selections From CQ Researcher*. SAGE Publications, 2010.

[41] The Independent. `http://www.independent.co.uk/news/world/europe/landmine-kills-three-children-in-bosnia-279712.html`.

[42] BBC News. `http://www.bbc.com/news/world-latin-america-11980034`.

[43] Physicians for Human Rights. The coward's war: Landmines in cambodia. `https://www.hrw.org/news/1991/09/02/cowards-war-landmines-cambodia`, September 1991.

[44] Williams J. and Ensler E. *My Name Is Jody Williams: A Vermont Girl's Winding Path to the Nobel Peace Prize*. University of California Press, 2013.

[45] NATO Association of Canada. http://natoassociation.ca/the-ottawa-process-two-decades-later/.

[46] CNN World News. http://edition.cnn.com/WORLD/9709/10/diana.angola/.

[47] BBC News. http://www.bbc.co.uk/news/special/politics97/news/08/0808/diana.shtml.

[48] BBC News. http://www.bbc.com/news/uk-england-cumbria-41111012.

[49] CNN World News. http://edition.cnn.com/WORLD/9709/17/land.mines/.

[50] Nobel Prize Official Website. http://www.nobelprize.org/nobel_prizes/peace/laureates/1997/press.html.

[51] International Committee of the Red Cross. http://www.icrc.org/eng/resources/documents/misc/57jnr5.htm.

[52] Human Rights Watch. http://www.hrw.org/news/2017/04/20/yemen-houthi-saleh-forces-using-landmines.

[53] Amnesty International. http://www.amnesty.org/en/latest/news/2017/09/myanmar-army-landmines-along-border-with-bangladesh-pose-deadly-threat-to-fleeing-rohingya/.

[54] Reuters. http://www.reuters.com/article/us-nigeria-security-chad/boko-haram-landmine-kills-four-chadian-soldiers-idUSKCN1120KY.

[55] Bottigliero I. *120 Million Landmines Deployed Worldwide: Fact Or Fiction?* Fondation Pro Victimis, 2000.

[56] NATO Standardization Office STANAG 2036. http://nso.nato.int/nso/.

[57] Lesser I., Arquilla J., Hoffman B., Ronfeldt D.F., and Zanini M. *Countering the New Terrorism*. RAND Corporation, 1999.

[58] Certini G., Scalenghe R., and Woods W.I. The impact of warfare on the soil environment. *Earth-Science Reviews*, 127:1 – 15, 2013.

[59] Habib M.K. Mechanical mine clearance technologies and humanitarian demining: Applicability and effectiveness. In *5th International Symposium on Technology and Mine Problem*, Monterey , CA, USA, 2002.

[60] Prada A.P. and Rodríguez M.C. Demining dogs in Colombia – a review of operational challenges, chemical perspectives, and practical implications. *Science & Justice*, 56(4):269 – 277, 2016.

[61] Bajic M., Ivelja T., Hadzic E., Balta A., Skelac G., and Grujic Z. Impact of flooding on Mine Action in Bosnia and Herzegovina, Croatia, and Serbia. *Journal of Conventional Weapons Destruction*, 19(1):43–49, 2015.

[62] Reuters. `http://www.reuters.com/article/us-balkans-flood-landmines/balkan-floods-may-have-undone-years-of-landmine-detection-idUSBREA4J0K220140520`.

[63] Keeley R. Understanding landmines and mine action. `http://mit.edu/demining/assignments/understanding-landmines.pdf`, September 2003.

[64] Habib M.K. Mine clearance techniques and technologies for effective humanitarian demining. *Journal of Conventional Weapons Destruction*, 6(1):62–65, 2002.

[65] Bruschini C. and Gros B. A survey of research on sensor technology for landmine detection. *Journal of Conventional Weapons Destruction*, 2(1):1–25, 2016.

[66] Schubert H. and Kuznetsov A. *Detection of Explosives and Landmines: Methods and Field Experience*, volume 66. Springer Science & Business Media, 2012.

[67] Daniels D.J. *EM detection of concealed targets*, volume 196. John Wiley & Sons, 2009.

[68] Acheroy M. Mine action: status of sensor technology for close-in and remote detection of anti-personnel mines. *Near Surface Geophysics*, 5(1):43–55, 2007.

[69] Collins L. and Gao P. Hypothesis testing for landmine detection with EMI images. In *IEEE International Conference on Fuzzy Systems Proceedings.*, volume 1, pages 237–240, Anchorage, AK, USA, 1998.

[70] Won I.J., Keiswetter D.A., and Bell T.H. Electromagnetic induction spectroscopy for clearing landmines. *IEEE Transactions on Geoscience and Remote Sensing*, 39(4):703–709, 2001.

[71] Sato M. Principles of mine detection by ground-penetrating radar. In *Anti-personnel Landmine Detection for Humanitarian Demining*, pages 19–26. Springer, 2009.

[72] Daniels D.J. A review of GPR for landmine detection. *Sensing and Imaging*, 7(3):90–123, 2006.

[73] Church P., McFee J.E., Gagnon S., and P P., Wort. Electrical impedance tomographic imaging of buried landmines. *IEEE Transactions on Geoscience and Remote Sensing*, 44(9):2407–2420, 2006.

[74] Metwaly M., El-Qady G., Matsushima J., Szalai S., Al-Arifi N.S.N., and Taha A. Contribution of 3-D electrical resistivity tomography for landmines detection. *Nonlinear Processes in Geophysics*, 15(6):977–986, 2008.

[75] Bowman A.P., Winter E.M., Stocker A.D., and Lucey P.G. Hyperspectral infrared techniques for buried landmine detection. In *2nd International Conference on the Detection of Abandoned Land Mines*, pages 129–133, Edinburgh, UK, 1998.

[76] McFee J.E., Anger C., Achal S., and Ivanco T. Landmine detection using passive hyperspectral imaging. In *Chemical and Biological Sensing VIII*, pages 655404–655404, 2007.

[77] Martinez P.L., Van Kempen L., Sahli H., and Cabello Ferrer D. Improved thermal analysis of buried landmines. *IEEE Transactions on Geoscience and Remote Sensing*, 42(9):1965–1975, 2004.

[78] Deans J., Gerhard J., and Carter L.J. Analysis of a thermal imaging method for landmine detection, using infrared heating of the sand surface. *Infrared Physics & Technology*, 48(3):202 – 216, 2006.

[79] Sabatier J.M. and Ning X. An investigation of acoustic-to-seismic coupling to detect buried antitank landmines. *IEEE Transactions on Geoscience and Remote Sensing*, 39(6):1146–1154, 2001.

[80] Scott W.R., Schroeder C.T., Martin J.S., and Larson G.D. Use of elastic waves for the detection of buried land mines. In *IEEE International Geoscience and Remote Sensing Symposium*, volume 3, pages 1116–1118, Sydney, Australia, 2001.

[81] Martin J.S., Larson G.D., and Scott Jr W.R. Surface-contacting vibrometers for seismic landmine detection. In *Detection and Remediation Technologies for Mines and Minelike Targets X*, volume 5794, pages 590–601, 2005.

[82] Petculescu A.G. and Sabatier J.M. Doppler ultrasound techniques for landmine detection. In *Detection and Remediation Technologies for Mines and Minelike Targets IX*, volume 5415, pages 30–35, 2004.

[83] Habib M.K. Controlled biological and biomimetic systems for landmine detection. *Biosensors and Bioelectronics*, 23(1):1 – 18, 2007.

[84] Poling A., Weetjens B., Cox C., Beyene N.W., Bach H., and Sully A. Using trained pouched rats to detect landmines: another victory for operant conditioning. *Journal of Applied Behavior Analysis*, 44(2):351–355, 2011.

[85] Steinfeld J.I. and Wormhoudt J. Explosives detection: a challenge for physical chemistry. *Annual Review of Physical Chemistry*, 49(1):203–232, 1998.

[86] Yinon J. Peer reviewed: Detection of explosives by electronic noses. *Analytical Chemistry*, 75(5):98 A–105 A, 2003.

[87] Gudmundson E., Jakobsson A., and Stoica P. NQR-based explosives detection; an overview. In *9th International Symposium on Signals, Circuits and Systems*, pages 1–4, Iasi, Romania, 2009.

[88] Garroway A.N., Buess M.L., Miller J.B., Suits B.H., Hibbs A.D., Barrall G.A., Matthews R., and Burnett L.J. Remote sensing by nuclear quadrupole resonance. *IEEE Transactions on Geoscience and Remote Sensing*, 39(6):1108–1118, 2001.

[89] Datema C.P., Bom V.R., and Van Eijk C.W.E. Landmine detection with the neutron backscattering method. *IEEE Transactions on Nuclear Science*, 48(4):1087–1091, 2001.

[90] McFee J.E., Faust A.A., Andrews H.R., Kovaltchouk V., Clifford E.T., and Ing H. A comparison of fast inorganic scintillators for thermal neutron analysis landmine detection. *IEEE Transactions on Nuclear Science*, 56(3):1584–1592, 2009.

[91] Harding G. X-ray scatter tomography for explosives detection. *Radiation Physics and Chemistry*, 71(3–4):869 – 881, 2004.

[92] Faust A.A., Rothschild R.E., Leblanc P., and McFee J.E. Development of a coded aperture X-ray backscatter imager for explosive device detection. *IEEE Transactions on Nuclear Science*, 56(1):299–307, 2009.

[93] DiFranco J. and Rubin B. *Radar detection*. SciTech Publishing Inc., 2004.

[94] Bach H. Scalable technical survey for improved land-release rates. *Journal of ERW and Mine Action*, 18(1):17–21, 2014.

[95] Bruschini C., Sahli H., Van Kempen L., Schleijpen R., and Den Breejen E. Achievements and bottlenecks in humanitarian demining EU-funded research: final results from the EC-DELVE project. In *Detection and Sensing of Mines, Explosive Objects, and Obscured Targets XIII*, volume 6953, page 69530E, 2008.

[96] Newnham P. and Daniels D.J. Market for advanced humanitarian mine detectors. In *Detection and Remediation Technologies for Mines and Minelike Targets VI*, volume 4394, pages 1213–1224, 2001.

[97] Soumekh M., Ton T., and Howard P. 3D wavefront image formation for NIITEK GPR. In *Radar Sensor Technology XIII*, volume 7308, pages 73080J–1, 2009.

[98] Daniels D.J., Curtis P., Amin R., and Hunt N. MINEHOUND production development. In *Detection and Remediation Technologies for Mines and Minelike Targets X*, volume 5794, pages 488–495, 2005.

[99] Daniels D.J. and Curtis P. MINEHOUND trials in Cambodia, Bosnia, and Angola. In *Detection and Remediation Technologies for Mines and Minelike Targets XI*, volume 6217, page 62172N, 2006.

[100] Sato M., Fujiwara J., Kido T., and Takahashi K. ALIS evaluation tests in Croatia. In *Detection and Sensing of Mines, Explosive Objects, and Obscured Targets XIV*, volume 7303, page 73031B, 2009.

[101] Geneva International Centre for Humanitarian Demining. `http://www.gichd.org/resources/publications/`.

[102] Cremer F., Schutte K., Schavemaker J.G.M., and Eric E., Den Breejen. A comparison of decision-level sensor-fusion methods for anti-personnel landmine detection. *Information fusion*, 2(3):187–208, 2001.

[103] Frigui H., Zhang L., and Gader P.D. Context-dependent multisensor fusion and its application to land mine detection. *IEEE Transactions on Geoscience and Remote Sensing*, 48(6):2528–2543, 2010.

[104] Doheny R.C., Burke S., Cresci R., Ngan P., Walls R., and Chernoff J. Handheld standoff mine detection system (HSTAMIDS) field evaluation in Namibia. volume 6217, page 62172K, 2006.

[105] Daniels D.J. and Curtis P. MINETECT. In *2nd International Workshop on Advanced Ground Penetrating Radar*, pages 110–114, Delft, Netherlands, 2003.

[106] Daniels D.J., Curtis P., Amin R., and Dittmer J. An affordable humanitarian mine detector. In *Detection and Remediation Technologies for Mines and Minelike Targets IX*, volume 5415, pages 1185–1194, 2004.

[107] Sato M., Fujiwara J., and Kazunori K., Takahashi. The development of the hand-held dual-sensor alis. In *Detection and Remediation Technologies for Mines and Minelike Targets XII*, volume 6553, page 65531C, 2007.

[108] Leimbach G. and Löwy H. Verfahren zur systematischen erforschung des erdinnern grosserer gebiete mittels elektrischer wellen. Patent, DE 237944, Filed on 15 June 1910.

[109] Waite A.H. and Schmidt S.J. Gross errors in height indication from pulsed radar altimeters operating over thick ice or snow. *Proceedings of the IRE*, 50(6):1515–1520, 1962.

[110] Ciarletti V. A variety of radars designed to explore the hidden structures and properties of the solar system's planets and bodies. *Comptes Rendus Physique*, 17(9):966–975, 2016.

[111] Conyers L.B. *Interpreting ground-penetrating radar for archaeology*. Routledge, 2016.

[112] Rotter A.J. *Light at the End of the Tunnel: A Vietnam War Anthology*. SR Books, 1999.

[113] Nilsson B. *Two Topics in Electromagnetic Radiation Field Prospecting*. PhD thesis, University of University of Luleå, 1978.

[114] Ruffell A. and McKinley J. *Geoforensics*. John Wiley & Sons, Ltd, 2008.

[115] BBC News. `http://news.bbc.co.uk/2/hi/uk_news/1019682.stm`.

[116] BBC News. `http://news.bbc.co.uk/2/hi/uk_news/7103836.stm`.

[117] Benedetto A. and Pajewski L. *Civil engineering applications of ground penetrating radar*. Springer, 2015.

[118] González-Huici M.A., Catapano I., and Soldovieri F. A comparative study of GPR reconstruction approaches for landmine detection. *IEEE Journal of Selected Topics in Applied Earth Observations and Remote Sensing*, 7(12):4869–4878, 2014.

[119] Nuzzo L., Alli G., Guidi R., Cortesi N., Sarri A., and Manacorda G. A new densely-sampled ground penetrating radar array for landmine detection. In *15th International Conference on Ground Penetrating Radar*, pages 969–974, Brussels, Belgium, 2014.

[120] Bruschini C., Gros B., Guerne F., Pièce P.Y., and Carmona O. Ground penetrating radar and imaging metal detector for antipersonnel mine detection. *Journal of Applied Geophysics*, 40(1):59 – 71, 1998.

[121] Webb A., Havens T.C., and Schulz T.J. GPR imaging with mutual intensity. In *Detection and Sensing of Mines, Explosive Objects, and Obscured Targets XXII*, volume 10182, page 101821B, 2017.

[122] Igel J. The small-scale variability of electrical soil properties–influence on GPR measurements. In *12th International Conference on Ground Penetrating Radar*, pages 16–19, Birmingham, UK, 2008.

[123] Nicolaescu I. and Van Genderen P. Performances of a stepped-frequency continuous-wave ground penetrating radar. *Journal of Applied Geophysics*, 82:59 – 67, 2012.

[124] Bleistein N. and Gray S.H. From the hagedoorn imaging technique to kirchhoff migration and inversion. *Geophysical Prospecting*, 49(6):629–643, 2001.

[125] Persico R., Leucci G., Matera L., de Giorgi L., Soldovieri F., Cataldo A., Cannazza G., and De Benedetto F. Effect of the height of the observation line on the the diffraction curve in GPR prospecting. *Near Surface Geophysics*, 13(3):243–252, 2015.

[126] Pramudita A.A., Kurniawan A., Suksmono A.B., and Lestari A.A. Effect of antenna dimensions on the antenna footprint in ground penetrating radar applications. *IET Microwaves, Antennas Propagation*, 3(8):1271–1278, 2009.

[127] Diamanti N. and Annan A.P. Characterizing the energy distribution around GPR antennas. *Journal of Applied Geophysics*, 99:83–90, 2013.

[128] Hines M.J., Piers A., Du K., Gonzalez-Valdes B., Martínez-Lorenzo J.Á., and Rappaport C.M. Localization of anti-personnel landmines using multi-bistatic ground-coupled ground penetrating radar. In *Radio Science Meeting (Joint with AP-S Symposium)*, pages 241–241, 2014.

[129] Eide E., Våland P.A., and Sala J. Ground-coupled antenna array for step-frequency GPR. In *15th International Conference on Ground Penetrating Radar*, pages 756–761, Brussels, Belgium, 2014.

[130] Diamanti N. and Annan A.P. Air-launched and ground-coupled GPR data. In *11th European Conference on Antennas and Propagation*, pages 1694–1698, Paris, France, 2017.

[131] Zhang Y., Orfeo D., Burns D., Miller J., Huston D., and Xia T. Buried nonmetallic object detection using bistatic ground penetrating radar with variable antenna elevation angle and height. In *Nondestructive Characterization and Monitoring of Advanced Materials, Aerospace, and Civil Infrastructure*, volume 10169, page 1016908, 2017.

[132] Lopera O., Milisavljević N., and Lambot S. Clutter reduction in GPR measurements for detecting shallow buried landmines: a Colombian case study. *Near Surface Geophysics*, 5(1):57–64, 2007.

[133] Paglieroni D.W., Chambers D.H., Mast J.E., Bond S.W., and Beer N.R. Imaging modes for ground penetrating radar and their relation to detection performance. *IEEE Journal of Selected Topics in Applied Earth Observations and Remote Sensing*, 8(3):1132–1144, 2015.

[134] Bernstein R., Oristaglio M., Miller D.E., and Haldorsen J. Imaging radar maps underground objects in 3-D. *Computer Applications in Power*, 13(3):20–24, 2000.

[135] Grasmueck M. and Weger R. 3D GPR reveals complex internal structure of pleistocene oolitic sandbar. *The Leading Edge*, 21:634–639, 2002.

[136] Lualdi M. and Zanzi L. 2D and 3D experiments to explore the potential benefit of GPR investigations in planning the mining activity of a limestone quarry. In

10th International Conference on Ground Penetrating Radar, pages 613 – 616, Delft, the Netherlands, 2004.

[137] Lorenzo H., Novo A., Rial F.I., and Solla M. Three dimensional ground-penetrating radar strategies over an indoor archaeological site convent of Santo Domingo (Lugo Spain). *Archaeological Prospecting*, 17:213–222, 2010.

[138] Zhao W.K., Tian G., Wang B.B., Shi Z.J., and Lin J.X. Application of 3D GPR attribute technology in archaeological investigations. *Applied Geophysics*, 9:261–269, 2012.

[139] Groenenboom J., Van der Kruk J., and Zeeman J.H. 3D GPR data acquisition and the influence of positioning errors on image quality. In *63rd EAGE Conference & Exhibition*, pages 1–4, Amsterdam, Netherlands, 2001.

[140] Lualdi M., Zanzi L., and Binda L. Acquisition and processing requirements for high quality 3D reconstructions from GPR investigations. In *International Symposium Non-Destructive Testing in Civil Engineering*, pages 1–13, Berlin, Germany, 2003.

[141] Lehmann F. and Green A.G. Semiautomated georadar data acquisition in three dimensions. *Geophysics*, 64(3):719–731, 1999.

[142] Grasmueck M., Weger R., and Horstmeyer H. How dense is dense enough for a 'real' 3D GPR survey? In *73rd SEG Annual lntemational Meeting*, pages 1180–1183, Dallas, TX, USA, 2003.

[143] Yilmaz Ö. *Seismic Data Analysis*. Society of Exploration Geophysicists, 2001.

[144] Nyquist H. Certain topics in telegraph transmission theory. *Transactions of the American Institute of Electrical Engineers*, 47(2):617–644, 1928.

[145] Doerksen K. Improved optical positioning for GPR-based structure mapping. In *9th International Conference on Ground Penetrating Radar*, pages 503–507, Santa Barbara, CA, USA, 2002.

[146] Sato M., Gaber A., Yokota Y., Grasmueck M., and Marchesini P. Ccd camera and igps tracking of geophysical sensors for visualization of buried explosive

devices. In *International Conference on Indoor Positioning and Indoor Navigation*, pages 1–4, Zurich, Switzerland, 2010.

[147] Forte E. and Pipan M. Review of multi-offset GPR applications: Data acquisition, processing and analysis. *Signal Processing*, 132:210 – 220, 2017.

[148] Berard B.B. and Maillol J.M. Multi-offset ground penetrating radar data for improved imaging in areas of lateral complexity — application at a Native American site. *Journal of Applied Geophysics*, 62(2):167 – 177, 2007.

[149] Sule S.D. and Paulson K.S. A comparison of bistatic and multistatic handheld ground penetrating radar (GPR) antenna performance for landmine detection. In *IEEE Radar Conference*, pages 1211–1215, Seattle, WA, USA, 2017.

[150] Diamanti N., Annan A.P., and Redman J.D. Anisotropy effect on gpr signals. In *8th International Workshop on Advanced Ground Penetrating Radar*, pages 1–5, Firenze, Italy, 2015.

[151] Forte E., Dossi M., Pipan M., and Colucci R.R. Velocity analysis from common offset GPR data inversion: theory and application to synthetic and real data. *Geophysical Journal International*, 197(3):1471–1483, 2014.

[152] Lavoué F., Brossier R., Métivier L., Garambois S., and Virieux J. Two-dimensional permittivity and conductivity imaging by full waveform inversion of multioffset GPR data: a frequency-domain quasi-newton approach. *Geophysical Journal International*, 197(1):248–268, 2014.

[153] Roberts R.L. and Daniels J.J. Analysis of GPR polarization phenomena. *Journal of Environmental and Engineering Geophysics*, 1(2):139–157, 1996.

[154] Borghese F., Denti P., Saija R., and Cecchi-Pestellini C. On the polarization and depolarization of the electromagnetic waves. *Journal of Physics: Conference Series*, 6(1):59–72, 2005.

[155] Leckebusch J. Problems and solutions with GPR data interpretation: Depolarization and data continuity. *Archaeological Prospection*, 18(4):303–308, 2011.

[156] Balanis C.A. *Advanced engineering electromagnetics*. John Wiley & Sons, 1989.

[157] Van der Kruk J., Arcone S.A., and Liu L. Fundamental and higher mode inversion of dispersed GPR waves propagating in an ice layer. *IEEE Transactions on Geoscience and Remote Sensing*, 45(8):2483–2491, 2007.

[158] Arcone S.A., Peapples P.R., and Liu L. Propagation of a ground-penetrating radar (GPR) pulse in a thin-surface waveguide. *Geophysics*, 68(6):1922–1933, 2003.

[159] Baker G.S. Applying AVO analysis to GPR data. *Geophysical Research Letters*, 25(3):397–400, 1998.

[160] Skolnik M. *Radar Handbook*. McGraw-Hill Education, 3 edition, 2008.

[161] Boniger U. and Tronicke J. Subsurface utility extraction and characterization: Combining GPR symmetry and polarization attributes. *IEEE Transactions on Geoscience and Remote Sensing*, 50(3):736–746, 2012.

[162] Radzevicius S.J. and Daniels J.J. Ground penetrating radar polarization and scattering from cylinders. *Journal of Applied Geophysics*, 45(2):111 – 125, 2000.

[163] Tsoflias G.P., Van Gestel J.P., Stoffa P.L., Blankenship D.D., and Sen M. Vertical fracture detection by exploiting the polarization properties of ground-penetrating radar signals. *Geophysics*, 69(3):803–810, 2004.

[164] Peichl M., Schreiber E., Heinzel A., and Dill S. Novel imaging radar technology for detection of landmines and other unexploded ordnance. *European Journal for Security Research*, 2(1):23–37, 2017.

[165] Cihlar J.B. and Bray J.R. Radar cross section modeling and measurement of electric detonators. In *IEEE Radar Conference*, pages 1–4, Ottawa, ON, Canada, 2013.

[166] Soldovieri F., Brancaccio A., Leone G., and Pierri R. Shape reconstruction of perfectly conducting objects by multiview experimental data. *IEEE Transactions on Geoscience and Remote Sensing*, 43(1):65–71, 2005.

[167] Giannakis I., Giannopoulos A., and Yarovoy A. Model-based evaluation of signal-to-clutter ratio for landmine detection using ground-penetrating radar. *IEEE Transactions on Geoscience and Remote Sensing*, 54(6):3564–3573, 2016.

[168] Reichman D., Morton K.D., Malof J.M., Collins L.M., and Torrione P.A. Target signature localization in GPR data by jointly estimating and matching templates. In *Detection and Sensing of Mines, Explosive Objects, and Obscured Targets XX*, volume 9454, page 945416, 2015.

[169] Borgatti L., Forte E., Mocnik A., Zambrini R., Cervi F., Martinucci D., Pellegrini F., Pillon S., Prizzon A., and Zamariolo A. Detection and characterization of animal burrows within river embankments by means of coupled remote sensing and geophysical techniques: Lessons from river panaro (northern italy). *Engineering Geology*, 226:277 – 289, 2017.

[170] Webb A., Havens T.C., and Schulz T.J. Spectral diversity for ground clutter mitigation in forward-looking GPR. In *Detection and Sensing of Mines, Explosive Objects, and Obscured Targets XXI*, volume 9823, page 98231M. International Society for Optics and Photonics, 2016.

[171] Metwaly M., Ismail A., and J. Matsushima. Evaluating some factors that affect feasility of using ground penetrating radar for landmine detection. *Applied Geophysics*, 4(3):221–230, 2007.

[172] Asimov I. and Shulman J.A. *Isaac Asimov's Book of Science and Nature Quotations*. Blue Cliff, 1988.

[173] Bucci O.M. and Isernia T. Electromagnetic inverse scattering: Retrievable information and measurement strategies. *Radio Science*, 32(6):2123–2137, 1997.

[174] Tellez O.L.L. and Scheers B. Ground-penetrating radar for close-in mine detection. In *Mine Action-The Research Experience of the Royal Military Academy of Belgium*. InTech, 2017.

[175] McGrath R. *Landmines And Unexploded Ordnance: A Resource Book*. Pluto Press, 2000.

[176] Daniels D.J. An assessment of the fundamental performance of GPR against buried landmines. *Detection and Remediation Technologies for Mines and Minelike Targets XII*, 6553:65530G, 2007.

[177] Savelyev T.G., van Kempen L., Sahli H., Sachs J., and Sato M. Investigation of time-frequency features for GPR landmine discrimination. *IEEE Transactions on Geoscience and Remote Sensing*, 45(1):118–129, 2007.

[178] Savelyev T.G. and Sato M. Optimal GPR bandwidth for time-frequency landmine discrimination. In *Detection and Remediation Technologies for Mines and Minelike Targets X*, volume 5794, pages 435–447, 2005.

[179] Sai B. and Ligthart L.P. GPR phase-based techniques for profiling rough surfaces and detecting small, low-contrast landmines under flat ground. *IEEE Transactions on Geoscience and Remote Sensing*, 42(2):318–326, 2004.

[180] Nasif A.O. and Hintz K.J. Observations on syntactic landmine detection using impulse ground-penetrating radar. In *Detection and Sensing of Mines, Explosive Objects, and Obscured Targets XVI*, volume 8017, page 80171M, 2011.

[181] Schofield J., Daniels D.J., and Hammerton P. A multiple migration and stacking algorithm designed for land mine detection. *IEEE Transactions on Geoscience and Remote Sensing*, 52(11):6983–6988, 2014.

[182] Carevic D., Craig M., and Chant I.J. Modeling GPR echoes from land mines using linear combinations of exponentially damped sinusoids. In *Detection and Remediation Technologies for Mines and Minelike Targets II*, volume 3079, pages 568–581, 1997.

[183] Roth F. *Convolutional Models for Landmine Identification with Ground Penetrating Radar*. PhD thesis, Delft University of Technology, 2005.

[184] Roth F., van Genderen P., and Verhaegen M. Processing and analysis of polarimetric ground penetrating radar landmine signatures. In *2nd International Workshop on Advanced Ground Penetrating Radar*, pages 70–75, Delft, Netherlands, 2003.

[185] Jacob R.W. and Urban T.M. Ground-penetrating radar velocity determination and precision estimates using Common-Midpoint (CMP) collection with hand-picking, semblance analysis and cross-correlation analysis: A case study and tutorial for archaeologists. *Archaeometry*, 58(6):987–1002, 2016.

[186] Booth A.D., Linford N.T., Clark R.A., and Murray T. Three-dimensional, multi-offset ground-penetrating radar imaging of archaeological targets. *Archaeological Prospection*, 15(2):93–112, 2008.

[187] Muller W. Self-correcting pavement layer depth estimates using 3D multi-offset ground penetrating radar (GPR). In *15th International Conference on Ground Penetrating Radar*, pages 887–892, Brussels, Belgium, 2014.

[188] Schennen S., Tronicke J., Wetterich S., Allroggen N., Schwamborn G., and Schirrmeister L. 3D ground-penetrating radar imaging of ice complex deposits in northern east siberia. *Geophysics*, 81(1):WA195–WA202, 2016.

[189] Ojowu Jr O., Wu Y., Li J., and Nguyenb L. SIRE: A MIMO radar for landmine/IED detection. In *Radar Sensor Technology XVII*, volume 8714, page 87140O, 2013.

[190] Shaw D., Ho K.C., Stone K., Keller J.M., Popescu M., Anderson D.T., Luke R.H., and Burns B. Explosive hazard detection using MIMO forward-looking ground penetrating radar. In *Detection and Sensing of Mines, Explosive Objects, and Obscured Targets XX*, volume 9454, page 94540Z, 2015.

[191] Burkholder R.J., Gupta L.J., and Johnson J.T. Comparison of monostatic and bistatic radar images. *IEEE Antennas and Propagation Magazine*, 45(3):41–50, 2003.

[192] Pauli M., Fischer C., and Wiesbeck W. Mine-detection using a multistatic antenna setup and non-linear inversion. In *10th International Conference on Ground Penetrating Radar*, volume 1, pages 83–85, Delft, The Netherlands, 2004.

[193] Counts T., Gurbuz A.C., Scott W.R., McClellan J.H., and Kangwook K. Multistatic ground-penetrating radar experiments. *IEEE Transactions on Geoscience and Remote Sensing*, 45(8):2544–2553, 2007.

[194] Lloyd D. and Longstaff I.D. Ultra-wideband multistatic SAR for the detection and location of landmines. *IEE Proceedings - Radar, Sonar and Navigation*, 150(3):158–164, 2003.

[195] Kim K., Gurbuz A.C., Scott Jr W.R., and McClellan J.H. A multi-static ground-penetrating radar with an array of resistively loaded vee dipole antennas for landmine detection. In *Detection and Remediation Technologies for Mines and Minelike Targets X*, volume 5794, pages 495–507, 2005.

[196] Ashtari A., Flores-Tapia D., Thomas G., and Pistorius S. A method for combining focused monostatic and bistatic GPR to reduce multipath effects. In *1st International Workshop on Computational Advances in Multi-Sensor Adaptive Processing*, pages 28–31, Puerto Vallarta, Mexico, 2005.

[197] Jin T., Lou J., and Zhou Z. Extraction of landmine features using a forward-looking ground-penetrating radar with MIMO array. *IEEE Transactions on Geoscience and Remote Sensing*, 50(10):4135–4144, 2012.

[198] Fischer C. and Wiesbeck W. Multistatic GPR for antipersonnel mine detection. In *International Geoscience and Remote Sensing Symposium*, volume 6, pages 2721–2723, Sydney, Australia, 2001.

[199] Fischer C. and Wiesbeck W. Multistatic antenna configurations and image processing for mine-detection GPR. In *3rd Demining Technology Information Forum workshop*, pages 23–24, Ispra, Italy, 2002.

[200] Zeng Z., Li J., Huang L., Feng X., and Liu F. Improving target detection accuracy based on multipolarization MIMO GPR. *IEEE Transactions on Geoscience and Remote Sensing*, 53(1):15–24, 2015.

[201] Dumanian A.J. and C.M. Rappaport. Enhanced detection and classification of buried mines with an uwb multistatic GPR. In *Antennas and Propagation Soci-*

ety International Symposium, volume 3B, pages 88–91, Washington, DC, USA, 2005.

[202] Fischer C., Herschlein A., Younis M., and Wiesbeck W. Detection of antipersonnel mines by using the factorization method on multistatic ground-penetrating radar measurements. *IEEE Transactions on Geoscience and Remote Sensing*, 45(1):85–92, 2007.

[203] Fischer C., Younis M., and Wiesbeck W. Multistatic antennas and non-linear inversion for mine-detection GPR. In *2nd International Workshop onAdvanced Ground Penetrating Radar*, pages 212–215, Delft, Netherlands, 2003.

[204] Stiles J.M., Apte A.V., and Beh B. A group-theoretic analysis of symmetric target scattering with application to landmine detection. *IEEE Transactions on Geoscience and Remote Sensing*, 40(8):1802–1814, 2002.

[205] Hayashi N. and Sato M. 3D subsurface visualization by suppressing ground reflection and direct wave with bistatic GPR. In *International Geoscience and Remote Sensing Symposium*, pages 4592–4595, Honolulu, HI, USA, 2010.

[206] Hayashi N. and Sato M. Fk filter designs to suppress direct waves for bistatic ground penetrating radar. *IEEE Transactions on Geoscience and Remote Sensing*, 48(3):1433–1444, 2010.

[207] van Zyl J.J., Zebker H.A., and Elachi C. Imaging radar polarization signatures: Theory and observation. *Radio Science*, 22(4):529–543, 1987.

[208] Born M. and Wolf E. *Principles of optics*. Cambridge Univ. Press, 1999.

[209] Deschamps G.A. Techniques for handling elliptically polarized waves with special reference to antennas: Part II - geometrical representation of the polarization of a plane electromagnetic wave. *Proceedings of the IRE*, 39(5):540–544, 1951.

[210] Huynen J.R. *Phenomenological theory of radar targets*. PhD thesis, Delft University of Technology, 1970.

[211] Huynen J.R. Measurement of the target scattering matrix. *Proceedings of the IEEE*, 53(8):936–946, 1965.

[212] Sinclair G. The transmission and reception of elliptically polarized waves. *Proceedings of the IRE*, 38(2):148–151, 1950.

[213] Kennaugh E.M. and Sloan R.W. Effects of type of polarization on echo characteristics. Technical report, DTIC Document, 1952.

[214] Heath G.E. Properties of the linear polarization bistatic scattering matrix. *IEEE Transactions on Antennas and Propagation*, 29(3):523–525, 1981.

[215] Bickel S.H. Some invariant properties of the polarization scattering matrix. *Proceedings of the IEEE*, 53(8):1070–1072, 1965.

[216] Shanmugan K.S., Narayanan V., Frost V.S., Stiles J.A., and Holtzman J.C. Textural features for radar image analysis. *IEEE Transactions on Geoscience and Remote Sensing*, GE-19(3):153–156, 1981.

[217] Ulaby F.T., Kouyate F., Brisco B., and Williams T.H.L. Textural infornation in sar images. *IEEE Transactions on Geoscience and Remote Sensing*, GE-24(2):235–245, 1986.

[218] Copeland J.R. Radar target classification by polarization properties. *Proceedings of the IRE*, 48(7):1290–1296, 1960.

[219] Daniels J.J., Wielopolski L., Radzevicius S., and Bookshar J. 3D GPR polarization analysis for imaging complex objects. In *16th Symposium on the Application of Geophysics to Environmental and Engineering Problems*, pages 1–13, San Antonio, TX, USA, 2003.

[220] Roberts R.L., Daniels J.J., and Peters Jr L. Improved GPR interpretation from analysis of buried target polarization properties. In *Symposium on the Application of Geophysics to Engineering and Environmental Problems*, pages 597–611, Oakbrook, IL, USA, 1992.

[221] Zhao W., Tian G., Forte E., Pipan M., Wang Y., Li X., Shi Z., and Liu H. Advances in GPR data acquisition and analysis for archaeology. *Geophysical Journal International*, 202(1):62–71, 2015.

[222] Radzevicius S.J., Guy E.D., and Daniels J.J. Pitfalls in GPR data interpretation: Differentiating stratigraphy and buried objects from periodic antenna and target effects. *Geophysical Research Letters*, 27(20):3393–3396, 2000.

[223] Radzevicius S.J., Daniels J.J., Guy E.D., and Vendl M.A. Significance of crossed-dipole antennas for high noise environments. In *Symposium on the Application of Geophysics to Environmental and Engineering Problems*, pages 407–413, Washington, DC, USA, 2000.

[224] Guy E.D., Daniels J.J., Radzevicius S.J., and Vendl M.A. Demonstration of using crossed dipole GPR antennae for site characterization. *Geophysical Research Letters*, 26(22):3421–3424, 1999.

[225] Stiles J.M., Parra-Bocaranda P., and Apte A. Detection of object symmetry using bistatic and polarimetric GPR observations. In *Detection and Remediation Technologies for Mines and Minelike Targets IV*, volume 3710, pages 992–1002, 1999.

[226] Chun E.H.Y. and Chun C.S.L. Polarimetric invariants for detection by forward-looking ground penetrating radar. In *IEEE Radar Conference*, pages 185–188, Kansas City, MO, USA, 2011.

[227] Villela A. and Romo J.M. Invariant properties and rotation transformations of the GPR scattering matrix. *Journal of Applied Geophysics*, 90:71–81, 2013.

[228] O'Neill K. Discrimination of uxo in soil using broadband polarimetric GPR backscatter. *IEEE Transactions on Geoscience and Remote Sensing*, 39(2):356–367, 2001.

[229] Alawneh I., Beine C., and Edenhofer P. Calculation of fingerprints of typical antipersonnel landmines by varying the observation point and incidence angles of excitations. In *6th European Conference on Antennas and Propagation*, pages 1068–1071, Prague, Czech Republic, 2012.

[230] Carin L., Kapoor R., and Baum C.E. Polarimetric sar imaging of buried landmines. *IEEE Transactions on Geoscience and Remote Sensing*, 36(6):1985–1988, 1998.

[231] Rosenberg D. and Stephens M. *Use Case Driven Object Modelling with UML. Theory and Practice*. Apress, 2007.

[232] Balanis C.A. *Antenna theory: analysis and design.* John Wiley & Sons, 2005.

[233] Yarovoy A.G., Savelyev T.G., Aubry P.J., and Ligthart L.P. Array-based GPR for shallow subsurface imaging. In *4th International Workshop on Advanced Ground Penetrating Radar*, pages 12–15, June 2007.

[234] Reynolds J.M. *An introduction to applied and environmental geophysics*. John Wiley & Sons, 2011.

[235] Topp G.C., Davis J.L., and Annan A.P. Electromagnetic determination of soil water content: Measurements in coaxial transmission lines. *Water Resources Research*, 16(3):574–582, 1980.

[236] Hunt A.G. Continuum percolation theory and archie's law. *Geophysical Research Letters*, 31(19):1–4, 2004.

[237] Friedman S.P. Soil properties influencing apparent electrical conductivity: a review. *Computers and Electronics in Agriculture*, 46(1):45 – 70, 2005.

[238] Peplinski N.R., Ulaby F.T., and Dobson M.C. Dielectric properties of soils in the 0.3-1.3-GHz range. *IEEE Transactions on Geoscience and Remote Sensing*, 33(3):803–807, 1995.

[239] Trang A.H. Simulation of mine detection over dry soil, snow, ice, and water. In *Detection and Remediation Technologies for Mines and Minelike Targets*, pages 430–441, 1996.

[240] Borchers B., Hendrickx J.M.H., Das B.S., and Hong S.H. Enhancing dielectric contrast between land mines and the soil environment by watering: modeling, design, and experimental results. In *Detection and Remediation Technologies for Mines and Minelike Targets V*, pages 993–1000, 2000.

[241] Wang P., Hu Z., Zhao Y., and Li X. Experimental study of soil compaction effects on GPR signals. *Journal of Applied Geophysics*, 126:128 – 137, 2016.

[242] Guillemoteau J., Bano M., and Dujardin J.R. Influence of grain size, shape and compaction on georadar waves: examples of aeolian dunes. *Geophysical Journal International*, 190(3):1455–1463, 2012.

[243] Igel J., Takahashi K., and Preetz H. Electromagnetic soil properties and performance of GPR for landmine detection: How to measure, how to analyse and how to classify? In *6th International Workshop on Advanced Ground Penetrating Radar*, pages 1–6, Aachen, Germany, 2011.

[244] Igel J., Preetz H., Takahashi K., and Loewer M. Landmine and UXO detection using EMI and GPR–limitations due to the influence of the soil. *First Break*, 31(8):43–51, 2013.

[245] Harrington R.F. *Field Computation by Moment Methods*. Wiley-IEEE Press, 1993.

[246] Taflove A. and Hagness S.C. *Computational Electrodynamics: The Finite-Difference Time-Domain Method.* Artech house, 2005.

[247] Box G.E.P. Robustness in the strategy of scientific model building. In Launer R.L. and Wilkinson G.N., editors, *Robustness in Statistics*, pages 201 – 236. Academic Press, 1979.

[248] Kunz K.S. and Luebbers R.J. *The finite difference time domain method for electromagnetics.* CRC Press, 1993.

[249] Giannopoulos A. *The investigation of Transmission-Line Matrix and Finite-Difference Time-Domain Methods for the Forward Problem of Ground Probing Radar*. PhD thesis, University of York, 1997.

[250] Yee K. Numerical solution of initial boundary value problems involving maxwell's equations in isotropic media. *IEEE Transactions on Antennas and Propagation*, 14(3):302–307, 1966.

[251] Courant R., Friedrichs K., and Lewy H. On the partial difference equations of mathematical physics. *IBM Journal of Research and Development*, 11(2):215–234, 1967.

[252] Gedney S.D. An anisotropic perfectly matched layer-absorbing medium for the truncation of fdtd lattices. *IEEE Transactions on Antennas and Propagation*, 44(12):1630–1639, 1996.

[253] Giannopoulos A. Modelling ground penetrating radar by gprmax. *Construction and Building Materials*, 19(10):755 – 762, 2005.

[254] Warren C., Giannopoulos A., and Giannakis I. gprmax: Open source software to simulate electromagnetic wave propagation for ground penetrating radar. *Computer Physics Communications*, 209:163 – 170, 2016.

[255] Marsland T.P. and Evans S. Dielectric measurements with an open-ended coaxial probe. *IEE Proceedings on Microwaves, Antennas and Propagation*, 134(4):341–349, 1987.

[256] Database of Demining Accidents. `http://www.ddasonline.com/index.html`.

[257] Maathuis B.H.P. and van Genderen J.L. A review of satellite and airborne sensors for remote sensing based detection of minefields and landmines. *International Journal of Remote Sensing*, 25(23):5201–5245, 2004.

[258] Cramer E.A. The mineseeker airship: 'supporting the u.n.'. *Journal of Mine Action*, 5(1):108–113, 2001.

[259] Mineseeker Foundation. `http://www.airships.narod.ru/mineseeker/dera.html`.

[260] Horizon magazine. `http://horizon-magazine.eu/article/how-speed-landmine-clearance.html`.

[261] García Fernández M., Álvarez López Y., Arboleya Arboleya A., González Valdés B., Rodríguez Vaqueiro Y., Las-Heras Andrés F., and Pino García A. Synthetic aperture radar imaging system for landmine detection using a ground penetrating radar on board a unmanned aerial vehicle. *IEEE Access*, 6:45100–45112, 2018.

[262] Colorado J., Devia C., Perez M., Mondragon I., Mendez D., and Parra C. Low-altitude autonomous drone navigation for landmine detection purposes. In *2017 International Conference on Unmanned Aircraft Systems (ICUAS)*, pages 540–546, June 2017.

[263] Peyton A. and Daniels D.J. `http://www.ingenia.org.uk/Ingenia/Articles/2f67b8a4-4fee-4fc2-88d7-f0c535b0dc89`.

[264] Newnham P. and Daniels D.J. Market for advanced humanitarian mine detectors. In *Detection and Remediation Technologies for Mines and Minelike Targets VI*, volume 4394, pages 1213–1225. International Society for Optics and Photonics, 2001.

[265] Daniels D.J., Braunstein J., and Nevard M. Using MINEHOUND in Cambodia and Afghanistan. *Journal of Conventional Weapons Destruction*, 18(2):14, 2015.

[266] Sharma P., Gaba S.P., and Singh D. Study of background subtraction for ground penetrating radar. In *2015 National Conference on Recent Advances in Electronics Computer Engineering (RAECE)*, pages 101–105, Feb 2015.

[267] Cagnoli B. and Ulrych T.J. Singular value decomposition and wavy reflections in ground-penetrating radar images of base surge deposits. *Journal of Applied Geophysics*, 48(3):175 – 182, 2001.

[268] VV. AA. Landmine free world 2015. `http://www.landminefree2025.org`, April 2017.